Innovative Techniques for the Characterization and Interpretation of Coastal Aquifers

Pumping Test Interpretation by means of the Drawdown Derivative to Estimate Aquifer Heterogeneity

Dissertation

zur Erlangung des akademischen Grades doctor rerum naturalium
(Dr. rer. nat.)

vorgelegt dem Rat der Chemisch-Geowissenschaftlichen Fakultät der
Friedrich-Schiller-Universität Jena

von Dipl.-Geol. Armin Pechstein
geboren am 05. November 1979 in Stollberg

Gutachter:

Prof. Dr. Sabine Attinger
Friedrich-Schiller-Universität Jena

Prof. Nadim K. Copty, PhD
Boğaziçi University, Istanbul

Tag der öffentlichen Verteidigung: 11. Mai 2016

Zusammenfassung

Grundwasser ist eine wertvolle natürliche Ressource und stellt einen unverzichtbaren Teil der Trinkwasserversorgung dar. Aufgrund des globalen Bevölkerungswachstums geraten die Grundwasserressourcen weltweit jedoch immer stärker unter Druck. Dies wird durch die Übernutzung und Verschmutzung des Grundwassers, sowie die steigende Nachfrage von Industrie und Landwirtschaft weiter verstärkt. Ein umfassendes Verständnis des Grundwasserflusses ist für den Schutz der Grundwasserreserven, sowie für die Entwicklung nachhaltiger Nutzungsstrategien von weitreichender Relevanz.

Grundwassernutzungskonzepte basieren heute hauptsächlich auf numerischen Grundwassermodellen. Die Entwicklung eines numerischen Grundwassermodells setzt eine Abschätzung der Grundwasserneubildung sowie eine umfassende hydrogeologische Beschreibung des untersuchten Grundwasserreservoirs voraus. Diese beinhaltet sowohl die Beurteilung von Randbedingungen, als auch die Unterteilung des Untergrundes in hydraulisch wirksame Einheiten oder Aquifere. Der Charakterisierung von Aquiferen kommt besondere Bedeutung zu, da ihre hydraulischen Eigenschaften maßgeblich Grundwasserfluss und Stofftransport bestimmen. Aufgrund ihrer geologischen Entwicklung sind Aquifere grundsätzlich heterogen ausgebildet, was die Abschätzung der hydraulischen Leitfähigkeit und des Speicherkoeffizienten erschwert. Die hydraulische Leitfähigkeit bzw. die Transmissivität ist dabei die bestimmende Eigenschaft von Aquiferen. Sie bestimmt Stärke und Richtung des Grundwasserflusses. Zudem ist die hydraulische Leitfähigkeit extrem variabel und kann sowohl kleinräumig im Bereich von Metern, als auch großräumig im Bereich von Kilometern, über mehrere Größenordnungen variieren. Die Heterogenität eines Aquifers beeinflusst somit wesentlich Grundwasserfluss und Stofftransport. Die adäquate Beschreibung und Abschätzung der hydraulischen Leitfähigkeit unter Berücksichtigung der Heterogenität eines Aquifers ist deshalb eine zentrale Fragestellung der hydrogeologischen Forschung.

Pumpversuche sind ein etabliertes Verfahren zu Bestimmung der hydraulischen Eigenschaften von Aquiferen. Die durch Pumpen verursachte Grundwasserabsenkung wird genutzt, um die hydraulischen Eigenschaften des untersuchten Aquifers abzuschätzen. Die Auswertung von Pumpversuchen basiert traditionell auf der Grundwassergleichung für die radiale Brunnenströmung von Theis [*Theis*, 1935], welche einen homogen ausgebildeten Aquifer voraussetzt. Die Anwendung von Theis-basierten Interpretationsverfahren auf die Grundwasserabsenkung in heterogenen Systemen ergibt deshalb interpretierte hydraulische Parameter, deren Beziehung zur originären Heterogenität des Aquifers bis dato nur unzureichend geklärt ist. Um den Einfluss von Heterogenität auf den Grundwasserfluss abschätzen zu können ist ein Verständnis dieser Beziehung, d.h., wie ein Interpretationsverfahren die originäre Heterogenität eines Aquifers wiedergibt, von fundamentaler Bedeutung. Die vor-

liegende Arbeit untersucht deshalb die Beziehung zwischen der Heterogenität eines Aquifers und den aus Pumpversuchen abgeleiteten interpretierten hydraulischen Aquiferparametern. Das Ziel ist, Theis-basierte Interpretationsverfahren für die Abschätzung des Einflusses von Heterogenität zu optimierten, um eine effizientere Beschreibung von Grundwasserleitern zu ermöglichen. Die theoretischen Arbeiten werden anschließend durch die Auswertung von realen Pumpversuchen, zur hydrogeologischen Erkundung eines stark tektonisch beeinflussten Aquifersystems im Norden Istanbuls, ergänzt.

Um den Zusammenhang zwischen Theis-basierten interpretierten Aquiferparametern und der zugrunde liegenden Heterogenität des Aquifers zu klären, werden zeitabhängige, räumliche Wichtungsfunktionen hergeleitet. Diese Wichtungsfunktionen ermöglichen es, eine skalierte Transmissivität von einer gegebenen heterogenen Transmissivitätsverteilung zu berechnen. Die skalierte Transmissivität wird anschließend mit der Theis-basierten interpretierten Transmissivität verglichen. Für diesen Vergleich werden unterschiedliche Interpretationsverfahren berücksichtigt, und zwar, die Cooper-Jacob Methode [*Cooper and Jacob*, 1946] und die Continuous-Derivation Methode [*Copty et al.*, 2011] für Pumpversuche in unbegrenzten Aquiferen, sowie, die Hantush Methode [*Hantush*, 1959] für Pumpversuche in Aquiferen, welche von einer linearen Randbedingung konstanten Drucks (BCH) begrenzt sind. In diesem Zusammenhang entwickelt diese Arbeit des Weiteren ein neues Interpretationsverfahren für Pumpversuche in BCH-Aquiferen. Dieses Verfahren basiert auf der zeitlichen Ableitung der Grundwasserabsenkung, und ist eine Erweiterung der Continuous-Derivation Methode. Es ermöglicht die Interpretation der Grundwasserabsenkung über die gesamte Dauer eines Pumpversuchs, und ist nicht wie die Cooper-Jacob oder Hantush Methode auf die Auswertung der späten Grundwasserabsenkung beschränkt. Somit erlaubt die Continuous-Derivation Methode für BCH-Systeme die kontinuierlich Abschätzung von zeitabhängigen Transmissivitäten.

Zu Beginn werden in Kapitel 2 die Grundlagen der Pumpversuchensauswertung eingeführt. Die oben genannten Interpretationsverfahren werden erläutert, und grundlegende Konzepte zur geostatistischen Beschreibung von Heterogenität sowie zur Skalierungstheorie erklärt. Der Fokus liegt auf der Beschreibung der heterogenen Leitfähigkeit bzw. der Transmissivität, welche als log-normal verteilte räumliche Zufallsfunktion modelliert wird. Zusätzlich werden Verfahren zur Untersuchung der Sensitivität der Grundwasserabsenkung bezüglich der Heterogenität des Aquifers vorgestellt. In diesem Zusammenhang wird der Fréchet Kernel eingeführt, welcher die Basis für die hergeleiteten räumlichen Wichtungsfunktionen ist.

Die Beziehung zwischen der originären Heterogenität und den interpretierten hydraulischen Parametern wird in Kapitel 3 zuerst für unbegrenzte Aquifere untersucht. Basierend auf dem Fréchet Kernel der Transmissivität werden zwei zeitabhängige, räumliche Wichtungsfunktionen abgeleitet und auf heterogene Transmissivitätsfelder angewendet. Die

erste Wichtungsfunktion nutzt den Fréchet Kernel als Wichtungsfaktor. Die resultierende, räumlich gewichtete Transmissivität ersetzt die originäre Heterogenität durch eine skalierte homogene Transmissivität, welche die Theis-Gleichung löst. Die zweite Wichtungsfunktion nutzt die Zeit-Ableitung des Fréchet Kernels als Wichtungsfaktor. Die resultierende, räumlich gewichtete Transmissivität ersetzt die originäre Heterogenität durch ein skaliertes heterogenes Transmissivitätsfeld. Für die Grundwasserabsenkung am Pumpbrunnen ist das skalierte heterogene Transmissivitätsfeld radial symmetrisch. Am Pumpbrunnen stimmt der skalierte Wert mit der originären Transmissivität am Brunnen überein, und nähert sich mit zunehmender Entfernung dem geometrischen Mittel des log-normal verteilten, originären Transmissivitätsfeldes. Der Übergang zwischen dem lokalen Wert und dem geometrischen Mittel erfolgt innerhalb von 15 bis 20 Korrelationslängen der log-normal Verteilung. Ein Pumpversuch in dem skalierten heterogenen Transmissivitätsfeld reproduziert die Grundwasserabsenkung im originär heterogenen Transmissivitätsfeld. Beide Wichtungsfunktionen wurden durch Monte Carlo Simulationen numerisch verifiziert. Der Vergleich der skalierten Transmissivitäten mit den interpretierten Transmissivitäten ergibt, dass das skalierte heterogene Transmissivitätsfeld gut mit den interpretieren Werten der Continuous-Derivation Methode übereinstimmt. Für die Cooper-Jacob Methode entspricht die interpretierte Transmissivität dem Endglied der skalierten heterogenen Transmissivität, da die Cooper-Jacob Methode lediglich die späte Grundwasserabsenkung für die Auswertung berücksichtigt.

Der Schwerpunkt dieser Arbeit liegt auf der Untersuchung von Küstenaquiferen. Deshalb wird das räumliche Wichtungsverfahren an BCH-Systeme angepasst. Dazu wird der Fréchet Kernel für BCH-Systeme abgeleitet und zur Abschätzung der skalierten homogenen Transmissivität genutzt. In den Kapiteln 4 und 5 erfolgt der Vergleich mit den interpretierten Transmissivitäten der Hantush Methode bzw. der Continuous-Derivation Methode für BCH-Systeme. Die Ergebnisse zeigen, dass die Beziehung zwischen interpretierter und originärer Transmissivität in BCH-Systemen vom vorherrschenden Fließregime abhängig ist. Unter instationären Bedingungen, wenn die Randbedingung die Grundwasserabsenkung noch nicht beeinflusst, korreliert die interpretierte Transmissivität mit dem skalierten heterogenen Transmissivitätsfeld. Für die stationäre Grundwasserabsenkung, wenn sich die Randbedingung auf die Grundwasserabsenkung auswirkt, entspricht die interpretierte Transmissivität jedoch der skalierten homogenen Transmissivität. Diesbezüglich ergeben die Hantush Methode und die Continuous-Derivation Methode für BCH-Systeme unter stationären Bedingungen die gleiche interpretierte Transmissivität.

Die oben zusammengefassten Ergebnissen zeigen, dass die Beziehung zwischen originärer und interpretierte Transmissivität davon abhängt, welche Eigenschaften der Theis-Gleichung für die Auswertung der Grundwasserabsenkung genutzt werden. Wird die Transmissivität mittels der zeitlichen Ableitung der Grundwasserabsenkung ermittelt, korre-

liert die interpretierte Transmissivität mit dem skalierten heterogenen Transmissivitätsfeld. Dies gilt für die Cooper-Jacob Methode und die Continuous-Derivation Methode in unbegrenzten Aquifern, sowie für die instationäre Grundwasserabsenkung in BCH-Systemen. Unter stationären Bedingungen geht die zeitliche Ableitung der Grundwasserabsenkung gegen null, und die interpretierte Transmissivität wird direkt aus der Grundwasserabsenkung ermittelt. Dementsprechend substituiert die interpretierte Transmissivität, welche aus der stationären Grundwasserabsenkung abgeleitet wird, die originär heterogene Verteilung durch einen homogenen Transmissivitätswert.

Ist die Transmissivität in einem heterogenen BCH-System log-normal verteilt, zeigen die Untersuchungen außerdem, dass das Verhältnis zweier Distanzen den Grundwasserfluss zum Brunnen, sowie die interpretierte Transmissivität wesentlich beeinflussen. Das entsprechende Verhältnis ergibt sich aus dem Quotienten der Distanz zwischen Pumpbrunnen und Randbedingung, und der Korrelationslänge der log-normal Verteilung der Transmissivität. Ist dieses Verhältnis klein, erschließt der Pumpversuch ein Areal welches nicht repräsentativ für den gesamten Aquifer ist. Das geometrische Mittel der heterogenen Transmissivität kann somit nicht abgeschätzt werde. Das Einzugsgebiet des Pumpversuches ist hingegen repräsentativ, wenn dieses Verhältnis einen Wert von 15 bis 20 übersteigt. Für hohe Werte, erlaubt die Continuous-Derivation Methode für BCH-Systeme die Ermittlung des geometrischen Mittels aus der Interpretation der instationären Grundwasserabsenkung. Unter stationären Bedingungen kann das geometrische Mittel hingegen nur in ausreichender Entfernung vom Pumpbrunnen und der Randbedingung approximiert werden. In diesem Zusammenhang zeigen die Untersuchung des Fréchet Kernels für BCH-Systeme, dass die stationäre Grundwasserabsenkung eine erhöhte Sensitivität für eine Region besitzt, welche zwischen dem Beobachtungsbrunnen, dem Pumpbrunnen und der Randbedingungen liegt. Je geringer die Entfernung eines Beobachtungsbrunnens von der Randbedingung, desto kleiner ist dieses Areal. Wie stark die lokale Transmissivität in diesem Bereich die interpretierte Transmissivität beeinflusst, ist vom Verhältnis zwischen Korrelationslänge und dem entsprechenden Areal abhängig.

Neben der Abschätzung der Transmissivität erlaubt die Anwendung von Theis-basierten Interpretationsverfahren die Berechnung des Speicherkoeffizienten. Dieser wird mittels der interpretierten Transmissivität berechnet und kann nicht direkt aus der Absenkung am Brunnen ermittelt werden. Der interpretierte Speicherkoeffizient wird deshalb mit dem zugehörigen Wert der interpretierten Transmissivität ausgewertet. Die numerischen Ergebnisse zeigen, dass der reale Speicherkoeffizient nur ermittelt werden kann, wenn der Einfluss der Heterogenität auf die interpretierte Transmissivität vernachlässigbar ist. Streng genommen ist dies nur der Fall, wenn die sehr frühe instationäre Grundwasserabsenkung am Pumpbrunnen zur Pumpversuchsauswertung genutzt wird, d.h., wenn die interpretierte und originäre Transmissivität übereinstimmen. In allen anderen Fällen entspricht die in-

terpretierte Transmissivität nicht der originären Transmissivität sondern einem, über das heterogene Transmissivitätsfeld gewichteten Wert. Der zugeordnete interpretierte Speicherkoeffizient beinhaltete dann weiterführende Informationen zur Konnektivität des heterogenen Transmissivitätsfeldes. Für Pumpversuche in unbegrenzten Aquiferen ergibt die Auswertung der quasi-stationären Grundwasserabsenkung am Pumpbrunnen, dass ein geringer interpretierter Speicherkoeffizient mit einer geringen lokalen Transmissivität am Brunnen korreliert. Ein hoher interpretierter Speicherkoeffizient zeigt hingegen eine hohe lokale Transmissivität am Pumpbrunnen an. In BCH-Systemen ist die Auswertung des interpretierten Speicherkoeffizienten komplizierter. Die Ergebnisse zeigen, dass der interpretierte Speicherkoeffizient unter stationären Bedingungen sowohl Informationen zur Konnektivität bezüglich des Pumpbrunnens, als auch zur Konnektivität bezüglich der Randbedingung beinhaltet. Darüber hinaus hängt der Wert des interpretierten Speicherkoeffizienten von der Variabilität der interpretierten Transmissivität ab, welche unter stationären Bedingungen relativ gering ist. Folglich ist die Variabilität des interpretierten Speicherkoeffizienten unter stationären Bedingungen ebenfalls gering, sodass dieser als Approximation des realen Speicherkoeffizienten aufgefasst werden kann. Nichtsdestotrotz beinhaltet der interpretierte Speicherkoeffizient Informationen über die Konnektivität der originären Transmissivitätsverteilung. Wird dieser Sachverhalt bei der Auswertung nicht berücksichtigt, kann dies zur unangemessenen Abschätzung des realen Speicherkoeffizienten führen.

Der theoretische Teil der vorliegenden Arbeit zeigt, dass die Interpretation der Grundwasserabsenkung in heterogenen System mittels Theis-basierter Interpretationsverfahren wichtige Informationen zur Aquiferheterogenität erbringen kann. Dabei muss berücksichtigt werden, dass die Bedeutung der interpretierten Transmissivität von den Eigenschaften der Theis-Gleichung abhängig ist, welche für die Interpretation genutzt werden. Der interpretierte Speicherkoeffizient entspricht im Allgemeinen nicht dem realen Speicherkoeffizienten des Aquifers, sondern ist als eine Variable zu verstehen, welche die Anwendung einer homogenen Theorie auf ein heterogenes Medium kompensiert. In diesem Zusammenhang beinhaltet der interpretierte Speicherkoeffizient weiterführende Informationen zur Heterogenität des Aquifers, und kann als ein Maß für die Konnektivität verstanden werden.

An den theoretischen Teil der Arbeit schließt sich mit Kapitel 6 ein praktischer Teil zur hydrogeologischen Erkundung eines Grundwasserreservoirs am Saritepe Campus der Boğaziçi Universität in Istanbul an. Dazu wurden Pumpversuche sowie geologische und hydrochemische Untersuchungen durchgeführt, welche die Installation von zwei neuen Brunnen am Standort beinhalteten. Das Ziel der Untersuchungen war die Erstellung eines konzeptionellen hydrogeologischen Modells zur Abschätzung von Meerwasserintrusionen am Standort. Die Auswertung der Pumpversuche zur Identifikation von Randbedingungen mittels der Zeit-Ableitung der Grundwasserabsenkung ergab, dass das untersuchte Grund-

wasserreservoir durch zwei undurchlässige, annähernd parallel verlaufende Störungszonen begrenzt ist, und in zwei Aquifere mit unterschiedlichen hydraulischen Eigenschaften unterteilt werden kann. Eine hydraulische Verbindung zum nahe gelegenen Schwarzen Meer wurde nicht festgestellt. Die Anwendung der Continuous-Derivation Methode für BCH-Systeme war somit nicht möglich. Die Unterteilung des Grundwasserreservoirs in zwei Aquifereinheiten wurde durch die geologischen und hydrochemischen Untersuchungen bestätigt. Demnach umfasst das Grundwasserreservoir zwei Paläo-Grundwasserkörper, deren Chemismus auf Grundwasser-Gesteins-Interaktion und lange Verweilzeiten zurückzuführen ist. Die Auswertung der δ^2H- und δ^{18}O-Daten ergaben, dass das Grundwasser nicht durch rezente meteorische Wässer beeinflusst ist, und ein Einfluss von Meerwasserintrusionen ausgeschlossen werden kann. Diese Ergebnisse bestätigen die Informationen der Pumpversuchsauswertung. In diesem Sinne zeigt diese Studie, dass die Auswertung von Pumpversuchen mittels der Zeit-Ableitung der Grundwasserabsenkung fundamentale Informationen über Randbedingungen und deren hydraulische Eigenschaften liefern kann, welche mit konventionellen geologischen bzw. geophysikalischen Untersuchungsmethoden nicht ohne Weiteres zugänglich sind.

Abstract

Groundwater flow and transport are strongly influenced by the heterogeneity of the subsurface, which complicates the estimation of subsurface flow parameters, such as transmissivity and storativity. The accurate definition of flow parameters is an essential step in any hydrogeological study. Accordingly, appraising the impact of aquifer heterogeneity on groundwater flow and the estimation of aquifer parameters became a key aspect of hydrogeologic research. Pumping tests are an established technique to estimate hydraulic aquifer parameters. Although aquifers are intrinsically heterogeneous, the interpretation of pumping tests is commonly performed under the assumption of aquifer homogeneity, by utilizing Theis' equation [*Theis*, 1935]. This yields interpreted hydraulic parameters whose relation to the underlying heterogeneity is uncertain.

The present thesis is therefore motivated by the requirement for an improved understanding on the interrelation between Theis-based interpreted hydraulic parameters and the true heterogeneity of aquifers. In this regard, it aims to optimize pumping test interpretation techniques which rely on Theis' equation for an application to heterogeneous systems. Various Theis-based interpretation techniques are considered, namely, the Cooper-Jacob method [*Cooper and Jacob*, 1946] and the Continuous-Derivation method [*Copty et al.*, 2011] for infinite aquifers, and, the Hantush method [*Hantush*, 1959] for pumping tests in the presence of an infinite linear constant head boundary (BCH). Furthermore, a new interpretation method is established by extending the Continuous-Derivation method for an application to BCH-domains. Whereas traditional interpretation methods like the Cooper-Jacob and the Hantush method just consider the late-time drawdown for the estimation of hydraulic parameters, the Continuous-Derivation method utilizes the entire time domain of the pumping test, by continuously evaluating the ratio of the drawdown and the drawdown derivative. Thus, the Continuous-Derivation method provides time-dependent hydraulic parameters.

To investigate the relation of Theis-based interpreted parameters to the underlying heterogeneity Fréchet kernels [*Knight and Kluitenberg*, 2005] are used. Fréchet kernels allow to examine the sensitivity of the drawdown to spatially distributed hydraulic parameters, and to estimate sub-domains to which the drawdown is most sensitive too. By utilizing the Fréchet kernel for transmissivity, two time-dependent spatial weighting functions are derived, which enable the estimation of upscaled transmissivity values from a given heterogeneous distribution. One uses the Fréchet kernel itself as spatial weight, providing an upscaled homogeneous transmissivity to substitute the true heterogeneous transmissivity distribution; the other uses the time derivative of the Fréchet kernel as spatial weight, providing an upscaled heterogeneous transmissivity field. The comparison of the upscaled transmissivities to the interpreted transmissivities from the above mentioned interpreta-

tion techniques reveals that the meaning of the interpreted transmissivity depends on the properties of the Theis' equation, used during the interpretation process. That is, if the interpreted transmissivity is estimated from the drawdown derivative, the resulting transmissivity relates to an upscaled heterogeneous transmissivity field. This relationship is valid for the interpreted transmissivity from the Cooper-Jacob method and the Continuous-Derivation method in infinite domains, as well as, for the interpreted transmissivity from the Continuous-Derivation method for BCH-domains, if the BCH does not affect the drawdown. On the contrary, at late pumping times in BCH-domains the drawdown derivative approaches zero, and, the interpreted transmissivity is directly related to the drawdown. As a result, the interpreted steady-state transmissivity in BCH-domains does not relate to an upscaled heterogeneous transmissivity field, but substitutes the true heterogeneous transmissivity distribution by a homogeneous transmissivity. In this regard, the late-time interpreted transmissivity from the Continuous-Derivation method for BCH-domains matches the interpreted steady-state transmissivity from Hantush's method.

By considering the transmissivity as log-normally distributed spatial random function and storativity to be uniform, the following information on aquifer heterogeneity can be potentially estimated from Theis-based pumping test interpretation techniques, with emphasis on the Continuous-Derivation method. For single-well pumping tests in infinite domains, the very early interpreted transmissivity matches the local transmissivity at the pumping well. At late pumping times, or, if the radius of the cone of depression exceeds 15 to 20 correlation lengths, respectively, the interpreted transmissivity approaches the geometric mean of the underlying transmissivity distribution. The interpreted storativity is understood as an indicator for flow connectivity, providing subsequent information on the heterogeneous transmissivity distribution. Thus, a small interpreted late-time storativity correlates with a small local transmissivity at the pumping well, and vice versa. Estimating the true storativity of the aquifer is only possible if the impact of heterogeneity on the interpreted transmissivity is negligible. Strictly speaking, only the very early interpreted storativity at the pumping well matches the true storativity of the aquifer.

Regarding interpreted hydraulic parameters from BCH-domains, early-time estimates contain the same information as in infinite domains, since the BCH does not affect the drawdown yet. Under steady-state conditions, the meaning of the interpreted transmissivity changes due to the influence of the BCH. Thus, the interpreted steady-state transmissivity does not generally allow to estimate the geometric mean of the transmissivity distribution. However, if the ratio of the distance between pumping well and BCH and the correlation length of the underlying transmissivity is larger than about 15 to 20, the geometric mean can be estimated from the transient interpreted transmissivity. In that case, the pumping test perturbs an aquifer volume considered representative for the entire aquifer. Under such conditions, even the interpreted steady-state transmissivity might be used to approx-

imate the geometric mean, if the observation well is sufficiently far from the pumping well and the BCH, respectively. The evaluation of the interpreted storativity in BCH-domains is complex. The numerical results show that even though the interpreted late-time storativity is less variable in BCH-domains, it includes information on flow connectivity in the vicinity of the pumping well and the BCH. In general, the numerical part of this thesis confirms that Theis-based hydraulic parameters include information on aquifer heterogeneity. Moreover, the established spatial weighting functions represent a tool to relate interpreted hydraulic parameter to the underlying heterogeneity, enhancing the information provided by Theis-based interpretation techniques.

The theoretical/numerical investigations are followed by an applied part, which evaluates real pumping tests in an aquifer system strongly affected by tectonics, at Saritepe Campus, Boğaziçi University, Istanbul. Pumping tests were accompanied by geological and hydrochemical investigations, which included the installation of two new wells drilled up to depths of 100 meters. The goal of investigations was to provide a conceptual hydrogeological model of the investigated groundwater reservoir to estimate the impact of the nearby Black Sea. By using the drawdown derivative for the identification of reservoir boundaries, pumping test interpretation revealed that the investigated groundwater reservoir is bounded by two impermeable faults, not showing a hydraulic connection to the sea. Furthermore, pumping test interpretation suggests that the investigated reservoir consists of two aquifers. The division of aquifers is supported by geological and hydrochemical findings. Accordingly, the investigated groundwater reservoir comprises two groundwater volumes of paleo-water, with the occurrence of brackish water being restricted to the deeper aquifer. However, an impact of seawater intrusion from the Black Sea can be excluded as hydrochemical results point to an origin of brackish water from water-rock interaction. These results basically confirm the pumping test interpretation model. In this regard, this study shows that pumping test interpretation which utilizes the time derivative for evaluation can provide fundamental information on reservoir boundaries and their hydrogeological properties, which are not easily accessible by conventional exploration methods.

Acknowledgements

The work of this thesis constitutes a collaboration of the Helmholtz-Centre for Environmental Research - UFZ and the Boğaziçi University, Istanbul to investigate effects of aquifer heterogeneity on pumping test interpretation. The author was supported by the following research fellowships: Research Fellowship of the Initiative and Networking Fund of the Helmholtz Association (IK-TR-14), Research Fellowship Program for Foreign Citizens (2216) of the Scientific and Technological Research Council of Turkey (TÜBITAK), UFZ-Fellowship of the Helmholtz-Centre for Environmental Research.

I would like to thank my advisor Prof. Dr. S. Attinger for the valuable scientific and financial support in the last years.

Special thanks to Prof. Dr. N. Copty for his guidance and the many, many discussions. His advises and amicable support helped me keeping track of my dissertation.

I'm thanking Dr. Ronald Krieg for his support during field campaigns, his administrative help and the memorable drives to Istanbul. I like to thank Prof. W. Gläßer for inspiring discussions during our geologic field trip, Prof. Dr. R. Merz, Prof. Dr. M. Martienssen and Prof. Dr. H. Weiss for their support in providing the field equipment. The support of Emre Otay and the staff at Saritepe Campus is largely appreciated.

For his scientific advise, support on funding and administrative help, special thanks to Dr. G. Strauch.

For a great time in Istanbul, support and kindness I would like to thank S. Sarioğlu, S. Kaptan and A. Cosentino.

Finally I'm thanking Edgar for his continuing support and patience. Without his help this thesis wouldn't have been possible. To my parents and my sister also a big "thank you" for their mental support during the last years.

List of Symbols and Abbreviations

Symbol	Unit	Quantity
β	[-]	ratio a_i/a
γ, γ_bch	[-]	Theis-based ratio $\frac{s}{\partial s/\partial \ln t}$, infinite and BCH-domain
ε	[-]	Euler-Mascheroni-constant
λ	[-]	ratio of L/l_Y
μ	[cp]	viscosity of fresh water
ϕ	[-]	porosity
σ^2_Y	[-]	variance of Y
∇		nabla operator
$\langle\,\rangle$		arithmetic ensemble mean
a, a_i	[m]	distance observation to pumping/imaginary well
B	[-]	formation factor
BCH		infinite linear constant head boundary
b	[m]	aquifer thickness
Corr	[-]	Pearson correlation coefficient
c_t	[bar^{-1}]	total compressibility
D	[m^{2}s^{-1}]	diffusivity defined as T_0/S_0
d	[m]	distance observation well to boundary
E_1		exponential integral or well-function
F_T		Fréchet kernel for transmissivity, infinite domain
F^B_T		Fréchet kernel for transmissivity, BCH-domain
F_S		Fréchet kernel for storativity
H	[m]	hydraulic head prior to pumping
h	[m]	hydraulic head
h_0	[m]	hydraulic head in homogeneous medium
IW		imaginary well
K	[ms^{-1}]	hydraulic conductivity
K_0, K_1		modified Bessel function of second kind of zero order, order one
K_ef	[ms^{-1}]	effective conductivity
K_efu	[ms^{-1}]	effective conductivity under uniform flow
K_G	[ms^{-1}]	geometric mean conductivity
k	[md]	permeability
L, L_1, L_2	[m]	distance boundary to pumping well

l_{Y}	[m]	correlation length of Y
ln		natural logarithm
log		logarithm to base 10
lu	[-]	length unit
m_{s}	[m]	slope of the late-time drawdown to $\log t$
m_{Ch}	[m]	slope drawdown to $\sqrt{t}$
m_{Y}	[-]	mean of ln-transmissivity
msl		mean sea level
NAFZ		North Anatolian Fault Zone
OW		observation well
PW		pumping well
q	[$\mathrm{m^3 s^{-1}}$]	pumping rate at the well
R_1 ... R_4	[m]	position vectors of an anomaly in T in BCH-domain
r, r_1, r_2	[m]	position vectors of an anomaly in T in infinite domain
r_{in}	[m]	interpreted radial distance
r_{w}	[m]	well radius
S	[-]	storativity
S_0	[-]	homogeneous storativity
S_{est}	[-]	indicator for flow connectivity, equal to $S_{\mathrm{in}}^{\mathrm{CJ}}$
S_{in}	[-]	interpreted storativity
$S_{\mathrm{in}}^{\mathrm{CD}}$	[-]	storativity from the Continuous-Derivation method
$S_{\mathrm{in}}^{\mathrm{CJ}}$	[-]	storativity from the Cooper-Jacob method
$S_{\mathrm{in}}^{\mathrm{Han}}$	[-]	storativity from the Hantush method
s	[m]	drawdown
s_0	[m]	drawdown in the homogeneous medium
s_{b}	[m]	build-up
s^{F}	[m]	drawdown in the F_{T}- or $F_{\mathrm{T}}^{\mathrm{B}}$-weighted domain
s^{RAD}	[m]	drawdown in the $\partial F_{\mathrm{T}}/\partial \ln t$- weighted domain
s_{m}	[m]	maximum drawdown
s_{p}	[m]	drawdown at the end of pumping period
T	[$\mathrm{m^2 s^{-1}}$]	transmissivity
$\tilde{T}$	[$\mathrm{m^2 s^{-1}}$]	transmissivity fluctuation from T_0
T_0	[$\mathrm{m^2 s^{-1}}$]	homogeneous transmissivity
T_{A}	[$\mathrm{m^2 s^{-1}}$]	arithmetic mean transmissivity
T_{G}	[$\mathrm{m^2 s^{-1}}$]	geometric mean transmissivity
T_{H}	[$\mathrm{m^2 s^{-1}}$]	harmonic mean transmissivity
T_{efu}	[$\mathrm{m^2 s^{-1}}$]	transmissivity under uniform flow

T_{eq}	$[\mathrm{m^2 s^{-1}}]$	equivalent transmissivity
$T_{\mathrm{eq}}^{\mathrm{F}}$, $T_{\mathrm{eq}}^{\mathrm{FB}}$	$[\mathrm{m^2 s^{-1}}]$	F_{T}- and $F_{\mathrm{T}}^{\mathrm{B}}$-weighted transmissivity
$T_{\mathrm{eq}}^{\mathrm{RAD}}$	$[\mathrm{m^2 s^{-1}}]$	spatially weighted transmissivity over $T_{\mathrm{in}}^{\mathrm{F}}(r_{\mathrm{in}})$
T_{in}	$[\mathrm{m^2 s^{-1}}]$	interpreted transmissivity
$T_{\mathrm{in}}^{\mathrm{CD}}$	$[\mathrm{m^2 s^{-1}}]$	transmissivity from Continuous-Derivation method
$T_{\mathrm{in}}^{\mathrm{CJ}}$	$[\mathrm{m^2 s^{-1}}]$	transmissivity from Cooper-Jacob method
$T_{\mathrm{in}}^{\mathrm{F}}$	$[\mathrm{m^2 s^{-1}}]$	$\partial F_{\mathrm{T}}/\partial \ln t$-weighted transmissivity
$T_{\mathrm{in}}^{\mathrm{Han}}$	$[\mathrm{m^2 s^{-1}}]$	transmissivity from Hantush method
T_{PW}	$[\mathrm{m^2 s^{-1}}]$	local transmissivity at the pumping well
t	[s]	time since pumping started
t'	[s]	time since pumping stopped, $t' = t - t_{\mathrm{p}}$
t_0	[s]	interception time, m_{s} intercepts $s = 0$
t_{a}	[s]	Agarwal time
t_{ip}	[s]	time at drawdown-inflection point in homogeneous BCH-domain
t_{p}	[s]	time when the pump is stopped
u	[-]	dimensionless time
u_{ip}	[-]	dimensionless time at drawdown-inflection point in homogeneous BCH-domain
u_γ	[-]	dimensionless time estimated from γ or γ_{bch}
$\mathbf{v}$	$[\mathrm{ms^{-1}}]$	Darcy velocity vector
W		spatial weighting function
$\mathbf{x}$, $\mathbf{x}'$	[m]	position vector of observation point, anomaly
Y		ln-transform of transmissivity

Contents

Chapter 1

Introduction

1.1 Motivation

Groundwater is a valuable natural resource that constitutes an important part of the drinking water supply worldwide. Due to global population growth the demand of this resource is under increasing pressure. Available drinking water resources are globally declining due to over-exploitation and pollution, which is aggravated by the requirements of agriculture and industry. An adapted and forward-looking management of water resources, including the preservation of subsurface water quality is therefore desperately needed.

Mathematical methods and numerical modeling have gained significant importance in hydrogeology, in particular for developing groundwater management strategies and remediation concepts. Establishing a numerical model for subsurface flow requires precise information on groundwater availability and renewability, as well as, a comprehensive characterization of the groundwater reservoir under investigation. This includes the estimation of reservoir delimiting boundary conditions, the reliable classification of aquifer units, and their hydraulic characterization by means of aquifer parameters, such as hydraulic conductivity, storativity and porosity. However, information on hydraulic aquifer properties is mostly scarce, as they are difficult to access. Moreover, groundwater flow and transport processes are dominated by the heterogeneity of the subsurface [e.g., *Sudicky*, 1986; *Dagan*, 1989], which complicates an adequate description of aquifer parameters. Accordingly, quantifying aquifer heterogeneity became a key interest of hydrological research. In this regard, the hydraulic conductivity was identified as one of the ruling aquifer parameters governing groundwater flow [e.g., *Gómez-Hernández and Gorelick*, 1989; *Butler et al.*, 1999].

A common and widely used technique to characterize aquifers is to perform a pumping test. That is, the drawdown induced by pumping a well is treated as system response of the perturbed aquifer system. The interpretation of the drawdown then allows to estimate

hydraulic properties of the investigated groundwater reservoir. Common pumping test interpretation methods rely on simplifying assumptions like aquifer homogeneity, namely by employing the Theis equation [*Theis*, 1935]. Consequently, Theis-based methods for pumping test interpretation do actually not consider the underlying aquifer to be heterogeneous. This can yield ambiguous estimates of hydraulic parameters and complicates appraising the impact of aquifer heterogeneity on groundwater flow. However, since Theis-based interpretation techniques are easy to apply, they are frequently used to estimate hydraulic aquifer parameters of heterogeneous systems.

In order to provide for a reliable characterization and quantification of aquifer heterogeneity, knowledge on how the underlying heterogeneity affects the drawdown at a well, and, on how pumping test interpretation methods render the drawdown signal is crucial. This applies in particular to Theis-based interpretation methods because they are widely-used. However, the understanding on the relation between aquifer heterogeneity and interpreted hydraulic parameters, obtained by applying Theis-based interpretation techniques to drawdown data from heterogeneous systems, is rather dissatisfying. Improving the understanding of this interrelation can enhance appraising aquifer heterogeneity at a particular site, and the understanding of governing processes of flow and transport in heterogeneous media in general.

Therefore, the study at hand is motivated by the requirement of an improved understanding and insight on how aquifer heterogeneity affects measurements of the hydraulic head during a pumping test, and accordingly, the estimation of hydraulic aquifer parameters. It explicitly focuses on what information on aquifer heterogeneity can be obtained by Theis-based interpretation techniques. In this regard, this work aims to close the existing gap between a more traditional approach of pumping test interpretation and recent advances, which are mostly mathematically challenging by considering pumping test analysis within a stochastic framework. Thus, the general objective is to improve the understanding of effects that may arise from aquifer heterogeneity on hydraulic measurements, as the need for a detailed characterization and quantification of aquifer heterogeneity is uncontroversial.

1.2 Outline

The following Chapter 2 outlines the principles of groundwater flow to wells and introduces common pumping test interpretation techniques. It gives a brief introduction on modeling aquifer heterogeneity in terms of a spatial random function within the framework of geostatistics. It further reviews established approaches to quantify aquifer heterogeneity, and summarizes the corresponding definitions of hydraulic aquifer parameters with particular emphasis on well flow. Concepts to investigate the sensitivity of the drawdown to aquifer

heterogeneity are introduced.

Theoretical and numerical investigations start with Chapter 3 by examining the meaning of Theis-based hydraulic parameters in infinite (unbounded) heterogeneous aquifers. For that purpose, the sensitivity of the drawdown to aquifer heterogeneity is investigated. By making use of Fréchet kernels a spatial relation between aquifer heterogeneity and Theis-based hydraulic parameters is established. It is demonstrated that even though common pumping test interpretation techniques rely on Theis' equation, corresponding estimates of hydraulic parameters include information on aquifer heterogeneity, in particular when evaluated from transient drawdown data.

In Chapter 4 the previously proposed procedure to investigate the sensitivity of the drawdown by means of Fréchet kernels is extended for an application to bounded heterogeneous aquifers in the presence of an infinite linear constant head boundary (BCH). Since Theis-based interpretation techniques for BCH-domains are commonly restricted to the evaluation of steady-state drawdown data, the sensitivity analysis focuses on this particular case. It is shown that, under steady-state conditions, the meaning of Theis-based hydraulic parameters in heterogeneous BCH-domains differs from the meaning of corresponding estimates in infinite domains.

Chapter 5 establishes a pumping test interpretation technique to evaluate transient drawdown data from BCH-domains, as results from Chapter 3 indicate that the interpretation of transient data can yield additional information on the underlying heterogeneity. Subsequently, estimated hydraulic parameters are related to the underlying heterogeneity by utilizing the previously established concept of Fréchet kernels for upscaling. Furthermore, synthetically generated pumping tests are used to illustrate limits and advantages of the proposed interpretation technique.

In Chapter 6 real world application of pumping test interpretation is demonstrated by means of hydrogeological investigations at Saritepe Campus, Boğaziçi University, Istanbul. A conceptual hydrogeological model for the site is established by considering geological and hydrochemical data. Unfortunately, the hydrogeologic situation at Saritepe Campus inhibited the application of the pumping test interpretation technique developed in Chapter 5. However, results emphasize the potential of an integrated approach of pumping test interpretation along with hydrochemical investigations for the characterization of complex groundwater reservoirs.

Finally, Chapter 7 summarizes findings and conclusions of previous chapters and puts them into a general context to answer the question on what information on aquifer heterogeneity can be obtained by applying Theis-based interpretation techniques to heterogeneous aquifers.

Chapter 2

Principles of Pumping Test Analysis in Confined Aquifers

2.1 Introduction

The interpretation of pumping tests is a common technique to characterize aquifers in terms of their hydraulic properties. Whereas early pumping test interpretation methods were limited to the estimation of well performance, the introduction of the drawdown derivative approach into pumping test analysis in the 1980's [e.g., *Bourdet et al.*, 1983, 1989] allowed to develop complex interpretation models that enabled hydrogeologists to identify detailed geologic features of the perturbed reservoir. A comprehensive summary on the evolution of well test analysis is given by *Gringarten* [2008].

Pumping analysis generally relies on the fact that groundwater flow can be described by equations, such as the groundwater flow equation. However, in order to derive a closed form solution for groundwater flow to a well, simplifying assumptions are needed, e.g., the assumption of aquifer homogeneity. Related equations and fundamental derivations, such as the Theis equation [*Theis*, 1935], are presented in Section 2.2. Section 2.3 then illustrates various pumping test interpretation techniques which rely on Theis' equation.

Nevertheless, natural aquifers are intrinsically heterogeneous. In this regard, the hydraulic conductivity is considered to be the parameter of major interest since it controls direction and magnitude of groundwater flow. The hydraulic conductivity is extremely variable, which in turn does not allow for a comprehensive deterministic description, nor to resolve its spatial distribution completely. In order to investigate effects of aquifer heterogeneity on estimated flow parameters, the hydraulic conductivity is modeled in terms of a stochastic spatial random function, as discussed in Section 2.4. Even though, such a stochastic approach can not account for geologic features like facies, it allows to quantify aquifer heterogeneity by means of the statistic properties of the spatial random function.

Therefore, modeling the hydraulic conductivity in a stochastic manner is herein used as a tool to investigate effects of aquifer heterogeneity on pumping test interpretation.

The general goal of pumping test analysis is to provide hydraulic parameters which characterize the investigated system with regard to a particular problem, e.g., to develop large-scale groundwater flow models, or, to investigate groundwater remediation problems on a local scale. Thus, finding hydraulic parameters which sufficiently describe aquifer heterogeneity also depends on the scale of the underlying problem. Moreover, estimated hydraulic parameters are known to depend on the prevailing flow regime. Consequently, estimated hydraulic parameters from pumping tests, i.e., from convergent groundwater flow to a well, are not necessarily a good description of hydraulic aquifer parameters when groundwater flow is uniform. Therefore, different concepts of upscaled hydraulic parameters are in use. A review on the issue of upscaling under uniform and convergent groundwater flow is given in Section 2.5.

Finally, Section 2.6 outlines recent advances to describe and quantify the sensitivity of the drawdown to aquifer heterogeneity. Hence, the concept of Fréchet kernels is introduced, which constitutes the basis for the numerical investigations in Chapters 3 to 5.

2.2 Principles of Groundwater Flow to Wells

This section deals with the basic principles of groundwater flow, stating related definitions and equations with emphasis on convergent groundwater flow to an extraction well. It is not aimed to give detailed derivations nor to discuss or expend the fundamentals of porous media theory. A detailed description of the theoretical background can be found for instance in *Bear* [1972], *Freeze and Cherry* [1979], *Kinzelbach and Rausch* [1995], *Fetter* [2000] and *Langguth and Voigt* [1980, 2004].

2.2.1 Aquifer as a Continuum

Aquifers consist of a solid aquifer matrix and voids in between, which are normally filled by gas or water. Therefore, aquifers are discontinuous on a microscopic scale with a particular point belonging to either matrix or void space. Within the framework of aquifer characterization by means of their hydraulic properties, a description of groundwater flow on a microscopic level is not feasible nor useful in most problems.

To bridge the gap between the discontinues microscopic scale and regarding the aquifer as a continuum, a representative elementary volume (REV) is defined. In hydrogeology the representative elementary volume is the smallest volume over which measurements can be made that yield a representative value for the domain under consideration. Thus, the representative elementary volume has to be sufficiently large for fluctuations on a micro-

scopic scale to be negligible, but it has to be small enough to be regarded as a point at the macroscopic scale. Accordingly, the actual aquifer medium is replaced by a fictitious continuum which allows for describing groundwater flow by means of partial differential equations [*Bear*, 1972]. Hydraulic aquifer parameters which are defined on the basis of the representative elementary volume, such as, porosity, storativity and hydraulic conductivity, or, transmissivity, respectively, are only valid above the scale of the representative elementary volume.

2.2.2 Theis' equation

Groundwater flow is mathematically described by means of partial differential equations which conserve basic properties such as mass, momentum and energy. The corresponding continuity equation is derived by applying the principle of mass conservation to the fluid, i.e., it describes the evolution of fluid flow in space and time by incorporating the capability of the aquifer to hold or release water.

The macroscopic mass balance equation of the fluid, averaged over a representative elementary volume, is given by

$$S(\mathbf{x})\frac{\partial h(\mathbf{x},t)}{\partial t} = -\nabla \mathbf{v}(\mathbf{x},t) + q(\mathbf{x}) \tag{2.1}$$

where $\mathbf{x}$ is the position vector in a Cartesian coordinate system, S is the storativity, h is the hydraulic head, t is time, $\mathbf{v}$ is the Darcy velocity vector, and, q a sink/source term of the fluid mass. The Darcy velocity is given by Darcy's law,

$$\mathbf{v}(\mathbf{x},t) = -K(\mathbf{x})\nabla h(\mathbf{x},t), \tag{2.2}$$

which relates changes in the hydraulic head to the hydraulic conductivity of the porous medium, K. Darcy's law thereby assumes that subsurface flow is laminar. Due to changes in pore size and geometry, flow through the pores of the aquifer is not generally linear. Thus, Darcy's law necessitates the assumption of a representative elementary volume and small water flow velocities, i.e., a small Reynolds number generally smaller than 10. Inserting (2.2) into (2.1), yields the time-dependent groundwater flow equation

$$S(\mathbf{x})\frac{\partial h(\mathbf{x},t)}{\partial t} - \nabla(K(\mathbf{x})\nabla h(\mathbf{x},t)) = q(\mathbf{x}). \tag{2.3}$$

In order to derive a closed form solution of (2.3) for convergent groundwater flow to an extraction well the following assumptions have to be made [*Kruseman et al.*, 1990]. 1) The aquifer is confined, i.e., a drop in the hydraulic head corresponds to an immediate release of water from storage. 2) The aquifer is infinite in areal extend, i.e., unbounded. 3) The aquifer is homogeneous, isotropic and of uniform thickness over the area influenced by pumping. 4) Prior to pumping, the piezometric surface is horizontal. 5) The aquifer is

pumped at a constant rate. 6) The well has an infinitesimal radius and is screened over the entire thickness of the aquifer, i.e., groundwater flow to the well is horizontal. Hence, convergent groundwater flow to a well can be described by

$$S\frac{\partial s}{\partial a} = T\left(\frac{\partial^2 s}{\partial a^2} + \frac{1}{a}\frac{\partial s}{\partial a}\right), \tag{2.4}$$

where s is the drawdown given by $s = H - h$, with H referring to the initial hydraulic head prior to pumping, a being the radial distance form the pumped well, and transmissivity $T = K \cdot b$, which b being the thickness of the aquifer.

In order to solve Equation (2.4) the following conditions are defined. The first condition

$$\frac{q}{2\pi T} = \lim_{a \to 0}\left(a\frac{\partial s}{\partial a}\right) \tag{2.5}$$

states that for all times $t \geq 0$, the well discharges at a constant rate q. Further conditions relate to the observed drawdown at particular locations, with

$$\begin{aligned} s(a, t = 0) &= 0 \\ s(a \to \infty, t) &= 0. \end{aligned} \tag{2.6}$$

Moreover, the drawdown $s(a, t)$ is related to the aquifer properties T and S by means of a dimensionless variable u, defined by *Theis* [1935]

$$u = \frac{a^2 S}{4Tt}. \tag{2.7}$$

Thus, $s(a, t)$ equals $s(u)$. Substituting $s(u)$ into (2.4) yields a ordinary differential equation of second order. By considering the above conditions, integration yields the Theis equation given by [*Theis*, 1935]

$$s(a, t) = \frac{q}{4\pi T}\int_u^\infty \frac{1}{u}\exp(-u)du = \frac{q}{4\pi T}E_1(u) \tag{2.8}$$

where $E_1(u)$ is the exponential integral function of u, also known as the well function.

2.3 Pumping Test Interpretation

Pumping test analysis, i.e., treating the observed drawdown induced by pumping as system response of the aquifer, is a common technique to estimate hydraulic properties of aquifers. Within the framework of signal theory, pumping a well at a specific rate constitutes the input signal to the system or the aquifer, respectively, whereas the resulting drawdown represents the output signal. If the input signal and aquifer properties are known, the output signal can be calculated without ambiguity, which is know as the direct problem or forward modeling. Alternatively, the input and the output signal are know, though the

aquifer properties are the unknown variable. This constitutes the inverse problem, which has an non-unique solution, i.e., several systems may exist which provide identical output signals [*Gringarten*, 2008].

The aim of analyzing a pumping test or drawdown data, respectively, is to find a sufficient and consistent characterization of the system perturbed by pumping. Thus, pumping test analysis usually consists of three steps. 1) Identification of the interpretation model of the perturbed system, which generally relates to solving the inverse problem by applying available interpretation techniques to estimate hydraulic aquifer parameters and to identify boundary conditions. 2) Calculation of the interpretation model parameters, which mainly comprises setting up a numerical model to solve the direct problem, to check and adjust estimated parameters. 3) Verification of the interpreted model and consistency checks. Most of the presented work relates to 1) and 2), i.e., to solving the inverse problem to identify aquifer parameters, and the ability of interpreted parameters to solve the direct problem.

2.3.1 Drawdown Derivative Approach for System Identification

Since the introduction of the drawdown derivative, pumping test analysis does not only allow for estimating hydraulic parameters, but is also used to investigate well conditions and system properties like reservoir boundaries. Characteristics of the drawdown derivative potentially allow to infer information on well-storage and skin [*Ehlig-Economides*, 1988; *Bourdet*, 2002], certain types of heterogeneity, and outer boundary conditions [*Bourdet et al.*, 1989; *Bourdet*, 2002; *Renard et al.*, 2009].

When utilized for system identification, it is common practice to evaluate the drawdown together with the drawdown derivative by means of diagnostic plots. The drawdown derivative is thereby defined as the derivative of s with respect to the natural logarithm of time, given by

$$\frac{\partial s}{\partial \ln t} = t\frac{\partial s}{\partial t}. \tag{2.9}$$

Figure 2.1 shows some examples of diagnostic plots. The typical characteristic of the drawdown derivative in infinite domains is its stabilization during late pumping times (Figure 2.1a), indicating radial infinite-acting flow. On the contrary, the drawdown derivative approaches zero for late pumping times if the investigated aquifer is delimited by a constant head boundary (Figure 2.1c). A medium of dual porosity shows a distinct valley in the drawdown derivative related to a change in hydraulic parameters (Figure 2.1b), which can hardly be identified by examining the drawdown. However, during late pumping times the drawdown derivative stabilizes at a constant value again, indicating radial infinite-acting flow. From Figure 2.1 it can be seen that the drawdown derivative is more sensitive to changes in aquifer properties, therefor enhancing the identification of prevail-

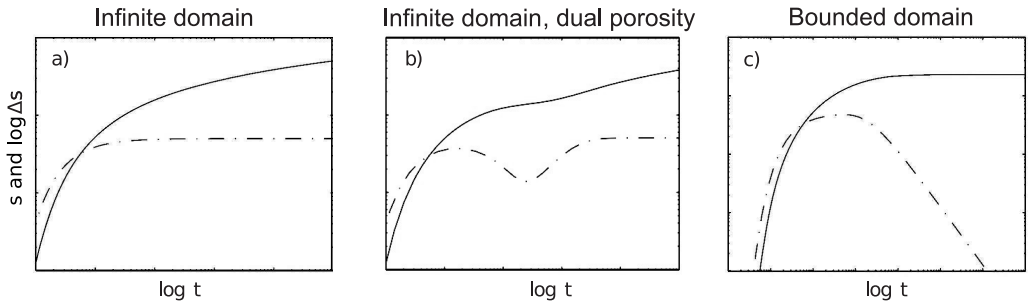

Figure 2.1: Diagnostic plots showing the drawdown s (solid) and the drawdown derivative (dashed) as a function of $\log t$ for a) an infinite domain, b) a medium of dual porosity, and c) for a domain bounded by an infinite linear constant head boundary.

ing flow regimes. There are several reviews available which illustrate the corresponding interpretation process, for instance, *Bourdet* [2002], *Gringarten* [2008], *Renard et al.* [2009].

The build-up, i.e., the recovery of the groundwater level after the pump is close at time t_p, can also be used for pumping test interpretation. For a shut-in after a single drawdown period, the corresponding derivative is commonly generated with respect to the equivalent Agarwal time [*Agarwal*, 1980]. Therefore, the build-up is defined by

$$s_\mathrm{b} = s_\mathrm{p} - s, \tag{2.10}$$

with s_p referring to the drawdown at time t_p, and s to the residual drawdown at t. By considering the Agarwal time, given by $t_\mathrm{a} = t_\mathrm{p}t'/(t_\mathrm{p} + t')$, with t' being the time since pumping stopped, i.e., $t' = t - t_\mathrm{p}$, the derivative of the build-up is given by [*Bourdet et al.*, 1989]

$$\frac{\partial s_\mathrm{b}}{\partial \ln t_\mathrm{a}} = \frac{t_\mathrm{p} + t'}{t_\mathrm{p}} t' \frac{\partial s_\mathrm{b}}{\partial t}. \tag{2.11}$$

Note that the build-up derivative matches type curves of the drawdown derivative when plotted against t'. However, distortions can be introduced when the flow regime deviates from radial infinite acting flow [*Bourdet*, 2002].

Besides the characterization of aquifers, the drawdown derivative has also been utilized by *Walker and Roberts* [2003] and *Beauheim et al.* [2004] to investigate dimensions of groundwater flow for constant rate pumping tests in domains with a Euclidean dimension of two. Their results reveal that aquifer heterogeneity is affecting flow dimensions, in particular during transient conditions.

2.3.2 Theis-based Interpretation Techniques

This section outlines Theis-based pumping test interpretation techniques by focusing on infinite domains, and domains delimited by an infinite linear constant head boundary (BCH). For the estimation of hydraulic parameters from pumping tests in infinite domains

the Cooper-Jacob method [*Cooper and Jacob*, 1946] and the Continuous-Derivation method [*Copty et al.*, 2011] are introduced. With regard to bounded domains the Hantush method [*Hantush*, 1959] is considered. However, there is a variety of Theis-based interpretation methods available. Comprehensive summaries are provided by, e.g., *Kruseman et al.* [1990] and *Langguth and Voigt* [2004].

Cooper-Jacob Method for Infinite Aquifer

For late pumping times, the cone of depression is considered to reach quasi steady-state conditions. As $t \to \infty$, u in Theis' equation (2.8) approaches 0. For small values of u, the exponential integral function is given by $E_1(u) = -\ln(u) - \varepsilon$, where $\varepsilon = 0.57721...$ is the Euler-Mascheroni-constant [*Abramowitz and Stegun*, 1964]. By using this property of $E_1(u)$, (2.8) reduces to

$$s = \frac{q}{4\pi T}(-\varepsilon - \ln u) \quad \text{as} \quad t \to \infty. \tag{2.12}$$

Equation (2.12) states the basis for several pumping test interpretation methods. The most common one, the Cooper-Jacob method [*Cooper and Jacob*, 1946], uses the transient drawdown, which is plotted as a function of $\log t$ to obtain estimates of transmissivity T and storativity S. T and S are then given by

$$\begin{aligned} T_{\text{in}}^{\text{CJ}} &= 0.183\frac{q}{m_{\text{s}}} \\ S_{\text{in}}^{\text{CJ}} &= \frac{2.25\, T_{\text{in}}^{\text{CJ}}\, t_0}{a^2} \end{aligned} \tag{2.13}$$

where m_{s} is the slope of the late-time drawdown with respect to $\log t$ and t_0 is obtained from the time at which the projection line of m_{s} intercepts the zero-drawdown axis. Both variables are commonly determined graphically. The subscript $_{\text{in}}$ indicates that corresponding estimates of T and S are obtained by applying an interpretation method; $^{\text{CJ}}$ indicates the application of the Cooper-Jacob method. *Cooper and Jacob* [1946] proofed that the above equations are valid if $u \leq 0.02$.

Continuous-Derivation Method for Infinite Aquifers

The Continuous-Derivation method, recently published by *Copty et al.* [2011], makes use of the drawdown derivative to infer estimates of transmissivity and storativity, $T_{\text{in}}^{\text{CD}}$ and $S_{\text{in}}^{\text{CD}}$. It evaluates the drawdown derivative over the entire time-domain of the pumping test, and is therefore not restricted to the evaluation of late-time drawdown data.

Starting from the Theis equation (2.8), the derivative of the drawdown s with respect to the natural logarithm of t is given by

$$\frac{\partial s}{\partial \ln t} = \frac{q}{4\pi T}\exp(-u). \tag{2.14}$$

Taking the ratio of s and $\frac{\partial s}{\partial \ln t}$ yields

$$\gamma = \frac{s}{\partial s / \partial \ln t} = E_1(u)\exp(u). \tag{2.15}$$

Accordingly, values of γ can be computed from the ratio $\frac{s}{\partial s/\partial \ln t}$, which in turn allows for estimating a value for u, denoted u_γ. Subsequently, $T_{\text{in}}^{\text{CD}}$ and $S_{\text{in}}^{\text{CD}}$ can be computed from the Theis equation and the estimated u_γ by

$$\begin{aligned} T_{\text{in}}^{\text{CD}}(t) &= \frac{q}{4\pi s(t)} E_1(u_\gamma) \\ S_{\text{in}}^{\text{CD}}(t) &= \frac{4 t u_\gamma T_{\text{in}}^{\text{CD}}}{a^2}. \end{aligned} \tag{2.16}$$

By making use of Fréchet kernels *Copty et al.* [2011] found that time-dependent estimates of $T_{\text{in}}^{\text{CD}}(t)$ can be converted into distance-dependent estimates by

$$r_{\text{in}} = \sqrt{\frac{4t\ T_{\text{in}}^{\text{CD}}}{1.6505\ S}}. \tag{2.17}$$

By applying the Continuous-Derivation method to synthetically generate pumping tests from aquifers heterogeneous in T and uniform in S, *Copty et al.* [2011] found that $T_{\text{in}}^{\text{CD}}$ includes some information about the underlying heterogeneity, namely, $T_{\text{in}}^{\text{CD}}(r_{\text{in}})$ is in good agreement with the spatial geometric mean over the underlying transmissivity distribution.

Hantush Method for Bounded Aquifers

Starting from the Theis equation (2.8) and utilizing the principle of superposition [e.g., *Ferris et al.*, 1962; *Bear*, 1972; *Kruseman et al.*, 1990], the drawdown in a domain unilaterally delimited by an infinite linear constant head boundary (BCH), is given by

$$s(t) = \frac{q}{4\pi T}[E_1(u) - E_1(\beta^2 u)], \tag{2.18}$$

where the ratio $\beta = a_i/a$ derives from applying the principle of superposition with a_i referring to the distance between the observation well and the imaginary recharging well. The underlying geometry for a Cartesian coordinate system with the BCH aligned to the y-axis, and the pumping well located at a distance L from the BCH, is given in Figure 2.2.

By letting t approach infinity, (2.18) reduces to $s_{\text{m}} = \frac{q}{2\pi T}\ln\beta$, where s_{m} is the steady-state drawdown. The interpreted Hantush transmissivity is then given by [*Hantush*, 1959]

$$T_{\text{in}}^{\text{Han}} = \frac{q}{2\pi s_{\text{m}}}\ln\beta. \tag{2.19}$$

Regarding the estimation of S, the Hantush method uses an inflection point which occurs as the BCH affects the drawdown at a particular observation. At the inflection point, the drawdown is given by

$$s = \frac{q}{4\pi T_{\text{in}}^{\text{Han}}}[E_1(u_{\text{ip}}) - E_1(\beta^2 u_{\text{ip}})] \tag{2.20}$$

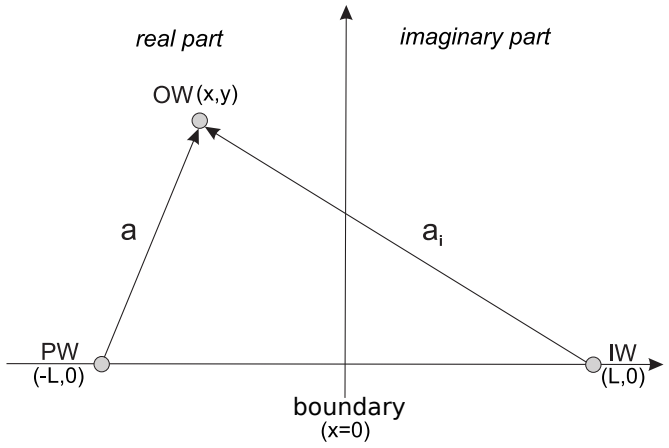

Figure 2.2: Geometry underlying Equation (2.18) to estimate the drawdown at an observation well (OW) in a BCH-domain. The pumping well (PW) is located at (-L,0) and the imaginary recharging well (IW) at (L,0), with L being the shortest distance between the PW and the boundary.

with $u_{\mathrm{ip}} = 2\ln\beta/(\beta^2-1)$. The interpreted storativity is then given by [*Hantush*, 1959]

$$S_{\mathrm{in}}^{\mathrm{Han}} = \frac{4t_{\mathrm{ip}}\,T_{\mathrm{in}}^{\mathrm{Han}}\,u_{\mathrm{ip}}}{a^2} \tag{2.21}$$

with t_{ip} being the time at which the inflection point of the drawdown is observed, commonly determined graphically.

Besides estimating T and S, the Hantush method also allows for the estimation of β and consequently L [e.g, *Hantush*, 1959; *Kruseman et al.*, 1990]. It therefor uses the slope of the drawdown at the inflection point. *Chapuis* [1994] investigate the performance of this inflection-point method and found that its accuracy decreases if $\beta < 20$, proposing a correction for the estimation of L.

2.4 Geostatistics in Hydrogeology

During their geologic evolution aquifers experience physical and chemical processes, such as, deposition, diagenesis, deformation and mineral precipitation under changing environments. As a result, aquifers are intrinsically heterogeneous in their hydraulic properties beyond the representative elementary volume. Field studies indicate that the hydraulic conductivity can vary by orders of magnitude over short distances of the order of meters [*Sudicky*, 1986; *Gelhar*, 1993]. Consequently, aquifer heterogeneity can not be fully described nor resolved by a deterministic approach, e.g., by sampling point measurements. Moreover, an description of aquifer heterogeneity also depends on the considered scale [*Dagan*, 1986; *Dagan et al.*, 2009]. On a local scale the aquifer might be considered heterogeneous, whereas the local scale is regarded as homogeneous when investigating aquifer systems on a regional scale.

In order to account for the impact of aquifer heterogeneity on groundwater flow, the theory of geostatistics has been developed since the 1960's [*Warren and Price*, 1961]. It attempts to find statistical characterizations to capture patterns of spatial variability, to

recognize and quantify the impact of aquifer heterogeneity on groundwater. A detailed discussion on multiple geostatistical aspects is given by, e.g., *Dagan* [1989]; *Gelhar* [1993] or *Rubin* [2003].

Within the framework of geostatistics, a spatially distributed quantity can be expressed in terms of a spatial random function, i.e., in terms of a spatially dependent random variable which exhibits a stochastic spatial structure. The random variable $Y(\mathbf{x})$ is then characterized by its statistical moments, the expected value or arithmetic mean, the variance, the auto-covariance and the semivariogram.

2.4.1 Transmissivity as Spatial Random Function

From the analysis of a large number of field data in different geological formations several studies, e.g., *Freeze* [1975], *Hoeksema and Kitanidis* [1985], *Gelhar* [1993], concluded that the hydraulic conductivity or the transmissivity, respectively, can be considered as log-normally distributed spatial random function, as one among other possibilities. That is, $Y(\mathbf{x}) = \ln T(\mathbf{x})$ is normally distributed with a Gaussian probability density function $\mathrm{pdf}_\mathrm{Y}(x) = \frac{1}{\sqrt{2\pi\sigma_\mathrm{Y}^2}} \exp\left(-\frac{(x-m_\mathrm{Y})^2}{2\sigma_\mathrm{Y}^2}\right)$, with m_Y and σ_Y^2 being the mean and the variance of Y, respectively. The probability density function of $T(\mathbf{x})$ is given by

$$\mathrm{pdf}_\mathrm{T}(x) = \frac{1}{x\sqrt{2\pi\sigma_\mathrm{Y}^2}} \exp\left[-\frac{(\ln x - m_\mathrm{Y})^2}{2\sigma_\mathrm{Y}^2}\right]. \tag{2.22}$$

Statistic characteristics, like the first moment T_A, the geometric and harmonic mean T_G and T_H, or the second moment σ_T^2 can then be calculated by

$$\begin{aligned} T_\mathrm{G} &= \exp(m_\mathrm{Y}), \\ T_\mathrm{A} &= \exp\left(m_\mathrm{Y} + \sigma_\mathrm{Y}^2/2\right), \\ T_\mathrm{H} &= \exp\left(m_\mathrm{Y} - \sigma_\mathrm{Y}^2/2\right), \\ \sigma_\mathrm{T}^2 &= \exp\left(2m_\mathrm{Y} + \sigma_\mathrm{Y}^2\right)\left[\exp(\sigma_\mathrm{Y}^2) - 1\right]. \end{aligned} \tag{2.23}$$

In practice, finding an appropriate model for $T(\mathbf{x})$ can be difficult. Commonly, spatially distributed measurements are log-transformed and interpreted to gain an experimental semi-variogram, or a covariance function, respectively. The data is then fitted to covariance models, e.g, exponential, Gaussian and spherical models, at which different models might lead to equivalent good results. Nevertheless, *Riva and Willmann* [2009] showed that mean values of quantities like transmissivity are not considerably impacted by the choice of the variogram type.

Besides treating heterogeneity as log-normally distributed spatial random function, several other techniques to describe aquifer heterogeneity are available, e.g., a multiple-point statistics approach, as discussed by *Renard* [2007]. To hydrogeologists, such an

approach might be more appealing since it also accounts for facies properties. However, from a practical point of view, the main advantage of geostatistics is their ability to quantify the uncertainty inherent to any geological study [*Winter*, 2004].

Modeling transmissivity as a log-normally distributed spatial random function is herein used as a tool to numerically investigate upscaling techniques in heterogeneous aquifers under convergent flow conditions. Thus, $Y = \ln T$ is considered as stationary multivariate Gaussian spatial random function with a Gaussian auto-covariance function referring to a finite correlation structure, expressed by the correlation length l_{Y}. The medium is assumed to be isotropic with equal l_{Y} in every direction. Transmissivity fields, with $m_{\mathrm{Y}} = 0$ and various values for σ^2_{Y} and l_{Y} were generated by using the Turning Bands method [*Mantoglou and Wilson*, 1982].

2.4.2 Quantifying Hydraulic Parameters in Stochastic Hydrogeology

Investigating flow in heterogeneous media can be achieved analytically or numerically. The analytic approach aims to find explicit expressions, which describe groundwater flow in a stochastic framework by solving the corresponding stochastic partial differential equations. Whereas, the numerical approach utilizes Monte Carlo simulations over an ensemble of synthetically generated heterogeneous realizations to provide numerical solutions. In this regard, an ensemble is understood as a collection of all realizations of a particular spatial random function, or a large number of realizations, respectively. Within the framework of this thesis the Monte Carlo approach is used.

The Monte Carlo approach is conceptually simple and needs no particular assumptions, allowing to investigate complex scenarios which are not accessible to analytic methods. The main steps of such a procedure are: 1) assuming a probability distribution of the input random variable, 2) generating an ensemble of realizations synthetically, 3) solving the groundwater flow equation with appropriate boundary conditions for every realization, 4) computing the statistics of the model output variables. Disadvantages of this approach are, that huge ensembles might be necessary, which can be time-consuming and computer resource demanding.

2.5 Upscaling

Considering aquifer parameters as heterogeneous quantities, e.g., in terms of a spatial random function, raises questions on how aquifer heterogeneity can be quantified. In this regard, upscaling basically aims to connect scales to find representative estimates which are capable of reproducing some average behavior of the heterogeneous system, though still accounting for aquifer heterogeneity by reducing the system complexity. Determin-

ing upscaled parameters for a certain problem can be quite challenging, in particular for complex flow regimes like convergent well flow. Two main concepts to estimate upscaled hydraulic parameters have evolved in literature, namely, effective parameters and equivalent parameters, which will be briefly summarized in the following. A detailed discussion on this problem is given by *Sanchez-Vila et al.* [2006].

The effective hydraulic conductivity K_{ef}, satisfies Darcy's law by

$$\langle \mathbf{v}(\mathbf{x}) \rangle = -K_{\mathrm{ef}} \langle \nabla h(\mathbf{x}) \rangle \tag{2.24}$$

where angle brackets indicate ensemble averaged quantities in the probability space. That is, averaging all the possible head and specific discharge fields that could be obtained with an ensemble of hydraulic conductivity fields. K_{ef} is a characteristic property of the medium, valid throughout the entire domain. However, the presence of boundaries or sink/sources causes K_{ef} to become variable in space. Due to its spatial dependence it is then often referred to as apparent or pseudo-effective conductivity since it is not a unique value, but relates to the prevailing flow regime.

The equivalent conductivity K_{eq}, satisfies Darcy's law by

$$\overline{\mathbf{v}(\mathbf{x})} = -K_{\mathrm{eq}} \overline{\nabla h(\mathbf{x})} \tag{2.25}$$

with the over bar referring to an average in the spatial or volumetric sense, respectively. That is, $\bar{\mathbf{v}} = V^{-1} \int_V \mathbf{v} \, \mathrm{d}V$, and, $\overline{\nabla h} = V^{-1} \int_V \nabla h \, \mathrm{d}V$. Thus, K_{eq} is a spatial average which refers to a single realization only. Equivalent parameters are associated with a particular geometry or boundary conditions, and can thus be defined for non-uniform flow conditions. They are not an intrinsic property of the heterogeneous aquifer medium, though spatially dependent and time-dependent. In case of ergodicity, ensemble averages can be replaced by spatial averages, i.e., the effective and equivalent conductivity are identical, $K_{\mathrm{ef}} = \langle K_{\mathrm{eq}} \rangle$ [*Sanchez-Vila and Tartakovsky*, 2007].

Furthermore, several studies point to the fact that as the cone of depression expands with continuous pumping, a pumping test also performs some upscaling over the heterogeneous aquifer, e.g., *Schad and Teutsch* [1994], *Copty and Findikakis* [2004], *Leven and Dietrich* [2006] and *Copty et al.* [2011]. Consequently, interpreted hydraulic parameters estimated by some pumping test interpretation method may also be regarded as upscaled parameters. However, how interpreted parameters relate to the underlying heterogeneity, or, to effective and equivalent parameters, respectively, is not clear. This is also pointed out in a recent review on representative hydraulic parameters in saturated groundwater flow by *Sanchez-Vila et al.* [2006] who emphasize the need for *"(1) further insights on when and under what conditions (pseudo-) effective, equivalent, and interpreted parameters are interchangeable; and, (2) an analysis of the relationship between representative hydraulic parameters and connectivity."*

2.5.1 Uniform Flow Conditions

Uniform groundwater flow in stationary isotropic log-normally distributed heterogeneous media is one of the particular cases where the effective conductivity is spatially independent, representing an intrinsic property of the medium, valid throughout the entire domain. Therefore, K_{ef} under uniform groundwater flow is often the desired value for modeling purposes and application, which is why it's explicitly denoted K_{efu}. K_{efu} is a characteristic property of the aquifer, given by $K_{\mathrm{efu}} = K_{\mathrm{G}} \exp\left(\sigma_{\mathrm{Y}}^2 \left(\frac{1}{2} - \frac{1}{n}\right)\right)$, with n being the dimension of the considered flow field [*Sanchez-Vila et al.*, 2006]. Accordingly, the effective transmissivity for uniform flow in two dimensions with $n = 2$, is given by $T_{\mathrm{efu}} = T_{\mathrm{G}}$.

2.5.2 Convergent Flow Conditions

Pumping groundwater from a well imposes a hydraulic gradient in direction to the pumped well, causing a convergent flow regime. If the aquifer is infinite, flow to the pumped well is radially convergent, if the aquifer is bounded the flow regime remains convergent but not necessarily symmetric. Due to convergent flow conditions K_{ef} or T_{ef}, respectively, become spatially dependent, not generally matching the effective value under uniform flow. During the last decades a lot of work has been dedicated to find expressions for upscaled hydraulic parameters under convergent flow, e.g., *Dagan* [1989], *Gómez-Hernández and Gorelick* [1989], *Ababou and Wood* [1990], *Desbarats* [1992], *Neuman and Orr* [1993], *Indelman and Abramovich* [1994], *Indelman et al.* [1996], *Sanchez-Vila* [1997], *Fiori et al.* [1998], *Riva et al.* [2001], *Dagan and Lessoff* [2007b,a], *Schneider and Attinger* [2008]. In the following, corresponding results are reviewed briefly by focusing on the effective and equivalent transmissivity .

Under radially convergent flow T_{ef} is a function of the radial distance from the pumped well. An analytic solution for T_{ef} under quasi steady-state conditions in an infinite domain was presented by *Sanchez-Vila* [1997]. He showed that T_{ef} increases monotonically from T_{H} at the pumped well to T_{G} within about two correlation scales, which is in agreement with previous studies by *Dagan* [1989] and *Indelman and Abramovich* [1994]. At the pumped well, the (pseudo-) effective hydraulic conductivity is dependent on the imposed boundary condition at the well. For a constant head boundary condition the effective hydraulic conductivity is the arithmetic mean, whereas when imposing a constant flux boundary condition it is the harmonic mean [e.g., *Dagan*, 1989; *Indelman et al.*, 1996]. In the far field T_{ef} approaches the geometric mean $T_{\mathrm{G}} = T_{\mathrm{efu}}$, and is independent of the boundary condition imposed at the pumped well.

The equivalent transmissivity is defined in physical space, with T_{eq} referring to a particular realization of the spatial random function. T_{eq} is commonly understood as a homogeneous substitute for the true heterogeneous distribution of a block that would pass the

same flux under the same pressure drop and maintained boundary conditions. *Desbarats* [1992] used an empirical approach to estimate T_{eq} under quasi steady-state conditions by weighting point transmissivities by a factor of $1/r^2$, which was subsequently validated analytically by *Sanchez-Vila et al.* [1999a]. *Dagan and Lessoff* [2007b,a] used an analytical approach to investigate conditional and unconditional statistics of T_{eq}. For the unconditional case they found $T_{\mathrm{eq}} \approx T_{\mathrm{H}}$; for the conditional case T_{eq} is practically deterministic and equal to the local transmissivity at the pumped well. *Schneider and Attinger* [2008] propose a more rigorous approach for spatial averaging by making use of the upscaling procedure Coarse Graining, which was introduced for uniform flow by *Attinger* [2003]. The fundamental idea is to perform a spatial filtering on the groundwater flow equation, which accounts for the non-uniform character of a pumping test. In other words, in the vicinity of the pumped well nearly no filtering is applied, whereas far from the well the filter volume is large. The resulting coarse grained transmissivity T^{CG} is equal to T_{H} at the pumped well, and approaches $T_{\mathrm{G}} = T_{\mathrm{efu}}$ within about 10 correlation scales, conditioning a Gaussian correlation structure. Numerical simulations showed that the ensemble averaged drawdown is reproduced very well by making use of T^{CG}.

Investigating equivalent and effective parameters under convergent flow in bounded domains is a quite recent field of research. *Riva et al.* [2001] derived an analytic expression for T_{ef} in a radial domain with centered pumping well, surrounded by a constant head boundary. They found T_{ef} to be equal to T_{H} in the vicinity of the pumped well. At intermediate radial distances T_{ef} tends towards T_{G}, peaks above T_{G}, and then declines as one approaches the external boundary. At the boundary, T_{ef} remains somewhat larger than T_{G}. If $\sigma_{\mathrm{Y}}^2 < 1$ this outer boundary effect is mild, becoming more pronounced with increasing variance of the spatial random function. The equivalent transmissivity T_{eq}, increases from T_{H} to T_{A} as the ratio L/l_{Y} increases from 0 to ∞, with L being the distance between the boundary and the pumped well. To the knowledge of the author, upscaled parameters for convergent flow in the presence of an infinite linear constant head boundary have not been considered in the literature yet.

2.6 Sensitivity Analysis in Heterogeneous Aquifers

A common approach to investigate the sensitivity of the drawdown to heterogeneous distributions are sensitivity coefficients. In general, sensitivity coefficients can be understood as a measure for a deviation in a parameter distribution and its effect on an observation. Within the framework of pumping tests, sensitivity coefficient directly relate a change in a hydraulic parameter to a change in the observed drawdown or hydraulic head, respectively. In this regard, deviations in T are generally considered uniform in a sub-domain i. The deviation in T then causes a deviation in the drawdown, when compared to the drawdown

from a corresponding homogeneous domain. The sensitivity coefficient is therefore defined by $I_\mathrm{i} = \partial s/\partial T_\mathrm{i}$ where i relates to a particular sub-domain. There are various methods available to calculate sensitivity coefficients [e.g., *Sun and Yeh*, 1985; *Yeh*, 1986; *Dietrich et al.*, 2005], which generally have to be evaluated numerically and are therefore computer resource demanding and time consuming.

A more general approach is to assume a non-uniform spatial distribution of hydraulic parameters where changes in T differ slightly from a uniform mean value, and to use a perturbation expansion to find the resultant small change in the measured output. Accordingly, the transmissivity is expressed as sum of a uniform mean T_0, and a fluctuations term $\tilde{T}$,

$$T(\mathbf{x}') = T_0 + \tilde{T}(\mathbf{x}') \tag{2.26}$$

with $\mathbf{x}' = (x, y)$ being the position vector of a particular anomaly in two dimensions. Similarly, the heterogeneous storativity can be written as a summation of S_0 and a fluctuations $\tilde{S}$.

Since an exact analytic solution of the hydraulic head for an arbitrary heterogeneous transmissivity distribution as defined above can not be found, the head is expanded by

$$h(\mathbf{x}, t) = h_0(\mathbf{x}, t) + h_1(\mathbf{x}, t) + h_2(\mathbf{x}, t) + \dots , \tag{2.27}$$

where $h_0(\mathbf{x}, t)$ is the hydraulic head at an observation point $\mathbf{x}$ in the homogeneous aquifer, characterized by T_0 and S_0. The other terms $h_\mathrm{j}(\mathbf{x}, t)$ for $j = 1, \dots$ are solutions of stochastic partial differential equations that describe deviations from the homogeneous solution. The first-order term of (2.27) is given by the Fréchet derivative [*Knight and Kluitenberg*, 2005]

$$h_1(\mathbf{x}, t) = -\int F_\mathrm{T}(\mathbf{x}, \mathbf{x}', t)\tilde{T}(\mathbf{x}')\, d\mathbf{x}' - \int F_\mathrm{S}(\mathbf{x}, \mathbf{x}', t)\tilde{S}(\mathbf{x}')\, d\mathbf{x}', \tag{2.28}$$

with F_S and F_T being the Fréchet kernels for storativity and transmissivity, respectively. By neglecting higher perturbation terms, inserting (2.28) in (2.27) yields

$$h(\mathbf{x}, t) = h_0(\mathbf{x}, t) - \int F_\mathrm{T}(\mathbf{x}, \mathbf{x}', t)\tilde{T}(\mathbf{x}')\, d\mathbf{x}' - \int F_\mathrm{S}(\mathbf{x}, \mathbf{x}', t)\tilde{S}(\mathbf{x}')\, d\mathbf{x}'. \tag{2.29}$$

Accordingly, the small change in the output signal is calculated using spatial convolution integrals known as Fréchet kernels, and the non-uniform spatial distributions of the hydraulic parameters.

Oliver [1990, 1993] derived the Fréchet kernels as convolution integrals, though they had to be evaluated numerically. Quite recently, *Knight and Kluitenberg* [2005] found explicit analytic expressions for the Fréchet kernels for transmissivity and storativity. They showed that the total sensitivity functions for uniform variations in the hydraulic parameters are the spatial integrals of the Fréchet kernels. In this regard, Fréchet kernels generalize

sensitivity coefficients for a dependence of $h(\mathbf{x}, t)$ on uniform changes in hydraulic parameters with one degree of freedom, to a spatial weighting which describes the dependence of $h(\mathbf{x}, t)$ on a non-uniform distribution with an infinite number of degrees of freedom.

Please note that since (2.27) is truncated after the first perturbation term, (2.29) constitutes an approximation of $h(\mathbf{x}, t)$. In other words, (2.29) assumes that the pumping well emits a hydraulic pressure signal, which is scattered by anomalies in the hydraulic parameters only once, neglecting second order scattering of the emitted signal.

Chapter 3

Estimating Transmissivity from Single-Well Pumping Tests in Infinite Heterogeneous Aquifers

3.1 Introduction

Subsurface formations are naturally heterogeneous with complex patterns of spatial variability. Determining subsurface flow parameters, such as transmissivity T, and storativity S, and appraising the impact of heterogeneity on groundwater flow and transport is an essential step in hydrogeological studies, and, in building groundwater flow models, in particular.

The interpretation of pumping tests, i.e. treating the drawdown induced by a pumped well as system response of the aquifer, is a common technique to estimate aquifer flow parameters. Conventional pumping test interpretation techniques generally rely on the Theis equation [*Theis*, 1935] which combines Darcy's law with the continuity equation by assuming the aquifer to be homogeneous (Section 2.2.2). Thus, the validity of Theis' equation is in principle limited to homogeneous aquifers. Nonetheless, since they are easy to apply, Theis-based interpretation techniques are widely used for parameter estimation in heterogeneous systems.

Cardwell and Parsons [1945] and *Matheron* [1967] already stated that a single representative value for the transmissivity does not exist if the aquifer is heterogeneous. Since then, finding representative descriptions of the hydraulic conductivity under convergent flow to a well has been the focus of numerous studies. Some of them utilize a stochastic approach to estimate the effective transmissivity or the effective hydraulic conductivity, respectively, defined as an average over an ensemble of realizations [e.g., *Neuman and Orr*, 1993; *Indelman et al.*, 1996; *Sanchez-Vila*, 1997; *Fiori et al.*, 1998; *Neuman et al.*, 2004; *Wu*

et al., 2005]. Another approach uses spatial averages of a single realization to estimate the equivalent transmissivity T_{eq} [e.g., *Desbarats*, 1992; *Sanchez-Vila et al.*, 1999a; *Dagan and Lessoff*, 2007a,b; *Schneider and Attinger*, 2008] to quantify aquifer heterogeneity. The equivalent transmissivity is thereby commonly regarded as homogeneous representation of a heterogeneous transmissivity distribution. A detailed review on the representative description of aquifer heterogeneity is given by *Sanchez-Vila et al.* [2006].

Neither the equivalent transmissivity T_{eq} nor the effective transmissivity fully match the interpreted transmissivity T_{in}, estimated from the transient drawdown by means of Theis-based interpretation techniques. However, the above studies reveal that for observations at the pumped well, T_{eq} is strongly dependent on the local transmissivity at the well. By considering an ensemble of T-realizations, and T as log-normally distributed spatial random function [*Gelhar*, 1993], the corresponding pseudo-effective transmissivity at the pumped well is given by the harmonic mean of transmissivity T_{H}. In the far field, the representative transmissivity approaches the asymptotic value of the effective transmissivity under uniform groundwater flow T_{efu}, equal to the geometric mean of transmissivity T_{G}. The transition between T_{H} and T_{G} is governed by the correlation length or the integral scale l_{Y}. Thus, the steady-state drawdown at an observation well far from the pumping well can potentially be used to infer T_{efu}. However, the drawdown at such distances of about 20 l_{Y} or more, might in practice be noisy and difficult to determine. A more rigorous approach to estimate statistical parameters of the spatial random function is proposed by *Schneider and Attinger* [2008]. Their extended Thiem-solution has been derived by applying the upscaling method of Coarse Graining to the groundwater head equation. Its application requires steady-state drawdown data at about 5 observation wells to assess T_{efu}, and further observation points to assess variance and correlation length of the transmissivity field [*Zech et al.*, 2015]. This is generally cost-intensive and seldom meets real data sets.

Among Theis-based interpretation techniques which use the transient drawdown to estimate hydraulic parameters, the Cooper-Jacob method [*Cooper and Jacob*, 1946], which is restricted to the interpretation of the late drawdown, has been the focus of a number of studies. *Meier et al.* [1998] and *Sanchez-Vila et al.* [1999b] show that the Cooper-Jacob method leads to a good approximation of T_{efu}, which was confirmed by several other studies [e.g., *Indelman*, 2003; *Copty and Findikakis*, 2004; *Wu et al.*, 2005]. However, the convergence to T_{efu} for heterogeneous aquifers occurs at much later times than the generally accepted validity criterion of the Cooper-Jacob method [*Copty and Findikakis*, 2004]. Furthermore, *Sanchez-Vila et al.* [1999b] show analytically that the storativity estimated by the Cooper-Jacob method provides information on flow connectivity, which was further investigated by *Trinchero et al.* [2008] and *Fernàndez-Garcia et al.* [2010]. By making use of the derivative approach for well test interpretation [e.g., *Bourdet et al.*, 1989;

Bourdet, 2002; *Gringarten*, 2008], *Copty et al.* [2011] recently proposed the Continuous-Derivation method for parameter estimation from heterogeneous aquifers. It utilizes the ratio of the drawdown and its time derivative over the entire time domain, allowing for the estimation of T_{in} even from very early pumping times. *Copty et al.* [2011] found time-dependent estimates of T_{in} to provide information about the underlying heterogeneity in T; specifically, T_{in} is equal to the transmissivity at the well for very early times and approaching T_{efu} during late pumping times.

It is recognized that a pumping test involves some upscaling over the heterogeneous aquifer as the cone of depression propagates with continuous pumping [e.g., *Schad and Teutsch*, 1994; *Leven and Dietrich*, 2006]. However, despite the progress in the field of the past few decades, the understanding of the relations between the various representative quantities of transmissivity remains incomplete [*Sanchez-Vila et al.*, 2006]. In order to maximize the information retrieved from pumping tests, an understanding of the interrelation between T_{in}, the transmissivity estimated by Theis-based interpretation techniques, and the equivalent transmissivity T_{eq}, is desirable. Thus, a spatial weighting which allows for reproducing T_{in} from a given heterogeneous distribution is required. Therefore, the aim of this study is to provide spatial weighting functions to approximate T_{in} and T_{eq}, to get further insight into the relationship of these quantities, and, to investigate how they relate to the underlying spatial distribution in T.

Starting from the Fréchet kernel [*Oliver*, 1990, 1993; *Knight and Kluitenberg*, 2005] and its relation to sensitivity coefficients [e.g., *Sun and Yeh*, 1985; *Yeh*, 1986; *Dietrich et al.*, 2005], we derive time-dependent spatial weighting functions for the computation of weighted averages of T_{in} and T_{eq} under radially convergent flow. The proposed spatial weighting functions are verified and investigated by means of Monte Carlo simulations. For the case of single-well pumping tests, i.e. for a configuration where the pumping well coincides with the observation well, we show numerically that the kernel-weighted transmissivities agree well to the corresponding Theis-based parameters. Thus, this study relates T_{in} and T_{eq} to the underlying heterogeneity. The influence of flow connectivity on estimated parameters is investigated. Moreover, implications for real world application are discussed with particular emphasis on pumping test interpretation by the Continuous-Derivation method [*Copty et al.*, 2011].

3.2 Fréchet Kernels as Spatial Weights

3.2.1 Spatial Weighting functions

The transmissivity is defined as a spatial random function which can be split into a uniform mean T_0, and fluctuations about the mean $\tilde{T}$, as given by Equation (2.26)

$$T(\mathbf{x}') = T_0 + \tilde{T}(\mathbf{x}')$$

with $\mathbf{x}' = (x, y)$ being the position vector of a particular anomaly in T in two dimensions. Similarly, the storativity is written as a summation of a uniform mean S_0 and a fluctuation term $\tilde{S}$.

Starting from a perturbation expansion, the transient head at an observation point $\mathbf{x}$, resulting from pumping in a heterogeneous domain can be expressed by (2.27)

$$h(\mathbf{x}, t) = h_0(\mathbf{x}, t) + h_1(\mathbf{x}, t) + h_2(\mathbf{x}, t) + \dots ,$$

where $h_0(\mathbf{x}, t)$ is the hydraulic head in the homogeneous aquifer with T_0 and S_0, and, the other terms $h_{\mathrm{j}}(\mathbf{x}, t)$ for $\mathrm{j} = 1, \dots$ are solutions of stochastic partial differential equations that describe deviations from the homogeneous solution. The first-order term of the above equation is given by the Fréchet derivative (2.28) [*Knight and Kluitenberg*, 2005]

$$h_1(\mathbf{x}, t) = -\int F_{\mathrm{T}}(\mathbf{x}, \mathbf{x}', t)\tilde{T}(\mathbf{x}')d\mathbf{x}' - \int F_{\mathrm{S}}(\mathbf{x}, \mathbf{x}', t)\tilde{S}(\mathbf{x}')d\mathbf{x}',$$

where F_{T} and F_{S} are the Fréchet kernels for transmissivity and storativity, respectively. By neglecting higher-order perturbation terms in (2.27) the head in a heterogeneous aquifer can be approximated by (2.29)

$$h(\mathbf{x}, t) = h_0(\mathbf{x}, t) - \int F_{\mathrm{T}}(\mathbf{x}, \mathbf{x}', t)\tilde{T}(\mathbf{x}')d\mathbf{x}' - \int F_{\mathrm{S}}(\mathbf{x}, \mathbf{x}', t)\tilde{S}(\mathbf{x}')d\mathbf{x}'.$$

The above equation states that the head at a particular location $\mathbf{x}$ in the heterogeneous aquifer is equal to the head in the homogeneous aquifer h_0, plus a spatial convolution integral in terms of the transmissivity and storativity fluctuations $\tilde{T}(\mathbf{x}')$ and $\tilde{S}(\mathbf{x}')$, respectively. The Fréchet kernels F_{T} and F_{S} are spatial weighting functions of the fluctuations of T and S.

Since transmissivity is the most salient feature of natural aquifers, we restrict our analysis to spatially variable T-fields, and assume the storativity to be uniform, which reduces (2.29) to

$$h(\mathbf{x}, t) = h_0(\mathbf{x}, t) - \int F_{\mathrm{T}}(\mathbf{x}, \mathbf{x}', t)\tilde{T}(\mathbf{x}')d\mathbf{x}'. \tag{3.1}$$

By assuming that the pumping well emits a pressure signal which spreads out radially to be scattered by anomalies in T, the hydraulic head at an observation $\mathbf{x}$ can be viewed

as the sum of all scattered signals from all involved anomalies. Thus, (3.1) can also be expressed as

$$h(\mathbf{x},t) = h_0(\mathbf{x},t) - \delta T_{\mathrm{eq}}(\mathbf{x},t) \int F_{\mathrm{T}}(\mathbf{x},\mathbf{x}',t)d\mathbf{x}' \tag{3.2}$$

with $\delta T_{\mathrm{eq}}(\mathbf{x},t)$ referring to the deviation between T_0 and T observed at the observation well, i.e. as $h(\mathbf{x},t)$ deviates from $h_0(\mathbf{x},t)$. It is important to note that although $\delta T_{\mathrm{eq}}(\mathbf{x},t)$ depends on the location of the observation point, it is a homogeneous parameter that comprises an average of the local fluctuations of T. This allows the $\delta T_{\mathrm{eq}}(\mathbf{x},t)$ to be taken outside the integration in (3.2). The equivalent transmissivity is then defined by

$$T_{\mathrm{eq}}(\mathbf{x},t) = T_0 + \delta T_{\mathrm{eq}}(\mathbf{x},t). \tag{3.3}$$

As one aim of this study is to provide a spatial weighting to approximate T_{eq} at a particular observation well, i.e. the homogeneous equivalent T which substitutes the true heterogeneous T-field, homogenization is intended. That is, $\delta T_{\mathrm{eq}}(\mathbf{x},t)$ is considered as constant fluctuation term. Thus, $T_{\mathrm{eq}}(\mathbf{x},t)$ is time-dependent and dependent on the point of observation. Moreover, as $T_{\mathrm{eq}}(\mathbf{x},t)$ is a homogeneous parameter, it should satisfy Theis' equation [*Theis*, 1935] by

$$h(\mathbf{x},t) = \frac{q}{4\pi T_{\mathrm{eq}}(\mathbf{x},t)} E_1(u) \tag{3.4}$$

where q is the constant pumping rate, and E_1 being the exponential integral function of $u = S_0 a^2/(4tT_{\mathrm{eq}}(\mathbf{x},t))$, a the distance between the pumping well and the observation well, and t the time since pumping started. However, as equations (3.1) and (3.2) rely on the assumption of a low order perturbation, they have to be regarded as an approximation of the corresponding T_{eq} in Theis' equation (3.4).

In order to derive a spatial weighting function to approximate T_{eq} from a given distribution of T, Equations (3.1) and (3.2) are equated which yields

$$\delta T_{\mathrm{eq}}(\mathbf{x},t) = \frac{\int F_{\mathrm{T}}(\mathbf{x},\mathbf{x}',t)\,\tilde{T}(\mathbf{x}')d\mathbf{x}'}{\int F_{\mathrm{T}}(\mathbf{x},\mathbf{x}',t)d\mathbf{x}'}. \tag{3.5}$$

By considering the definition of T_{eq} as given by (3.3), and transmissivity to be log-normally distributed, i.e. $Y = \ln T$, we obtain the spatial weighting to estimate T_{eq} by means of the corresponding Fréchet kernel,

$$T_{\mathrm{eq}}^{\mathrm{F}}(\mathbf{x},t) = \exp\left(\frac{\int F_{\mathrm{T}}(\mathbf{x},\mathbf{x}',t)\,Y(\mathbf{x}')d\mathbf{x}'}{\int F_{\mathrm{T}}(\mathbf{x},\mathbf{x}',t)d\mathbf{x}'}\right) \tag{3.6}$$

with index $^{\mathrm{F}}$ stating that the Fréchet kernel is used as a weight.

In addition to the spatial weighting for the equivalent transmissivity which satisfies Theis' equation as defined above, we present below a modified weighting expression which is denoted T_{in}, the interpreted transmissivity. One of the most commonly used methods for the interpretation of transient drawdown data is the Cooper-Jacob method [*Cooper and*

Jacob, 1946] which uses the derivative of the drawdown with respect to the logarithm of time. More recently, the Continuous-Derivation method [*Copty et al.*, 2011] also employs the time derivative of the drawdown to estimate T_{in}. In general, interpreting the drawdown derivative became a common tool for reservoir characterization, and system identification in particular [e.g., *Bourdet et al.*, 1989; *Bourdet*, 2002; *Gringarten*, 2008], as it is much more sensitive to variations of hydraulic aquifer properties than the drawdown itself. In line with these interpretation methods, we empirically define a weighted transmissivity according to (3.6), with the time derivative of the Fréchet kernel as spatial weighting function. Thus, the corresponding time-dependent spatial weighting reads

$$T_{\mathrm{in}}^{\mathrm{F}}(\mathbf{x},t) = \exp\left(\frac{\int \frac{\partial F_{\mathrm{T}}(\mathbf{x},\mathbf{x}',t)}{\partial \ln t} Y(\mathbf{x}')d\mathbf{x}'}{\int \frac{\partial F_{\mathrm{T}}(\mathbf{x},\mathbf{x}',t)}{\partial \ln t} d\mathbf{x}'}\right). \tag{3.7}$$

Because the above expression is based on the time derivative of the Fréchet kernel, we refer to the transmissivity as an interpreted transmissivity, even though it is based on a spatial weighting.

Equations (3.6) and (3.7) can be regarded as an application for the Fréchet kernels to approximate T_{in} and T_{eq} from a given heterogeneous distribution of T. In this regard they provide a tool to investigate the relation between both transmissivities, and the underlying heterogeneity. The validity of (3.6) and (3.7) is investigated and verified numerically in Section 3.3.

Please note that the Cooper-Jacob and the Continuous-Derivation method, respectively, allow for the estimation of the storativity only by its relation to T_{in} and u. Consequently, it is not possible to directly relate changes in the hydraulic head to the interpreted storativity. In this regard, we follow the existing view of treating the interpreted storativity as an indicator of flow connectivity, as proposed by, e.g., *Meier et al.* [1998], *Sanchez-Vila et al.* [1999b], *Trinchero et al.* [2008], *Fernàndez-Garcia et al.* [2010].

3.2.2 Properties of the Transmissivity Fréchet Kernel

In this section we summarize the properties of the Fréchet kernel and its time derivative. By considering a single-well pumping test configuration, where the pumping well (PW) coincides with the observation well (OW), F_{T} is given by *Knight and Kluitenberg* [2005]

$$F_{\mathrm{T}}(r,t) = -\frac{q}{8\pi^2 T_0^2 Dt} \exp\left(-\frac{r^2}{2Dt}\right) K_1\left(\frac{r^2}{2Dt}\right) \tag{3.8}$$

where D is the diffusivity of the aquifer equal to T_0/S_0, and $K_1(z)$ is the modified Bessel function of the second kind of order one. Equation (3.8) relies on the geometry of a radial coordinate system with OW=PW at its origin. Consequently, F_{T} is radially symmetric and dependent on r, the distance between a particular anomaly in T and OW=PW. The

derivative of F_T with respect to $\ln t$, needed to evaluate (3.7), is given by

$$\frac{\partial F_T(r,t)}{\partial \ln t} = -\frac{qr^2}{16\pi^2 D^2 T_0^2 t^2} \exp\left(-\frac{r^2}{2Dt}\right)\left(K_0\left(\frac{r^2}{2Dt}\right) + K_1\left(\frac{r^2}{2Dt}\right)\right) \tag{3.9}$$

where $K_0(z)$ is the modified Bessel function of the second kind of zero order.

Figure 3.1 shows F_T, as well as its derivative $\partial F_T/\partial \ln t$, for two anomalies located at different distances from OW=PW. In general, the absolute magnitude of F_T decreases as the distance of an anomaly from OW=PW increases. Accordingly, the impact of an anomaly close to OW=PW will be larger than that of a similar anomaly but further away from the well. With proceeding time, F_T approaches a fixed value only dependent on position, $F_T(r,t) \to -\frac{q}{4\pi^2 T_0^2 r^2}$ as $t \to \infty$ for $r \neq 0$ [*Knight and Kluitenberg*, 2005].

The derivative of F_T increases rapidly as the cone of depression reaches an anomaly (Figure 3.1). After a distinct peak, $\partial F_T(r,t)/\partial \ln t$ approaches zero as pumping continues, indicating that the impact of an anomaly in T on the drawdown is restricted to a rather short period. Along with the derivation of the Continuous-Derivation method, *Copty et al.* [2011] found that the dimensionless derivative of the Fréchet kernel, $\partial F_T(1/u)/\partial(1/u)$, peaks at a dimensionless time of $1/u = 1.6505$. This led them to conclude that continuous estimates of $T_{in}(t)$ can be associated to a radial distance, given by

$$r_{in} = \sqrt{\frac{4t\, T_{in}(t)}{1.6505\, S_0}}. \tag{3.10}$$

That is, for single-well pumping tests (3.10) allows to relate transient estimates of the interpreted transmissivity to a particular distance r_{in} from the well. Note that due to the way Equation (3.10) was derived, it treats the domain from which parameters are estimated to be only variable in T. Storativity is assumed uniform, and to be known.

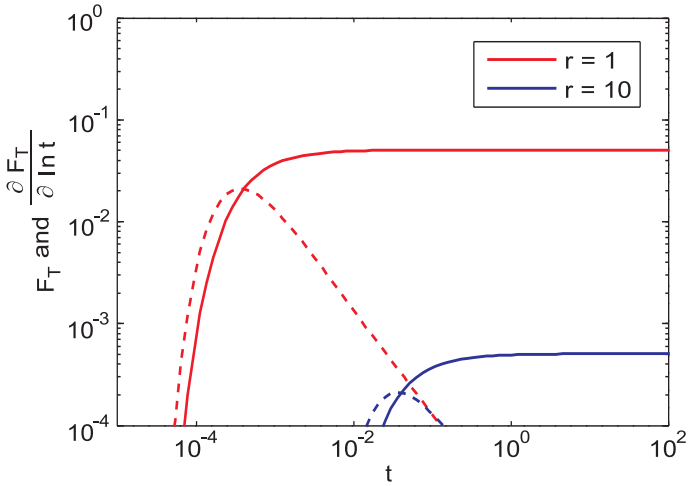

Figure 3.1: Absolute value of the Fréchet kernel F_T (solid), and its derivative $\partial F_T/\partial \ln t$ (dashed), as functions of time. F_T and $\partial F_T/\partial \ln t$ are depicted for two anomalies at different distances from the pumping well, which coincides with the observation well.

3.3 Numerical Application and Discussion

The validity of the spatial weighting functions (3.6) and (3.7), and the relation between the corresponding transmissivities $T_{\mathrm{eq}}^{\mathrm{F}}$ and $T_{\mathrm{in}}^{\mathrm{F}}$ is investigated numerically and presented in this section. For that purpose, transmissivity was modeled as multivariate Gaussian log-normally distributed spatial random function $Y = \ln T$, with mean m_{Y}, variance σ_{Y}^2, and a Gaussian covariance model expressed by the correlation length l_{Y}. Statistic parameters of examined ensembles are given in Table 3.1. Transmissivity fields were generated on a regular grid of 481 by 481 cells of 1 by 1 lu using the Turning Bands Method [*Mantoglou and Wilson*, 1982]. Storativity was assumed uniform with $S_0 = 5 \cdot 10^{-4}$.

Numerical simulations were performed using regularly spaced cells of 0.2 by 0.2 lu. A pumping well is placed at the center of the domain and a pumping test is simulated using MODFLOW [*Harbaugh et al.*, 2000]. A Neumann condition of zero flux is imposed at the outer boundaries. Preliminary simulations were performed to assure that for the duration of pumping, the drawdown at the observation well, assumed to coincide with the pumping well, is not impacted by the boundary conditions. The simulated drawdown was then interpreted with the Cooper-Jacob and the Continuous-Derivation method, respectively. According to *Desbarats* [1992] and *Peaceman* [1983], the equivalent radius of the pumping well is $r_{\mathrm{w}} = 0.0397$ lu, based on the defined computational grid.

The spatial integrals of F_{T} and its derivative $\partial F_{\mathrm{T}}/\partial \ln t$ were computed as discrete sums over a grid identical to the one used for numerical simulations. Equations (3.6) and (3.7) further require to define T_0. This is an important difference from the traditional stochastic approach. Following the traditional stochastic approach, T_0 is a constant value, equal to the expected value of the random variable, e.g. the arithmetic or geometric mean, respectively. However, by taking the transient nature of pumping tests into account, the observed drawdown relates to an increasing aquifer volume as pumping continues. Consequently, the transmissivity observed at the well gradually changes from the transmissivity at the well to some spatial average of the perturbed aquifer volume surrounding the well. To account for this fact, a progressively changing value of T_0 was used with (3.6) and (3.7). That is, the kernel-weighted T of the previous time step is used as T_0 for the following time step. Preliminary tests conducted to investigate the effect of different T_0 numerically indicated

Table 3.1: Statistical parameters of log-normally distributed ensembles of $Y = \ln T$.

ensemble	22	30	31	32	38	42
σ_{Y}^2	1	0.25	0.5	1	2	1
l_{Y} [lu]	4	8	8	8	8	14
m_{Y}			0			

that better agreement was obtained with a progressively changing T_0, in particular for intermediate times.

3.3.1 Equivalent Transmissivity

As given by the Theis equation (3.4), T_{eq} is a homogeneous parameter which, when assigned to the entire flow domain, reproduces the drawdown obtained from pumping in the true heterogeneous domain, under the given boundary conditions. To verify the proposed spatial weighting for T_{eq}, (3.6) along with (3.8), we compare the drawdown simulated with the true heterogeneous domain s, to the drawdown estimated by means of the spatially weighted $T_{\mathrm{eq}}^{\mathrm{F}}(t)$ and S_0 using (3.4), latter referred to s^{F}. Figure 3.2 compares s to s^{F} for an ensemble of 200 realizations at four selected times, including the corresponding Pearson correlation coefficients.

For an ensemble of $\sigma_{\mathrm{Y}}^2 = 1$ the agreement between s and s^{F} is very good, with correlation coefficients consistently exceeding 0.99. For early pumping times the correlation is almost perfect, becoming slightly weaker with continuous pumping. For all tested ensembles, i.e., for variances up to 2 and correlation lengths between 4 and 14 lu, correlation coefficients of > 0.99 indicate a very good agreement between s and s^{F}, at which the agreement slightly decreases as the degree of heterogeneity increases (Table 3.2). Thus, it can be concluded that the spatial weighting given by (3.6) provides a good approximation of the equivalent transmissivity in a heterogeneous domain.

Furthermore, results for $T_{\mathrm{eq}}^{\mathrm{F}}$ at $t = 1$ day, i.e. under near steady-state conditions, are in

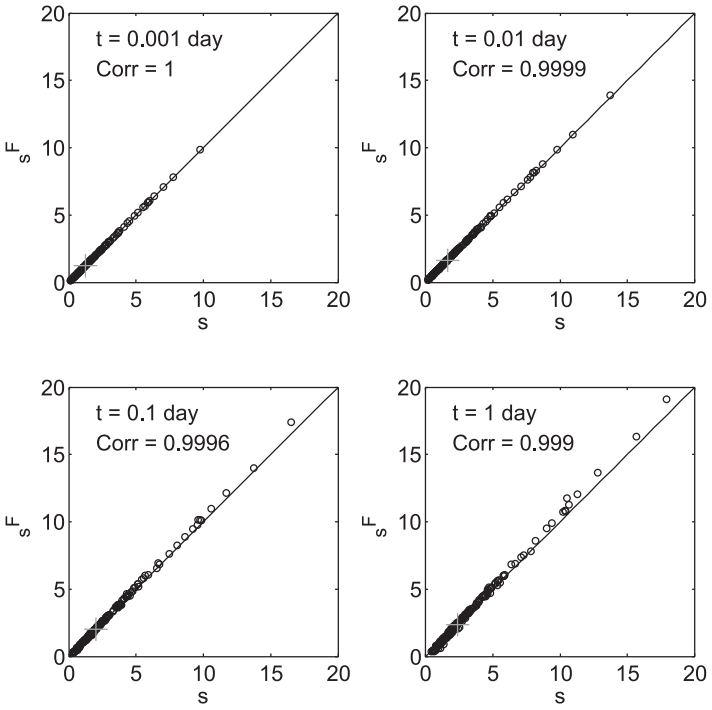

Figure 3.2: Drawdown in the true heterogeneous domain, s, compared to the drawdown computed from $T_{\mathrm{eq}}^{\mathrm{F}}(t)$ and S_0 using the Theis equation s^{F}, at four selected times. Ensemble statistics are $\sigma_{\mathrm{Y}}^2 = 1$, $l_{\mathrm{Y}} = 8$ lu, $m_{\mathrm{Y}} = 0$, ensemble size is 200. The cross marks s in a homogeneous domain characterized by $T_0 = T_{\mathrm{G}}$ and S_0.

Table 3.2: Pearson correlation coefficients comparing the drawdown in the true heterogeneous domain s to s^{F}, the drawdown computed by means of $T_{\mathrm{eq}}^{\mathrm{F}}(t)$ and S_0 using Theis' equation, at four selected time steps, and, for ensembles varying in σ_{Y}^2 and l_{Y}. Ensemble size is 200.

ensemble	22	30	31	38	42
σ_{Y}^2	1	0.25	0.5	2	1
l_{Y} $[lu]$	4	8	8	8	14
Corr (t = 0.001 day)	0.9999	1	1	0.9988	1
Corr (t = 0.01 day)	0.9998	0.9999	0.9999	0.9987	1
Corr (t = 0.1 day)	0.9996	0.9995	0.9996	0.9982	0.9999
Corr (t = 1 day)	0.9992	0.9989	0.9990	0.9974	0.9997

very good agreement with results from *Desbarats* [1992] who proposed a weighted spatial average with weights $1/r^2$ to estimate T_{eq}. Note that for late pumping times, F_{T} is radially symmetric, dependent only on position with $1/r^2$, which agrees to the geometric weight used by Desbarats. This weight was also confirmed analytically by *Sanchez-Vila et al.* [1999a].

3.3.2 Interpreted Transmissivity

The interpreted transmissivity T_{in}, as given by (3.7), does not satisfy the Theis equation. However, because (3.7) utilizes $\partial F_{\mathrm{T}}(r,t)/\partial \ln t$ continuously, $T_{\mathrm{in}}^{\mathrm{F}}(t)$ can be associated to a sub-domain which changes with time as the magnitude of $F_{\mathrm{T}}(r,t)$ changes. Thus, time-dependent estimates of $T_{\mathrm{in}}^{\mathrm{F}}(t)$ can be converted to distance-dependent estimates $T_{\mathrm{in}}^{\mathrm{F}}(r_{\mathrm{in}})$, by making use of the time-to-distance conversion in (3.10). This in turn allows for the estimation of radially-symmetric heterogeneous $T_{\mathrm{in}}^{\mathrm{F}}$-fields. In other words, $T_{\mathrm{in}}^{\mathrm{F}}(r_{\mathrm{in}})$ is assigned to rings centered at OW=PW, with ring widths dependent on the elapsed time between consecutive time steps, as also discussed qualitatively by *Butler* [1990].

Figure 3.3 compares three true heterogeneous domains to their radially heterogeneous counterparts $T_{\mathrm{in}}^{\mathrm{F}}(r_{\mathrm{in}})$. For small r_{in}, $T_{\mathrm{in}}^{\mathrm{F}}$ equals the local transmissivity at the pumping well T_{PW}. At large interpreted distances, $T_{\mathrm{in}}^{\mathrm{F}}$ approaches the geometric mean of T, i.e. $m_{\mathrm{Y}} = 0$. Verifying the spatial weighting for $T_{\mathrm{in}}^{\mathrm{F}}$ as proposed in (3.7) now becomes possible by comparing the drawdown in the true heterogeneous domain s, to the drawdown in the radially heterogeneous domain s^{RAD}, which is computed numerically using the radial transmissivity distribution $T_{\mathrm{in}}^{\mathrm{F}}(r_{\mathrm{in}})$.

Figure 3.4 compares s to s^{RAD} for an ensemble of 200 realizations at four selected times. Pearson correlation coefficients illustrate the agreement between both sets of data. For early pumping times the correlation is almost perfect, becoming slightly weaker with increasing time. The illustrated procedure was repeated for various ensembles with variances

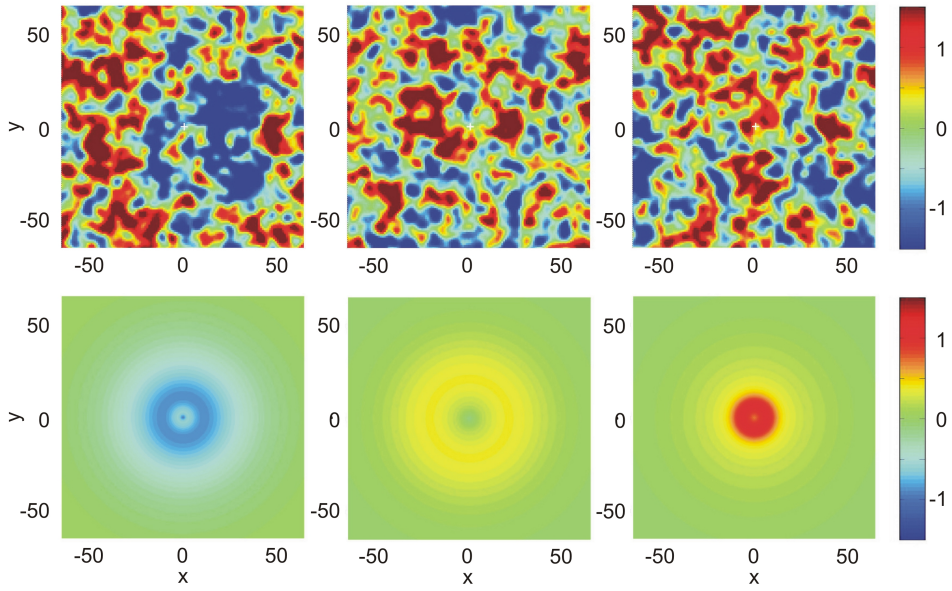

Figure 3.3: Generated $Y = \ln T$ fields and their radially heterogeneous counterparts, $T_{\text{in}}^{\text{F}}(r_{\text{in}})$. Ensemble statistics are $\sigma_{\text{Y}}^2 = 1$, $l_{\text{Y}} = 4$ lu, $m_{\text{Y}} = 0$. Only the central sub-domain of 131 by 131 lu is shown, with OW=PW at the center of the domain.

up to 2 and correlation lengths between 4 and 14 lu (Table 3.3). Correlation coefficients of > 0.99 indicate a very good agreement between s and s^{RAD}. Thus, radially heterogeneous T_{in}^{F}-fields obtained from the spatial weighting given by (3.7) and the time-distance conversion (3.10) are a good representation of the true heterogeneous domains.

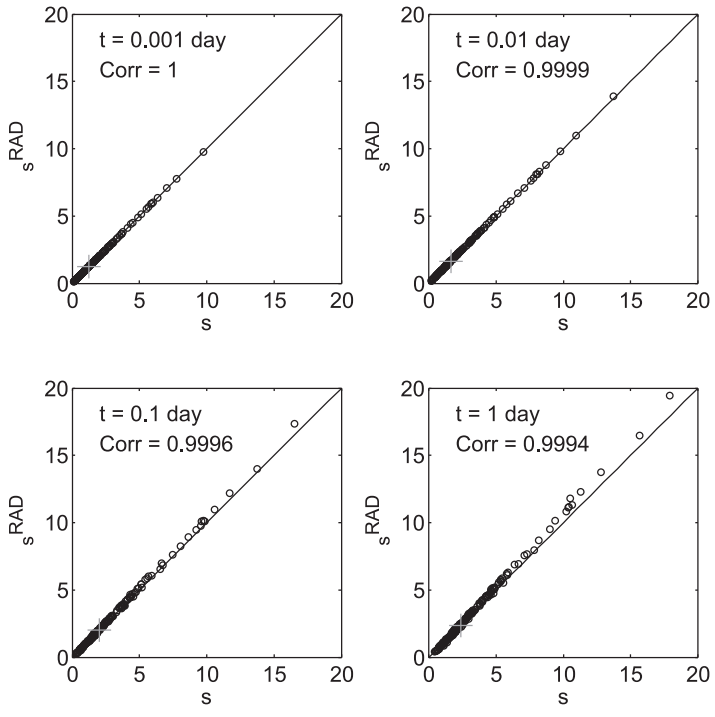

Figure 3.4: Drawdown in the true heterogeneous domain s compared to s^{RAD}, the drawdown in the radially heterogeneous domain which is computed from $T_{\text{in}}^{\text{F}}(r_{\text{in}})$, at four selected times. Ensemble statistics are $\sigma_{\text{Y}}^2 = 1$, $l_{\text{Y}} = 8$ lu, $m_{\text{Y}} = 0$, ensemble size is 200. The cross marks s in a homogeneous domain characterized by $T_0 = T_{\text{G}}$ and S_0.

Table 3.3: Pearson correlation coefficients comparing the drawdown in the true heterogeneous domains, s to s^{RAD}, the drawdown in the radially heterogeneous domains $T_{\mathrm{in}}^{\mathrm{F}}(r_{\mathrm{in}})$, at four time steps, and, for several ensembles varying in σ_{Y}^2 and l_{Y}. Ensemble size is 200.

ensemble	22	30	31	38	42
σ_{Y}^2	1	0.25	0.5	2	1
l_{Y} $[lu]$	4	8	8	8	14
Corr (t = 0.001 day)	1	1	1	0.9988	1
Corr (t = 0.01 day)	0.9998	0.9999	0.9999	0.9986	1
Corr (t = 0.1 day)	0.9996	0.9995	0.9995	0.9982	0.9998
Corr (t = 1 day)	0.9996	0.9993	0.9994	0.9977	0.9995

3.3.3 Relating Equivalent to Interpreted Transmissivity

The equivalent transmissivity of a radially heterogeneous domain, centered at the pumping well, is given by the harmonic average over point values of T, as demonstrated by *Cardwell and Parsons* [1945]. By considering single-well pumping tests, the spatially weighted interpreted transmissivity $T_{\mathrm{in}}^{\mathrm{F}}(r_{\mathrm{in}})$ is radially symmetric with respect to OW=PW (Figure 3.3). Thus, the equivalent transmissivity can be understood as the harmonic average over the corresponding radially heterogeneous $T_{\mathrm{in}}^{\mathrm{F}}(r_{\mathrm{in}})$-field.

The relation between the equivalent and interpreted transmissivity for single-well pumping tests can therefore be expressed by

$$T_{\mathrm{eq}}^{\mathrm{RAD}}(t) = W \left[\int_{r_{\mathrm{w}}}^{r_{\mathrm{in}}(t)} \frac{dr_{\mathrm{in}}}{T_{\mathrm{in}}^{\mathrm{F}}(r_{\mathrm{in}})\; r_{\mathrm{in}}^2} \right]^{-1} \quad \text{where} \quad W = \int_{r_{\mathrm{w}}}^{r_{\mathrm{in}}(t)} \frac{dr_{\mathrm{in}}}{r_{\mathrm{in}}^2} \tag{3.11}$$

and (3.10) relating times to radial distances. The index $^{\mathrm{RAD}}$ indicates that the equivalent transmissivity is obtained from the corresponding radially heterogeneous $T_{\mathrm{in}}^{\mathrm{F}}$-field. Note that the upper limit of the integral in (3.11) is time-dependent with $r_{\mathrm{in}}(t)$ referring to the radius of influence of the pumping test. A similar approach was utilized by *Leven and Dietrich* [2006], who used changes in the sensitivity distribution to investigate heterogeneous aquifers by means of single-well pumping tests. However, it is worthwhile to recall that $T_{\mathrm{in}}^{\mathrm{F}}(r_{\mathrm{in}})$ is assigned to rings centered at OW=PW (Figure 3.3); it does not refer to a single value which represents the entire domain perturbed by pumping.

Verification of (3.11) is again achieved numerically by computing the error between $T_{\mathrm{eq}}^{\mathrm{RAD}}(t)$ and $T_{\mathrm{eq}}^{\mathrm{F}}(t)$. $T_{\mathrm{eq}}^{\mathrm{RAD}}(t)$ is the spatial harmonic average over the radially heterogeneous $T_{\mathrm{in}}^{\mathrm{F}}$-field, and $T_{\mathrm{eq}}^{\mathrm{F}}(t)$ the spatial kernel-based average over the true heterogeneous T-field. Box plots in Figure 3.5 show the statistical analysis for the deviation of $T_{\mathrm{eq}}^{\mathrm{RAD}}$ from $T_{\mathrm{eq}}^{\mathrm{F}}$ at selected times, and, for ensembles of varying σ_{Y}^2. Even for a moderate variance

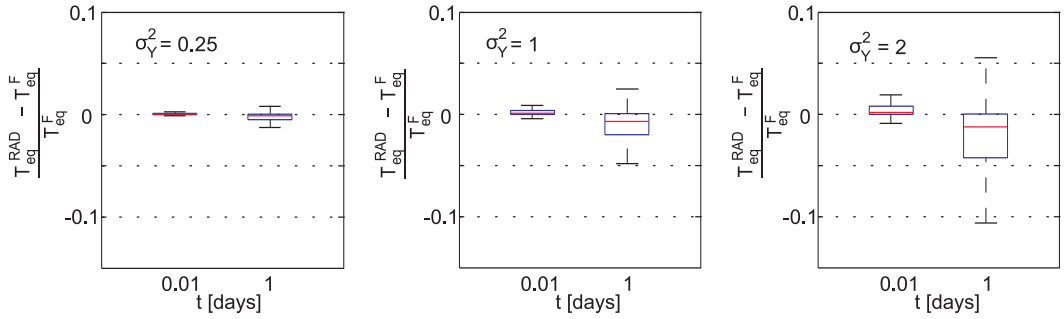

Figure 3.5: Statistics of the difference between the two T_{eq} estimates at selected times, and, for ensembles of varying σ_{Y}^2. $T_{\mathrm{eq}}^{\mathrm{RAD}}$ is estimated from radially heterogeneous $T_{\mathrm{in}}^{\mathrm{F}}$-fields. $T_{\mathrm{eq}}^{\mathrm{F}}$ is computed from the true heterogeneous distribution in T. Ensemble size is 200, $l_{\mathrm{Y}} = 8$ lu, $m_{\mathrm{Y}} = 0$.

of $\sigma_{\mathrm{Y}}^2 = 2$, the deviation between the different methods to compute T_{eq} is quite small. Deviations between both estimates of T_{eq} are due to discretization in space and time, limited by computational resources. However, presented results clearly show that (3.11) allows for approximating the equivalent transmissivity from $T_{\mathrm{in}}^{\mathrm{F}}$, provided that the storativity of the aquifer S_0 is known.

3.3.4 Spatial Weighting versus Flow Connectivity

It is well known that flow connectivity has an important impact on the estimation of flow parameters. It is also obvious that a simple spatial weighting can not capture this effect. Therefore, in this section, we investigate the impact of flow connectivity on estimated parameters, specifically on the interpreted transmissivity.

According to *Meier et al.* [1998] and *Sanchez-Vila et al.* [1999b], the interpreted storativity estimated by means of the Cooper-Jacob method [*Cooper and Jacob*, 1946], $S_{\mathrm{in}}^{\mathrm{CJ}}$ (2.13), serves as an indicator for flow connectivity. However, in order to emphasize that the corresponding storativity is used as an indicator for flow connectivity in the following, the abbreviation S_{est} is used, with

$$S_{\mathrm{est}} = S_{\mathrm{in}}^{\mathrm{CJ}} = \frac{2.25 t_0 T_{\mathrm{in}}^{\mathrm{CJ}}}{a^2}. \tag{3.12}$$

$T_{\mathrm{in}}^{\mathrm{CJ}} = 0.183 q/m_{\mathrm{s}}$ is the transmissivity estimated by the Cooper-Jacob method (2.13), with m_{s} being the slope of the late-time drawdown curve when plotted against $\log t$, and t_0 being obtained from the time at which the projection line of the slope intercepts the zero-drawdown axis. By considering a single-well pumping test configuration, a reduces to the radius of the pumping well.

To investigate the impact of flow connectivity on the interpretation of single-well pumping tests, we estimate the error between the drawdown in the true heterogeneous domain s, and the drawdown in the spatially weighted, radially heterogeneous domain s^{RAD}. Hence,

the corresponding error is a measure on how the spatially averaged $T_{\mathrm{in}}^{\mathrm{F}}$-field, which does not actually account for flow connectivity, renders groundwater flow to the pumping well in the true heterogeneous domain, which is related to S_{est} in the following.

Figure 3.6 shows the deviation of s^{RAD} from s during late pumping times as a function of S_{est}, for different ensembles varying in σ_{Y}^2. In addition, different colors in Figure 3.6 depict the local transmissivity at the well. It can be seen that $S_{\mathrm{est}} < S_0$ correlates with a small T_{PW}, indicating a well which is weakly connected to the domain. On the contrary, $S_{\mathrm{est}} > S_0$ correlates with a large T_{PW}, with the well being well connected to the domain. It is interesting to note that relations between S_{est} and S_0 are reverse when the pumping and observation well are not coinciding [e.g., *Sanchez-Vila et al.*, 1999b; *Trinchero et al.*, 2008]. Note that if OW=PW, t_0 in (3.12) correlates with the ratio of the near-field to far-field transmissivities. On the other hand, when the wells are not coinciding, t_0 rather depends on how fast the drawdown signal reaches the OW.

However, with regard to the impact of flow connectivity, Figure 3.6 shows that deviations between s^{RAD} and s are rather small for variances up to 0.5, barely exceeding $\pm 10\%$. If OW=PW is well connected to the domain s^{RAD} underestimates s, whereas s^{RAD} overestimates s for weakly connected wells. With increasing variance, S_{est} scatters over an increasing range of up to 40 orders of magnitude. Interestingly, if flow connectivity

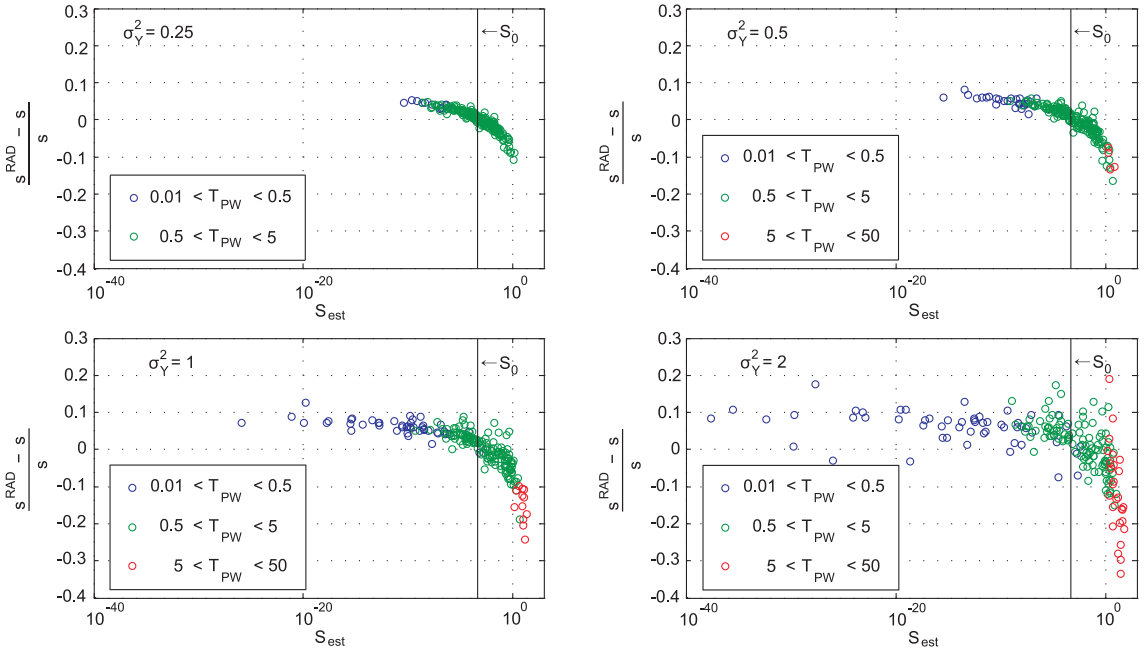

Figure 3.6: Deviation of the drawdown in the radial heterogeneous domain s^{RAD}, from the drawdown in the true heterogeneous domain s, as a function of flow connectivity S_{est}, at t=1 day. Plots relate to ensembles of 200 realizations each, with different σ_{Y}^2, $l_{\mathrm{Y}} = 8$ lu, $m_{\mathrm{Y}} = 0$. $S_0 = 5 \cdot 10^{-4}$ is the storativity assumed uniform during simulations. T_{PW} is the local transmissivity at OW=PW.

between the well and the domain is weak, the error between s^{RAD} and s exceeds 10% only occasionally, even for $\sigma_{\mathrm{Y}}^2 = 2$. On the contrary, the error between s^{RAD} and s is much more pronounced for a well connected well, in particular for realizations with $S_{\mathrm{est}} > 1$. In this regard, Figure 3.6 gives additional information to Figure 3.4, where deviations of s^{RAD} from s seem to be restricted to a large drawdown. Figure 3.6 reveals that relative deviations are much more pronounced for realizations with a small drawdown, or $T_{\mathrm{PW}} \gg T_0$, respectively, which agrees with a pronounced impact of flow connectivity.

The above discussion shows that $T_{\mathrm{in}}^{\mathrm{F}}$ can generally not capture the impact of flow connectivity. However, the impact of flow connectivity is almost negligible if $\sigma_{\mathrm{Y}}^2 \leq 0.5$, since s deviates from s^{RAD} just in the range of about $\pm 10\%$. As the degree of heterogeneity increases, the impact of flow connectivity increases as well. Considering the available set of simulations, the spatially weighted $T_{\mathrm{in}}^{\mathrm{F}}$-field still provides a good representation of the true heterogeneous domain for variances up to 2, if $S_{\mathrm{est}} < 1$. Under this condition the error between s and s^{RAD} does not exceed $\pm 20\%$. In other words, the spatial weighting given by equation (3.7) agrees well to how an extraction well averages over a heterogeneous domain, if OW=PW. Furthermore, the above procedure was also applied to the kernel-weighted equivalent transmissivity $T_{\mathrm{eq}}^{\mathrm{F}}$, which yielded comparable results.

3.4 Implications for Pumping Test Interpretation

3.4.1 Concepts of Equivalent and Interpreted Transmissivity

Figure 3.7 compares the spatially weighted equivalent and interpreted transmissivity, $T_{\mathrm{eq}}^{\mathrm{F}}$ and $T_{\mathrm{in}}^{\mathrm{F}}$, for three randomly selected realizations. $T_{\mathrm{eq}}^{\mathrm{F}}$ and $T_{\mathrm{in}}^{\mathrm{F}}$ are plotted as a function of the interpreted distance from OW=PW normalized by l_{Y}. As pumping starts, both $T_{\mathrm{eq}}^{\mathrm{F}}$ and $T_{\mathrm{in}}^{\mathrm{F}}$ are equal to the local transmissivity at the pumped well T_{PW}. As the cone of depression propagates in time, which corresponds to an increase in distance in Figure 3.7, $T_{\mathrm{eq}}^{\mathrm{F}}$ remains rather close to T_{PW}, which is in agreement with findings by *Dagan and Lessoff* [2007a,b]. However, Figure 3.7 also shows that if T_{PW} is considerably higher than T_0, $T_{\mathrm{eq}}^{\mathrm{F}}$ starts to deviate from T_{PW} as pumping continues.

Contrary to $T_{\mathrm{eq}}^{\mathrm{F}}$, which is relatively stable as pumping propagates, $T_{\mathrm{in}}^{\mathrm{F}}$ shows pronounced variations. At large distances, $T_{\mathrm{in}}^{\mathrm{F}}$ approaches the effective transmissivity under uniform groundwater flow $T_{\mathrm{efu}} = T_{\mathrm{G}}$, for every individual realization (Figure 3.7). By considering the arithmetic ensemble mean of the spatially weighted interpreted transmissivity $\left\langle T_{\mathrm{in}}^{\mathrm{F}} \right\rangle$, Figure 3.8 shows $\left\langle T_{\mathrm{in}}^{\mathrm{F}} \right\rangle / T_{\mathrm{G}}$ as a function of the normalized interpreted distance from OW=PW. It can be seen that for all considered variances, $\left\langle T_{\mathrm{in}}^{\mathrm{F}} \right\rangle$ starts at the corresponding arithmetic mean of T, approaching $T_{\mathrm{efu}} = T_{\mathrm{G}}$ after 15 to 20 correlation lengths.

Moreover, it is important to note that the meaning of r_{in} in Figure 3.7 is different for

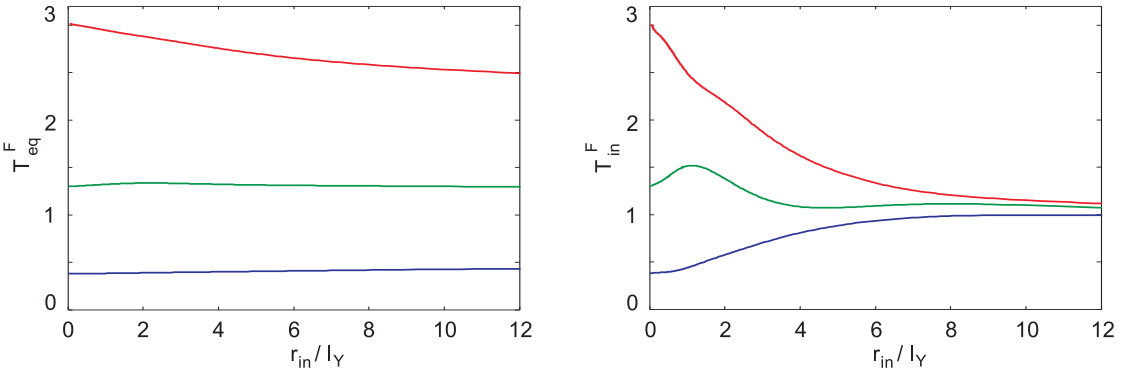

Figure 3.7: Equivalent transmissivity T_{eq}^{F}, and interpreted transmissivity $T_{\mathrm{in}}^{\mathrm{F}}$, as a function of r_{in} (normalized by l_{Y}) for three selected T-fields. Ensemble statistics are $\sigma_{\mathrm{Y}}^2 = 0.5$, $l_{\mathrm{Y}} = 8$ lu, $m_{\mathrm{Y}} = 0$ ($T_{\mathrm{G}} = 1$).

$T_{\mathrm{eq}}^{\mathrm{F}}$ and $T_{\mathrm{in}}^{\mathrm{F}}$. For $T_{\mathrm{in}}^{\mathrm{F}}$, r_{in} allows for estimating the radially heterogeneous $T_{\mathrm{in}}^{\mathrm{F}}$-field, since (3.10) explicitly relates T_{in} to r_{in}. As illustrated by Figure 3.4, radially heterogeneous $T_{\mathrm{in}}^{\mathrm{F}}$-fields allow for reproducing the drawdown in the true heterogeneous domain, at which $T_{\mathrm{in}}^{\mathrm{F}}$ approaches T_{G} within a few l_{Y} (Figure 3.7). However, when related to $T_{\mathrm{eq}}^{\mathrm{F}}$, r_{in} is understood as an approximation for the radius of influence at a particular point in time [*Copty et al.*, 2011]. The homogeneous $T_{\mathrm{eq}}^{\mathrm{F}}$ is then assigned to the entire domain perturbed by pumping to reproduce the drawdown in the true heterogeneous domain by means of Theis' equation.

The above discussion already reveals the limits of the concept of T_{eq} for single-well pumping tests in heterogeneous domains. That is, relating T_{eq} to s does potentially not allow to infer information about the underlying heterogeneity, since T_{eq} is essentially sensitive to the local transmissivity at OW=PW, with $T_{\mathrm{eq}} \approx T_{\mathrm{PW}}$ for the entire duration of pumping [*Dagan and Lessoff*, 2007a,b]. However, T_{in} is sensitive to the underlying het-

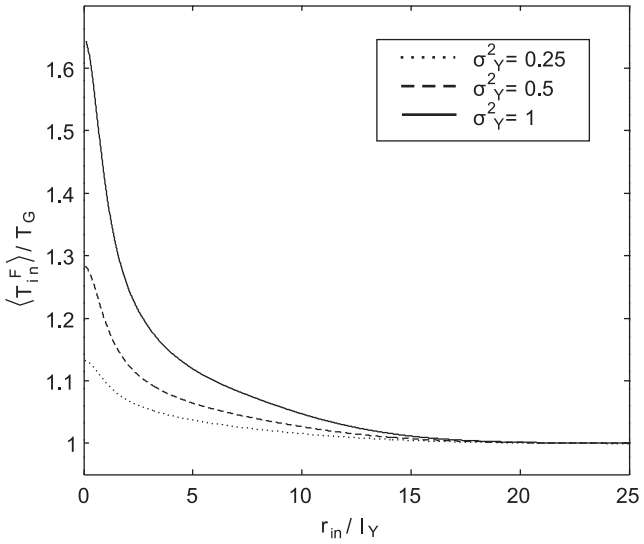

Figure 3.8: Ensemble means of the interpreted transmissivity $\langle T_{\mathrm{in}}^{\mathrm{F}} \rangle$, for ensembles with different σ_{Y}^2, $l_{\mathrm{Y}} = 8$ lu, $m_{\mathrm{Y}} = 0$. For depicted ensembles the arithmetic mean is given by $T_{\mathrm{A}} = 1.133$, 1.284 and 1.649. Interpreted distances r_{in}, are normalized by l_{Y}. Each ensemble comprises 500 realizations.

erogeneity allowing for estimating $T_{\mathrm{efu}} = T_{\mathrm{G}}$ from late pumping times [e.g., *Sanchez-Vila et al.*, 1999b; *Indelman*, 2003; *Copty and Findikakis*, 2004], and, for the generation of radially heterogeneous T_{in}-fields to reproduce the drawdown in a forward simulation.

3.4.2 Methods for Pumping Test Interpretation

In this section we examine the spatially weighted interpreted transmissivity determined from Equation (3.7) to the transmissivities estimated with the Continuous-Derivation method [*Copty et al.*, 2011] and the Cooper-Jacob method [*Cooper and Jacob*, 1946]. The recently developed Continuous-Derivation method uses the time derivative of the drawdown to compute a continuous function of radial distance-dependent estimates of the transmissivity $T_{\mathrm{in}}^{\mathrm{CD}}(r_{\mathrm{in}})$.

Figure 3.9 compares $T_{\mathrm{in}}^{\mathrm{CD}}(r_{\mathrm{in}})$ estimated from the drawdown in the true heterogeneous domain to the spatial weight over the underlying T-field $T_{\mathrm{in}}^{\mathrm{F}}(r_{\mathrm{in}})$, for three individual realizations of single-well pumping tests from two different ensembles. It can be seen that the agreement between both T_{in} is very good for $\sigma_{\mathrm{Y}}^2 = 0.25$ but decreases with an increase in variance, showing deviations in magnitude and interpreted distances, r_{in}. Deviations in magnitude are inherent to the Fréchet kernel weighting, which relies on a first order perturbation approach, assuming variations in $\tilde{T}$ to be small. Thus, $T_{\mathrm{in}}^{\mathrm{F}}$ does not reproduce every peak from $T_{\mathrm{in}}^{\mathrm{CD}}$ in highly heterogeneous domains. Deviations with respect to r_{in} are attributed to the impact of flow connectivity, which can not be captured by a simple spatial weighting of point transmissivities, as already discussed in Section 3.3.4.

However, Figure 3.9 clearly shows that $T_{\mathrm{in}}^{\mathrm{F}} \approx T_{\mathrm{in}}^{\mathrm{CD}}$. Consequently, $T_{\mathrm{in}}^{\mathrm{F}}$ as given by Equation (3.7) sufficiently describes how changes in the hydraulic head relate to the underlying

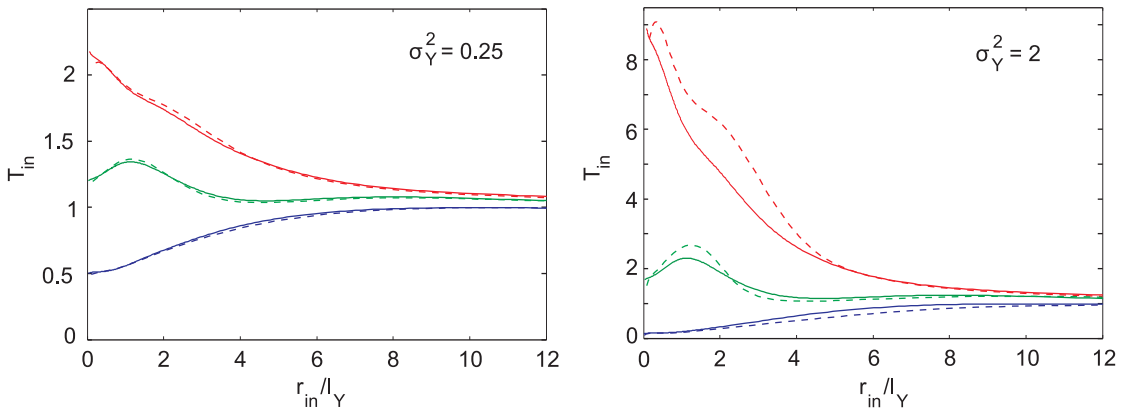

Figure 3.9: Spatially weighted transmissivity $T_{\mathrm{in}}^{\mathrm{F}}$ (solid lines) estimated by (3.7) compared to the transmissivity from the Continuous-Derivation method $T_{\mathrm{in}}^{\mathrm{CD}}$ (dashed lines) as functions of the interpreted radial distance (normalized by l_{Y}), for three individual realizations from two different ensembles of $\sigma_{\mathrm{Y}}^2 = 0.25$ and 2, $l_{\mathrm{Y}} = 8$ lu, $m_{\mathrm{Y}} = 0$ ($T_{\mathrm{G}} = 1$).

heterogeneity. Thus, properties of $T_{\mathrm{in}}^{\mathrm{F}}$ also apply to $T_{\mathrm{in}}^{\mathrm{CD}}$, which implies the estimation of radially heterogeneous T_{in}-fields, and the approximation of the equivalent transmissivity by making use of (3.11).

Furthermore, the Continuous-Derivation method potentially allows for estimating T_{PW} from very early drawdown data of single-well pumping tests. However, with regard to field data, early drawdown data at OW=PW might be strongly influenced by well effects like storage and skin, which can mask the actual aquifer response. Distortions during the early-time drawdown will also affect $T_{\mathrm{in}}(r_{\mathrm{in}})$ and consequently limit the applicability of equation (3.11). In that case, an observation well in the close vicinity of PW might be used for pumping test evaluation, provided that the distance between OW and PW is much smaller than l_{Y}. However, for late pumping times, $T_{\mathrm{in}}^{\mathrm{CD}} = T_{\mathrm{in}}^{\mathrm{F}}$ is equal to T_{G}, thus, approximating T_{efu} which is independent of T_{PW}.

The Cooper-Jacob method and the Continuous-Derivation method yield equal results for transmissivity and storativity when applied to late drawdown data. In this scope, the Continuous-Derivation method might be understood as an extension of the Cooper-Jacob method, releasing the restriction of interpreting late-time drawdown data for utilizing the entire drawdown for parameter estimation.

With regard to the interpreted storativity S_{est}, this study confirms that for single-well pumping tests, estimates from the Cooper-Jacob method can not be used to assess the real storativity of the aquifer [e.g. *Schad and Teutsch*, 1994; *Meier et al.*, 1998; *Sanchez-Vila et al.*, 1999b]. $S_{\mathrm{est}} = S_{\mathrm{in}}^{\mathrm{CJ}}$ is in general inferred from $T_{\mathrm{in}}^{\mathrm{CJ}}$. Thus, both estimates are dependent on the spatial weighting which utilizes the temporal derivative of the Fréchet kernel for transmissivity. Consequently, S_{est} has to be regarded as a property of the interpreted transmissivity, and is treated as an indicator for flow connectivity.

3.5 Conclusions

Pumping tests are a well established technique to characterize aquifer hydraulic properties. Even though aquifers are intrinsically heterogeneous, the interpretation of pumping tests is commonly performed by assuming the medium to be homogeneous. In doing so, the naturally heterogeneous system is substituted by an idealized homogeneous one, providing interpreted hydraulic parameters which are averaged over a domain of uncertain extent.

By making use of Fréchet kernels we investigated how two spatially averaged properties, denoted the equivalent and interpreted transmissivity, T_{eq} and T_{in}, relate to the underlying heterogeneity, and to estimates obtained by applying Theis-based interpretation techniques to drawdown data from heterogeneous T-fields. Focusing on single-well pumping tests, the spatial weighting functions were applied to multivariate-Gaussian log-normally distributed transmissivity fields. The interrelation of these two transmissivity estimates as well as

their relation to the underlying heterogeneity was discussed. The impact of connectivity was also investigated. Finally, we state implications for the concepts of T_{eq} and T_{in}, and, for real world applications, respectively. Note that well effects like skin and well-bore storage are not considered herein. Nevertheless, presented results provide insight on how the interpreted transmissivity, estimated by Theis-based interpretation techniques, relates to the underlying heterogeneity of the perturbed aquifer system. The findings of this study can be summarized as follows:

1. The interpreted time-dependent transmissivity T_{in}, starts from the local transmissivity at the pumping well T_{PW}, approaching at late pumping times the effective transmissivity under uniform groundwater flow, if the area perturbed by pumping exceeds about 15 to 20 correlation lengths. Consequently, T_{in} potentially allows for inferring information about the underlying heterogeneity. Within the framework of spatial weighting, T_{in} can be approximated by utilizing the temporal derivative of the Fréchet kernel as spatial weight, as given by (3.7).

2. The equivalent time-dependent transmissivity T_{eq}, starts from T_{PW} as well, but does not approach a global value for late pumping times. For weakly heterogeneous systems T_{eq} approximates T_{PW} for the entire duration of pumping. With increasing degree of heterogeneity, T_{eq} becomes time-dependent, differing significantly from T_{PW} at late pumping times. As T_{eq} is essentially sensitive to the local transmissivity at the well, its applicability to investigate aquifer heterogeneity is limited. Within the framework of spatial weighting, T_{eq} can be approximated by utilizing the Fréchet kernel itself as spatial weight, as given by (3.6).

3. Transient estimates of T_{in}, obtained from (3.7), or by interpreting the transient drawdown at the pumped well by means of the Continuous-Derivation method [*Copty et al.*, 2011], respectively, allow for mapping radially heterogeneous T_{in}-fields. Provided that the storativity of the aquifer (assumed uniform) is know, T_{eq} can be approximated by a spatial harmonic mean with weights $1/r_{\mathrm{in}}^2$ over a radially heterogeneous T_{in}-field, as given by (3.11).

4. The impact of flow connectivity S_{est}, can not be captured by spatially weighting point transmissivities. However, for weakly heterogeneous aquifers with variances up to 0.5, the impact of flow connectivity is almost negligible. In that case, the spatial weighting functions, (3.6) and (3.7), comprehensively describe how an extraction well averages over the heterogeneous T-field. As heterogeneity increases, this agreement decreases. However, by considering the available set of simulations with variances up to 2, the proposed spatial weightings for T_{eq} and T_{in} still provide a reasonable approximation of the underlying heterogeneity, if $S_{\mathrm{est}} < 1$. Moreover, for the case of an observation well coinciding with the pumping well considered here, it was found that high connectivity correlates with a large transmissivity at the well.

5. This study further indicates that instead of replacing the heterogeneous domain by an equivalent homogeneous one, an upscaled heterogeneous domain is a promising approach for a more comprehensive interpretation of pumping tests in heterogeneous domains.

The presented approach of using Fréchet kernels as a spatial weight could be potentially modified to the more general case where pumping and observation well are not coinciding. However, for a description of the underlying heterogeneity, transient drawdown data recorded at or close to the pumping well is preferred, since it comprises the drawdown response of the entire domain affected by pumping. Using drawdown data from an observation well further away from the pumping well, would minimize the response from anomalies in the vicinity of the pumping well, which is not desirable.

Chapter 4

Estimating Transmissivity from Steady-State Pumping Tests in Heterogeneous Aquifers in the Presence of a Linear Constant Head Boundary

4.1 Introduction

Aquifers are intrinsically heterogeneous with complex patterns of heterogeneity reflecting their geologic evolution. The estimation of aquifer parameters, like transmissivity T and storativity S, is commonly performed by interpreting drawdown data from pumping tests. Pumping test interpretation techniques are traditionally based on the Theis equation [*Theis*, 1935] which presumes aquifer homogeneity. Applying Theis-based interpretation techniques to drawdown data from heterogeneous aquifers then yields interpreted hydraulic parameters which are averaged over an area of uncertain extend, disguising their relation to the underlying heterogeneity.

Finding representative descriptions of transmissivity under convergent flow to a well has been the focus of numerous studies. Given the difficulty of quantifying aquifer heterogeneity, two different concepts have emerged in literature. One utilizes a stochastic approach to estimate the effective transmissivity which refers to an average in the probability space [e.g., *Neuman and Orr*, 1993; *Indelman et al.*, 1996; *Sanchez-Vila*, 1997; *Fiori et al.*, 1998; *Indelman*, 2003], i.e., to an ensemble of heterogeneous realizations of an aquifer. The other approach uses spatial averaging techniques to estimate the equivalent transmissivity [e.g., *Desbarats*, 1992; *Sanchez-Vila et al.*, 1999a; *Dagan and Lessoff*, 2007a,b; *Schneider and*

Attinger, 2008]. The equivalent transmissivity T_{eq} relates to a single realization of the heterogeneous aquifer, and is commonly defined as homogeneous substitute for the true heterogeneous transmissivity distribution. Properties of the equivalent and effective transmissivity have already been outlined in Sections 2.5 and 3.1. However, available studies mostly concentrate on infinite heterogeneous aquifer disregarding the more complex case of bounded aquifers.

Nevertheless, several studies investigate the effective and equivalent transmissivity under various boundary configurations by considering T as log-normally distributed Gaussian spatial random function and S to be uniform, e.g., *Rubin and Dagan* [1988]; *Neuman and Orr* [1993]; *Osnes* [1995]; *Paleologos et al.* [1996]; *Osnes* [1998]; *Guadagnini and Neuman* [1999a,b]; *Tartakovsky et al.* [2002]; *Guadagnini and Riva* [2003]. These studies show that even under uniform groundwater flow, a unique representative value of transmissivity does not exist if the domain is bounded. Though, if the domain size relative to the correlation scale of the transmissivity distribution l_{Y} is large, the effective transmissivity approaches the geometric mean of point transmissivities. A review on this problem is included in *Sanchez-Vila et al.* [2006]. However, introducing a pumping well into a bounded domain further complicates the analysis since the flow geometry becomes convergent towards the well, but is generally not symmetric.

Studies which consider the effect of outer boundaries on well flow and the estimation of transmissivity are few. By investigating 2D steady-state convergent flow in a radially bounded aquifer centered around a pumping well, *Riva et al.* [2001] found the effect of the outer constant head boundary to be mild and confined to the close vicinity of the boundary, if the variance of the spatial random function σ_{Y}^2 is smaller than 1. The equivalent transmissivity then increases from the harmonic to the arithmetic mean of T as the ratio L/l_{Y} increases from 0 to ∞, with L being the shortest distance between the boundary and the pumped well. By considering a rectangular heterogeneous domain bounded by two opposing constant-head and no-flow boundaries, *Lu and Vesselinov* [2015] developed an analytical approach to investigate the sensitivity of the hydraulic head with respect to heterogeneous distributions in T, under mean uniform flow and convergent well flow. However, to the authors knowledge, convergent flow to a well in a heterogeneous domain unilaterally delimited by an infinite linear constant head boundary (BCH) has not been explicitly considered in the literature yet, although it is often of interest, for example for characterizing coastal aquifers.

The analysis of drawdown data from BCH-domains is commonly realized by the Hantush method [*Hantush*, 1959], which relies on Theis' equation. Consequently, the application of Hantush's method presumes the aquifer to be homogeneous. Since it is easy to apply, the Hantush method is often used to estimate hydraulic parameters from heterogeneous aquifers. Though, studies on how the interpreted Hantush transmissivity relates to

the underlying heterogeneity, or to equivalent or effective quantities, respectively, are not available.

In this regard, this study investigates how estimates of transmissivity, obtained by interpreting the steady-state drawdown by the Hantush method [*Hantush*, 1959], relate to the underlying heterogeneity. It therefore develops a spatial weighting to approximate the equivalent transmissivity in BCH-domains from a given heterogeneous transmissivity distribution. For that purpose, the procedure presented in the previous chapter is applied. That is, the sensitivity of the drawdown on the heterogeneous transmissivity is examined by means of Fréchet kernels [*Oliver*, 1990, 1993; *Knight and Kluitenberg*, 2005]. Accordingly, the Fréchet kernel for transmissivity for BCH-domains is derived. Subsequently, the resulting spatially averaged transmissivity and the interpreted transmissivity from Hantush's method are numerically investigated by means of Monte Carlo simulations.

4.2 Applying Hantush's Method to Drawdown Data from Heterogeneous Aquifers

By considering Theis' equation [*Theis*, 1935] and applying the principle of superposition [e.g., *Ferris et al.*, 1962; *Bear*, 1972; *Kruseman et al.*, 1990], the transient drawdown for a fully penetrating well in a homogeneous BCH-domain is given by the superposed Theis' equation (2.18)

$$s(t) = \frac{q}{4\pi T}[E_1(u) - E_1(\beta^2 u)],$$

where s is the drawdown, q is the constant pumping rate and T is transmissivity. The dimensionless variable $u = \frac{a^2 S}{4tT}$ involves the radial distance of an observation well (OW) from the pumping well (PW) a, the storativity of the aquifer S, the elapsed time since pumping started t, and again T. The ratio $\beta = a_\mathrm{i}/a$ derives from applying the principle of superposition. The geometry underlying the superposed Theis' equation is given in Figure 2.2. As outlined in Section 2.3.2, the superposed Theis' equation reduces under steady-conditions to $s_\mathrm{m} = \frac{q}{2\pi T} \ln \beta$. Accordingly, the interpreted Hantush transmissivity is given by (2.19) [*Hantush*, 1959]

$$T_\mathrm{in}^\mathrm{Han} = \frac{q}{2\pi s_\mathrm{m}} \ln \beta,$$

where s_m is the steady-state drawdown at a particular OW. In order to emphasize that the Hantush transmissivity is obtained by applying an interpretation technique to the drawdown, the index $_\mathrm{in}$ is added.

Even though the application of Hantush's method presumes aquifer homogeneity, it is commonly used to estimate the transmissivity from the drawdown in heterogeneous systems. In order to illustrate the impact of applying Hantush's method to heterogeneous

aquifers, Figure 4.1 compares the true heterogeneous distribution of T (Figure 4.1a) to estimates of $T_{\text{in}}^{\text{Han}}$ (Figures 4.1b to d). Therefor, $T_{\text{in}}^{\text{Han}}$ was calculated from the steady-state drawdown of synthetically generated pumping tests, with the PW being located at various distances L from the BCH, in this particular domain (Figure 4.1a). That is, to estimate $T_{\text{in}}^{\text{Han}}$, every point in the domain is considered a potential OW. For details on the numerical setup please see Section 4.4.

From Figure 4.1, it is apparent that even under steady-state conditions $T_{\text{in}}^{\text{Han}}$ is dependent on the locations of the observation and pumping well, or, the local transmissivities in the surrounding of these wells, respectively. Moreover, the distance between the pumping well and the boundary L, seems to influence estimates of $T_{\text{in}}^{\text{Han}}$. In this regard, it is interesting to note that the location-dependence of $T_{\text{in}}^{\text{Han}}$ is in contrast to estimates of T obtained from interpreting the late-time drawdown in infinite domains by Theis-based interpretation techniques, like the Cooper-Jacob method [*Cooper and Jacob*, 1946] or the Continuous-Derivation method [*Copty et al.*, 2011], respectively. However, Figure 4.1 also shows that $T_{\text{in}}^{\text{Han}}$ appears to be related to the underlying heterogeneous transmissivity distribution.

Please note that besides estimating $T_{\text{in}}^{\text{Han}}$, the Hantush method also allows for the estimation of β and consequently L, as well as, for the estimation of storativity. It therefor

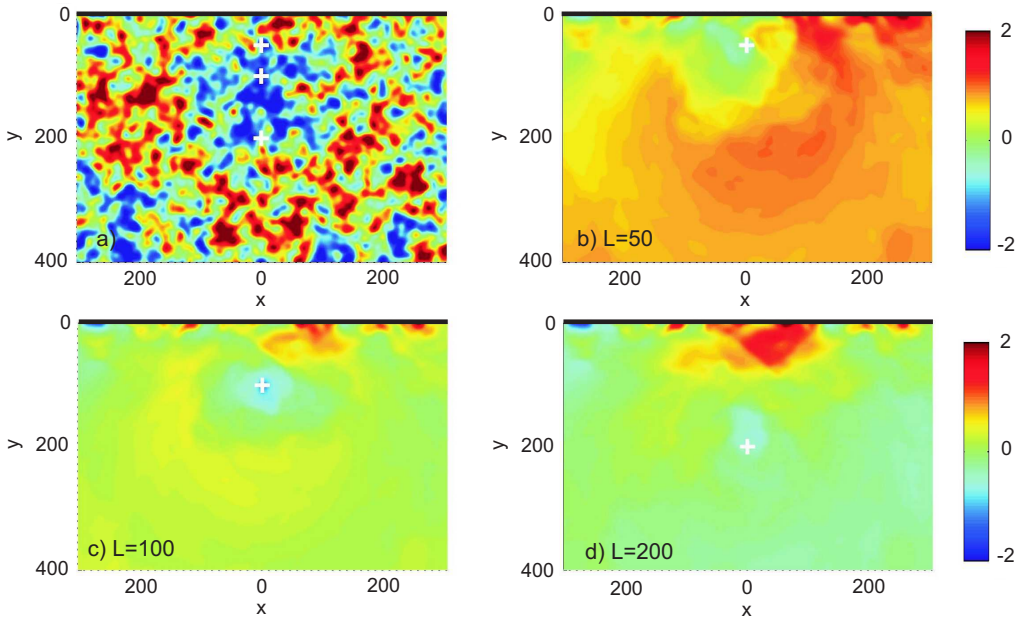

Figure 4.1: True heterogeneous distribution of T (a) compared to $T_{\text{in}}^{\text{Han}}$ (b to d), estimated from the simulated steady-state drawdown by means of Equation (2.19); for pumping at various locations in the heterogeneous BCH-domain presented in plot a. The BCH delimits the domain to the North in x-direction at y=0. T is depicted in terms of $\ln(T)$. Crosses indicate locations of the PW. Statistics of underlying transmissivity distribution are $\sigma_{\text{Y}}^2 = 1$, $l_{\text{Y}} = 10$ lu, $m_{\text{Y}} = 0$ ($T_{\text{G}} = 1$).

uses the slope of the transient drawdown at an inflection point which occurs as the BCH starts to affect the drawdown at an OW (Section 2.3.2). However, since the estimation of theses parameters involves transient drawdown data, they are not considered in this chapter, but will be discussed in Chapter 5.

4.3 Fréchet Kernel for Transmissivity in BCH-domains

4.3.1 Fréchet Kernel for Transmissivity

Analytic expressions of the Fréchet kernel for transmissivity in infinite domains F_{T}, were derived by *Knight and Kluitenberg* [2005] by using explicit Laplace transform inversions. For an observation well which does not coincide with the pumping well, F_{T} is given by

$$F_{\mathrm{T}}(\mathbf{x},\mathbf{x}',t) = -\frac{q(r^2-a^2/4)}{8\pi^2 T_0^2 D r_1 r_2 t}\exp\left(-\frac{r^2+a^2/4}{2Dt}\right)K_1\left(\frac{r_1 r_2}{2Dt}\right) \tag{4.1}$$

where D is the diffusivity defined by T_0/S_0, and $K_1(z)$ is the modified Bessel function of the second kind, of order one. Equation (4.1) relates to the geometry of a Cartesian coordinate system (Figure 4.2a) with the PW and the OW located at distances $a/2$ from its origin. For the case of single-well pumping tests where the OW coincides with the PW, (4.1) reduces to (3.8).

Starting from F_{T} in infinite domains, the Fréchet kernel for transmissivity in BCH-domains is derived by applying the principle of superposition. Therefor, an imaginary domain is introduced, i.e. the heterogeneous domain is mirrored along the BCH to obtain an extended infinite domain. The extended domain then consists of a real part accommodating the PW, the OW and the real heterogeneous T-field, and an imaginary part which accommodates the recharging imaginary well (IW) and the imaginary heterogeneous T-field. Figure 4.2b shows the geometry of the extended domain and relevant distances, for the case when the BCH delimits the real domain to the East (in y-direction at x=0). The corresponding distances are given by

$$\begin{aligned} R_1 &= \sqrt{(L+x')^2+y'^2}, \quad R_2 = \sqrt{(L-x')^2+y'^2}, \\ R_3 &= \sqrt{(x'-x)^2+(y'-y)^2}, \quad R_4 = \sqrt{(x'+x)^2+(y'-y)^2}. \end{aligned} \tag{4.2}$$

Accordingly, the Fréchet kernel for transmissivity in a BCH-domain can be expressed as the sum of four sub-signals/Fréchet kernels in the infinite extended domain. The corresponding Fréchet kernels in the infinite extended domain relate to the following sub-signals: (1) the pressure signal scattered by a real anomaly in T due to pumping at the PW and observing at the OW, (2) the pressure signal scattered by an imaginary anomaly in T due to pumping at the PW and observing at the OW, (3) the pressure signal scattered by a real anomaly in T due to recharging at the IW and observing at the OW, and, (4) the

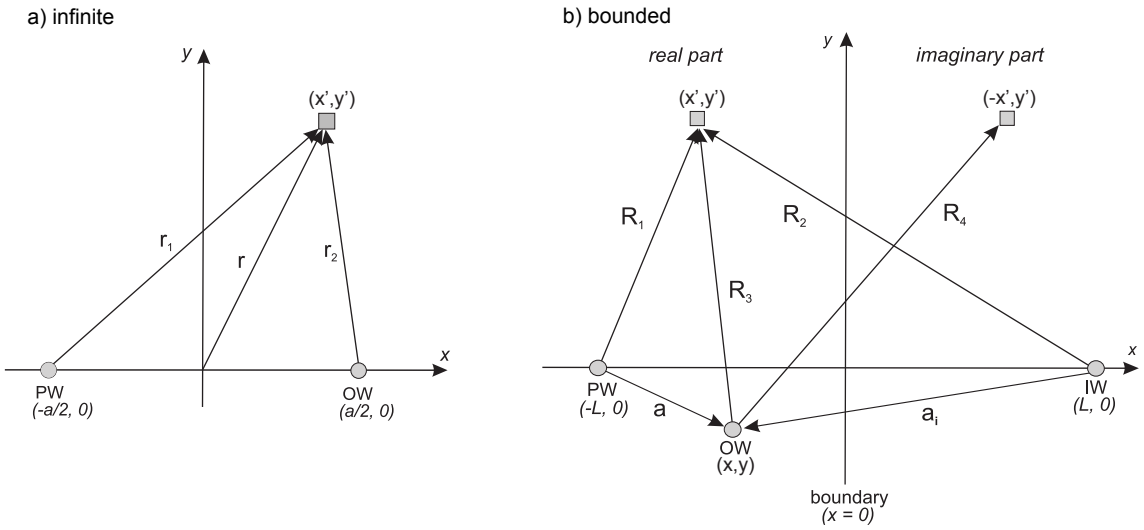

Figure 4.2: Geometry underlying the calculation of the Fréchet kernel in a) infinite and b) bounded domains. The Fréchet kernel is estimated at the location of the anomaly (x', y'). For the infinite case, PW and OW are separated by distance a; r, r_1 and r_2 are position vectors of the anomaly in T. For the bounded case, the y-axis coincides with the BCH, delimiting the real BCH-domain to the East. L is the shortest distance between BCH and PW or IW, respectively. Position vectors R_1 to R_4 are given by (4.2). Distances equivalent to r in the infinite domain are not depicted for the bounded case. These distances are calculated by the median line of the triangles which correspond to the four sub-signals described in the text. The corresponding triangles are aR_1R_3, aR_2R_4, $a_\mathrm{i}R_2R_3$ and $a_\mathrm{i}R_1R_4$.

pressure signal scattered by an imaginary anomaly in T due to recharging at the IW and observing at the OW.

Applying the principle of superposition as demonstrated yields the Fréchet kernel for transmissivity in BCH-domains, given by

$$\begin{aligned} F_\mathrm{T}^\mathrm{B}(\mathbf{x},\mathbf{x}',t) = -\frac{q}{16\pi^2 T_0^2 Dt}\Bigg[& \frac{R_1^2+R_3^2-a^2}{R_1R_3}\exp\left(-\frac{R_1^2+R_3^2}{4Dt}\right)K_1\left(\frac{R_1R_3}{2Dt}\right) \\ & +\frac{R_2^2+R_4^2-a^2}{R_2R_4}\exp\left(-\frac{R_2^2+R_4^2}{4Dt}\right)K_1\left(\frac{R_2R_4}{2Dt}\right) \\ & -\frac{R_2^2+R_3^2-a_i^2}{R_2R_3}\exp\left(-\frac{R_2^2+R_3^2}{4Dt}\right)K_1\left(\frac{R_2R_3}{2Dt}\right) \\ & -\frac{R_1^2+R_4^2-a_i^2}{R_1R_4}\exp\left(-\frac{R_1^2+R_4^2}{4Dt}\right)K_1\left(\frac{R_1R_4}{2Dt}\right)\Bigg]. \end{aligned} \tag{4.3}$$

For the special case of a single-well pumping test, when the OW coincides with the PW, Equation (4.3) reduces to

$$\begin{aligned} F_\mathrm{T}^\mathrm{B}(\mathbf{x},\mathbf{x}',t) = -\frac{q}{8\pi^2 T_0^2 Dt}\Bigg[& \exp\left(-\frac{R_1^2}{2Dt}\right)K_1\left(\frac{R_1^2}{2Dt}\right)+\exp\left(-\frac{R_2^2}{2Dt}\right)K_1\left(\frac{R_2^2}{2Dt}\right) \\ & -\frac{R_1^2+R_2^2-4L^2}{R_1R_2}\exp\left(-\frac{R_1^2+R_2^2}{4Dt}\right)K_1\left(\frac{R_1R_2}{2Dt}\right)\Bigg]. \end{aligned} \tag{4.4}$$

Under steady-state conditions, the Fréchet kernels can be further simplified by letting t approach infinity in the above equations. By making use of the Bessel function property $K_1(z) \sim z^{-1}$ for small z [*Abramowitz and Stegun*, 1964], it can be shown that $F_{\mathrm{T}}^{\mathrm{B}}$ as given by (4.3) approaches a fixed value, only dependent on the position of the T-anomaly,

$$F_{\mathrm{T}}^{\mathrm{B}}(\mathbf{x}, \mathbf{x}') \rightarrow \frac{qa^2}{8\pi^2 T_0^2} \frac{(R_1^2 R_3^2 + R_2^2 R_4^2) - \beta^2 (R_1^2 R_4^2 + R_2^2 R_3^2)}{R_1^2 R_2^2 R_3^2 R_4^2} \quad \text{as} \quad t \rightarrow \infty. \tag{4.5}$$

For the case of a single-well pumping test (4.4) reduces to

$$F_{\mathrm{T}}^{\mathrm{B}}(\mathbf{x}, \mathbf{x}') \rightarrow -\frac{qL^2}{\pi^2 T_0^2 R_1^2 R_2^2} \quad \text{as} \quad t \rightarrow \infty. \tag{4.6}$$

4.3.2 Properties of the Fréchet Kernel for Transmissivity

Properties of the Fréchet kernel for transmissivity in BCH-domains are discussed in this section. The focus is on the steady-state Fréchet kernel in BCH-domains $F_{\mathrm{T}}^{\mathrm{B}}(t \rightarrow \infty)$. Properties of the transient Fréchet kernels are discussed in Section 5.4, which also includes a comparison of $F_{\mathrm{T}}^{\mathrm{B}}$ and F_{T}.

Figure 4.3 depicts the spatial distribution of $F_{\mathrm{T}}^{\mathrm{B}}(t \rightarrow \infty)$ for various observation wells. Note that $F_{\mathrm{T}}^{\mathrm{B}}$ is depicted in terms of $\log_{10} |F_{\mathrm{T}}^{\mathrm{B}}|$ for reasons of better presentation. In general, anomalies in T located close to the BCH have larger weight than those located farther from the BCH, on the other side of the pumping well. For a single-well pumping test configuration (Figure 4.3a), $F_{\mathrm{T}}^{\mathrm{B}}$ is negative in the entire domain. That is, an anomaly in T with $T > T_0$ reduces the drawdown when compared to the drawdown in the homogeneous domain with $T = T_0$. On the contrary, an anomaly of $T < T_0$ increases the resulting drawdown. If the PW and the OW are not coinciding (Figure 4.3b to f), $F_{\mathrm{T}}^{\mathrm{B}}$ is positive within a circular-shaped region between the wells, and negative outside this region. For positive values of the Fréchet kernel, i.e, for an anomaly in T located between the OW and the PW, the above relations are reverse, with $T > T_0$ leading to an increased drawdown. Anomalies in T located on the circle, where the kernel changes from positive to negative, have minimal influence on the drawdown.

Symmetry for the spatial distribution of $F_{\mathrm{T}}^{B}(t \rightarrow \infty)$ is only given for particular configurations. If the OW is located on a line perpendicular to the BCH intersecting the PW, $F_{\mathrm{T}}^{\mathrm{B}}$ is symmetric with respect to this line (Figure 4.3b and d). If the OW is located on a line parallel to the BCH intersecting the PW, F_{T}^{B} is symmetric with respect to a line perpendicular to the BCH at $a/2$ (Figure 4.3c). For other pumping test configurations, the spatial distribution of $F_{\mathrm{T}}^{\mathrm{B}}$ is non-symmetric (Figure 4.3e and f). Furthermore, it can be seen that an anomaly located in the vicinity of the wells generally overshadows the impact of an anomaly farther from the wells. However, the magnitude of F_{T}^{B} is not only dependent on the location of an anomaly in T with respect to the PW and the OW, like in infinite domains, but depends additionally on its location with respect to the BCH.

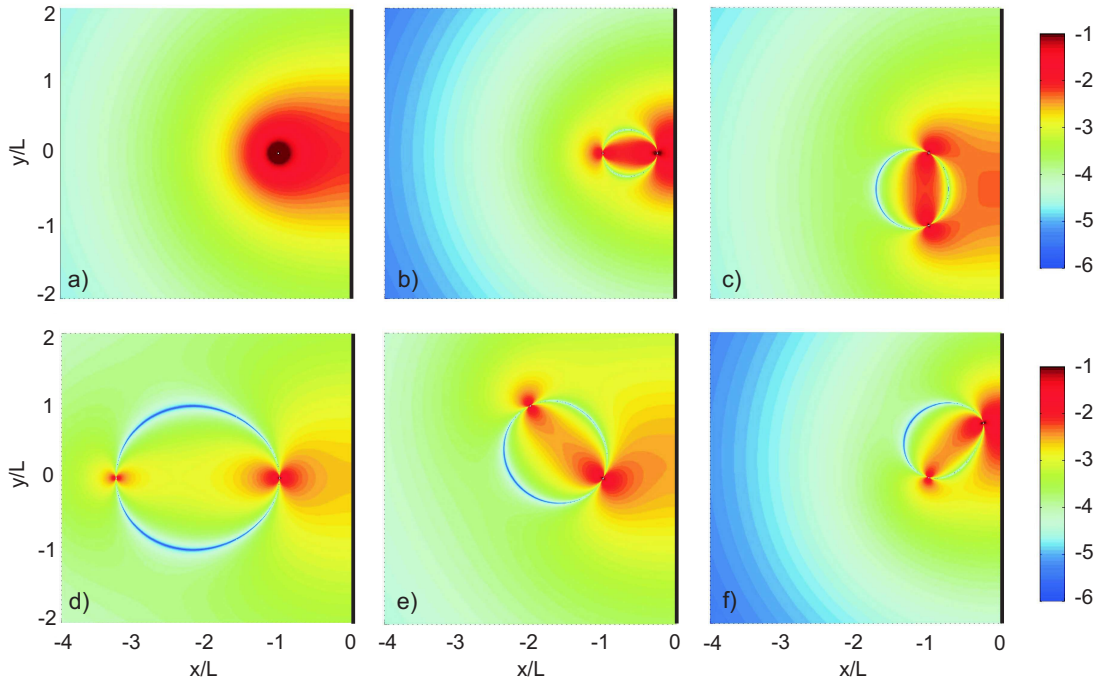

Figure 4.3: Contour plots of the steady-state Fréchet kernel in BCH-domains, $F_{\mathrm{T}}^{\mathrm{B}}$ $(t \to \infty)$, for selected OWs. Distances are normalized by L. The BCH is East of the PW (-1,0). $F_{\mathrm{T}}^{\mathrm{B}}$ is depicted in terms of $\log_{10}|F_{\mathrm{T}}^{\mathrm{B}}|$. For a) single-well pumping tests $F_{\mathrm{T}}^{\mathrm{B}}$ is negative in the entire domain. For b) to f) with OW≠PW, $F_{\mathrm{T}}^{\mathrm{B}}$ is positive inside a circular-shaped sub-domain between the OW and the PW, and negative outside.

4.3.3 Fréchet Kernels as Spatial Weights

In this section a spatial weighting function to approximate the transmissivity which solves the superposed Theis' equation (2.18) for the correct drawdown in the true heterogeneous BCH-domain is established. The transmissivity is considered to be spatially variable with uniform mean T_0 and fluctuations about the mean $\tilde{T}$ (2.26),

$$T(\mathbf{x}') = T_0 + \tilde{T}(\mathbf{x}').$$

Similarly, the storativity can be written as a summation of a uniform mean S_0 and a fluctuations term $\tilde{S}$.

Starting from a perturbation expansion, the hydraulic head at an observation point $\mathbf{x}$, resulting from pumping in a heterogeneous domain can be expressed by (2.27)

$$h(\mathbf{x},t) = h_0(\mathbf{x},t) + h_1(\mathbf{x},t) + h_2(\mathbf{x},t) + \dots .$$

Truncating the above equation after the first perturbation term, and substituting $h_1(\mathbf{x},t)$ by the Fréchet derivative (2.28) yields an approximation of $h(\mathbf{x},t)$, as discussed for infinite domains in Section 2.6. In order to account for groundwater flow to a well in a BCH-domain, the Fréchet kernels for infinite domains in Equation (2.29) are substituted by the

Fréchet kernels for BCH-domains, which yields

$$\begin{aligned} h(\mathbf{x},t) &= h_0(\mathbf{x},t) + h_1(\mathbf{x},t) \\ &= h_0(\mathbf{x},t) - \int \tilde{T}(\mathbf{x}')F_{\mathrm{T}}^{\mathrm{B}}(\mathbf{x},\mathbf{x}',t)\,d\mathbf{x}' - \int \tilde{S}(\mathbf{x}')F_{\mathrm{S}}^{\mathrm{B}}(\mathbf{x},\mathbf{x}',t)\,d\mathbf{x}'. \end{aligned} \tag{4.7}$$

Accordingly, $h_0(\mathbf{x},t)$ is the hydraulic head in the homogeneous domain characterized by S_0 and T_0, and, $h_1(\mathbf{x},t)$ relates to the first perturbation term which can be expressed by a spatial convolution integral in terms of the transmissivity and storativity fluctuations $\tilde{T}(\mathbf{x}')$ and $\tilde{S}(\mathbf{x}')$. The Fréchet kernels $F_{\mathrm{T}}^{\mathrm{B}}$ and $F_{\mathrm{S}}^{\mathrm{B}}$ are spatial weighting functions for the fluctuations in T and S. Physically, the above equation assumes that the PW emits a pressure signal which spreads out to be scattered by anomalies in T and S. However, as the perturbation expansion is truncated after the first perturbation term, the above equation has to be considered an approximation of $h(\mathbf{x},t)$, i.e., it assumes that second order scattering of the emitted pressure signal can be ignored.

The derivation of the spatial weighting function to approximate the transmissivity which solves the superposed Theis' equation for BCH-domains (2.18) follows the corresponding derivation for infinite domains as presented in Section 3.2.1. Thus, the aquifer is considered to be variable in T but uniform in S. Moreover, the equivalent transmissivity is defined by $T_{\mathrm{eq}}(\mathbf{x},t) = T_0 + \delta T_{\mathrm{eq}}(\mathbf{x},t)$, as given by (3.3). The resulting time-dependent spatial weighting function for the equivalent transmissivity in BCH-domains then reads

$$T_{\mathrm{eq}}^{\mathrm{FB}}(\mathbf{x},t) = \exp\left(\frac{\int F_{\mathrm{T}}^{\mathrm{B}}(\mathbf{x},\mathbf{x}',t)Y(\mathbf{x}')\,d\mathbf{x}'}{\int F_{\mathrm{T}}^{\mathrm{B}}(\mathbf{x},\mathbf{x}',t)\,d\mathbf{x}'}\right), \tag{4.8}$$

with index $^{\mathrm{FB}}$ indicating that the Fréchet kernel for BCH-domains is used as a spatial weight.

Under steady-state conditions, $F_{\mathrm{T}}^{\mathrm{B}}$ becomes independent of time, as given by Equations (4.5) and (4.6). Accordingly, the spatial weighting to approximate the equivalent transmissivity (4.8) can be simplified to

$$T_{\mathrm{eq}}^{\mathrm{FB}}(\mathbf{x},t\to\infty) = \exp\left(\frac{\int W(\mathbf{x},\mathbf{x}')Y(\mathbf{x})\,d\mathbf{x}'}{\int W(\mathbf{x},\mathbf{x}')\,d\mathbf{x}'}\right). \tag{4.9}$$

For the general case, when the OW and the PW are not coinciding, $W(\mathbf{x},\mathbf{x}')$ is given by

$$W(\mathbf{x},\mathbf{x}') = \frac{(R_1^2R_3^2 + R_2^2R_4^2) - \beta^2(R_1^2R_4^2 + R_2^2R_3^2)}{R_1^2R_2^2R_3^2R_4^2}, \tag{4.10}$$

which reduces for a single-well pumping test configuration to

$$W(\mathbf{x},\mathbf{x}') = (R_1R_2)^{-2}. \tag{4.11}$$

It it interesting to note that under steady-state conditions, the spatial weights are independent of T_0.

4.4 Numerical Application and Discussion

In this section the relation between the spatially weighted $T_{\mathrm{eq}}^{\mathrm{FB}}$ and $T_{\mathrm{in}}^{\mathrm{Han}}$ is investigated numerically. For that purpose, the transmissivity in the BCH-domain was modeled as multivariate Gaussian log-normally distributed spatial random function, $Y = \ln T$, with mean m_{Y}, variance σ_{Y}^2, and a Gaussian covariance model expressed by the correlation length l_{Y}. The Turning Bands Method [*Mantoglou and Wilson*, 1982] was used to generate spatially variable transmissivity fields. Since transmissivity is considered to be the most salient feature of natural aquifers, storativity was assumed uniform with $S_0 = 5 \cdot 10^{-4}$.

Under steady-state conditions, the area perturbed by pumping is considerably large in BCH-domains. Thus, a grid of 4001 by 2495 cells was selected to simulate steady-state pumping tests, which corresponds to a domain of $3.06 \cdot 10^5$ by $3 \cdot 10^5$ length units (lu). The domain consists of a heterogeneous sub-domain of 2901 by 1901 regularly spaced cells of 0.5 by 0.5 lu which is aligned with the center of the BCH. A transmissivity of $T_0 = T_{\mathrm{G}}$ was assigned to the rest of the domain which is non-regular and described by a vector which increases about 1.55% for each cell, starting at the edge of the heterogeneous sub-domain. A Dirichlet condition was imposed at all outer boundaries. Pumping tests with the pumped well located at various distances L from one constant head boundary were simulated using MODFLOW [*Harbaugh et al.*, 2000]. The distance between the pumped well and the BCH is commonly expressed by the ratio $\lambda = L/l_{\mathrm{Y}}$.

Preliminary simulations were performed to assure that the remaining outer boundaries do not impact the drawdown at considered observation wells. Thus, the numerical setup ensures that the impact of the remaining outer boundaries is negligible for OWs located within the heterogeneous sub-domain. The simulated drawdown was then interpreted by the Hantush method and evaluated by means of Monte Carlo simulations.

Fréchet kernels were evaluated on computational grids identical to the heterogeneous sub-domain. Related integrals were computed as discrete sum over the corresponding mesh.

4.4.1 Approximating the Hantush Transmissivity

The interpreted transmissivity $T_{\mathrm{in}}^{\mathrm{Han}}$ is estimated from the simulated drawdown in a heterogeneous domain by utilizing Hantush's method. It is recognized that Equation (2.19) directly relates $T_{\mathrm{in}}^{\mathrm{Han}}$ to the steady-state drawdown. Consequently, $T_{\mathrm{in}}^{\mathrm{Han}}$ is a homogeneous representation of the underlying heterogeneous transmissivity, which solves the direct problem along with S_0. This can also be verified numerically.

In order to examine the ability of the spatially weighted $T_{\mathrm{eq}}^{\mathrm{FB}}(t \to \infty)$ to approximate $T_{\mathrm{in}}^{\mathrm{Han}}$, Figure 4.4 compares both estimates by means of Monte Carlo simulations over ensembles of 200 realizations with variance $\sigma_{\mathrm{Y}}^2 = 1$ and $\lambda = 5$. Each plot refers to a different OW, as illustrated by the geometry-sketch, and provides the Pearson correlation coefficient

as a measure of agreement for the corresponding data. Pearson correlation coefficients for further Monte Carlo simulations over ensembles of varying σ_Y^2 and λ are presented in Table 4.1.

From Figure 4.4 and Table 4.1, it can be seen that the Fréchet kernel weighted transmissivity $T_{eq}^{FB}(t \to \infty)$ approximates the interpreted transmissivity T_{in}^{Han} well. For variances up to 1, correlation coefficients are generally > 0.9, whereas the correlation at some OWs decreases to about 0.87 for $\sigma_Y^2 = 2$. The decrease in correlation with increasing degree of heterogeneity is attributed to the pronounced impact of flow connectivity, which can not be captured by a spatial weighting, as discussed in the previous chapter for single-well pumping tests in infinite domains. Thus, T_{in}^{Han} which is estimated from head data is considered to comprise the effect of flow connectivity, whereas the spatially weighted T_{eq}^{FB} does not. Further examination of Figure 4.4 shows that even though the correlation

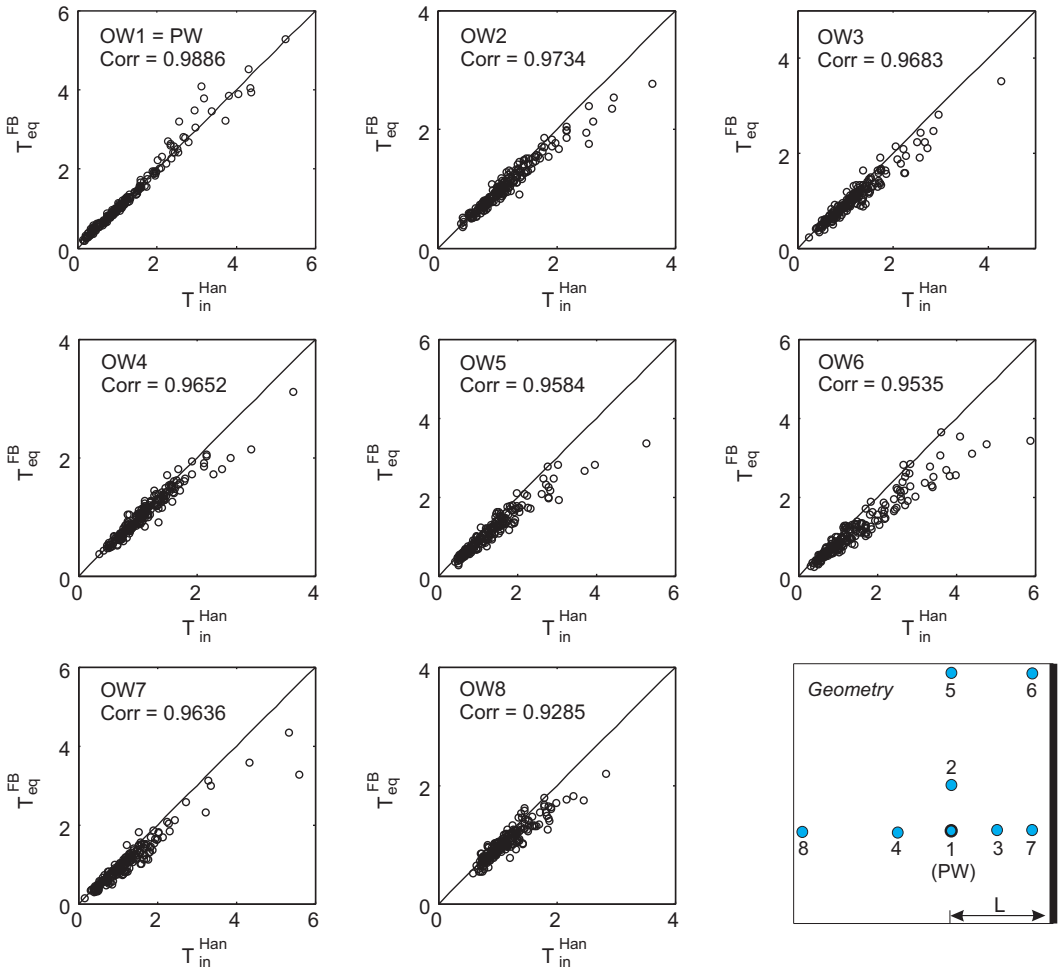

Figure 4.4: Comparison of the transmissivity estimated from the Hantush method T_{in}^{Han}, and the spatially weighted T_{eq}^{FB} (Equation 4.9), at eight OWs and for an ensemble of 200 realizations. Locations of considered OWs are illustrated in the geometry plot. The BCH is located East of the PW, $\lambda = 5$. Statistic parameters for the ensemble are $\sigma_Y^2 = 1$, $l_Y = 10$, $m_Y = 0$ ($T_G = 1$).

Table 4.1: Pearson correlation coefficients comparing $T_{\text{in}}^{\text{Han}}$ to $T_{\text{eq}}^{\text{FB}}$ under steady-state conditions for ensembles of 200 realizations. Locations of selected OWs are illustrated by the geometry plot in Figure 4.4. Mean and correlation length of all considered ensembles are equal to $m_{\text{Y}} = 0$ and $l_{\text{Y}} = 10$.

σ_{Y}^2	0.5		1	2	
λ	5	10	10	5	10
OW 1 = PW	0.9955	0.9928	0.9827	0.9668	0.9508
OW 2	0.9863	0.9773	0.9515	0.9504	0.8967
OW 3	0.9836	0.9766	0.9503	0.9430	0.8920
OW 4	0.9824	0.9697	0.9379	0.9341	0.8765
OW 5	0.9807	0.9804	0.9604	0.9259	0.9213
OW 6	0.9830	0.9815	0.9632	0.9672	0.9363
OW 7	0.9826	0.9719	0.9418	0.9221	0.8935
OW 8	0.9835	0.980	0.9613	0.9341	0.9246

is good, $T_{\text{eq}}^{\text{FB}}$ tends to underestimate $T_{\text{in}}^{\text{Han}}$, in particular for OWs farther from the PW, and, for transmissivity estimates that are much larger than T_0. This trend is attribute to the fact that $T_{\text{eq}}^{\text{FB}}$ constitutes an approximation in terms of a lowest order perturbation. The approximate character of $T_{\text{eq}}^{\text{FB}}$ and the impact of flow connectivity in BCH-domains is discussed in more detail in the following sections.

In summary, the good agreement between $T_{\text{in}}^{\text{Han}}$ and $T_{\text{eq}}^{\text{FB}}$ for heterogeneous systems with variances up to 2 implies that the geometric relations given by Equations (4.5) and (4.6) are a valid description for how Hantush's method renders the underlying heterogeneity. This implies that the Fréchet kernels for transmissivity specify the sub-domain which influences the drawdown (Figure 4.3). Moreover, the presented results show that it is not possible to generally estimate $T_{\text{G}} = T_{\text{efu}}$ from interpreting pumping test data by the Hantush method. Even though the range over which $T_{\text{in}}^{\text{Han}}$ scatters becomes more narrow for OWs farther from the PW and the BCH, respectively, $T_{\text{in}}^{\text{Han}}$ does not generally approach T_{G}, which is equal to 1 for all considered realizations in Figure 4.4.

In this regard, it has to be emphasized that the above relation, which states that the Theis-based interpreted transmissivity equals the equivalent homogeneous transmissivity, exclusively applies to steady-state conditions in BCH-domains. In infinite domains, Theis-based interpretation techniques which evaluate the transient late-time drawdown, like the Cooper-Jacob method [*Cooper and Jacob*, 1946] or the Continuous-Derivation method [*Copty et al.*, 2011], respectively, do not yield the equivalent homogeneous transmissivity. As discussed in Chapter 3, the corresponding interpreted transmissivity in infinite domains is considered to relate to an upscaled heterogeneous transmissivity field, which

corresponds to a spatial weighting by the time derivative of the Fréchet kernel. On the contrary, $T_{\text{in}}^{\text{Han}}$ relates to a spatial weighting by the Fréchet kernel itself. Note that the Hantush method uses the absolute drawdown to estimate T, whereas the Cooper-Jacob and the Continuous-Derivation method use the time derivative of the transient drawdown.

4.4.2 Ensemble Quantities of the Hantush Transmissivity

In order to describe groundwater flow within the framework of stochastic hydrogeology, ensemble quantities are often of interest. Thus, this section numerically evaluates the ensemble quantities $\left\langle T_{\text{in}}^{\text{Han}} \right\rangle$ and $\left\langle T_{\text{eq}}^{\text{FB}} \right\rangle$, with angular brackets denoting the arithmetic ensemble mean. The focus is on $\left\langle T_{\text{in}}^{\text{Han}} \right\rangle$, which is subsequently compared to $\left\langle T_{\text{eq}}^{\text{FB}} \right\rangle$.

Figure 4.5 shows $\left\langle T_{\text{in}}^{\text{Han}} \right\rangle$ for three ensembles of equal variance $\sigma_{\text{Y}}^2 = 0.5$, but varying in $\lambda = L/l_{\text{Y}}$. Figure 4.5a to c show the spatial distribution of $\left\langle T_{\text{in}}^{\text{Han}} \right\rangle$, which is symmetric with respect to a line perpendicular to the BCH intersecting the PW, located at $(0, -1)$. Therefore, just half of the BCH-domains are depicted. Figure 4.5d to g then show transects of $\left\langle T_{\text{in}}^{\text{Han}} \right\rangle$ as indicated by the arrows next to the corresponding $\left\langle T_{\text{in}}^{\text{Han}} \right\rangle$-fields. All distances are normalized by L. With regard to the numerical setup, the distance between the PW and the BCH was fixed at $L = 100$ lu, but correlation lengths of considered ensembles varied between 5 and 20 lu.

From Figure 4.5a to c it can be seen that λ influences $\left\langle T_{\text{in}}^{\text{Han}} \right\rangle$ considerably. That is, the effect of the BCH on $\left\langle T_{\text{in}}^{\text{Han}} \right\rangle$ is more pronounced for small λ than for large values of λ. If λ is small, $\left\langle T_{\text{in}}^{\text{Han}} \right\rangle$ exceeds the geometric mean of T considerably in the entire domain, being closest to T_{G} in the vicinity of the PW. For large values of λ the effect of the BCH on $\left\langle T_{\text{in}}^{\text{Han}} \right\rangle$ is much weaker, and $\left\langle T_{\text{in}}^{\text{Han}} \right\rangle$ is close to T_{G} in most of the domain. However, in a sub-domain between the PW and the BCH, $\left\langle T_{\text{in}}^{\text{Han}} \right\rangle$ approaches the arithmetic mean of transmissivity T_{A} at the BCH. This effect is attributed to the geometry of the flow regime, which is linear at the BCH, but approaches a more radially convergent flow regime with increasing distance form the BCH, or, with decreasing distance towards the PW, respectively.

In general, the results from Figure 4.5 agree with findings by *Riva et al.* [2001], *Tartakovsky et al.* [2002] and *Guadagnini and Riva* [2003], who state that ensemble quantities of T approach T_{G} if the domain size is large relative to the correlation scale, which corresponds in our case to large values of λ. Furthermore, *Riva et al.* [2001] found the influence of the constant head boundary to be restricted to a few correlation lengths which is also in agreement with the presented results. However, Figure 4.5a also shows that if the PW is located within a few correlation lengths from the BCH, the boundary affects $\left\langle T_{\text{in}}^{\text{Han}} \right\rangle$ in the entire domain, even for a small variance of 0.5 considered in this analysis. Moreover, *Riva et al.* [2001] state that the apparent transmissivity peaks at some distance. This behavior

can also be observed for $\langle T_{\text{in}}^{\text{Han}} \rangle$ as shown by Figure 4.5d. On a line perpendicular to the BCH intersecting the PW, the peak occurs at about -5y/L for $\lambda = 5$, at -3y/L for $\lambda = 10$, and at -2y/L for $\lambda = 20$, respectively. That is, the peak occurs on that line at about $20 l_{\text{Y}}$ from the PW, independent from λ. Behind the peak, $\langle T_{\text{in}}^{\text{Han}} \rangle$ decreases to a certain value above T_{G}, which depends again on λ. The larger λ, the closer $\langle T_{\text{in}}^{\text{Han}} \rangle$ to T_{G}.

With regard to the sub-domain between the PW and the BCH, it is interesting to note that $\langle T_{\text{in}}^{\text{Han}} \rangle$ exceeds T_{A} under certain conditions. In Figure 4.5a to c, areas with $\langle T_{\text{in}}^{\text{Han}} \rangle > T_{\text{A}}$ are indicated by a brownish color. Additional information on the magnitude of $\langle T_{\text{in}}^{\text{Han}} \rangle$ is provided by Figure 4.5d and e. It can be seen that if λ is large, $\langle T_{\text{in}}^{\text{Han}} \rangle$ at the

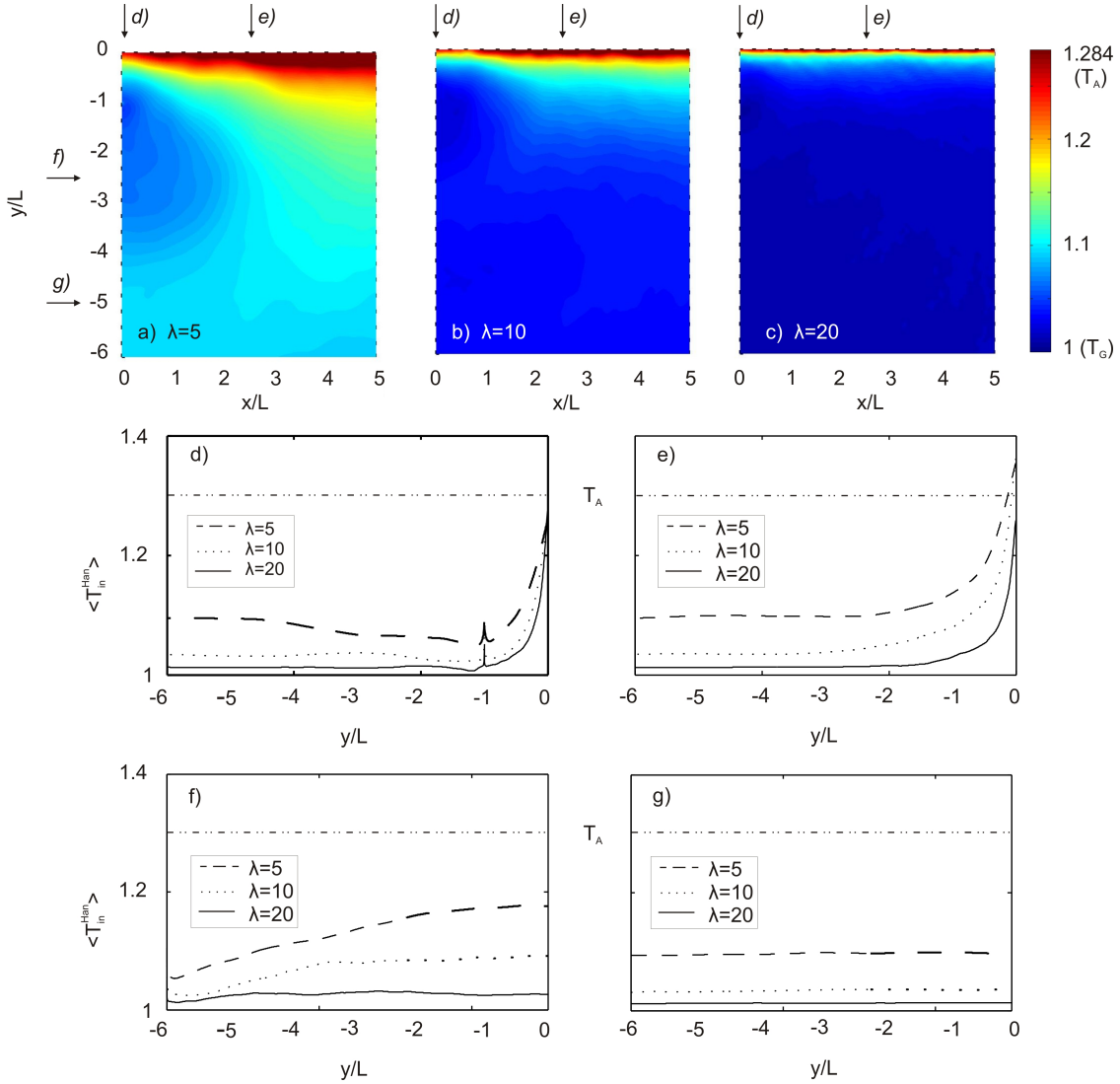

Figure 4.5: $\langle T_{\text{in}}^{\text{Han}} \rangle$-fields for different ensembles of varying λ (a to c), and, $\langle T_{\text{in}}^{\text{Han}} \rangle$ along several transects perpendicular (d, e) and parallel (f, g) to the BCH. Ensemble size is 1000. Distances are normalized by L. Parameters of the ensembles are $l_{\text{Y}} = 20, 10, 5$, thus, $\lambda = 5, 10, 20$; $\sigma_{\text{Y}}^2 = 0.5$, $m_{\text{Y}} = 0$ ($T_{\text{G}} = 1$) and $S_0 = 5 \cdot 10^{-4}$.

BCH approximates T_{A}, but increases above T_{A} as λ decreases. Moreover, the width of the corresponding wedge-shaped sub-domain where $\left\langle T_{\mathrm{in}}^{\mathrm{Han}}\right\rangle > T_{\mathrm{A}}$ increases with decreasing λ. On a line perpendicular to the BCH intersecting the PW, $\left\langle T_{\mathrm{in}}^{\mathrm{Han}}\right\rangle$ approaches T_A as an OW is closer to BCH (Figure 4.5d). However, if an OW is located farther from this line and close to BCH, $\left\langle T_{\mathrm{in}}^{\mathrm{Han}}\right\rangle$ exceeds T_{A} if λ is small (Figure 4.5e).

The observed effect of $\left\langle T_{\mathrm{in}}^{\mathrm{Han}}\right\rangle > T_{\mathrm{A}}$ is attributed to the impact of flow connectivity between the PW and the BCH, even though a proof can not be presented, since there is no technique available yet to quantify the impact of flow connectivity in BCH-domains. However, it seems reasonable that flow connectivity is more pronounced in domains of small λ, as the development of preferential flow paths between the PW and the BCH is more likely than in domains with large λ. For a PW which is well connected to the BCH, flow through preferential flow paths leads to a small drawdown, which in turn yields high transmissivity estimates. In that case, groundwater flow between the BCH and the PW is considered to be dominated by flow connectivity (Figure 4.5a, $\lambda = 5$). On the contrary, the probability of preferential flow paths between the PW and the BCH decreases as λ increases. For large values of λ, the flow connectivity between the PW and the BCH is almost negligible, as groundwater flow between both sources is not governed by preferential flow paths, but rather by some average value of the point transmissivities between the PW and the BCH. Consequently, $\left\langle T_{\mathrm{in}}^{\mathrm{Han}}\right\rangle$ does not exceed T_{A} at OWs in the vicinity of the BCH for large λ (Figure 4.5c, $\lambda = 20$).

Another interesting property of $\left\langle T_{\mathrm{in}}^{\mathrm{Han}}\right\rangle$ is the transmissivity at the PW or in its very close vicinity, respectively. From Figure 4.5d it can be seen that $\left\langle T_{\mathrm{in}}^{\mathrm{Han}}\right\rangle$ peaks at the PW. This peak is attributed to the enhanced sensitivity of the drawdown on the local transmissivity at the pumping well T_{PW} (Figure 4.3a). In infinite domains the equivalent homogeneous transmissivity at the PW is basically equal to T_{PW} as demonstrated by *Dagan and Lessoff* [2007a,b], and in Chapter 3. The arithmetic ensemble mean of T_{PW} thus equals T_{A}. However, in BCH-domains, $\langle T_{\mathrm{PW}}\rangle$ deviates from T_{A}, which is attributed to the pronounced sensitivity of the drawdown to the sub-domain between the PW and the BCH, as well as, to the the impact of flow connectivity between the PW and the BCH.

In order to compare $\left\langle T_{\mathrm{eq}}^{\mathrm{FB}}\right\rangle$ to $\left\langle T_{\mathrm{in}}^{\mathrm{Han}}\right\rangle$, Figure 4.6 shows $\left\langle T_{\mathrm{eq}}^{\mathrm{FB}}\right\rangle$-fields for a variance of 0.5 and different values of $\lambda = 5$ and 10, respectively, as well as $\left\langle T_{\mathrm{eq}}^{\mathrm{FB}}\right\rangle$ along a transect perpendicular to the BCH intersecting the PW. By comparing Figure 4.6 to Figure 4.5 it can be seen that $\left\langle T_{\mathrm{eq}}^{\mathrm{FB}}\right\rangle$ generally underestimated $\left\langle T_{\mathrm{in}}^{\mathrm{Han}}\right\rangle$, not reaching T_{A} at BCH. The tendency of $T_{\mathrm{eq}}^{\mathrm{FB}}$ to underestimate $T_{\mathrm{in}}^{\mathrm{Han}}$ is in agreement with findings from Figure 4.4, which already revealed its approximate character. However, both quantities exhibit a similar shape. Furthermore, the before mentioned peaks at about $20l_{\mathrm{Y}}$ from the PW can also be observed for $\left\langle T_{\mathrm{eq}}^{\mathrm{FB}}\right\rangle$, even though they occur slightly farther from the PW. The peak in the close vicinity of the PW also appears in a comparable magnitude for $\left\langle T_{\mathrm{eq}}^{\mathrm{FB}}\right\rangle$,

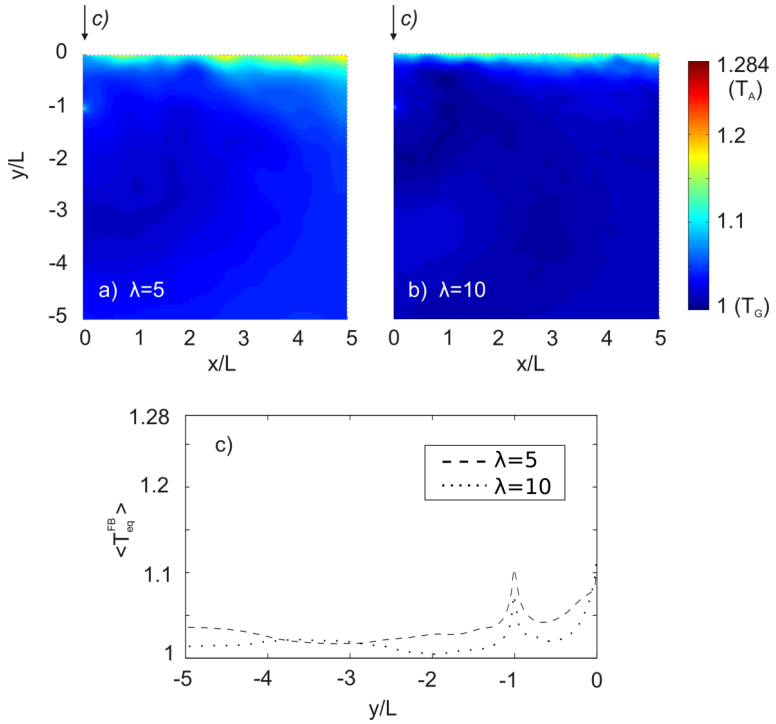

Figure 4.6: $\langle T_{\mathrm{eq}}^{\mathrm{FB}} \rangle$-fields for two values of λ , and, along a transect perpendicular to the BCH intersecting the PW. Ensemble size is 1000. Distances are normalized by L. Parameters of the ensembles are $\sigma_{\mathrm{Y}}^2 = 0.5$, $m_{\mathrm{Y}} = 0$ ($T_{\mathrm{G}} = 1$) and $S_0 = 5 \cdot 10^{-4}$.

though the width of the peak is more narrow for $\langle T_{\mathrm{in}}^{\mathrm{Han}} \rangle$.

In summary, both ensemble transmissivities exhibit comparable characteristics. Thus, the presented results show that $\langle T_{\mathrm{eq}}^{\mathrm{FB}} \rangle$ provides a reasonable approximation of $\langle T_{\mathrm{in}}^{\mathrm{Han}} \rangle$. However, $\langle T_{\mathrm{eq}}^{\mathrm{FB}} \rangle$ slightly underestimates $\langle T_{\mathrm{in}}^{\mathrm{Han}} \rangle$ as it is an approximation in terms of a lowest order perturbation, and does not account for the impact of flow connectivity. The impact of flow connectivity on T-estimates is more pronounced in BCH-domains than in infinite domains, due to the existence of multiple sources. Accordingly, the flow connectivity between the PW and the BCH can considerably affect T-estimates. This applies in particular to ensembles of small λ. In that case $\langle T_{\mathrm{in}}^{\mathrm{Han}} \rangle$ deviates from T_{G} in the entire domain, even exceeding T_{A} in the close vicinity of the BCH. With increasing λ, the impact of flow connectivity between the PW and the BCH decreases. For large values of $\lambda \geq 20$, the influence of flow connectivity between the PW and the BCH is almost negligible, with $\langle T_{\mathrm{in}}^{\mathrm{Han}} \rangle \approx T_{\mathrm{G}}$ in most of the domain.

4.4.3 Implications for Pumping Test Interpretation

By considering the transmissivity as log-normally distributed spatial random function, the aim of pumping test interpretation is to estimate hydraulic parameters which describe the underlying heterogeneity by means of their statistic properties. In infinite domains, the interpretation of pumping tests by, e.g., the Cooper-Jacob method [*Cooper and Jacob*, 1946] or the Continuous-Derivation method [*Copty et al.*, 2011], respectively, allows to estimate the geometric mean of the underlying transmissivity distribution $T_{\mathrm{G}} = T_{\mathrm{efu}}$ from the

transient late-time drawdown, irrespective of the location of the observation well [*Sanchez-Vila et al.*, 1999b; *Copty and Findikakis*, 2004]. In BCH-domains, the Hantush method [*Hantush*, 1959] does not generally yield an estimate of T_G from interpreting the drawdown at an arbitrary observation well. However, since Figure 4.5 reveals that $\langle T_{in}^{Han} \rangle$ approaches T_G in systems with $\lambda \geq 20$, the question arises whether T_{in}^{Han} possibly approaches T_G for a single realization as well.

In this regard, Figure 4.7 compares statistics of T_{in}^{Han} for ensembles of variances 0.5 and 1, with $\lambda = 5$ and 20. Statistics are shown for 8 OWs, including OW=PW (OW1), at which the directions of the OWs with respect to the PW are illustrated by the geometry plot in Figure 4.4. For better comparability distances of the OWs from the PW and the BCH, respectively, are normalized by l_Y. Accordingly, OWs 2 to 4 illustrate the variability of T_{in}^{Han} at $a/l_Y = 2.5$ from the PW, and OWs 5 and 8 relate to observations at $a/l_Y = 25$. For OWs 6 and 7, the perpendicular distance between the OW and the BCH, d, is fixed to $d/l_Y = 1.5$.

From Figure 4.7 it can be seen that the variability of T_{in}^{Han} generally decreases as λ increases. Thus, for large values of λ, T_{in}^{Han} might be used to approximate T_G if the OW is located behind the PW and far from the BCH, or, at a sufficient normalized distance from the PW, respectively. However, even under such conditions T_{in}^{Han} has to be regarded as

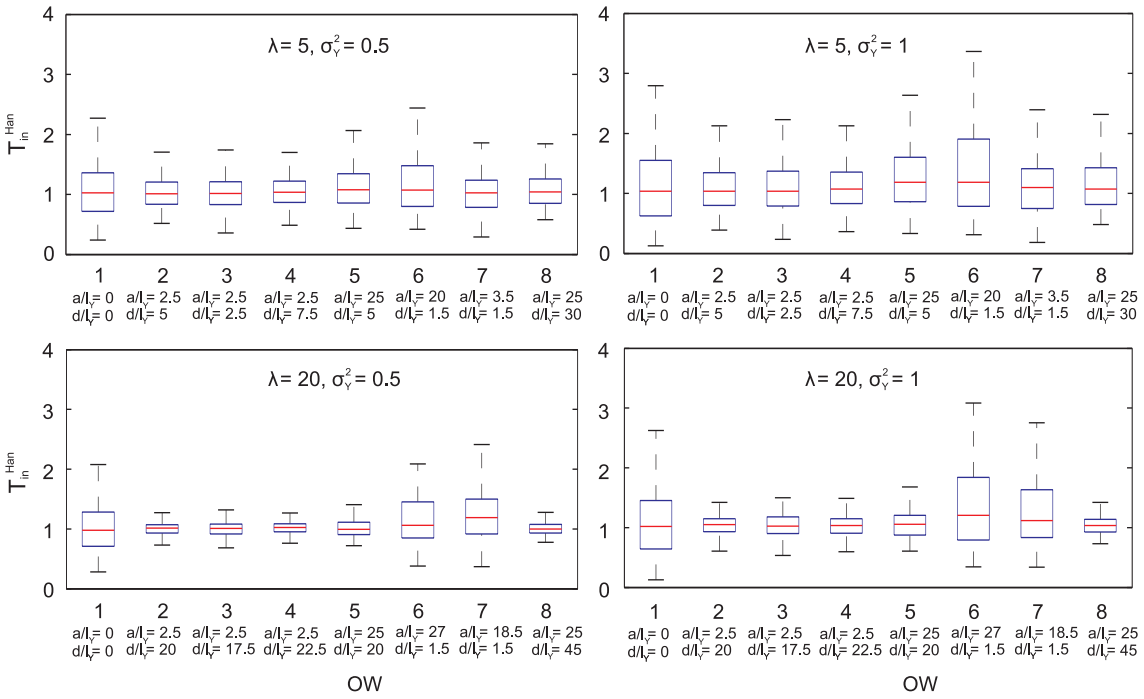

Figure 4.7: Statistics of T_{in}^{Han} at different observation wells, for ensembles varying in $\lambda = L/l_Y$ and variance σ_Y^2. Directions of considered OWs are illustrated by the geometry plot in Figure 4.4. Locations of OWs are described by a and d, normalized by l_Y. Ensemble size is 200, $m_Y = 0$ ($T_G = 1$).

an approximation, not matching T_G exactly. Not surprisingly, the accuracy of $T_{in}^{Han} \approx T_G$ increases as the degree of heterogeneity decreases. However, estimates of T_{in}^{Han} obtained by interpreting the drawdown at an observation well close to a source, i.e., close to the BCH or at the PW, respectively, should not be used to approximate T_G, irrespective of λ.

4.5 Conclusions

Natural aquifers are intrinsically heterogeneous with regard to their hydraulic parameters transmissivity and storativity. The interpretation of pumping tests is an established technique to estimate aquifer parameters. In infinite aquifers, the impact of aquifer heterogeneity on the interpretation of pumping tests has been extensively studied. However, studies which investigate the impact of heterogeneity on the drawdown in the presence of an infinite linear constant head boundary (BCH) are rare, even though the characterization of such aquifers is of considerable interest, for example, regarding the description of coastal reservoirs.

The Hantush method [*Hantush*, 1959] is widely used to evaluate drawdown data from BCH-domains. Since the Hantush method relies on Theis' equation, it presumes aquifer homogeneity. Applying the Hantush method to drawdown data from heterogeneous BCH-domains yields an interpreted transmissivity denoted T_{in}^{Han} which is location dependent, and satisfies the superposed Theis equation for the correct drawdown in the true heterogeneous domain. However, how T_{in}^{Han} relates to the underlying heterogeneity is not clear.

In order to improve the understanding of T_{in}^{Han} in heterogeneous systems, the Fréchet kernel for transmissivity for BCH-domains was derived and its properties were discussed, with particular emphasis on steady-state conditions. Subsequently, the Fréchet kernel for BCH-domains was used within a spatial weighting to estimate the equivalent homogeneous transmissivity T_{eq}^{FB}, which was compared to T_{in}^{Han} by means of Monte Carlo simulations in log-normally distributed transmissivity fields. The findings from this work can be summarized as follows:

1. The Fréchet kernel for transmissivity for BCH-domains allows for a description of sub-domains to which the steady-state drawdown at a particular observation well is most sensitive too. Using the steady-state Fréchet kernel as spatial weight allows for approximating T_{in}^{Han}, as given by Equations (4.9) to (4.11).

2. The flow connectivity between the pumping well and the BCH has significant impact on estimated parameters in the entire domain. If flow connectivity is large, which correlates with a small λ, $\langle T_{in}^{Han} \rangle$ does even exceed the arithmetic mean of the transmissivity distribution T_A, in a wedge-shaped sub-domain in the vicinity of the BCH. As λ increases, the impact of flow connectivity between the pumping well and the BCH decreases. If λ exceeds about 15 to 20, the impact of flow connectivity is almost negligible, with $\langle T_{in}^{Han} \rangle$

approaching T_A at the BCH. The influence of the BCH is then restricted to a rather narrow sub-domain of a few correlation lengths in the vicinity of the BCH.

3. Provided that λ is large, i.e., exceeding about 20, T_{in}^{Han} can potentially be used to approximate T_G from an observation well sufficiently far from the BCH and the pumping well, respectively, even from a single realization. However, in practice, observation wells are often located relatively close to the pumping well which would cast some doubt on the meaning of the interpreted transmissivity T_{in}^{Han} relative to the underlying heterogeneity.

4. Regarding the relation between T_{in}^{Han} and the underlying heterogeneity of the aquifer, the meaning of the interpreted transmissivity T_{in}^{Han} is basically different from the meaning of the interpreted transmissivity estimated from the late-time drawdown in infinite domains, by utilizing the Copper-Jacob method [*Cooper and Jacob*, 1946] or the Continuous-Derivation method [*Copty et al.*, 2011], respectively. Corresponding late-time estimates are independent form the location of the observation well, and relate to an upscaled heterogeneous transmissivity field. On the contrary, T_{in}^{Han} depends on the location of the observation well, and relates to an upscaled homogeneous transmissivity.

Please note that the focus of the study at hand is on investigating the conceptual understanding of the interpreted transmissivity in heterogeneous BCH-domains. It does therefore not consider the influence of well effects on the drawdown, like well-bore storage and skin.

Chapter 5

Evaluating Transient Pumping Tests in Heterogeneous Aquifers in the Presence of a Linear Constant Head Boundary

5.1 Introduction

The estimation of hydraulic parameters from pumping tests is commonly performed by pumping test interpretation methods which rely on Theis' equation [*Theis*, 1935]. Thus, investigated aquifers are treated as homogeneous during the interpretation process, even though natural aquifers are intrinsically heterogeneous. In order to clarify the relation of Theis-based interpreted hydraulic parameters to the underlying heterogeneity, Chapters 3 and 4 investigate the meaning of Theis-based estimates under transient conditions in infinite domains, and, under steady-state conditions in the presence of an infinite linear constant head boundary (BCH). For that purpose, spatial weighting functions were derived which allow for relating the interpreted hydraulic parameters to the underlying heterogeneity. The spatial weighting functions are based on the Fréchet kernels for transmissivity, and were applied to heterogeneous log-normally distributed transmissivity fields. These investigations revealed that when estimated from the transient drawdown in infinite domains, the interpreted transmissivity relates to an upscaled heterogeneous transmissivity, described by the time derivative of the corresponding Fréchet kernel. On the contrary, steady-state estimates of the interpreted transmissivity in BCH-domains relate to an upscaled homogeneous transmissivity, described by the corresponding Fréchet kernel. Moreover, the upscaled transmissivities basically reproduce the main features of the interpreted transmissivities.

Pumping test interpretation in infinite heterogeneous domains, e.g., by the Cooper-Jacob method [*Cooper and Jacob*, 1946] or the Continuous-Derivation method [*Copty et al.*, 2011] respectively, can yield the geometric mean of the transmissivity distribution T_{G}, irrespective form the location of the observation well [e.g., *Sanchez-Vila et al.*, 1999b; *Copty and Findikakis*, 2004; *Wu et al.*, 2005; *Sanchez-Vila et al.*, 2006; *Copty et al.*, 2011]. Furthermore, as the Continuous-Derivation method allows for estimating time-dependent interpreted hydraulic parameters, the local transmissivity at the pumping well T_{PW} can be potentially obtained from the very early drawdown at the pumped well [*Copty et al.*, 2011]. The interpreted storativity is considered to provide subsequent information on the underlying heterogeneity, in terms of an indicator for flow connectivity [e.g., *Meier et al.*, 1998; *Sanchez-Vila et al.*, 1999b; *Knudby and Carrera*, 2005; *Trinchero et al.*, 2008]. Moreover, it can yield information on how the transmissivity at the pumping well relates to the overall transmissivity of the aquifer.

Estimating hydraulic parameters from drawdown data in BCH-domains is currently restricted to the interpretation of the steady-state drawdown by the Hantush method [*Hantush*, 1959]. Even though investigations in Chapter 4 improved the evaluation of the Hantush transmissivity $T_{\mathrm{in}}^{\mathrm{Han}}$, by providing a description of the sub-domain to which the drawdown is most sensitive too, it also showed that overall features of the underlying heterogeneity, e.g. the geometric mean T_{G}, are not easily accessible. In fact, the interpretation in BCH-domains is more complicated, as the impact of flow connectivity between the pumping well and the BCH has to be considered. However, if flow connectivity between the pumping well and the BCH is weak, $T_{\mathrm{in}}^{\mathrm{Han}}$ may be used to approximate T_{G}, if the observation well is sufficiently far from BCH and PW, respectively. Moreover, whether the interpreted storativity in BCH-domains may include information on flow connectivity has not been the scope of investigations yet.

Because groundwater flow and contaminant transport are strongly influenced by the heterogeneity of the aquifer, developing efficient techniques for pumping test interpretation is highly desirable. This applies in particular to BCH-domains, since the characterization of coastal aquifers gains in importance, e.g., with regard to the impact of seawater intrusions. In this regard, this chapter proposes a pumping test interpretation method to evaluate transient drawdown data in BCH-domains, thus releasing the restriction of interpreting the steady-state drawdown for considering the entire time domain of the pumping test for the estimation of hydraulic parameters. For that purpose, the Continuous-Derivation method for infinite domains [*Copty et al.*, 2011] is extended for an application to BCH-domains. Subsequently, the meaning of time-dependent estimates of transmissivity and storativity, is investigated by means of Fréchet kernels [e.g., *Oliver*, 1990, 1993; *Knight and Kluitenberg*, 2005]. Finally, the proposed interpretation method is applied to synthetically generated pumping test data. Accordingly, benefits and limitations are discussed.

5.2 Mathematical Derivation

We consider transient two dimensional groundwater flow towards a fully penetrating well in a heterogeneous confined aquifer which is bounded by an infinite linear constant head boundary (BCH). The BCH delimits the aquifer over its entire thickness.

By considering the Theis equation [*Theis*, 1935] along with the principle of superposition [e.g. *Ferris et al.*, 1962; *Bear*, 1972; *Kruseman et al.*, 1990], the transient drawdown for a fully penetrating well in a homogeneous confined aquifer, unilaterally delimited by a BCH, is given by the superposed Theis' equation (2.18)

$$s(t) = \frac{q}{4\pi T}[E_1(u) - E_1(\beta^2 u)]$$

where s is the drawdown, q is the constant pumping rate and T is transmissivity, i.e. the hydraulic conductivity integrated over the depth of the aquifer. The non-dimensional quantity $u = \frac{a^2 S}{4tT}$ involves the distance of an observation well (OW) from the pumping well (PW) a, the storativity of the aquifer S, the elapsed time since pumping started t, and, again T. $E_1(z)$ is the exponential integral function. The ratio $\beta = a_i/a$ derives from applying the principle of superposition with a_i referring to the distance between the OW and the imaginary recharging well (IW). The geometry underlying the superposed Theis' equation is given in Figure 2.2.

In order to obtain time-dependent estimates of the interpreted transmissivity and storativity we follow *Copty et al.* [2011] by taking the derivative of the superposed Theis equation (2.18) with respect to the natural logarithm of time,

$$\frac{\partial s}{\partial \ln t} = \frac{q}{4\pi T}[\exp(-u) - \exp(-\beta^2 u)]. \tag{5.1}$$

Taking the ratio of the superposed Theis equation (2.18) and (5.1) yields

$$\gamma_{\text{bch}} = \frac{s}{\partial s/\partial \ln t} = \frac{E_1(u) - E_1(\beta^2 u)}{\exp(-u) - \exp(-\beta^2 u)}. \tag{5.2}$$

A plot of γ_{bch} as a function of the dimensionless time $1/u$ and for different values of β is given in Figure 5.1. Additionally, Figure 5.1 shows γ for infinite domains (2.15), which is independent from the location of the observation well. For observation wells far from the BCH and the PW, or, very close to the BCH, respectively, $\beta \to 1$. In that case, γ_{bch} approaches a straight line with a slope of unity, when plotted as function of $1/u$ on log-log scale. If the pumping well and the observation well are coinciding, $\beta \to \infty$. Accordingly, the second terms in the nominator and denominator on the right hand side of (5.2) approach zero, and $\gamma_{\text{bch}} \to \gamma$. That is, the effect of the BCH on the drawdown at OW=PW is virtually negligible. However, for realistic values of β, γ_{bch} matches γ during early times, when the drawdown is not influenced by the BCH. Once the drawdown at an

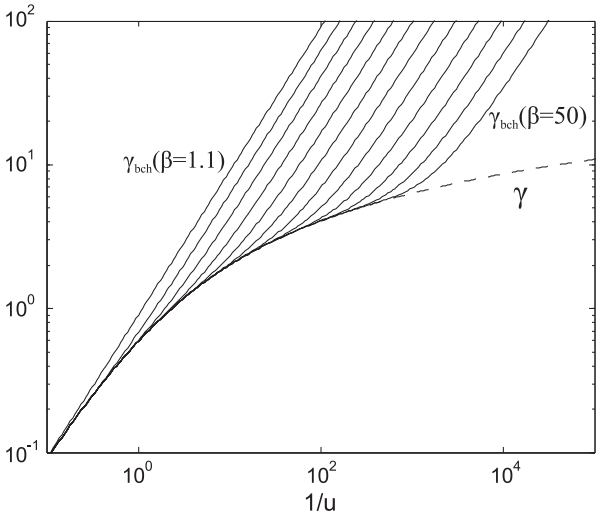

Figure 5.1: Plot of γ_{bch} as a function of the dimensionless time $1/u$ (solid) for different values of β between 1.1 and 50, and, compared to γ in an infinite domain (dashed).

OW is affected by the BCH, γ_{bch} starts to deviate from γ, quickly approaching a straight line.

Provided that β is known, a function of γ_{bch} can be computed from (5.2) for every OW. Utilizing the ratio of the drawdown and its time derivative then allows for estimating u for any particular value of $\gamma_{\mathrm{bch}} = \frac{s}{\partial s/\partial \ln t}$, which we denote u_γ. Subsequently, the interpreted transmissivity $T_{\mathrm{in}}^{\mathrm{CD}}$ and storativity $S_{\mathrm{in}}^{\mathrm{CD}}$ are computed from (5.3) and (5.4), and the definition of u_γ, respectively.

$$T_{\mathrm{in}}^{\mathrm{CD}}(t) = \frac{Q}{4\pi s(t)}[E_1(u_\gamma) - E_1(\beta^2 u_\gamma)] \tag{5.3}$$

$$S_{\mathrm{in}}^{\mathrm{CD}}(t) = \frac{4tT_{\mathrm{in}}^{\mathrm{CD}}u_\gamma}{a^2} \tag{5.4}$$

Equations (5.2) to (5.4) provide a simple and fast way to obtain time-dependent estimates of flow parameters from the ratio of the drawdown to the drawdown derivative. However, note that the definition of $S_{\mathrm{in}}^{\mathrm{CD}}$ in (5.4) is equal to the corresponding definition in an infinite domain (2.16). $S_{\mathrm{in}}^{\mathrm{CD}}$ is related to the drawdown by means of $T_{\mathrm{in}}^{\mathrm{CD}}$ and u_γ, though not directly.

Within the context of extending the Continuous-Derivation method to BCH-domains, a corresponding approach for a potential application to domains delimited by an infinite linear no-flow boundary has also been investigated. The corresponding derivation basically follows the above procedure, but starts from the superposed Theis equation which considers the presence of a no-flow boundary, $s(t) = \frac{q}{4\pi T}[E_1(u) + E_1(\beta^2 u)]$. The resulting γ_{bnf} is presented in Figure 5.2. From Figure 5.2 it can be seen that γ_{bnf} is not necessarily monotonically increasing, in particular, if β is larger than about 12. Thus, an unique estimation of u_γ is not provided for OWs with $\beta > 12$. This limits the applicability of the Continuous-Derivation method to such systems. Moreover, γ_{bnf} approaches γ as $\beta \to 1$.

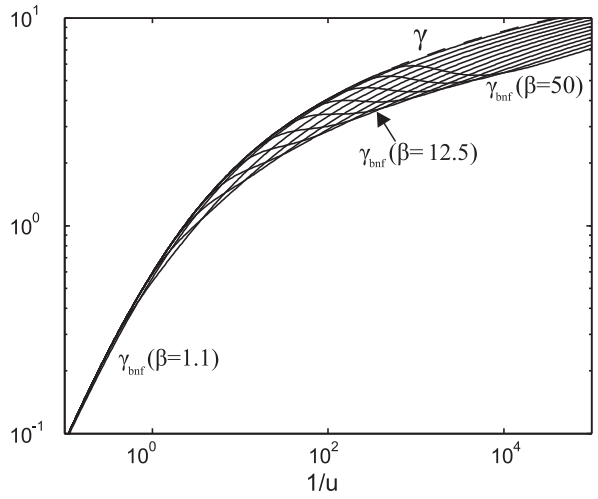

Figure 5.2: Plot of γ_{bnf} as a function of the dimensionless time $1/u$ (solid) for different values of β between 1.1 and 50, and, compared to γ in an infinite domain (dashed).

5.3 Relation to Hantush's Method

This section examines how interpreted hydraulic parameters estimated by the Hantush method [*Hantush*, 1959] relate to corresponding estimates from the Continuous-Derivation method for BCH-domains. As the time since pumping started approaches infinity u approaches 0, with t being proportional to $1/u$. For small values of u, the exponential integral function is given by $E_1(u) = -\ln(u) - \varepsilon$, where $\varepsilon = 0.57721...$ is the Euler constant [*Abramowitz and Stegun*, 1964]. Using this property, it can be shown that $T_{\mathrm{in}}^{\mathrm{CD}}$ in (5.3) reduces under steady-state conditions to

$$T_{\mathrm{in}}^{\mathrm{CD}}(t \to \infty) = \frac{q}{2\pi s_{\mathrm{m}}} \ln \beta, \tag{5.5}$$

with s_{m} being the maximum drawdown at an observation well. Equation (5.5) is equivalent to (2.19), the equation provided by *Hantush* [1959]. Thus, $T_{\mathrm{in}}^{\mathrm{CD}}(t \to \infty) = T_{\mathrm{in}}^{\mathrm{Han}}$, provided that L is known. This includes that $T_{\mathrm{in}}^{\mathrm{CD}}(t \to \infty)$ relates to an upscaled homogeneous transmissivity. Consequently, $T_{\mathrm{in}}^{\mathrm{CD}}(t \to \infty)$ is dependent on the location of the observation well, as demonstrated for $T_{\mathrm{in}}^{\mathrm{Han}}$ in the previous chapter.

The Hantush method further allows for the estimation of β or L, and the interpreted storativity $S_{\mathrm{in}}^{\mathrm{Han}}$, respectively. It therefore uses the drawdown derivative at an inflection point of the transient drawdown in the homogeneous medium, which occurs due to the influence of the BCH at time t_{ip}. To estimate the time t_{ip}, the Hantush method uses the drawdown slope over the transient drawdown period, which is commonly determined graphically [*Kruseman et al.*, 1990]. In order to illustrate the effect of aquifer heterogeneity on the transient drawdown and its time derivative, Figure 5.3 shows s and $\partial s / \partial \ln t$ recorded at OW=PW for 50 realizations of a heterogeneous medium with $\sigma_{\mathrm{Y}}^2 = 1$. Additionally, s and $\partial s / \partial \ln t$ in the homogeneous domain with $T = T_{\mathrm{G}}$ are given by bold lines. From Figure 5.3 it can be seen that aquifer heterogeneity considerably influences the drawdown

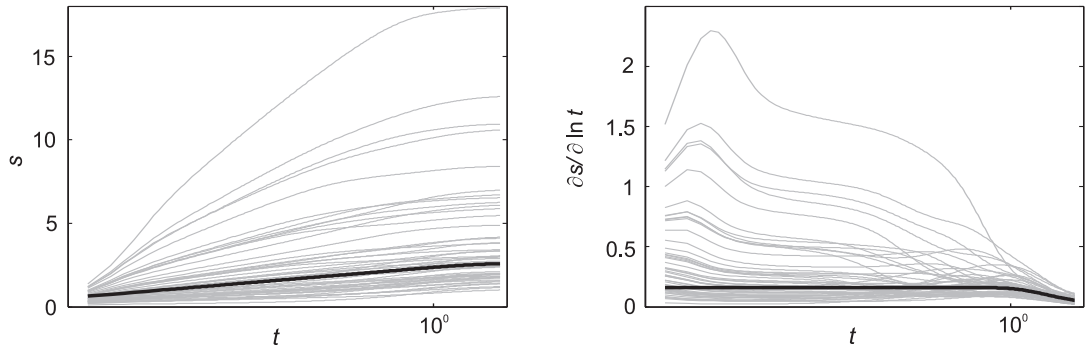

Figure 5.3: Simulated drawdown s and its time derivative $\partial s/\partial \ln t$ as functions of time, for 50 pumping tests in heterogeneous BCH-domains (grey). The drawdown is recorded at OW=PW, and compared to the corresponding data from a homogeneous BCH-domain with $T_0 = T_\mathrm{G}$ (black). Statistical parameters of the ensemble are $\sigma_\mathrm{Y}^2 = 1$, $l_\mathrm{Y} = 8$ and $m_\mathrm{Y} = 0$ ($T_\mathrm{G} = 1$). The distance between the PW and the BCH is $L = 10 l_\mathrm{Y}$.

and its time derivative, and consequently the estimation of t_ip. For detailed information on the numerical setup, please see Section 5.5.

As a result, for realizations considered in Figure 5.3, Hantush estimates of L vary between 9 length units (lu) and $1.21 \cdot 10^3$ lu, whereas the real distance between the PW and the BCH is $L = 80$ lu. Repeating computations for an OW located at $L/2$ from the PW opposite of the BCH, yields estimates of L varying between 46 and 141 lu. Thus, Figure 5.3 sends out a sign of caution when estimating L from drawdown data in heterogeneous aquifers by the Hantush method.

Regarding the estimation of the interpreted storativity, the Hantush method uses $T_\mathrm{in}^\mathrm{Han}$ and t_ip to estimate the storativity by $S_\mathrm{in}^\mathrm{Han} = \frac{4 t_\mathrm{ip} T_\mathrm{in}^\mathrm{Han} u_\mathrm{ip}}{a^2}$ (2.21), where $u_\mathrm{ip} = 2 \ln \beta / (\beta^2 - 1)$ again relies on the Hantush estimate of L. Thus, the Hantush method combines drawdown data from transient and steady-state conditions to estimate β and $S_\mathrm{in}^\mathrm{Han}$. Moreover, $T_\mathrm{in}^\mathrm{Han}$ is not necessarily a reliable representation of the overall reservoir transmissivity, as discussed in the previous chapter. In this regard, Hantush estimates of β and $S_\mathrm{in}^\mathrm{Han}$ are somehow ambiguous, when inferred from heterogeneous aquifers. The estimation of $S_\mathrm{in}^\mathrm{CD}$ is regarded more rigorous, as it does not combine drawdown data from different pumping times.

5.4 Sensitivity of the Drawdown

Fréchet kernels, which can be regarded as a measure for how an anomaly in T influences the drawdown at a particular observation well, are used to examine the sensitivity of the drawdown to a heterogeneous transmissivity distribution. The corresponding equations have already been discussed in previous chapters and are state again briefly. For pumping a well at a constant rate in an infinite domain, the Fréchet kernel for transmissivity is given

by Equation (4.1) [*Knight and Kluitenberg*, 2005]

$$F_{\mathrm{T}}(\mathbf{x},\mathbf{x}',t) = -\frac{q(r^2-a^2/4)}{8\pi^2 DT_0^2 r_1 r_2 t}\exp\left(-\frac{(r^2+a^2/4)}{2DT}\right)K_1\left(\frac{r_1 r_2}{2DT}\right)$$

with distances relating to a Cartesian coordinate system as shown in Figure 4.2a, diffusivity D being defined by $D = T_0/S_0$, and, K_1 the modified Bessel function of the second kind, of order one. For a BCH-domain, the corresponding Fréchet kernel is given by Equation (4.3)

$$\begin{aligned} F_{\mathrm{T}}^{\mathrm{B}}(\mathbf{x},\mathbf{x}',t) = -\frac{q}{16\pi^2 T_0^2 Dt}\Bigg[& \frac{R_1^2+R_3^2-a^2}{R_1R_3}\exp\left(-\frac{R_1^2+R_3^2}{4Dt}\right)K_1\left(\frac{R_1R_3}{2Dt}\right) \\ & +\frac{R_2^2+R_4^2-a^2}{R_2R_4}\exp\left(-\frac{R_2^2+R_4^2}{4Dt}\right)K_1\left(\frac{R_2R_4}{2Dt}\right) \\ & -\frac{R_2^2+R_3^2-a_i^2}{R_2R_3}\exp\left(-\frac{R_2^2+R_3^2}{4Dt}\right)K_1\left(\frac{R_2R_3}{2Dt}\right) \\ & -\frac{R_1^2+R_4^2-a_i^2}{R_1R_4}\exp\left(-\frac{R_1^2+R_4^2}{4Dt}\right)K_1\left(\frac{R_1R_4}{2Dt}\right)\Bigg] \end{aligned}$$

with distances according to Figure 4.2b. In order to illustrate the sensitivity of the drawdown with respect to heterogeneity, this section compares the Fréchet kernel in BCH-domains $F_{\mathrm{T}}^{\mathrm{B}}$ to its counterpart in infinite domains F_{T}.

The influence of particular anomalies in T on the drawdown at the pumping well (OW=PW) is exemplified in Figure 5.4. Each plot depicts $F_{\mathrm{T}}^{\mathrm{B}}$ for three selected anomalies at equal distances from OW=PW but in different directions, i.e., at different distances from the IW. In addition, Figure 5.4 shows the corresponding Fréchet kernels for infinite domains F_{T}, which are solely a function of the distance between OW=PW and the anomaly. From Figure 5.4, it can be seen that for early pumping times $F_{\mathrm{T}}^{\mathrm{B}}$ equals F_{T} in an infinite

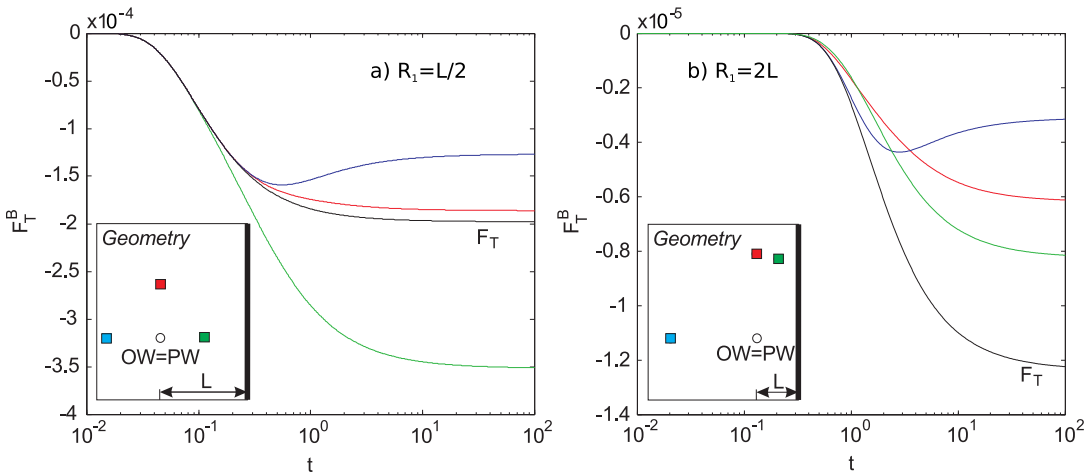

Figure 5.4: Fréchet kernel for infinite domains F_{T}, compared to the Fréchet kernel for BCH-domains $F_{\mathrm{T}}^{\mathrm{B}}$, for selected anomalies at equal distances of a) $L/2$ and b) $2L$ from OW=PW. Geometry plots illustrate locations of considered anomalies, with the BCH located East of the PW.

domain. The farther an anomaly in T from OW=PW and the closer it is to the boundary, the shorter this period. As pumping continues, $F_{\mathrm{T}}^{\mathrm{B}}$ starts to deviate from F_{T}, with the deviation occurring later the farther an anomaly form the BCH or the IW, respectively. Furthermore, by considering the given geometry with the BCH East of the PW at $x = 0$ (Figure 4.2b), $F_{\mathrm{T}}^{\mathrm{B}}$ is monotonically increasing if the anomaly is located at $x > -L$. For anomalies at $x < -L$, $F_{\mathrm{T}}^{\mathrm{B}}$ peaks at a particular time, characteristic for every anomaly, before decreasing to a constant value under steady-state conditions.

Figures 5.5 to 5.7 examine the spatial distribution of F_{T} in infinite domains (plots a to c) and $F_{\mathrm{T}}^{\mathrm{B}}$ in BCH-domains (plots d to f), for observations at different wells at selected times, including steady-state conditions. Additionally, Figures 5.5 to 5.7 show the ratio $F_{\mathrm{T}}^{\mathrm{B}}/F_{\mathrm{T}}$ (plots g to i) to illustrate the area where deviations between F_{T} and $F_{\mathrm{T}}^{\mathrm{B}}$ are most pronounced. In general, Figures 5.5 to 5.7 show that for very early pumping times (t=0.1), the magnitudes of F_{T} and $F_{\mathrm{T}}^{\mathrm{B}}$ are equal, indicated by a ratio of $F_{\mathrm{T}}^{\mathrm{B}}/F_{\mathrm{T}}$=1. That is, the drawdown at a particular observation is not affected by the BCH during very early times, which was already concluded from the discussion on γ_{bch} in Section 5.2. With continuous pumping $F_{\mathrm{T}}^{\mathrm{B}}$ in the vicinity of the BCH generally exceeds F_{T}.

For a single-well pumping test configuration, Figure 5.5 shows that F_{T} and $F_{\mathrm{T}}^{\mathrm{B}}$ are most pronounced in the vicinity of OW=PW. Regarding the ratio $F_{\mathrm{T}}^{\mathrm{B}}/F_{\mathrm{T}}$, anomalies in T located between OW=PW and the BCH gain pronounced impact on the drawdown in the BCH-domain as pumping continuous (Figure 5.5i). Anomalies in the rest of the domain show a weaker impact on the drawdown if the domain is bounded. However, since the absolute magnitudes of $F_{\mathrm{T}}^{\mathrm{B}}$ within the sub-domain of pronounced sensitivity is considerably smaller than $F_{\mathrm{T}}^{\mathrm{B}}$ in the vicinity of OW=PW, the impact of the corresponding anomalies on the drawdown is rather weak. Thus, for single-well pumping tests in BCH-domains, the drawdown is most sensitive to the local transmissivity in the direct vicinity of the well T_{PW}, even under steady-state conditions.

Figure 5.6 shows the kernels and their ratio for an OW located between the PW and the BCH. In the infinite domain, F_{T} is most pronounced at the wells, though much smaller than for the case of OW=PW. The spatial distribution of the kernels is characterized by a circle which intersects both wells. Inside this circle the kernels are positive, and negative outside. For very early times F_{T} and $F_{\mathrm{T}}^{\mathrm{B}}$ are equal, with $F_{\mathrm{T}}^{\mathrm{B}}/F_{\mathrm{T}} = 1$. As pumping continues, $F_{\mathrm{T}}^{\mathrm{B}}$ starts to exceed F_{T} in a sub-domain between the wells, the BCH and the mentioned circle. Interestingly, as $t \to \infty$, $F_{\mathrm{T}}^{\mathrm{B}}$ in the close vicinity of the OW even exceeds $F_{\mathrm{T}}^{\mathrm{B}}$ in the vicinity of the PW (Figure 5.6f). That is, the local transmissivity in the vicinity of the OW has a more pronounced impact on the corresponding drawdown than T_{PW}. This is contrary to F_{T} in infinite domains, where the local transmissivities in the vicinity of the OW and the PW influence the drawdown at the OW by equal parts (Figure 5.6c). Furthermore, the magnitude of $F_{\mathrm{T}}^{\mathrm{B}}$ exceeds F_{T} significantly in a quite narrow sub-domain

between the OW, the PW and the BCH (Figure 5.6i). Since the magnitude of F_T^B in this sub-domain does not deviate much from F_T^B in the vicinity of the PW, anomalies in T located within this sub-domain have pronounced influence on the drawdown at the OW. Moreover, the sensitivity for anomalies behind the wells is generally small. For anomalies on the circle, where F_T^B and F_T change from positive to negative, the ratio F_T^B/F_T also deviates significantly from 1. However, as F_T^B for these anomalies is generally small, their impact on the drawdown is negligible.

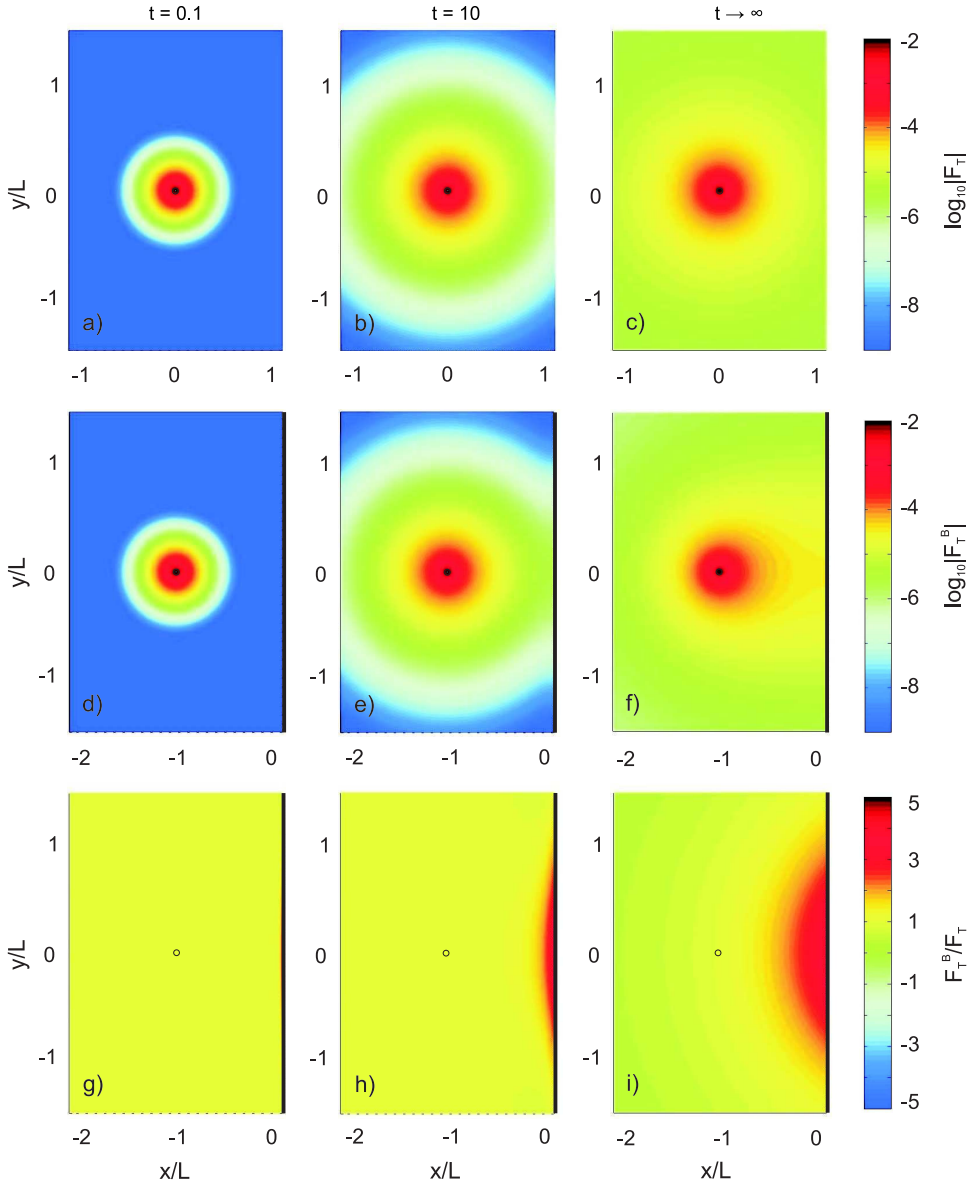

Figure 5.5: Comparison of the spatial distribution of the Fréchet kernels in infinite domains F_T (a to c) and bounded domains F_T^B (d to f), for a single-well pumping test with OW=PW, at different times. The Fréchet kernels are depicted in terms of $\log_{10}|F|$. Plots g to i show the ratio F_T^B/F_T. The BCH is East of the PW, which is indicated by a circle. Distances are normalized by L.

Figure 5.7 now shows the spatial distribution of the kernels and their ratio for an OW located behind the PW, opposite of the BCH. Considering the unbounded case, the local transmissivities in the vicinity of the wells influence the drawdown at the OW again by equal parts (Figure 5.7a to c). With regard to the bounded case, the PW is now closer to the BCH. Thus, $F_{\mathrm{T}}^{\mathrm{B}}$ in the vicinity of the PW exceeds $F_{\mathrm{T}}^{\mathrm{B}}$ in the vicinity of the OW as pumping continues, yet just slightly (Figure 5.7f). The ratio $F_{\mathrm{T}}^{\mathrm{B}}/F_{\mathrm{T}}$ shows that deviations

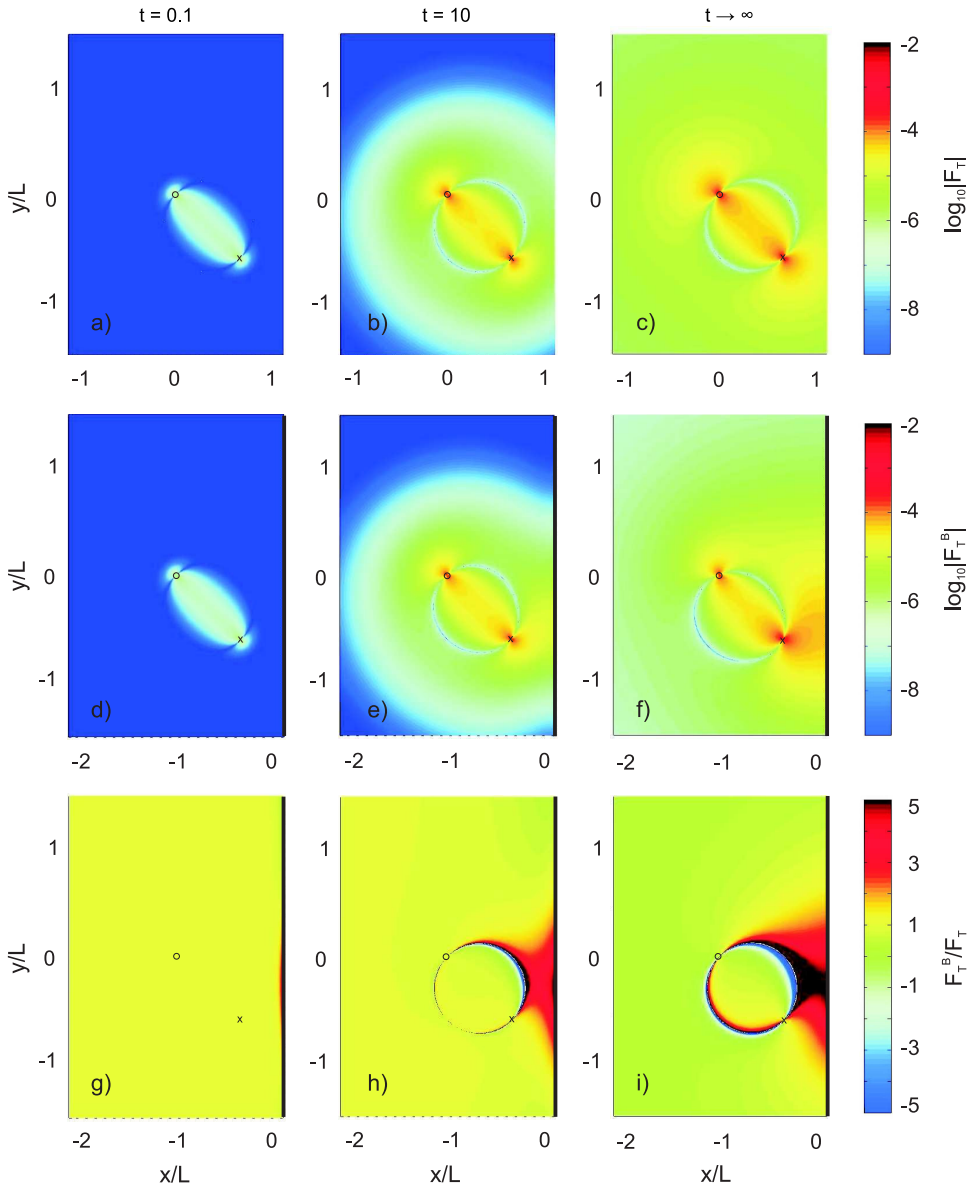

Figure 5.6: Comparison of the spatial distribution of the Fréchet kernels in infinite domains F_{T} (a to c) and bounded domains $F_{\mathrm{T}}^{\mathrm{B}}$ (d to f), for observations at an OW located between the PW and the BCH, at different times. The Fréchet kernels are depicted in terms of $\log_{10}|F|$. Plots g to i show the ratio $F_{\mathrm{T}}^{\mathrm{B}}/F_{\mathrm{T}}$. The BCH is East of the PW, which is indicated a circle. The location of the OW is marked by a cross. Distances are normalized by L.

between both kernels are again most pronounced in a sub-domain between the OW, the PW and the BCH, though, deviations are smaller than for the case of an OW located close to the BCH. Moreover, the corresponding sub-domain is considerably larger if the OW is located behind the PW. For anomalies located behind the OW, $F_{\mathrm{T}}^{\mathrm{B}}/F_{\mathrm{T}} < 1$. Consequently, the drawdown at the OW is most sensitive to the local transmissivities at the wells, at which the influence of T_{PW} slightly prevails, and, some average of the point transmissivities in

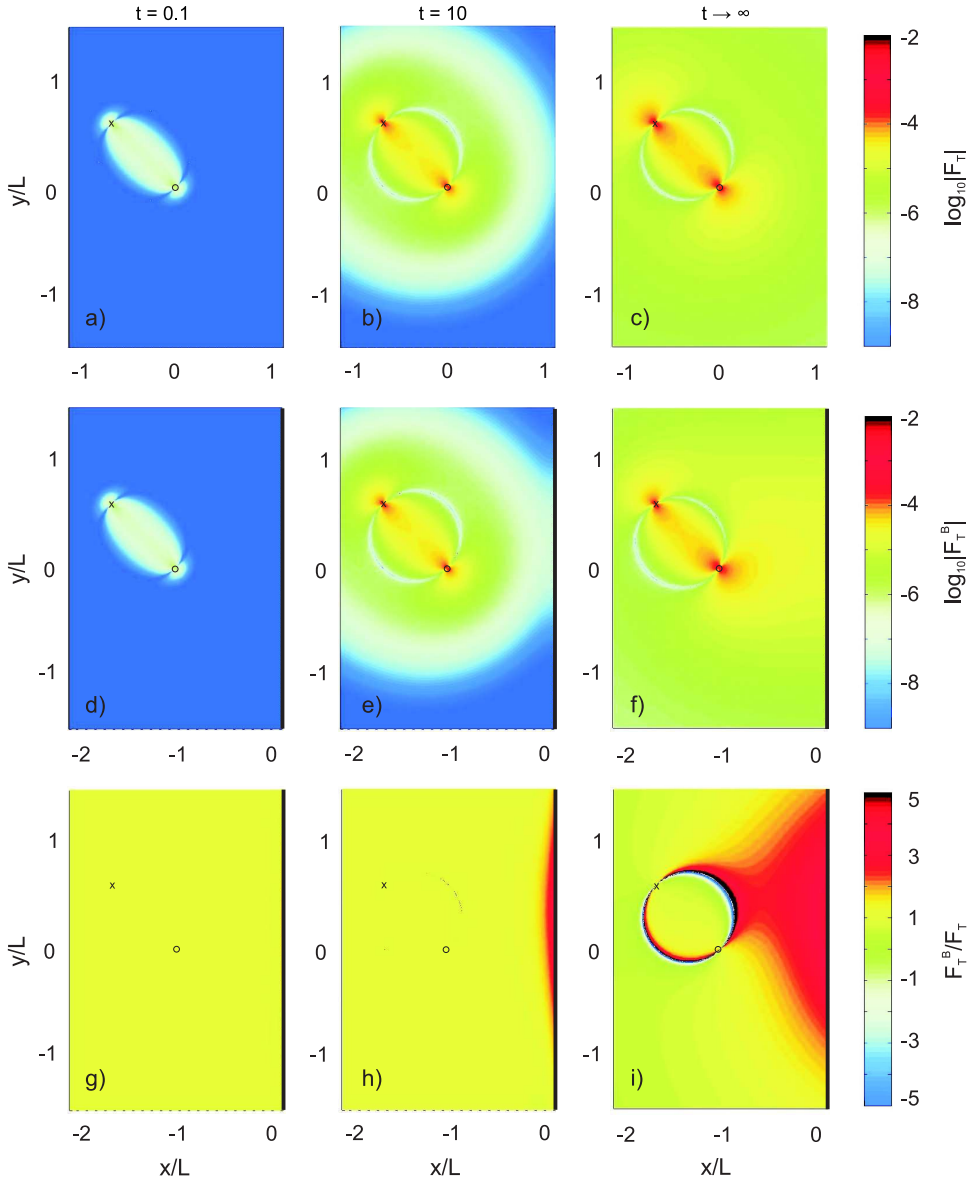

Figure 5.7: Comparison of the spatial distribution of the Fréchet kernels in infinite domains F_{T} (a to c) and bounded domains $F_{\mathrm{T}}^{\mathrm{B}}$ (d to f), for observations at an OW located behind the PW, opposite of the BCH, at different times. Fréchet kernels are depicted in terms of $\log_{10}|F|$. Plots g to i show the ratio $F_{\mathrm{T}}^{\mathrm{B}}/F_{\mathrm{T}}$. The BCH is East of the PW, with a circle indicating PW. The location of the OW is marked by a cross. Distances are normalized by L.

the sub-domain where $F_{\mathrm{T}}^{\mathrm{B}}/F_{\mathrm{T}} > 1$.

In summary, the above discussion illustrates some important characteristics of BCH-domains: (1) During early pumping times the existence of the BCH does not affect the drawdown at an observation well. (2) After the BCH is affecting, the drawdown at an OW is basically sensitive to the local transmissivities at the OW and the PW, and, to a sub-domain located between the wells and the BCH. With regard to the local transmissivities at the wells, the transmissivity at the well which is closest to the BCH prevails. Regarding the sub-domain of pronounced sensitivity between the wells and the BCH, the closer an OW to BCH, the more narrow this sub-domain becomes, and, the more pronounced the impact of this sub-domain on the drawdown at the OW. (3) Under steady-state conditions, the sensitivity of the drawdown at the OW to point transmissivities located behind the OW and the PW, opposite of the BCH, is almost negligible.

5.5 Estimating Time-Dependent Hydraulic Parameters

In this section the meaning of transient estimates of $T_{\mathrm{in}}^{\mathrm{CD}}$ and $S_{\mathrm{in}}^{\mathrm{CD}}$ is investigated numerically. Since the transmissivity is considered to be the most salient characteristic of natural aquifers, numerical investigations consider the transmissivity to be spatially variable, and storativity to be uniform, equal to $S_0 = 5 \cdot 10^{-4}$. The transmissivity was modeled as multivariate Gaussian log-normally distributed spatial random function, $Y = \ln T$, with mean m_{Y}, variance σ_{Y}^2, and a Gaussian covariance model expressed by the correlation length l_{Y}. The Turning Bands Method [*Mantoglou and Wilson*, 1982] was used to generate heterogeneous transmissivity fields.

Transient pumping tests were simulated in a domain of 481 by 481 lengths units with uniformly spaced cells of 0.2 by 0.2 lu. A Dirichlet condition was imposed at all outer boundaries. Pumping tests, with the pumped well located at various distances from one outer boundary, were simulated using MODFLOW [*Harbaugh et al.*, 2000]. Preliminary simulations were performed to assure that the remaining outer boundaries do not impact the drawdown at considered observation wells. The numerical setup ensures that the impact of the remaining outer boundaries on the drawdown is negligible for OWs located within an area of about 1.5 L from the PW. The simulated drawdown was interpreted by means of the Continuous-Derivation method for BCH-domains.

5.5.1 Interpreted Transmissivity

Since $T_{\mathrm{in}}^{\mathrm{CD}}(t \to \infty) = T_{\mathrm{in}}^{\mathrm{Han}}$, as demonstrated in Section 5.3, steady-state estimates of $T_{\mathrm{in}}^{\mathrm{CD}}$ are understood in terms of an upscaled homogeneous transmissivity, i.e., they solve the superposed Theis equation (2.18) along with S_0 for the correct drawdown in the true

heterogeneous domain. Thus, the question arises whether transient estimates of $T_{\text{in}}^{\text{CD}}$ in BCH-domains also relate to an upscaled homogeneous transmissivity. The discussions on γ_{bch} and the Fréchet kernels already indicate that the early-time drawdown is unaffected by the BCH. Consequently, it is suggested that the meaning of early-time estimates of $T_{\text{in}}^{\text{CD}}$ in BCH-domains agrees with the meaning of $T_{\text{in}}^{\text{CD}}$-estimates in infinite domains. In this regard, it is recalled that in infinite domains, transient estimates of $T_{\text{in}}^{\text{CD}}$ relate to an upscaled heterogeneous transmissivity, whereas steady-state estimates in BCH-domains relate to an upscaled homogeneous transmissivity. However, in order to check the meaning of time-dependent estimates of $T_{\text{in}}^{\text{CD}}$ in BCH-domains, it seems reasonable to interpret transient drawdown data from a BCH-domain by means of the Continuous-Derivation method for infinite domains.

Figure 5.8 shows $T_{\text{in}}^{\text{CD}}$ as a function of time estimated from the simulated drawdown in three heterogeneous realizations of BCH-domains, at (a) OW=PW and (b) an observation well which is located at $L/2$ from the PW. Solid lines show $T_{\text{in}}^{\text{CD}}$ estimated by the Continuous-Derivation method for BCH-domains; dashed lines refer to $T_{\text{in}}^{\text{CD}}$ estimated from the same drawdown by the Continuous-Derivation method for infinite domains. It can be seen that during early pumping times, when the BCH does not affect the drawdown, both methods yield equal results, starting to deviate as the BCH is felt at the observation well. After the BCH affects the drawdown, $T_{\text{in}}^{\text{CD}}$ estimated by the Continuous-Derivation method for BCH-domains stabilizes rather quickly at the homogeneous transmissivity under steady-state conditions, whereas $T_{\text{in}}^{\text{CD}}$ estimated by the Continuous-Derivation method for infinite domains increases steeply.

Consequently, two different flow periods have to be distinguished when interpreting

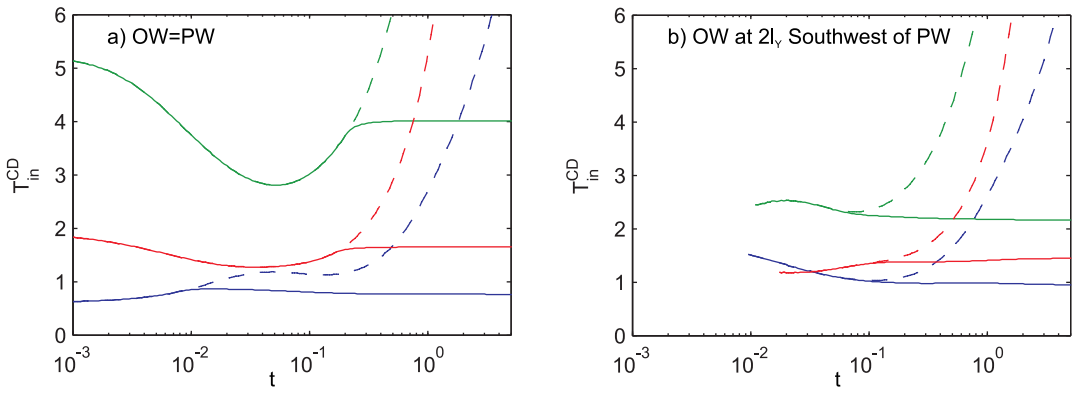

Figure 5.8: Interpreted transmissivity $T_{\text{in}}^{\text{CD}}$ estimated from the drawdown at two different OWs, in different realizations of BCH-domains. $T_{\text{in}}^{\text{CD}}$ was estimated by the Continuous-Derivation method for BCH-domains (solid) and for infinite domains (dashed). Statistical parameters of the ensemble are $l_{\text{Y}} = 8$, $\sigma_{\text{Y}}^2 = 1$, $m_{\text{Y}} = 0$ ($T_{\text{G}} = 1$). The BCH is at $L = 4l_{\text{Y}}$ North of the PW, and $S_0 = 5 \cdot 10^{-4}$.

drawdown data in BCH-domains, namely, a transient period of radial infinite-acting flow, and, a non-radial steady-state flow period. The meaning of $T_{\text{in}}^{\text{CD}}$-estimates, or its relation to the underlying heterogeneity, differs accordingly. During radial infinite-acting flow the meaning of $T_{\text{in}}^{\text{CD}}$ in BCH-domains equals that in infinite domains, relating to an upscaled heterogeneous transmissivity field, with $T_{\text{in}}^{\text{CD}}$ being sensitive to a sub-domain where changes of the Fréchet kernels are significant. Under non-radial steady-state flow, estimates of $T_{\text{in}}^{\text{CD}}$ stabilize rather quickly at the location-dependent, homogeneous transmissivity, which can be assigned to the entire domain.

Furthermore, Figure 5.8 shows that $T_{\text{in}}^{\text{CD}}$ increases steeply during late pumping times, if the presence of the BCH is ignored during the interpretation process. When information on the investigated reservoir is limited, this increase might be used to conclude that a constant head boundary exists.

5.5.2 Interpreted Storativity

The interpreted storativity $S_{\text{in}}^{\text{CD}}$ is calculated from $T_{\text{in}}^{\text{CD}}$ and u_γ (5.4). Accordingly, $S_{\text{in}}^{\text{CD}}$ is understood as a property of $T_{\text{in}}^{\text{CD}}$. In infinite domains, the interpreted late-time storativity is treated as an indicator for flow connectivity [e.g., *Sanchez-Vila et al.*, 1999b; *Trinchero et al.*, 2008], with $S_{\text{in}}^{\text{CD}}$ being estimated from $T_{\text{in}} \approx T_{\text{G}}$. Evaluating the steady-state drawdown in BCH-domains yields an interpreted transmissivity which does not generally match T_{G}. How does this affect the meaning of the interpreted storativity?

To investigate the meaning of the interpreted storativity in BCH-domains, Figure 5.9 shows statistics on late-time estimates of $S_{\text{in}}^{\text{CD}}$ at different OWs, and for different ensembles. The considered ensembles vary in variance σ_{Y}^2 and in the ratio $\lambda = l_{\text{Y}}/L$. Figure 5.9 suggests that late-time estimates of $S_{\text{in}}^{\text{CD}}$ can be understood as an approximation of S_0, in particular, when evaluated at OWs far from the BCH and the PW (OW 10 and 48). However, in the vicinity of sources, i.e., for OWs close to the PW or the BCH, respectively, deviations between $S_{\text{in}}^{\text{CD}}$ and S_0 are rather pronounced. This suggests that $S_{\text{in}}^{\text{CD}}$ also includes information on flow connectivity.

As recommended by *Knudby and Carrera* [2005], T_{PW} can be used as an indicator for flow connectivity. That is, if $T_{\text{PW}} > T_0$, the PW is considered well connected to the domain, whereas the connection is weak if $T_{\text{PW}} < T_0$. In this regard, Figure 5.10 compares T_{PW} to late-time estimates of $S_{\text{in}}^{\text{CD}}$ at OW=PW, for ensembles of different σ_{Y}^2 and λ . It can be seen that $T_{\text{PW}} < T_0$ correlates with $S_{\text{in}}^{\text{CD}} < S_0$, and vice versa. Consequently, $S_{\text{in}}^{\text{CD}}$ also includes information on flow connectivity and subsequent information on T_{PW}. Furthermore, the cloud of points in Figure 5.10 is more narrow for large λ, which is in agreement with previous findings. That is, the influence of flow connectivity between the PW and the BCH on estimated parameters increases with decreasing λ (Section 4.4.2).

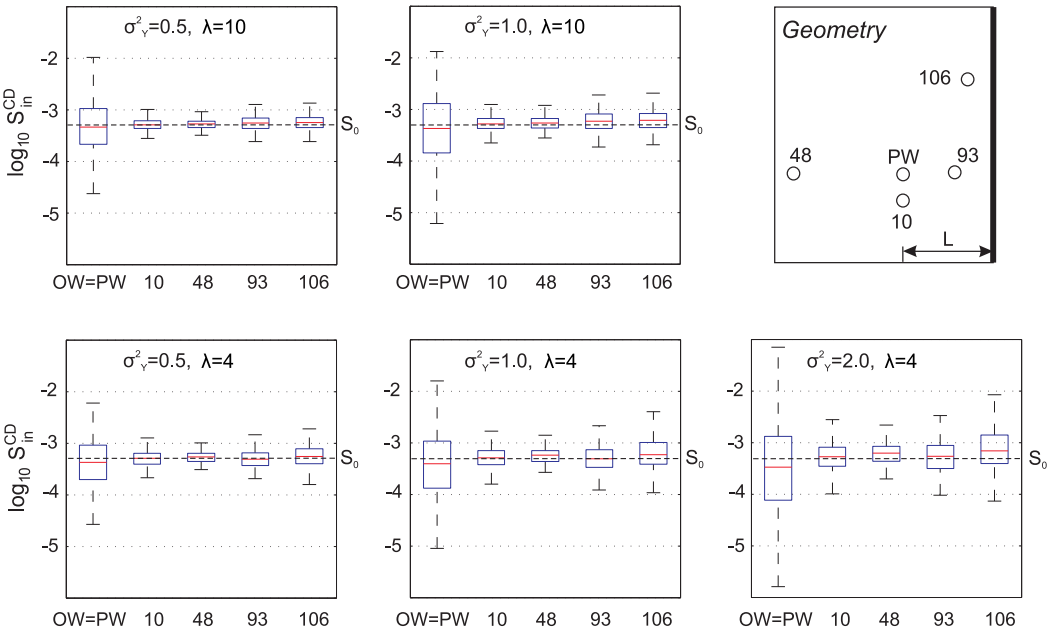

Figure 5.9: Statistics on the interpreted storativity $S_{\text{in}}^{\text{CD}}$, estimated from the steady-state drawdown at various OWs in BCH-domains, for an ensemble of size 200. The geometry plot illustrates locations of OWs (not to scale). Statistics of ensembles are $m_{\text{Y}} = 0$, $l_{\text{Y}} = 8$ lu.

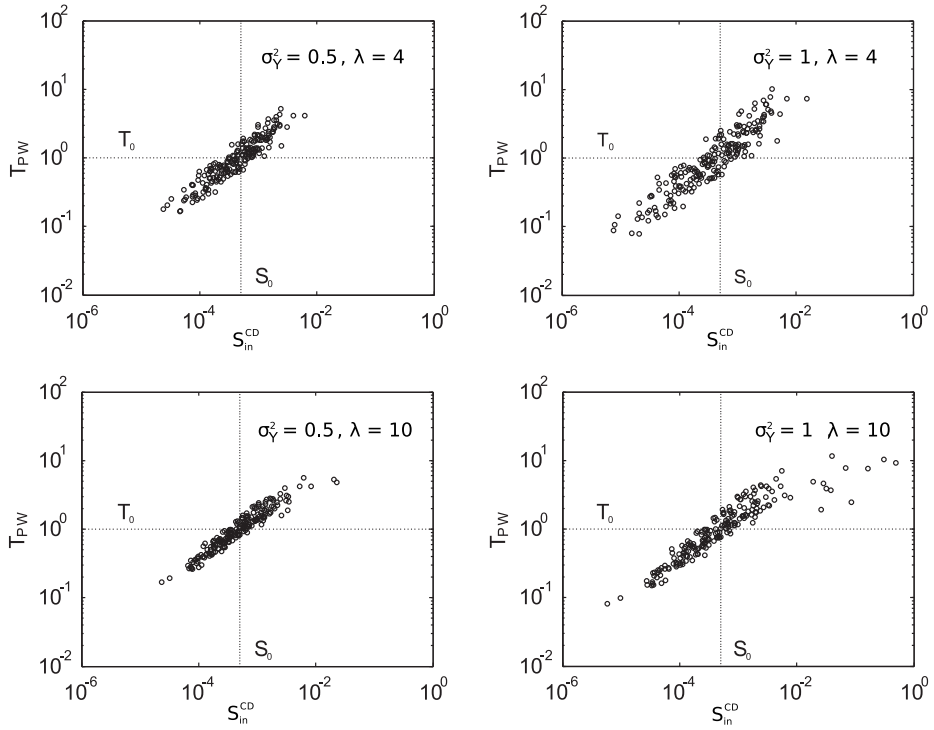

Figure 5.10: Comparison of T_{PW} and $S_{\text{in}}^{\text{CD}}$ estimate from the steady-state drawdown at OW=PW, for ensembles of different variance σ_{Y}^2 and λ. Ensemble size is 200 realizations each. Statistics of ensembles are $m_{\text{Y}} = 0$, $l_{\text{Y}} = 8$ lu.

The presented results reveal some interesting properties of the interpreted storativity. As the interpreted storativity depends on the interpreted transmissivity, it seems also to depend on its variability. For example, with regard to late-time estimates of the interpreted transmissivity from single-well pumping tests in infinite domains, $T_{\mathrm{in}} \approx T_{\mathrm{G}}$, often deviates considerably from T_{PW}. Consequently, the associated interpreted storativity can vary over up to 40 orders of magnitude (Section 3.3.4). Under steady-state conditions in BCH-domains, $T_{\mathrm{in}}^{\mathrm{CD}} = T_{\mathrm{in}}^{\mathrm{Han}}$ becomes a homogeneous (equivalent) parameter, which does differ only slightly from T_{PW} (Figure 4.7, OW1). Note that for single-well pumping tests in infinite domains, the equivalent transmissivity basically approximates T_{PW} [*Dagan and Lessoff*, 2007a]. Figure 5.9 and 5.10 now show that the variability of the interpreted storativity in BCH-domains decreases accordingly, with late-time estimates of $S_{\mathrm{in}}^{\mathrm{CD}}$ appearing to be an approximation of the true storativity of the aquifer S_0, varying just over a view orders of magnitude. Thus, the magnitude of the interpreted storativity itself does not include unambiguous information on flow connectivity. In fact, the magnitude of $S_{\mathrm{in}}^{\mathrm{CD}}$ is dependent on the properties of the corresponding interpreted transmissivity.

In this regard, the interpreted storativity is understood to compensate for flow properties in heterogeneous T-fields, which cannot be captured by the assumption of aquifer homogeneity. In other words, the interpreted storativity contains information about the storativity of the aquifer, but at the same time, includes relicts of applying pumping test interpretation techniques which presume aquifer homogeneity (Theis' equation) to heterogeneous systems. Accordingly, the interpreted storativity approximates the real storativity in certain cases. That is, when the impact of heterogeneity on the interpreted transmissivity is negligible. Strictly speaking, there is only one such case, namely, interpreting the very early drawdown at OW=PW, when the interpreted transmissivity equals T_{PW}. Estimated parameters at OWs different from the PW, as well as, at later times at OW=PW, are impacted by heterogeneity, and consequently by flow connectivity. However, as the interpreted transmissivity becomes a homogeneous (equivalent) parameter under steady-state conditions, late-time estimates of $S_{\mathrm{in}}^{\mathrm{CD}}$ from observation wells far from the PW and the BCH, respectively, may provide also a rather good approximation of S_0 (Figure 5.9).

The above discussion mainly focuses on the evaluation of the late-time interpreted storativity, which is already complex and somehow unambiguous. The Continuous-Derivation method allows for estimating transient estimates of $S_{\mathrm{in}}^{\mathrm{CD}}$, which may include further information on flow connectivity. An attempt to evaluate this information is included in the next section. Nevertheless, the Continuous-Derivation method can potentially give an estimate of the real storativity by interpreting the very early drawdown at OW=PW. Though, very early drawdown data at the pumping well is more noisy and influenced by well effects, making the estimation of S_0 quite difficult in practice.

5.5.3 Interpretation of Synthetic Pumping Test Examples

This section illustrates the evaluation of transient drawdown data in BCH-domains by means of three synthetically generated pumping tests. In this regard it summarizes what information on aquifer heterogeneity can be potentially obtained by the Continuous-Derivation method for BCH-domains. Please note that the interpretation does not consider the influence of well effects, like well-bore storage and skin, which can mask the actual aquifer response. Furthermore, as the evaluation involves computing the drawdown derivative, it is prone to errors caused by noisy data. Different types of filters can be used for the removal of noise, e.g., a smoothing differentiation expression [*Bourdet et al.*, 1989; *Spane and Wurstner*, 1993] or splines [*Illman and Neuman*, 2001]. However, for the following evaluation of synthetically generated pumping tests no filtering was needed.

Figure 5.11 shows three different realizations of heterogeneous BCH-domains (A to C) with $\sigma_Y^2 = 1$ and $l_Y = 8$. The transmissivity is depicted in terms of $Y = \ln T$. The BCH is located at $L = 4l_Y$ North of the PW, i.e., $\lambda = 4$. For each realization, a pumping test was simulated and the drawdown at four observation wells was evaluated with the Continuous-Derivation method for BCH-domains, including OW=PW (OW1). The following discussion evaluates transient estimates of T_{in}^{CD} and S_{in}^{CD} at considered OWs, and relates observed characteristics to the underlying transmissivity. In this regard, the presented analysis aims to maximize the information that can be obtained from pumping tests. Further details about the spatial heterogeneity may be determined by solving the inverse problem, provided more detailed data of the subsurface is available.

Evaluation and Interpretation of the Transmissivity T_{in}^{CD}

With regard to the evaluation of T_{in}^{CD}, pumping test interpretation can be summarized as follows. For OW=PW (OW1), Figure 5.11 shows that at very early pumping times $T_{in}^{CD} = T_{PW}$. When T_{PW} is known, pumping test interpretation may continue by evaluating T_{in}^{CD} from the other OWs. Since early-time estimates of T_{in}^{CD} relate to radial infinite-acting flow, their meaning corresponds to those obtained in infinite domains, as discussed in Section 5.5.2 and by *Copty et al.* [2011]. Thus, even early-time estimates of T_{in}^{CD} do not generally match the local transmissivity at a particular OW (except for the case when OW=PW), as the drawdown is also sensitive to T_{PW} and the perturbed aquifer volume. In other words, the estimated transmissivity is not unique but dependent on the locations of the OW and the PW, or, the corresponding local transmissivities, respectively. Consequently, if OW≠PW, T_{in}^{CD} only allows for inferring qualitative information with respect to a known value of T, preferably T_{PW}.

Knowing T_{PW}, pumping test interpretation for realization A may lead to the following results. Transient estimates of T_{in}^{CD} from early drawdown data at OW84-A indicate that

the transmissivity in the vicinity of this OW is slightly larger than T_{PW}. Under steady-state conditions, $T_{\mathrm{in}}^{\mathrm{CD}}$ stabilizes at a much larger value (even above T_{G}). This indicates that the transmissivity between OW84-A and the BCH, i.e., in the sub-domain to which the steady-state drawdown at this OW is most sensitive too (Figure 5.6f and i), is much larger than T_{PW}. Similar conclusions can be drawn for OW95-A, with the transmissivity between OW95-A and the BCH being larger than between OW84-A and the BCH, and much larger than T_{PW}. The interpretation for early estimates of $T_{\mathrm{in}}^{\mathrm{CD}}$ from OW57-A is slightly different, since it is farther from the BCH, located behind the PW. Accordingly, the drawdown signal has already sampled a significant part of the domain when reaching OW57-A. Thus, the early-time $T_{\mathrm{in}}^{\mathrm{CD}}$ indicates that the average transmissivity between OW57-A and the PW exceeds T_{PW}. Under steady-state conditions, the sub-domain over which OW57-A averages is considerably larger than for OW84-A and OW95-A, respectively (Figure 5.7f and i). Thus, the late-time $T_{\mathrm{in}}^{\mathrm{CD}}$ at OW57-A might be regarded as an approximation of T_{G} (Section 4.4.3, Figure 4.7). However, in order to get an reliable approximation of T_{G}, λ should be large. For simulations in Figure 5.11 $\lambda = 4$ is quite small. In this regard, presented results show that additional data on λ is needed to approximate T_{G} from steady-state estimates of T. Otherwise, results can be misleading like in realization B where the steady-state $T_{\mathrm{in}}^{\mathrm{CD}}$ at OW57-B overestimates T_{G}.

Having a closer look at realization B, it is interesting to note that OW95-B is located at the edge of a lens with $T \gg T_{\mathrm{PW}}$. However, corresponding values of $T_{\mathrm{in}}^{\mathrm{CD}}$ from late times are much smaller than T_{PW}. This confirms that the steady-state drawdown at OW95-B is basically sensitive to the area between OW84-B, OW95-B and the BCH, as suggested by Figure 5.7i, not comprising the nearby lens of large T. For OW84-B, $T_{\mathrm{in}}^{\mathrm{CD}}$ is somehow constant, also not recognizing the nearby lens of large transmissivity in the East of the OW. Estimates of $T_{\mathrm{in}}^{\mathrm{CD}}$ from OW57-B start at a relatively low transmissivity, when compared to T_{PW}; followed by a continuing increase, and a stabilization at a transmissivity even larger than T_{PW}. This indicates that OW57-B is located in a relatively large area of $T \ll T_{\mathrm{PW}}$, whereas the average transmissivity in the sub-domain which corresponds to steady-state conditions is close to T_{PW}. This is confirmed by the transmissivity distribution of realization B. With regard to realization C, estimates of $T_{\mathrm{in}}^{\mathrm{CD}}$ at all OWs, including OW=PW (OW1), stay at a relatively high level, making it impossible to discover that all OWs, except of OW57-C, are screened in an quite large sub-domain of large transmissivity, which does not represent the transmissivity distribution of the entire aquifer.

The above evaluation of $T_{\mathrm{in}}^{\mathrm{CD}}$ illustrates that information on the sub-domain to which the drawdown is most sensitive too is essential for the interpretation process. Depending on the location of the observation well, transient estimates of $T_{\mathrm{in}}^{\mathrm{CD}}$ can yield information about the underlying heterogeneity in T. However, statistic parameters of the underlying heterogeneity are not readily inferable.

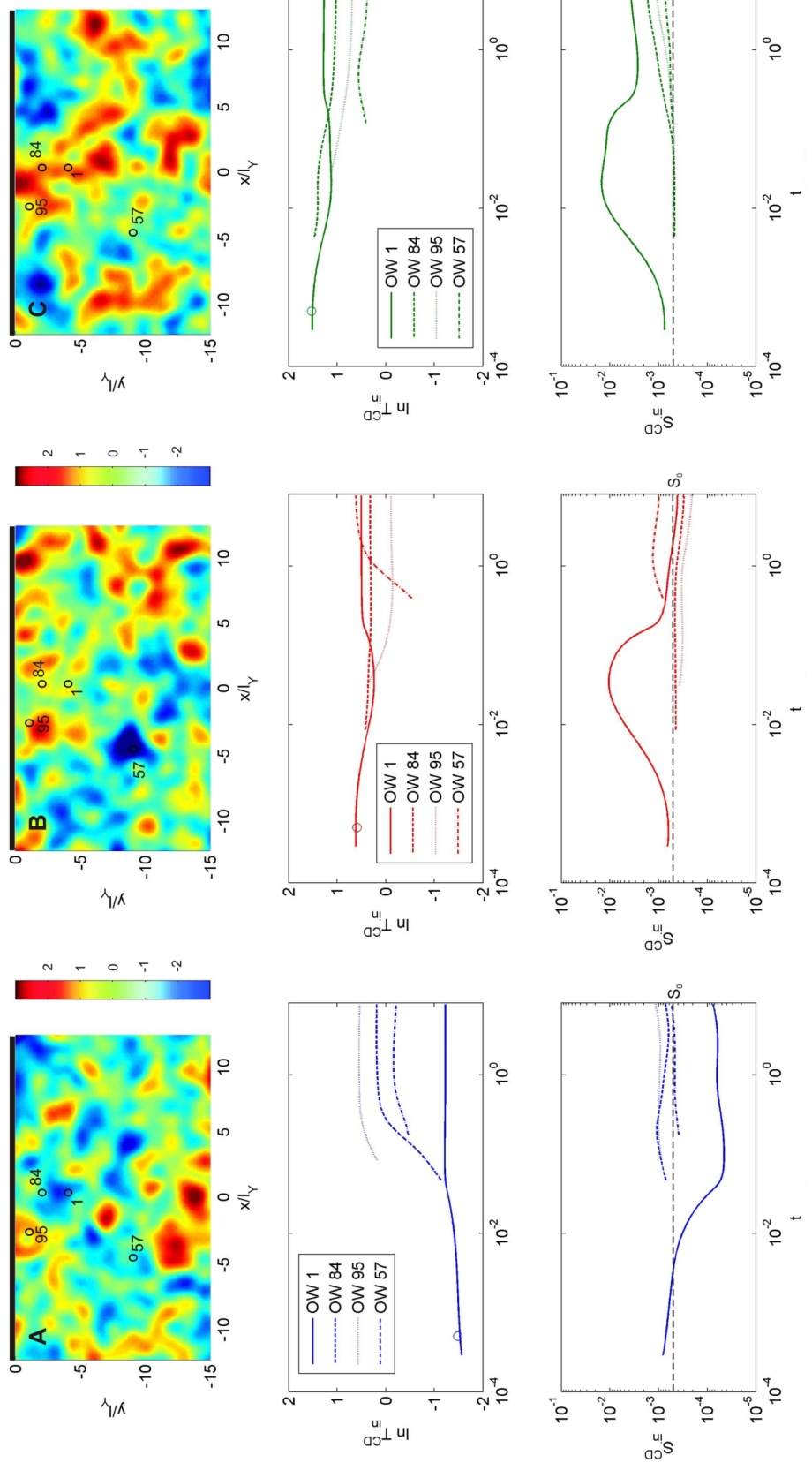

Figure 5.11: Interpreted transmissivity and storativity, $T_{\text{in}}^{\text{CD}}$ and $S_{\text{in}}^{\text{CD}}$, estimated from the synthetically generated drawdown at four different OWs in three realizations of T-fields (A to C). Distances are normalized by the correlation length $l_Y = 8$; $\sigma^2 = 1$, $m_Y = 0$ ($T_{\text{G}} = 1$). The transmissivity is illustrated in terms of $Y = \ln T$. The BCH is North of the PW at $L = 4l_Y$, i.e. $\lambda = 4$. Circles in $T_{\text{in}}^{\text{CD}}$-plots indicate T_{PW}. $S_0 = 5 \cdot 10^{-4}$ is the storativity assumed constant during simulations.

Please note that for the given examples with $\lambda = 4$, variations in $T_{\text{in}}^{\text{CD}}$ during the radial infinite-acting flow period are relatively small. Though, as λ increases, the drawdown signal samples an increasing number of l_{Y} before the BCH affects the drawdown. Thus, if λ exceeds values of about 15 to 20, estimates of $T_{\text{in}}^{\text{CD}}$ potentially approach T_{G} during radial infinite-acting flow, as discussed in Sections 3.3.2 and 3.4.2. However, even if T_{G} is reached during transient flow condition, the steady-state $T_{\text{in}}^{\text{CD}}$ does generally deviate from T_{G}, as discussed above and in Section 4.4.3. Accordingly, the information which can be derived from pumping tests in BCH-domains largely depends on λ, i.e., on whether the aquifer volume sampled by the pumping test is representative for the entire aquifer. This is the case if λ is large.

Evaluation and Interpretation of the Storativity $\mathbf{S_{in}^{CD}}$

The evaluation of $S_{\text{in}}^{\text{CD}}$ as an indicator for flow connectivity is generally complex in BCH-domains. In infinite domains, late-time estimates with $S_{\text{in}}^{\text{CD}} > S_0$ at OW=PW indicate a PW which is well connected to the domain (Section 3.3.4), whereas, if OW≠PW the same expression indicates that the connection between the PW and the OW is weak [*Sanchez-Vila et al.*, 1999b; *Trinchero et al.*, 2008]. In BCH-domains the evaluation of $S_{\text{in}}^{\text{CD}}$ is further complicated by the fact that the meaning of $T_{\text{in}}^{\text{CD}}$ changes from an upscaled heterogeneous parameter under radial infinite-acting flow, to an upscaled homogeneous parameter under non-radial steady-state flow, with the BCH constituting an additional source. This, in turn affects the magnitude of $T_{\text{in}}^{\text{CD}}$ and consequently $S_{\text{in}}^{\text{CD}}$, as discussed in Section 5.5.2. $S_{\text{in}}^{\text{CD}}$ from the radial infinite-acting flow period is therefore considered to relate to the flow connectivity between the OW and the PW, as discussed above. Whereas, under non-radial steady-state flow, $S_{\text{in}}^{\text{CD}}$-estimates are considered to represent an average of the flow connectivity between the OW and the PW, and, the flow connectivity between the OW and the BCH, which would in turn relate to the sub-domain to which the drawdown (and consequently $T_{\text{in}}^{\text{CD}}$) is most sensitive too.

Regarding the evaluation of the synthetic pumping tests, Figure 5.11 confirms the results from Section 5.5.2. That is, for very early pumping times at OW=PW (OW1), $S_{\text{in}}^{\text{CD}}$ approximates the true storativity of the aquifer S_0. Furthermore, late-time estimates of $S_{\text{in}}^{\text{CD}}$ at OW=PW provide subsequent information on T_{PW}. Thus, for realization A, $S_{\text{in}}^{\text{CD}} < S_0$ indicates that $T_{\text{PW}} < T_0$, which is in agreement with the true transmissivity distribution. Accordingly, T_{PW} is close to T_0 in realization B as $S_{\text{in}}^{\text{CD}}$ is close to S_0, and for realization C, $S_{\text{in}}^{\text{CD}} > S_0$ indicates that $T_{\text{PW}} > T_0$.

Moreover, Figure 5.11 allows for some suggestions on what information transient estimates of $S_{\text{in}}^{\text{CD}}$ may include. For example, in realization B, $S_{\text{in}}^{\text{CD}}$ for OW=PW (OW1-B) peaks at intermediate times, decreasing to $S_{\text{in}}^{\text{CD}} \approx S_0$ during late times. Therefore, it

seems reasonable to conclude that the PW is located in an area of $T_{\mathrm{PW}} > T_0$, whereas the connectivity between the PW and the BCH is not pronounced, which is supported by the given transmissivity distribution of realization B. On the contrary, transient estimates of $S_{\mathrm{in}}^{\mathrm{CD}}$ for all OWs in realization C are continuously increasing. This increase might indicate that flow to the wells is mainly through preferential flow paths between the PW and the BCH. Thus, the estimated transmissivity in realization C is not representative for the entire system. With regard to realization A, $S_{\mathrm{in}}^{\mathrm{CD}}$ at OW=PW (OW1-A) keeps basically decreasing as pumping continues, indicating that OW1-A is located in an area of low T, with the PW being weakly connected to the BCH. For $T_{\mathrm{PW}} < T_0$, investigations on infinite domains showed that the impact of flow connectivity is not negligible but weak (Section 3.3.4). Accordingly, it seems reasonable that late-time estimates of $S_{\mathrm{in}}^{\mathrm{CD}}$ for the other wells in realization A plot around S_0.

Thus, the above evaluation suggests that transient estimates of $S_{\mathrm{in}}^{\mathrm{CD}}$ potentially include information on how flow connectivity evolves with time, or, as the cone of depression propagates, respectively.

5.6 Conclusions

Natural aquifers are intrinsically heterogeneous with regard to their hydraulic parameters transmissivity and storativity. The evaluation of pumping tests is an established method to estimate aquifer parameters, commonly performed by applying Theis-based interpretation techniques. Several studies as well as previous chapters of this work confirm that even though Theis-based interpretation techniques presume aquifer homogeneity, their application to heterogeneous aquifers yields interpreted hydraulic parameters, which include information on aquifer heterogeneity, in particular, when evaluating transient drawdown data. However, the estimation of hydraulic parameters in domains unilaterally bounded by an infinite linear constant head boundary (BCH) is currently restricted to the interpretation of the steady-state drawdown by Hantush's method [*Hantush*, 1959].

In order to allow for the estimation of hydraulic parameters from transient drawdown data in BCH-domains, a new pumping test interpretation method for BCH-domains was derived, by extending the Continuous-Derivation method [*Copty et al.*, 2011] for an application to BCH-domains. Subsequently, Fréchet kernels were used to investigate the relation between the resulting time-dependent interpreted hydraulic parameters, $T_{\mathrm{in}}^{\mathrm{CD}}$ and $S_{\mathrm{in}}^{\mathrm{CD}}$, and the underlying heterogeneity. Finally, the Continuous-Derivation method for BCH-domains was applied to synthetically generated pumping tests from multivariate Gaussian log-normally distributed transmissivity fields to illustrate the interpretation process. It was found that the Continuous-Derivation method for BCH-domains allows for a more detailed description of aquifer heterogeneity, in particular when drawdown data from sev-

eral observation wells is evaluated. The main findings of this study can be summarized as follows:

1. Two flow periods have to be distinguished in BCH-domains, namely, radial infinite-acting flow when the BCH does not influence the drawdown at an observation well, and, non-radial steady-state flow when the BCH influences the drawdown. The meaning of interpreted hydraulic parameters is dependent on the flow period.

2. During the radial infinite-acting flow period, the drawdown at an observation well is most sensitive to the local transmissivities at the OW and the PW, which influence the drawdown by equal parts. Under non-radial steady-state flow conditions, the drawdown is most sensitive to the local transmissivity in the vicinity of the well which is closest to the BCH, and, to a sub-domain between the wells and the BCH.

3. Time-dependent estimates of $T_{\mathrm{in}}^{\mathrm{CD}}$ from the radial infinite-acting flow period bear the same information as in infinite domains. Accordingly, they are understood as an upscaled heterogeneous transmissivity field. Thus, very early estimates of $T_{\mathrm{in}}^{\mathrm{CD}}$ at the pumping well potentially allow to infer the local transmissivity at the well T_{PW}. Under non-radial steady-state flow, $T_{\mathrm{in}}^{\mathrm{CD}}$ relates to an upscaled homogeneous transmissivity, with $T_{\mathrm{in}}^{\mathrm{CD}} = T_{\mathrm{in}}^{\mathrm{Han}}$, the transmissivity estimated by the Hantush method.

4. The estimation of statistic parameters of the underlying heterogeneous transmissivity distribution is difficult in BCH-domains. It is found that the ratio $\lambda = L/l_{\mathrm{Y}}$ is significant. If λ is small, the pumping test perturbs an aquifer volume which is not generally representative for the entire aquifer. On the contrary, if λ exceeds about 15 to 20, the perturbed aquifer volume is representative for the entire aquifer, potentially allowing to estimate the geometric mean of transmissivity from late estimates of the radial infinite-acting flow period.

5. The interpreted storativity $S_{\mathrm{in}}^{\mathrm{CD}}$ should be treated as a property of $T_{\mathrm{in}}^{\mathrm{CD}}$. Under certain conditions $S_{\mathrm{in}}^{\mathrm{CD}}$ approximates the true storativity of the aquifer S_0, namely, during very early pumping times at OW=PW. If the pumping test perturbs a representative aquifer volume (large λ) the late-time $S_{\mathrm{in}}^{\mathrm{CD}}$ may also be used to approximate S_0, if the observation well is sufficiently far from the pumping well and the BCH, respectively.

6. Investigations further suggest that transient estimates of $S_{\mathrm{in}}^{\mathrm{CD}}$ may provide time-dependent information on flow connectivity, i.e., as the cone of depression propagates in time. However, appraising the impact of flow connectivity in BCH-domains is complex, since different sources exist, namely, the PW during radial infinite-acting flow, and, the PW and the BCH during non-radial steady-state flow. In this regard, a continuous increase of $S_{\mathrm{in}}^{\mathrm{CD}}$ at several observation wells under non-radial steady-state flow might indicate that flow connectivity between the PW and the BCH has a pronounced impact on well flow.

Along with extending the Continuous-Derivation method for an application to BCH-domains, its potential use for evaluating pumping tests in domains, which are unilaterally

bounded by an infinite linear no-flow boundary was also investigated. It was found that if the boundary is impermeable, the Continuous-Derivation method does not allow for an unambiguous estimation of hydraulic parameters from the drawdown at observation wells close to the pumped well (with $\beta > 12$), which limits its applicability to such systems.

Please note that this study does not consider the impact of well effects like skin and well-bore storage, which can mask the actual aquifer response, in particular during early pumping times.

Chapter 6

Investigating an Aquifer System by Hydraulic Testing - Saritepe Campus, Boğaziçi University, Istanbul

6.1 Introduction

6.1.1 Exploring Saritepe Campus

Saritepe Campus of Boğaziçi University is located 25 km North of the center of Istanbul, West of the village of Kilyos. Figure 6.1 shows Saritepe Campus and its surrounding. It also shows the locations of six wells which have been used within the scope of this study to investigate the hydrogeological situation at the site. Wells K1 to K4 were installed by the university prior to 2010 to establish an independent drinking water supply for the campus. Unfortunately three out of four wells (K1, K2, K3) have been producing brackish groundwater. Hence, the university decided to install well K4 about 850 m East of the other wells. Nowadays, K4 produces fresh groundwater, whereas the other wells are abandoned.

The aim of this study is to develop a conceptual hydrogeologic model of the site to answer questions on the origin of the brackish water at wells K1, K2 and K3. Furthermore, it should be investigated whether well K4 might also be affected by brackish water in the future. Currently, brackish groundwater is assumed to be related to seawater intrusion form the Black Sea. In this regard, the pumping test interpretation method derived in Section 5 may be applied for the estimation of hydraulic aquifer parameters. Moreover, the prospective use of the site to investigate salinization problems in coastal aquifer regions should be estimated.

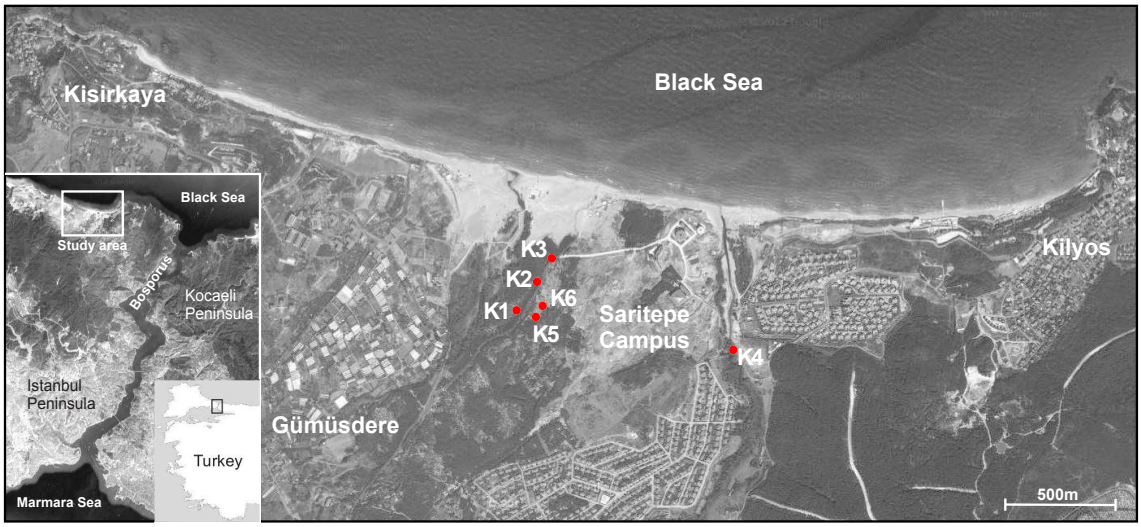

Figure 6.1: Satellite image of Saritepe Campus/Boğaziçi University.

To answer the questions raised above, the following investigations were conducted. Two new wells (K5 and K6) were installed to get insight on the local geology at the site, as no data on the existing wells was available. After well installation in 2011, pumping tests were conducted in 2012 to determine hydraulic aquifer properties and boundary conditions of the tapped reservoir. Pumping tests were accompanied by groundwater sampling campaigns for a hydrochemical and isotopic characterization of the reservoir under investigation.

This chapter evaluates the conducted investigations. It starts with a review on the geology of Northern Istanbul, with emphasis on its tectonic evolution. Section 6.2 then focuses on geologic investigations, including the evaluation of drilling K5 and K6. Sections 6.3 and 6.4 interpret conducted pumping tests and hydrochemical investigations. Finally, a conceptual hydrogeological model of the site is established and discussed in Section 6.5.

6.1.2 Regional Geologic Framework

The geologic evolution of Turkey is closely related to the closure of the multi-branched Neo-Tethyan ocean, i.e., to the collision of different terranes during the Alpide orogeny [*Stampfli*, 2000; *Moix et al.*, 2008]. Since the Oligocene Turkey can be regarded as a single landmass [*Okay*, 2008]. *Yilmaz et al.* [1997] and *Okay and Tüysüz* [1999] distinguish four independently functioning plate tectonic elements (Figure 6.2), namely, from North to South: 1) the Pontides, which comprise the terranes of Istanbul Zone, Rhodope-Strandja Massif and Sakarja Zone, 2) the Kırşehir Massif, 3) the Anatolide-Tauride Block and 4) the Arabian Platform. Within this classification the study site is located in the NE of the Istanbul Zone.

Istanbul Zone has a Late Precambrian crystalline basement unconformably overlain by a thick Ordovician to Carboniferous sedimentary sequence [*Görür et al.*, 1997]. A

discordance separates Paleozoic rocks from a Triassic sedimentary sequence while Jurassic and Lower Cretaceous sequences are missing. The Paleozoic to Early Mesozoic sequences show similarities to the Moesian Platform (Figure 6.2), i.e., Istanbul Zone formed part of the passive continental margin of Laurasia until Cretaceous times [*Okay et al.*, 1994; *Yilmaz et al.*, 1997; *Tüysüz*, 1999; *Okay et al.*, 2001; *Yilmaz*, 2007; *Okay*, 2008]. During the Alpide orogeny the northward subducting Neo-Tethys induced back-arc rifting North of the Istanbul Zone. This led to the initial rifting of the West Black Sea Basin and southward drift [*Görür*, 1988; *Okay et al.*, 1994; *Nikishin et al.*, 2003], accompanied by an Upper Cretaceous magmatic arc [*Okay et al.*, 2001; *Yilmaz*, 2007]. From the Early Maastrichtian up to the end of the Paleocene, arc magmatism was replaced by the deposition of marly limestones [*Okay et al.*, 2006].

The collision between the Pontic domain and the Southern terranes (Anatolide-Tauride-Block, Kırşehir Massif) continued until the Late Paleocene to Early Eocene [*Okay*, 2008]. Due to continuous terrane amalgamation and subduction South of the Istanbul Zone, the northernmost branch of the Neo-Tethys closed during the Late Cretaceous to Paleocene. Thereupon, Istanbul Zone collided with the Rhodope-Strandja Massif and Sarkaya Zone

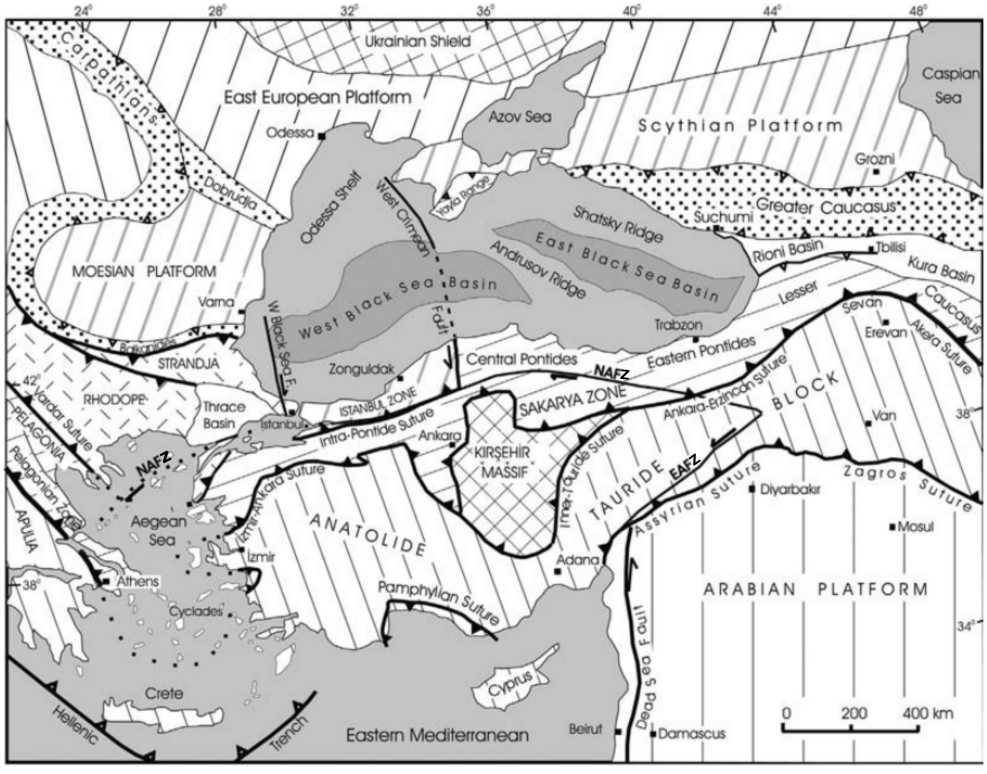

Figure 6.2: Tectonic map of the Eastern Mediterranean region showing the major terranes and the bounding sutures. The filled triangles indicate the polarity of the subduction (modified by *Okay et al.* [2006] from *Okay and Tüysüz* [1999]). NAFZ, North Anatolian Fault Zone; EAFZ, East Anatolian Fault Zone.

during the Early Eocene forming the Intra-Pontide suture [*Şengör and Yilmaz*, 1981; *Okay et al.*, 1994]. Within this compressive regime the Paleozoic to Early Mesozoic province of Istanbul Zone was thrusted northward over the Cretaceous magmatic arc, followed by an uplift in tandem with extensive erosion from Eocene times on [*Akartuna*, 1963; *Özgül*, 2011]. Post-collisional compressive stress continued until Late Eocene to Early Miocene leading to fold and thrust belts trending approximately parallel to the Intra-Pontide suture.

During the Middle Miocene the right-lateral North Anatolian Fault Zone (NAFZ) formed in the East of Turkey (Figure 6.2), reaching the Istanbul and Marmara region about 200 ka ago [*Şengör et al.*, 2005]. With a dextral slip rate of 2 cm/a [*Reilinger et al.*, 1997] the NAFZ is still the major driving force affecting the Istanbul region. Due to continuous N-S compression created by the northward movement of the Arabian Plate, the Anatolian Block escaped westerly along the NAFZ. Accordingly, East Anatolia was affected by compression whereas West Anatolia experienced transpressional tectonics and shear related deformation. Within this extensional regime which affected the Istanbul region prior to the entry of the NAFZ from Late Miocene to Early Pliocene [*McClusky et al.*, 2000; *Reilinger et al.*, 1997; *Gökaşan et al.*, 2003], the Istanbul region is assumed to have developed as a horst structure bounded by two normal oblique faults [*Yilmaz*, 2007]. The tectonic regime changed to dextral-shear when the southern oblique fault was possibly captured by the NAFZ, forming its western extension [*Demirbag et al.*, 2003].

Recent studies indicate that this new tectonic regime established in the Marmara region since Upper Pleistocene. According to *Gökaşan et al.* [1997], *Demirbag et al.* [1999] and *Oktay et al.* [2002], the region is developing under compressive tectonics again, with compression in the NNW-SSE direction around the NE of the Istanbul Peninsula. *Oktay et al.* [2002] give evidence for a conceptual tectonic model of block rotation within this compressive regime, affecting the region since the Würm Glacial age. This temporally correlates with the origination of a new rupture at the Northern strand of the NAFZ. Accordingly, block rotation results from right-lateral shearing between two zone bounding faults, namely, the new rupture of the NAFZ within the Sea of Marmara, and a scarp on the SW shelf of the Black Sea [*Gökaşan et al.*, 2001b]. Within this context, the Bosporus is regarded as sinistral block bounding shear-zone between the tectonic blocks of the Istanbul peninsula and the Kocaeli peninsula. The establishment of the new compressive regime may also have led to the uplift of the areas North of Istanbul [*Oktay and Eren*, 1995; *Gökaşan et al.*, 1997; *Demirbag et al.*, 1999; *Koral*, 2007], and the reactivation of faults previously regarded as inactive [*Özgül*, 2011]. Compressive stresses may also give way to regional strike-slip faulting and related structures, such as pull-apart basins, pressure ridges and grabens, besides the uplifting by crustal shortening and thickening as mentioned by *Demirbag et al.* [1999].

6.1.3 Local Geology at Saritepe Campus

An overview on the local geology of Saritepe Campus and its surrounding is given by the geological map in Figure 6.3. The north-vergent, NW-SE striking fault zone of the Şile-Sarıyer-Fault is the most prominent structure of the region. It separates the pre-Cretaceous basement which mainly comprises Carboniferous sedimentary rocks in the South, to a Cretaceous to Paleocene volcano-sedimentary sequence of volcano-clastic beds with minor lava flows in the North. Within the fault zone Mezosoic units crop out. A Oligocene to Quaternary sequence of mostly unconsolidated sediments of neritic to terrestrial facies covers Paleozoic and Mezosoic units unconformably.

The *pre-Cretaceous* basement mainly comprises the Carboniferous sequence of Trakya formation, consisting of turbeditic sandstone, shale and limestone, dated to the Tournaisian to Viséan [*MTA*, 2005]. They form part of an Ordovician to Carboniferous sedimentary sequence which crops out at both sides of the Bosporus. Along the Şile-Sarıyer-Fault the Carboniferous sequence is thrusted northward over Cretaceous to Paleocene rocks. Within the fault zone, outcrops of Permian volcanic rock as well as Triassic sediments and intrusive rocks are bounded by parallel north-vergent thrusts and reverse faults [*MTA*, 2012a,b].

Cretaceous to Paleocene sequences relate to Sarıyer formation, which comprises deposits of mainly volcanic and volcano-sedimentary facies, related to the opening of the Black Sea by back-arc-spreading and accompanying arc volcanism [*Okay*, 2008; *Okay et al.*, 1994; *Görür*, 1988]. Lithologically, Sarıyer formation is divided into three conformable members, namely, Bozhane, Garipçe, and Kısırkaya member [*Keskin et al.*, 2003]. Bozhane member consists of siliclastic turbidites representing a flysch facies dated to Santonian to Campanian [*Yilmaz et al.*, 2009]. Garipçe and Kısırkaya member overlay Bozhane member transitionally. On the European side, both members are summarized as Riva formation made up of volcanic ejecta, andesite-basalt, agglomerate, spilite, dacite, rhyolite and trachyandesite with intermediate layers of tuff, sandstone and shale [*MTA*, 2005; *Yilmaz et al.*, 2009]. *Keskin et al.* [2003] describe both members as discrete. Accordingly, Garipçe member consists of mainly volcano-clastic deposits (hyaloclastic, volcanic breccia and epiclastic sandstone) produced by debris flows with minor lava flows (<1-2%). It comprises up to 98% of Sarıyer formation and is approximately 2000 meter thick. Layer thickness is up to 50 m. Kısırkaya member finishes Sarıyer formation. It is composed of olivine-basalt and its epi- and pyroclastic equivalents with a calcarenit level of <10 m in its upper part. Direct dating for Upper Cretaceous volcanics is not available close to the study site. However, dating a basaltic andesite lava in the vicinity of Iğneada which is assumed stratigraphically equivalent with Riva formation [*Yilmaz et al.*, 2009] yielded 74.3 ± 3.1 Ma (Campanian/ Maastrichtian) [*Ercan et al.*, 1998]. For Kısırkaya formation *Keskin et al.* [2003] propose Maastrichtian age due to the fossil bearing calcarenit layer in its upper part.

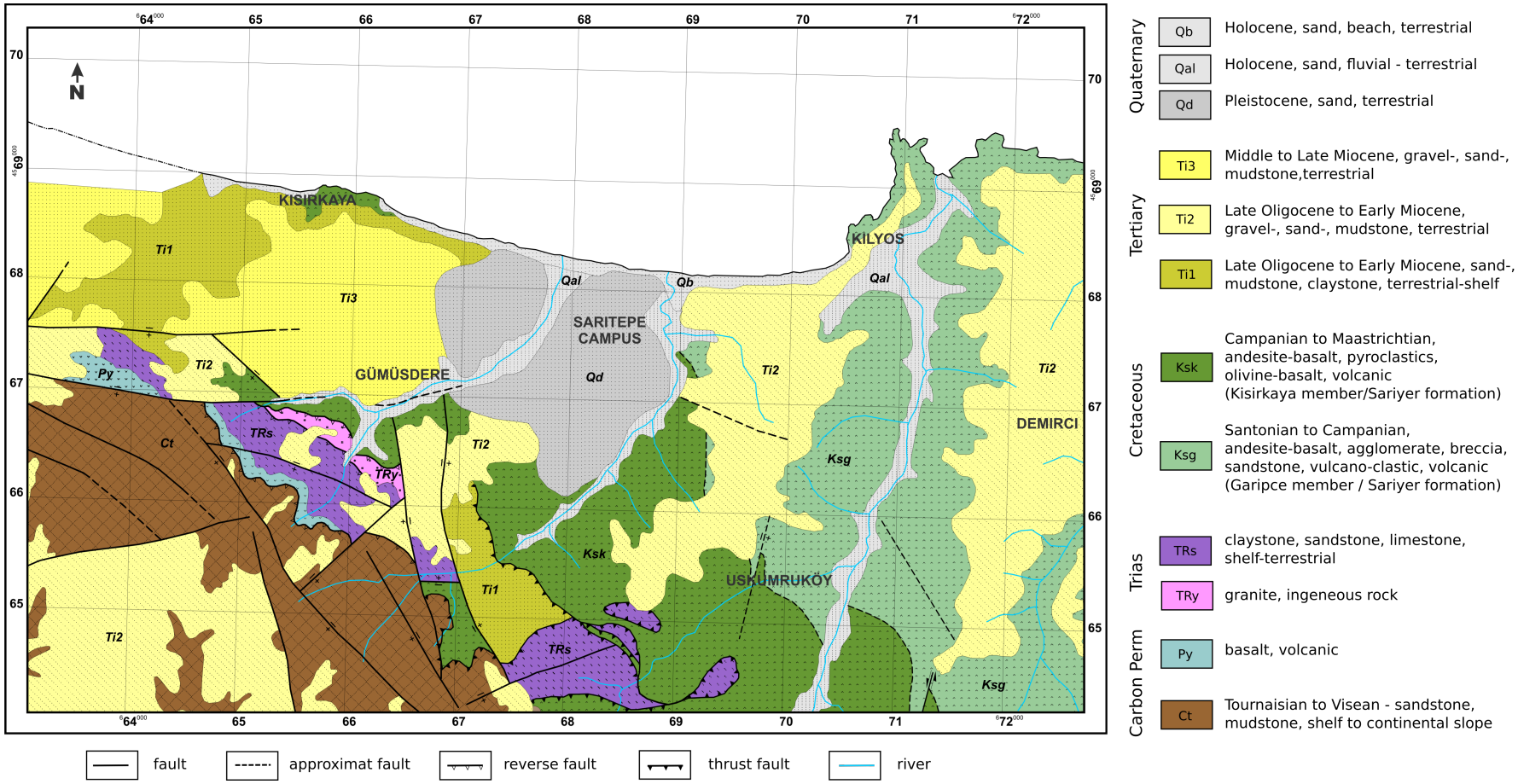

Figure 6.3: Geological map of Saritepe Campus and its surrounding, compiled after *MTA* [2005, 2012a,b,c] and *Keskin et al.* [2003].

Oligocene to Quaternary sediments overlay the Paleozoic to Paleocene rocks unconformable, which had served as parent rock. The succession starts with Oligocene to Lower Miocene sediments. Lagoonal to lacustrine sediments of Meştepe formation merge vertically and horizontally with lake-river-fan deposits of Kayalıtepe formation, at which the amount of coarser sediments increases upwards representing a fluvial facies [*MTA*, 2005, 2012a,b,c]. Meşetepe formation comprises mainly greenish-gray to gray-colored claystone, marl and shale interbedded with coal blended, white, reddish brown to pink fine sand. Kayalıtepe formation is characterized by poorly sorted quartz sandstone and conglomerates containing claystone lenses [*Yilmaz et al.*, 2009]. They are unconformably covered by Middle to Upper Miocene terrestrial sediments [*MTA*, 2012c] of Çukurçeşme formation comprising yellowish-gray to red-brown gravel-sand deposits containing flint and relatively high amounts of mica [*Özgül et al.*, 2005]. Tertiary sediments are discordantly overlain by Quaternary deposits, e.g., dunes, beach sediments and fluvial deposits in valleys.

Please note that notations for stratigraphic units vary with location. Thus, equivalent formations may be called differently on the Anatolian and European side, in particular Tertiary formations. This might be due to the fact that literature for the European side focuses on areas around the Sea of Marmara and corresponding catchments within Paleozoic rocks, whereas literature for the Anatolian side focuses on catchments within the Cretaceous parent around the Black Sea. On the European side Cretaceous rocks are restricted to rather small areas including the study site. In view of this, the stratigraphy of the Anatolian side is adopted.

6.2 Geological Investigations

In order to explore the geology at Saritepe Campus two wells were installed in 2011. In addition, several surface outcrops in the surrounding of the campus have been investigated to provide a basis for the classification of drilled material. Locations of investigated outcrops are given in Figure 6.4.

Sediments and bedrock have been classified according to *DIN 4022* [1987]. Sediments are defined by their major constituents (gain size), their degree of roundness, carbonate content, fabric and texture, as well as color. Volcano sedimentary deposits are described according to the petrographic facies of the matrix and clasts, but are defined by their sedimentary lithological properties, e.g. basaltic breccia. Measurements of tectonic features are in Clar-notation, given in the text in parenthesis.

Section 6.2.1 evaluates geologic investigations, including the drillings of wells K5 and K6. As geologic results indicate that the site is strongly affected by tectonics, Section 6.2.2 evaluates geomorphological data in combination with measurements of tectonic features recorded in the field. A geologic model of the site is presented in Section 6.2.3.

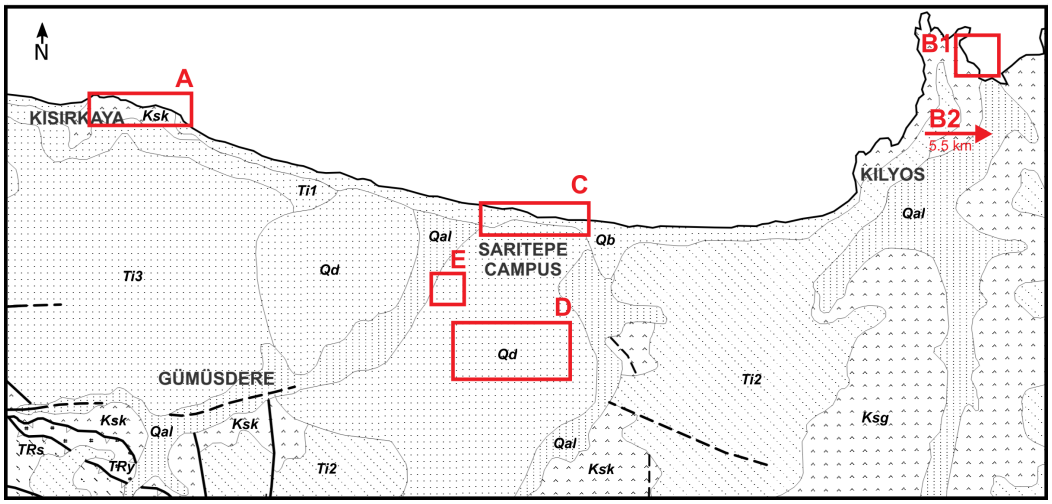

Figure 6.4: Locations of investigated geological outcrops. Notations are according to Figure 6.3. Locations represent (A) Kısırkya member and (B) Garipçe member of Sarıyer formation, (C) Tertiary and (D) Quaternary units. Location (E) relates to the drillings of wells K5 and K6.

6.2.1 Drilling and Field Observations

Outcrop A follows the cliffs below Kısırkaya village on a length of 550 m, and is located about 2.5 km NW of Saritepe Campus (Figure 6.4). According to the geological map in Figure 6.3, this outcrop represents Kısırkaya member of Sarıyer formation.

The outcrop starts in the East with a volcanic fragment breccia (Figure 6.5a) made up of basaltic lava which forms cliffs of approximately 5 m height. Particle size of the breccia ranges from a few millimeters to some decimeters. Within the breccia, debris of flow textured basalt and pillow lava as well as block lava have been observed. The breccia appears dark grey and reddish-grey. The reddish color and the occurrence of pillow lava indicates a partly hyaloclastic deposition of the lava the breccia was derived from, which is addressed as A'a-lava. Thus, the breccia is assumed to have derived from submarine extruded lava on steep flanks, whereupon the flanks became over steepened, unstable and collapsed. Fractures are filled with quartz, mainly sticking WNW-ESE (200/50).

To the West, lithology changes after about 70 m along a WNW-ESE striking fault (195/47) to pyroclastic flow deposits (Figure 6.5b). The fault shows a yellow clayey gouge of a few centimeters in width within an older cataclastic weathered fault zone of some decimeters width. It further cuts an older cataclastic fault which strike NNW-SSE (250/50). The fault which shows the gouge might be regarded as reactivated.

The pyroclastic formation (Figure 6.5d) is layered and contains basaltic clasts in basaltic to andesitic matrix. Blocks are black to dark grey, the matrix is light grey to reddish grey. A coarse lower part is followed by finer grained, stratified deposits with clasts ranging from some millimeters to some centimeters in size. Within the matrix sporadic blocks bigger

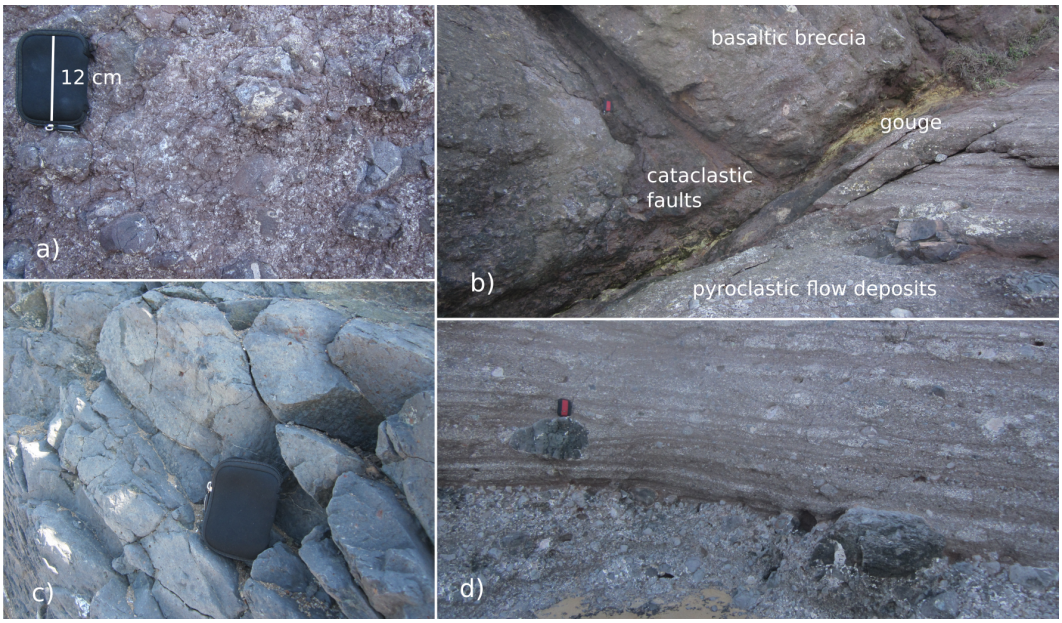

Figure 6.5: Outcrop A below Kısırkya village: a) basaltic fragment breccia, b) fault separating basaltic breccia and pyroclastic flow deposits, c) basalt with weathered olivine minerals, d) pyroclastic flow deposits.

than 10 cm are observed, e.g., vesicular basalt bearing weathered olivine minerals. The pyroclastic deposits can be followed for about 200 m along the beach, forming cliffs of about 4 m. Thereby, layers generally strike E-W dipping slightly North with about 10-15°. The formation is further cut by fractures. Two main sets of intersecting quartz-filled fractures were identified, striking NW-SE (210/30) and ENE-WSW (340/80).

A roughly N-S striking thrust fault (262/28) delimits the pyroclastic flow deposits in the West, again to a basaltic breccia which continues for about 40 m along the beach. Within the basaltic breccia another NE-SW striking, NW dipping fault zone (315/45) is developed, about 5 meters in width. It is characterized by several red gouges and fault breccia. Towards the West, the intensively disturbed basaltic breccias is delimited by a left-lateral NE-SW striking strike slip-fault (332/71) which constitutes the tectonic boundary to an olivine basalt. Thus, faults within the basaltic breccia are considered to relate to an old tectonic regime, whereas the strike-slip fault may relate to neotectonics.

The olivine basalt (Figure 6.5c) is intensively fractured at which the main set of fractures strikes NW-SE dipping SW (230/60). Its color is grey to greenish gray, indicating hydrothermal alteration. Weathered olivine minerals (iddingsite) can be seen with the naked eye and are numerous. The basalt extends approximately 65 m along the beach. The height of the cliffs changes with the occurrence of the basalt abruptly to approximately 10 m. To the West the olivine basalt is again followed by black to reddish black volcanic breccia for another 160 m along the beach. Cliffs are much lower (2-4 m) and are overlain

by light yellowish to reddish brown clay forming landslides, partially burying the breccia and the contact to the olivine basalt.

Outcrops B1 and B2 relate to Garipçe member of Sarıyer formation. Outcrop B1 is situated NE of the village of Kilyos, approximately 3 km NE of Saritepe Campus; B2 is located at the Northern end of the Bosporus close to Rumeli Feneri, about 8.5 km E of Saritepe Campus (Figure 6.4).

Both outcrops mainly comprise volcano-clastic sediments. At Kilyos an approximately 14 m thick layered pyroclastic flow sequence crops out. The base of this sequence is characterized by a matrix-supported tuffaceous breccia (Figure 6.6a). The matrix appears mainly andesitic. The prevalence of angular to sub-angular volcanic clasts in the range of cobbles to pebbles implies a local source, and thus contemporaneous volcanism and sedimentation. However, bombs have been observed too. Andesitic clasts are prevailing showing a high proportion of feldspar minerals which are intensively weathered. The color of the breccias ranges from light to dark grey. In the lower part, weathered, seasonally water-bearing parts show a yellowish rusty color, due to the precipitation of iron-oxides. The breccia is cut by a NE-SW striking fault (310/65). To the top, the breccia is followed by a tuffaceous clay-/siltstone sequence. Within the tuff, clods of pillow lava in the range of several meters were observed. The tuffaceous clay-/siltstone sequence is layered, at which layer thickness varies from centimeters to decimeters, including sporadic layers of welded tuff.

At Rumeli Feneri a volcanic fragment breccia (Figure 6.6b) whose appearance is almost equivalent to the one encountered at the outcrop near Kilyos forms cliffs at the Black Sea shore of about 15 m. However, at Rumeli Feneri andesitic rocks are prevailing and no pillow lava has been encountered. Finer pyroclastic flow deposits are missing and the formation is more weathered, appearing yellowish to brownish grey.

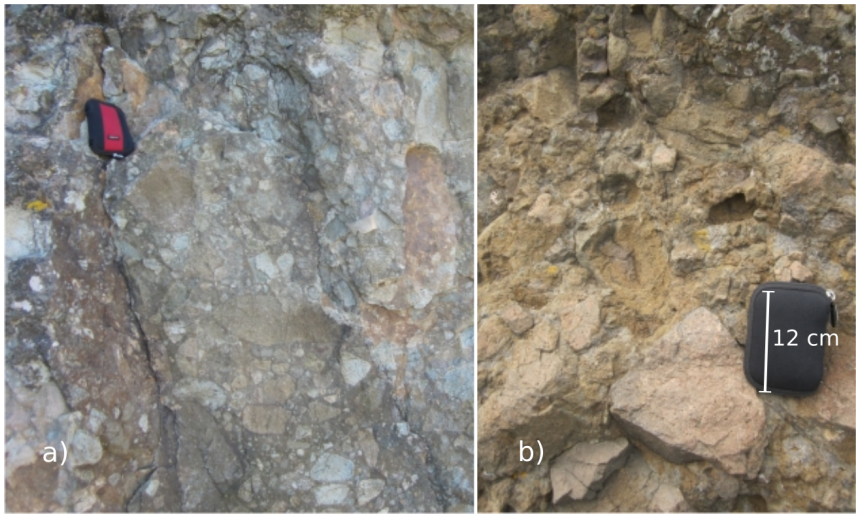

Figure 6.6:
Outcrops B1 and B2: a) basaltic-andesitic fragment breccia at Kilyos, b) weathered andesitic fragment breccia at Rumeli Feneri.

Outcrop C relates to Cenozoic units encountered at the cliffs of Saritepe Campus. It starts in the West with a grey cohesive clay showing rusty patches (Figure 6.7a), transitionally overlain by a reddish clay. The facies of these clays is considered to be lagoonal to neritic, whereas the reddish stains point to a terrestrial influence and pedogenesis. On the top of the clay groundwater leaks. Within the clay a normal fault plain of dark red claystone was identified, striking NW-SE, dipping NE (047/65).

A fluvial terrace of white to yellowish grey coarse sand, with intercalated layers of fine gravel, follows above the clay units unconformably, containing no mica and carbonate. The fluvial terrace is located at an elevation of about 5 to 8 m msl. At the lower level of the terrace, yellow layers with high clay content show iron and manganese concretions, indicating paleo-pedogenesis (hard pan, Figure 6.7b). The terrace is intersected by a fault striking NE-SW, dipping NW (307/83). This fault is regarded as strike-slip fault, as no vertical displacement is observed.

The sequence described above does not continue eastwards, but is delimited by a small valley. East of the valley, below the main building of the campus, a formation of loosely consolidated medium sand crops out at sea level (Figure 6.7c). The yellowish brown sand is carbonate free, contains up to 30% of clay and silt, and about 10 to 20% of fine sand. The amount of clay and silt increases to the bottom of the sequence.

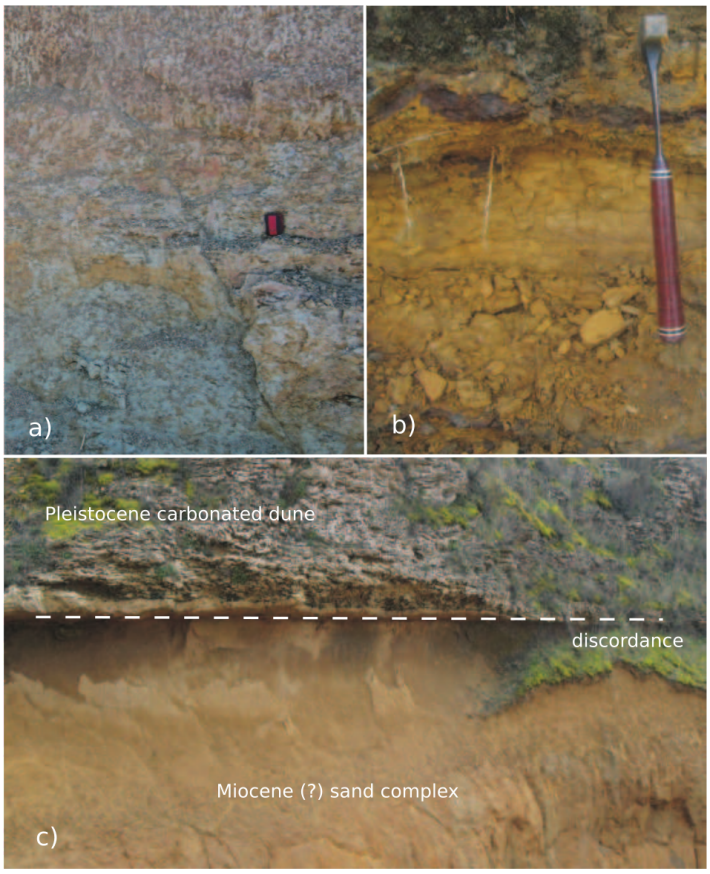

Figure 6.7: Cenozoic sediments at Outcrop C: a) Miocene clay, b) bottom of fluvial terrace showing hard pan, c) Miocene sand sequence discordantly overlain by a carbonated Pleistocene dune.

The entire sequence along the beach is considered to have accumulated during the Miocene to Quaternary. However, it is unclear whether it belongs to the Meştepe or Kayalıtepe formation, or to younger units, respectively. It is discordantly overlain by carbonated dune sediments, as discussed in the following.

Outcrops D comprises the most prominent geological structure at the Campus, a Quaternary dune. Its top elevation is about 70 m msl with the wells situated at its Western flank. The dune does not reach the Black Sea but is considered to overlay Tertiary sediments discordantly, which form the cliffs at the shoreline (outcrop C).

The dune itself shows typical cross-bedding. Bedding inclines with 25 to 35° ESE to SE, striking roughly NE-SW, at which layers which contain a higher amount of silt and clay incline with lower angles. Sediments show an intermediate carbonate content. The dune is addressed as transverse dune. Thus, the prevailing paleo-wind direction was about NW-SE, perpendicular to the strike of bedding. Sand grains are dark yellow to reddish yellow and matte, indicating that dune development started prior to Holocene during Pleistocene.

Where the dune reaches the cliffs, a carbonate skeleton develops (Figure 6.7c). The carbonation affects only the first decimeters of the formation on the seaside, and is restricted to the coarser parts of the sediment. The carbonate skeleton is therefore considered to derive from the precipitation of carbonates, dissolved by ocean spay and seepage water, respectively. Carbonate precipitation is restricted to evaporation within the coarser parts. Finer sediment particles are blown out. Behind the carbonate skeleton a reddish brown carbonate bearing medium/fine sand is encountered, showing a high clay and silt content. Bolder of comparable carbonate skeletons can be found all over the dune. However, when occurring at higher elevations their derivation is slightly different and related to precipitation.

Outcrop E refers to the newly installed wells K5 and K6. Drilling work started in June 2011 and extended until March 2012, as the drilling company was badly prepared, which resulted in a collapsed borehole at well K6. Accordingly, the petrographic and lithological description of drilled material was difficult to realize as upper units contaminated newly drilled material. Thus, features such as, carbonate-, mica-, or clay-content could not be documented for deeper units. Nevertheless, rock samples were taken for every meter out of the drilling suspension and classified with regard to the prevailing constitutes. Regarding the classification of bedrock formations, drilled material was washed prior to examination. Boreholes were drilled at diameters of 266.7 mm and 193.7 mm, respectively, at which drilling diameter changed to smaller size when bedrock was reached. PVC tubes with diameters of 200 mm and 140 mm have been used for well construction (even within bedrock). Slot size of screens is 2 mm. Gravel-pack and clay seals were used to separate hydraulic units.

Figure 6.8 presents the geologic profiles for wells K5 and K6, summarizing the petro-

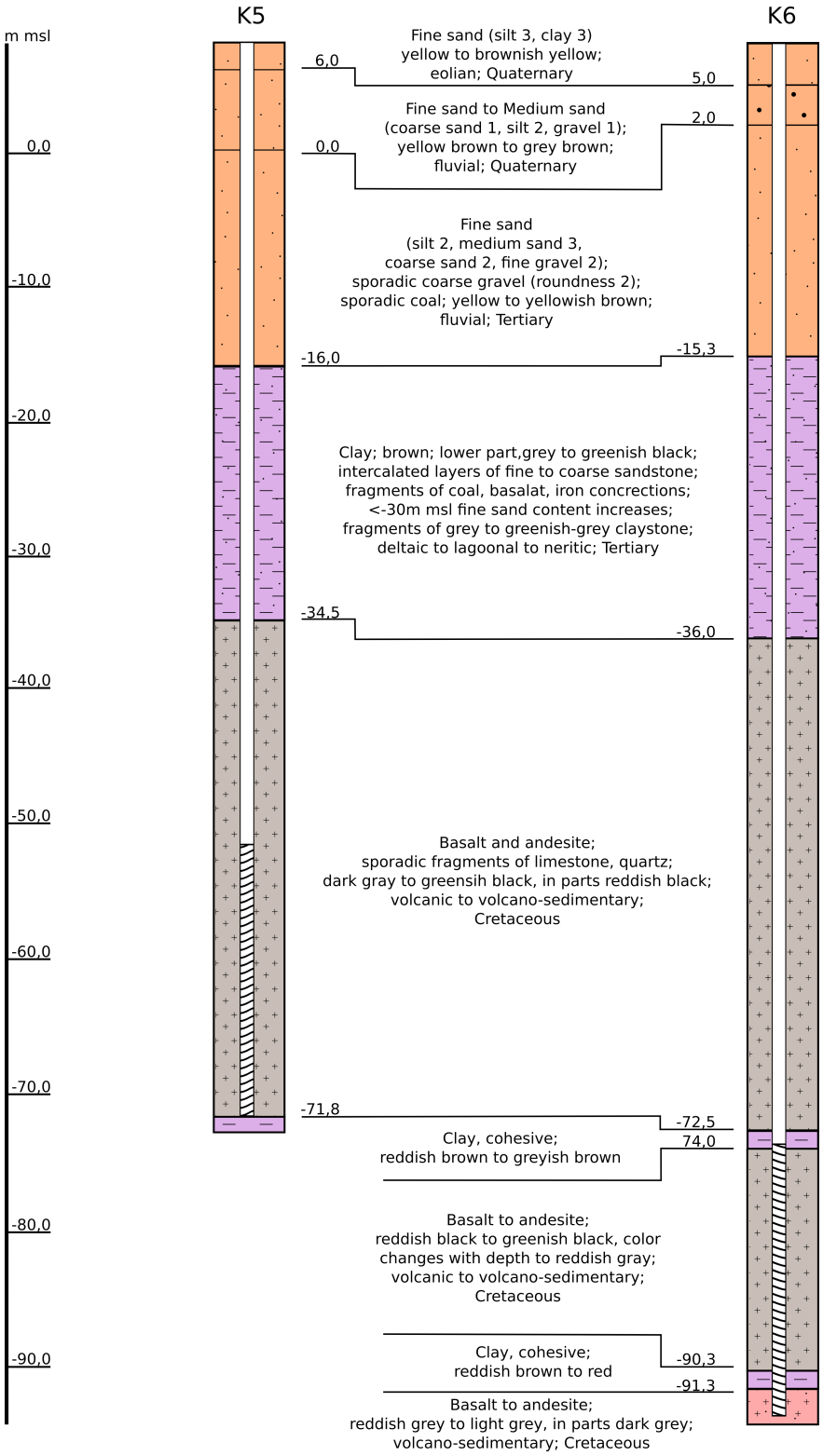

Figure 6.8: Geologic profiles of wells K5 and K6. Main constitutes are mentioned first, numbers describe properties/quantities on a scale from 1 (weak) to 6 (high). Depths were estimated from the number of used drilling rods and are approximations. Dashed section indicate the well screen.

graphic description. In general, the geologic profiles of both wells correlate well. Thus, the bedrock surface is encountered at about -35 m msl. Cretaceous bedrock is overlain by a clay sequence of about 20 m in thickness. At its bottom clay is grey to greenish black, changing to a brownish color upwards. The lower part of the clay sequence further shows a higher content of fine sand and fragments of greenish grey to dark grey clay stone, indicating bedding. Upwards, the fine sand content within the clay decreases, though intercalated sand layers become more evident. Sand layers are considered to reach a thickness of up to 2 m, bearing weakly rounded fragments of basalt and iron concretions. Thus, they indicate a nearby catchment. Stratigraphically, the clay sequences is addressed as part of the Meştepe formation. Upwards, the clay sequence is followed by a sequence of fine sand with varying amounts of medium to coarse sand. The entire sand sequence indicates a fluvial facies, again related to a nearby catchment. However, assigning a stratigraphic unit to this sequence is difficult as no particular characteristics could be identified. The occurrence of mica, characteristic for Çukurçeşme formation [*Özgül et al.*, 2005], was first recognized at about sea level, as drilling continued mica content was varying but generally decreasing with depth. However, fine sand between 0 and -16 m msl is considered to be of Miocene age, relating to Çukurçeşme or Kayalıatepe formation, respectively. Above mean seal level, Tertiary sediment are followed by fluvial and eolian Quaternary sediments.

Within the Cretaceous bedrock, the basaltic facies generally prevails over andesitic components. Thus, drilled bedrock is considered to relate to geologic units encountered at the nearby outcrop A, i.e., to Kısırkaya member of Sarıyer formation, rather than to Garıpçe member. However, investigations at outcrop A indicate that Kısırkaya member comprises different units, namely basaltic andesitic breccia, pyroclastic flow deposits and olivine basalt. In this regard, both wells are considered to be screened within a formation comparable to the basaltic breccia, encountered at outcrop A for several times.

During drilling, several layers of cohesive clay were observed within the Cretaceous formation, at depths of about -72 m msl and -90 m msl (Fgiure 6.8). Below the second clay layer, the bedrock facies changes, as rock color becomes lighter, turning from reddish/greenish black to reddish grey. By comparing drilled material to units at outcrop A, bedrock below -90 m msl is considered to relate to pyroclastic deposits (Figure 6.5d). Though, whether the Cretaceous clay layers relate to a tectonic discordance, i.e., to fault gouge, or may constitute alteration zones or bedding could not eventually be resolved.

6.2.2 Geomorphological and Tectonic Investigations

Figure 6.9a shows the Digital Terrain Model of the Northern part of the Istanbul Peninsula. The Digital Terrain Model was composed by using SRTM-data (3 arcsec) provided by the US Geological Survey. White lines in Figure 6.9a emphasize morphological linea-

ments, basically tracing the drainage system of the Northern Istanbul area. By considering that the drainage system often follows tectonic structures, lineaments can be used for a corresponding analysis. In addition to the drainage system, the dashed blue line indicates the main watershed of the region. It is interesting to note that the watershed basically approximates the trace of the Şile-Sarıyer-fault. South of Saritepe Campus it strikes NW-SE, but changes to NE-SW direction before reaching the Bosporus. Northern rivers drain into the Black Sea, whereas Southern rivers drain to the Sea of Marmara.

The drainage system is considered to have developed on a Pliocene to Quaternary etch-plain, and is therefore related to the neotectonic regime, i.e., to dextral shear and associated block rotation [e.g., *Gökaşan et al.*, 2001a; *Yilmaz*, 2007]. Figure 6.9b summarizes strike-direction of morphological lineaments, identified in Figure 6.9a. Two strike-directions are prevailing, a NE-SW direction and a roughly N-S direction. In addition, Figure 6.9b shows the strike of two faults (green lines) identified at outcrop C. As both faults cut Neogene to Quaternary units, they are considered neotectonic. It can be seen that the strike-slip fault meets the prevailing lineament direction quite well. Note that equivalent sets of lineaments, trending NE-SW, i.e., parallel to the Northern branch of the Bosporus, have also

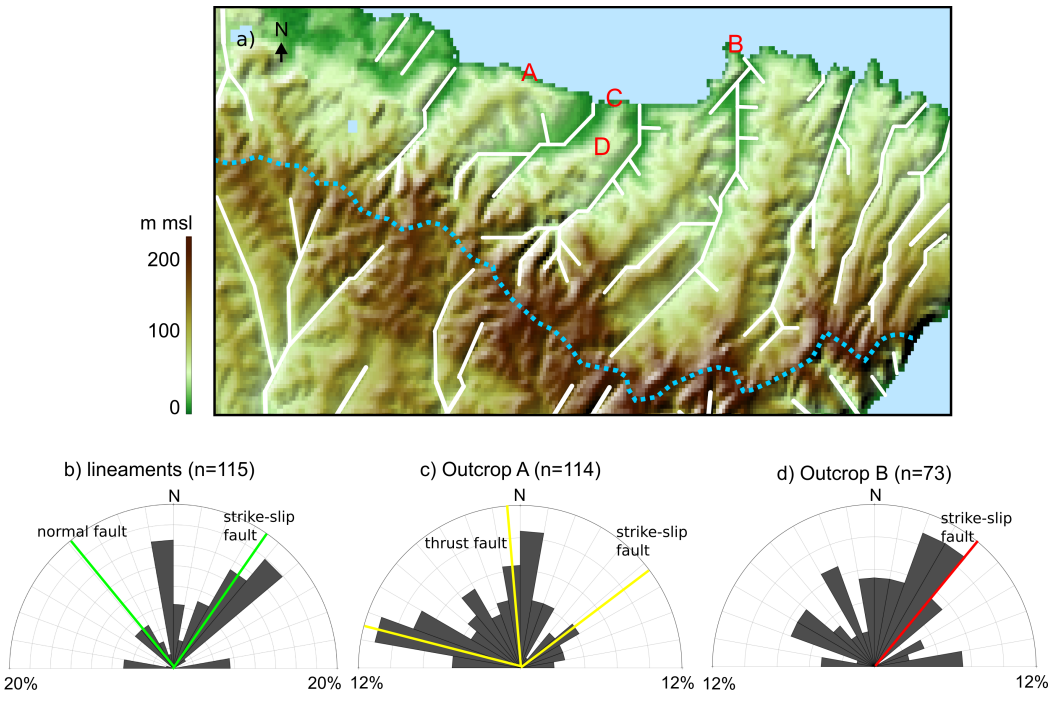

Figure 6.9: Digital Terrain Model of Northern Istanbul (a) showing prevailing geomorphological lineaments (white), as well as the main watershed of the region (blue). Capital letters indicate the investigated geological outcrops. Plot b) summarizes strike directions of geomorphological lineaments and shows the strike of neotectonic faults (green) at outcrop C. Plots c) and d) summarize strike directions of tectonic elements (fractures + faults) at outcrops A and B. Colored lines indicate the strike directions of encountered faults.

been observed by *Gökaşan et al.* [2001a]. On a regional scale, which comprises the Istanbul and Kocaeli peninsulas, they are cut by WNW-ESE to NW-SE striking lineaments which are more continuous and show right-lateral displacement [*Gökaşan et al.*, 2001a]. However, the strike of the normal fault at outcrop C seems to relate to a secondary direction.

Figures 6.9c and 6.9d evaluate measurements of tectonic features at outcrops A and B, respectively. At outcrop A, tectonic measurements mainly comprise fractures within the olivine basalt. Two main strike-directions can be identified, one set strikes roughly N-S whereas the second set strikes WNW-ESE. A fault zone with comparable strike, classified as reactivated fault showing yellowish gouge was identified in the field. The corresponding trend is given by the WNW-ESE oriented yellow line in Figure 6.9c. Thus, this direction is considered to relate to an old (Paleogene) tectonic regime, reactivated by neotectonics. In addition, Figure 6.9c shows strike directions of two other faults which, were encountered at the complex fault zone within the basaltic breccia (Outrcop A). A N-S striking thrust was identified, which is cut by NE-SW trending sinistral strike-slip fault. Accordingly, the N-S striking thrust is considered to relate to paleotectonics, whereas the strike-slip fault might relate to neotectonics.

Figure 6.9d summarizes strike directions of fractures at outcrop B, at which a red line indicates another NE-SW striking fault. The strike of this fault deviates about 15° from that of the strike-slip fault at outcrop A, and follows the main direction of fractures. Moreover, these directions agree with the main strike-direction of the drainage system.

6.2.3 Geologic Model of Saritepe Campus

At Saritepe Campus, the top of Cretaceous bedrock or basis of Tertiary sediments, respectively, is encountered at about -35 m msl. At Kısırkaya (outcrop A) the equivalent geologic boundary is at about 7 m msl; South and West of the campus, Cretaceous units crop out at even higher elevations. With regard to the occurrence of Tertiary formations, Middle to Late Miocene sediments are restricted to the areas West of Saritepe Campus. East and South of the campus, Late Oligocene to Lower Miocene sediments form the uppermost units, which crop out at higher elevations than the corresponding units in the West. Based on these observations, it can be concluded that Saritepe Campus is situated within a structural depression. In this regard, the existence of the Pleistocene dune at the site is considered to be directly related to tectonically induced local subsidence. Consequently, the campus experienced more pronounced subsidence then the surrounding areas during the Quaternary.

The driving force which lead to the current geologic situation at Saritepe Campus is considered to be related to the neotectonic regime of dextral shear and block rotation. In this regard, Figure 6.10 shows a simplified conceptual model for block rotation. Ac-

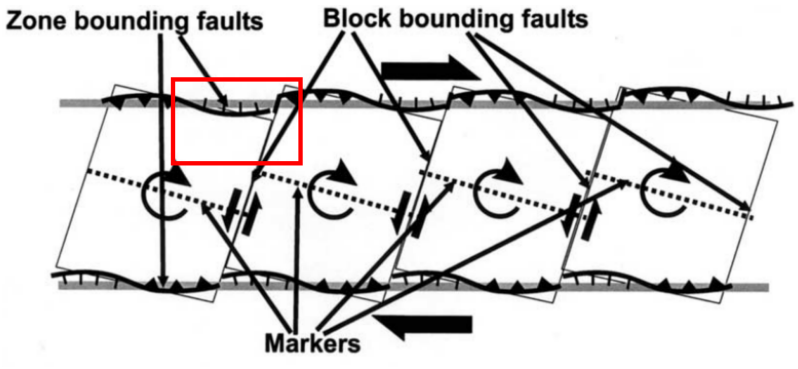

Figure 6.10: Conceptual model of block rotation from *Oktay et al.* [2002]. The rectangle indicates the suggested position of Saritepe Campus within the theoretical model, with the upper corners relating to the villages of Kilyos and Kısırkaya.

cordingly, tectonic movements along right-lateral zone bounding faults lead to rotating tectonic blocks delimited by left-lateral block-bounding faults. The size of the tectonic block in which Saritepe Campus is situated is difficult to estimate. *Oktay et al.* [2002] and *Gürbüz* [2009] apply this model on a regional scale, considering the Bosporus as sinistral block-bounding fault, which separates the tectonic blocks of the Istanbul peninsula and the Kocaeli peninsula. However, *Kaymakci et al.* [2007] investigated block rotation on a more local scale, along the Tekirdağ and Gnasos fault, West of the Sea of Marmara. They found that the extension of tectonic blocks may range from a few kilometers to a few tens of kilometers at which blocks are relatively equidimensional. In this regard, it is interesting to note that another Quaternary dune of similar extent than the one at Saritepe Campus is developed about 15 km West of Saritepe Campus, close to the village of Agaçlı [*MTA*, 2012c]. Moreover, the Bosporus is about 15 km East of the campus. Thus, it is suggested that Saritepe Campus is located West of a sinistral NE-SW trending strike-slip fault, which continuous to the village of Kilyos. Conceptually, this strike-slip fault is understood as block-bounding fault. The position of Saritepe Campus with regard to the conceptual model of block rotation is indicated by the red rectangle in Figure 6.10. Thus, the tectonic situation at the site is quite complex. However, NE-SW trending left-lateral strike-slip faults are considered the main tectonic structures of the area. In general, Saritepe Campus is expected to be intersected by various faults which potentially constitute hydraulic boundaries for groundwater reservoirs.

6.3 Hydraulic Testing

To investigate the hydrogeological situation at Saritepe Campus pumping tests were conducted in 2012. This section summarizes details on pumping test performance and evaluates the obtained data to derive the pumping test interpretation model, by utilizing the

derivative approach as outlined in Section 2.3.1. Subsequently hydraulic aquifer parameters of the investigated groundwater reservoir are estimated. Hydraulic testing was accompanied by groundwater sampling. The corresponding data is evaluated in Section 6.4. Finally, the conceptual hyrogeological model of Saritepe Campus is presented and discussed in Section 6.5.

6.3.1 Pumping Test Setup and Well Conditions

Preliminary tests and investigations, such as camera inspections and well cleaning were conducted in 2010/2011. They revealed that well K1 is the only well at the site suitable for pumping. K2 is artesian year-round and had to be capped to ensure hydraulic head recordings. Wells K3, K5 and K6 do not allow for extracting a considerable amount of groundwater. Well K4 currently provides water supply for Saritepe Campus, but shows no influence on the other wells. Thus, well K1 was used as pumping well. Well data, including well depths and screened sections is provided in Table 6.1. An overview on well locations is given in Figure 6.1.

In order to get a first impression of the hydrogeological situation of the reservoir perturbed by pumping, Figure 6.11 shows the hydraulic head h, at considered wells from May to August 2012. Additionally, Figure 6.11 gives the daily rate of precipitation, recorded at the nearby village of Kilyos. It can be seen that the pumping tests were conducted over a dry period, with a decreasing seasonal trend in h. Closer examination of Figure 6.11 reveals that the hydraulic head at wells K5 and K6 deviates significantly from that of the other wells, suggesting that these wells tap different aquifers. Furthermore, h at well K3 is below h at wells K1 and K2 in May 2012, eventually exceeding h at K2 after a preliminary

Table 6.1: Dimensioning of wells at Saritepe Campus.

	K1	K2	K3	K5	K6
UTM x	667960.0	668005.7	668038.4	668001.3	668004.7
UTM y	4567526.2	4567618.2	4567694.0	4567531.3	4567541.3
Elevation					
ground [m msl]	7.84	5.37	9.41	8.14	7.76
well bottom [m msl]	-87.97	-131.53	-124.74	-71.86	-92.24
Screen					
top [m msl]	-43.66[1]	-55.13[1]	-55.09[1]	-51.86	-72.24
length [m]	44.31	76.40	69.65	20	20
diameter [mm]	110	110	110	140	140
Distance for K1 [m]	-	101.60	184.70	39.90	49.80

[1] not screened, top-elevation indicates the end of casing/start of open-hole

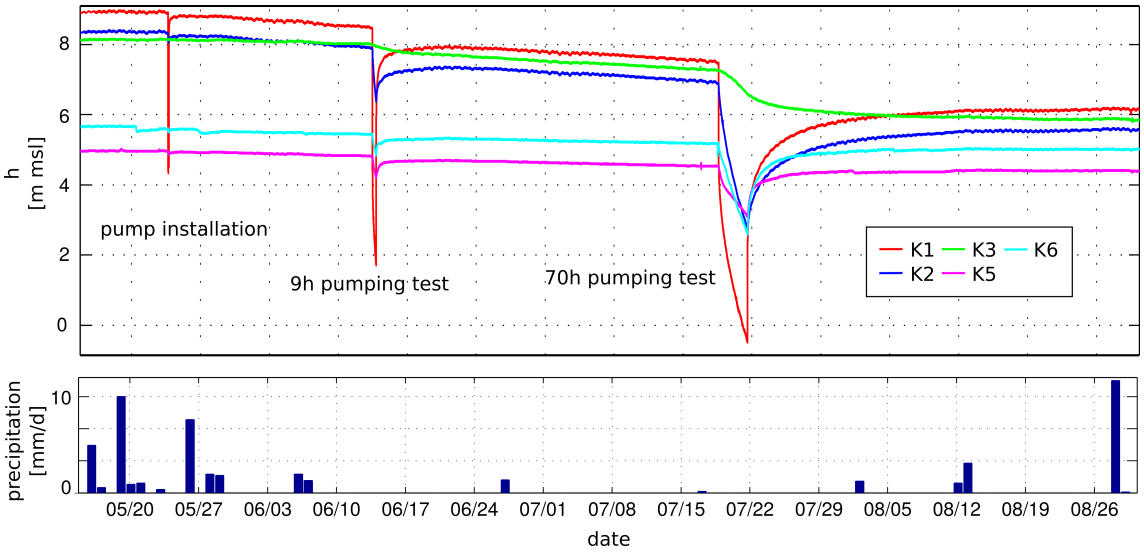

Figure 6.11: Hydraulic head at considered wells and rate of precipitation over a period from spring to autumn 2012.

test in June 2012. Even though h at K3 responds to pumping at K1, the response is delayed and no recovery is observed. Thus, it is concluded that well K3 is partly isolated from the aquifer reservoir investigated by pumping, most likely by a semi-permeable fault.

Based on the above observations and by considering the results from geological investigations in Section 6.2, Figure 6.12 provides a preliminary hydrogeological model which will serve as a basis for pumping test interpretation in the following. Accordingly, the investigated reservoir consists of three aquifer units. Cretaceous bedrock is overlain by Quaternary to Tertiary sediments, which are summarized to aquifer unit A. The deeper parts of unit A comprise a clay complex which acts as confining layer. Thus, aquifer unit A does not contribute to groundwater flow in the deeper units. The Cretaceous bedrock formation is divided into two aquifer units, with unit B relating to a basaltic breccia, and unit C to pyroclastic deposits. Both units are assumed to dip with about 10-15° North, as suggested by field measurements. They are separated by confining clay layers. Due to

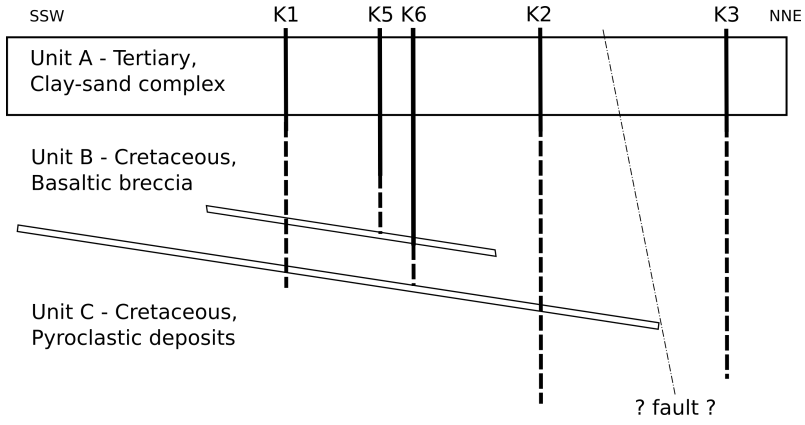

Figure 6.12: Preliminary hydrogeological model of the investigated reservoir, based on geologic information from drilling wells K5 and K6, and long term records of h.

lack of additional data, clay layers are regarded continuous, and the potential relation to a fault zone is neglected.

Wells K1 and K2 are screened over both aquifer units B and C. Well K1 is considered to tap just the upper part of unit C, whereas K2 taps the deeper part of the pyroclastic deposits. Wells K5 and K6 tap aquifer unit B. Please note that due to the wells being screened in different aquifers, providing a meaningful contour map of the hydraulic head is not possible.

6.3.2 Data Processing

Prior to pumping test interpretation, hydraulic head data had to be corrected for variations in the seasonal trend and for the influence of sea tides, respectively. Regarding the seasonal trend, the correction was performed by fitting a linear model to the hydraulic head data recorded over two weeks prior to pumping. The obtained trend was extended over the duration of the pumping test for a linear correction.

The correction for tides was a bit more complicated. Even though the amplitude of Black Sea tides is rather small, an impact on the hydraulic head was noticed, and correction was required. However, tidal data which is usually needed for a correction [e.g., *Chapuis et al.*, 2006; *Toll and Rasmussen*, 2007] was not available for the Black Sea. Thus, an attempt was made to correct the data by means of synthetically generated tides.

Therefor, the hydraulic head from well K1 was used, recorded over a three months period from January to March 2012. The corresponding data was corrected for the seasonal trend and a synthetic tidal model was fitted using the Tidal Fitting Toolbox [*Grinsted*, 2014] in MATLAB, which uses ordinary least squares to fit tidal components. Subsequently, the fitted model was used for tidal prediction over the duration of the pumping test, and the hydraulic head was corrected accordingly. Figure 6.13 compares variations in the hydraulic head at well K1 to the fitted model. Even though, the tidal model does not fit the underlying data perfectively, both data sets agree well. The fitted tidal model is thus regarded sufficient for data correction.

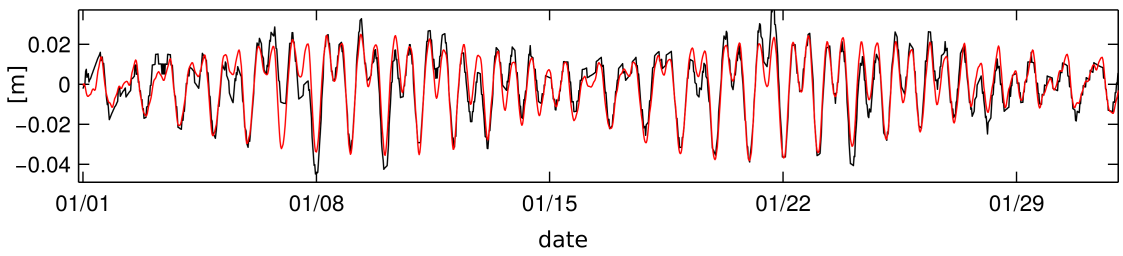

Figure 6.13: Variations of the hydraulic head at well K1 in January 2012 (black) compared to the fitted tidal model (red), used for the correction of pumping test data.

As pumping test evaluation by diagnostic plots (Section 2.3.1) relies on the time derivative of the hydraulic head, artifacts which originate from noise require further processing. In order to minimize these artifacts several studies propose numerical differentiation schemes such as smoothing the data prior to the computation of the derivative, or smoothing the derivative [e.g., *Bourdet et al.*, 1989; *Spane and Wurstner*, 1993; *Horne*, 1996; *Illman and Neuman*, 2001]. Within this study, the following procedure was used for data differentiation and the removal of noise.

After the correction for the seasonal trend and tides, the data was sampled on regular intervals to reduce the number of data points. Afterwards, a zero-phase digital filtering, which processes the data in both the forward and reverse direction [*Oppenheim and Schafer*, 1999] was applied, by using the *filtfilt*-function in MATLAB. For taking the derivative, the numerical differentiation scheme proposed by *Bourdet et al.* [1989] was utilized. It uses one point before and one point after the point of interest i, calculates the corresponding derivative, and places their weighted mean at the point considered [*Bourdet et al.*, 1989],

$$\left(\frac{\partial h}{\partial \tau}\right)_{\mathrm{i}} = \frac{(\Delta h_1/\Delta\tau_1)\Delta\tau_2 + (\Delta h_2/\Delta\tau_2)\Delta\tau_1}{\Delta\tau_1 + \Delta\tau_2}, \tag{6.1}$$

where subscript 1 refers to a point before i, subscript 2 to a point after, and τ to the time function $\ln \Delta t$. When working with build-up data, the equivalent Agarwal time t_{a} was used instead of t (Section 2.3.1).

6.3.3 Pumping Test Interpretation

This section evaluates drawdown and build-up data of a 70-hours pumping test, which started on July 18th, 2012. The pumping test was performed at a constant rate of 3.9492 m^3/h with a Grundfos SQE 7-40 pump installed at 50 m below surface level on May 23$^{\mathrm{rd}}$, 2012. The hydraulic head was recorded at intervals of 10 seconds at the pumping well K1, and each minute at the remaining wells. Vented gauges which automatically compensate for changes in barometric pressure were used.

With regard to the preliminary hydrogeological model presented in Figure 6.12, pumping test interpretation aims to answer the following questions: 1) Is the reservoir bounded? 2) Is the proposed division into aquifer units appropriate? 3) Can information on aquifer heterogeneity be estimated?

Diagnostic Plots

Figure 6.14 summarizes typical flow regimes which can be identified by means of the drawdown derivative with respect to $\ln t$, plotted as a function of time on log-log scale. The slope of the drawdown derivative allows for associating flow regimes to reservoir properties and boundary conditions. As long as there is no flow barrier between the wells, the outer

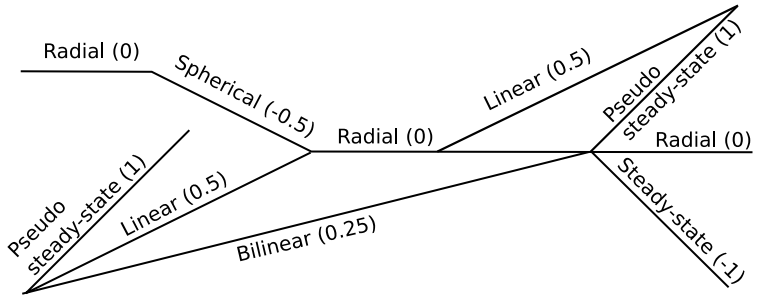

	time range Early	Intermediate	Late
0	Double porosity restricted	Homogeneous behavior	Semi-infinite reservoir
0.25	Finite conductivity fracture	Finite conductivity fault	Double porosity unrestricted with linear flow
0.5	Infinte conductivity fracture	Horizontal well	Two parallel sealing boundaries
1	Wellbore storage	Layered no crossflow with boundaries	Closed reservoir (drawdown)
-1		Conductive fault	Constant head boundary
-0.5		Well in partial penetration	

Figure 6.14: Flow regime identification scheme (compiled from *Ehlig-Economides et al.* [1994]; *Bourdet* [2002]; *Renard et al.* [2009]), representing schematically the $\ln t$-derivative of the drawdown/build-up as a function of $\log t$. The slope of the derivative, which is given in parenthesis, allows for associating flow regimes to reservoir properties, at different times of the pumping test.

reservoir boundaries have a similar influence on the hydraulic response at the pumped well and the observation wells. Accordingly, the characteristic derivative behaviors presented in Figure 6.14 can also be observed on interference test data [*Bourdet*, 2002]. Note that the drawdown is commonly more prone to fluctuations in the pumping rate than the build-up.

Figure 6.15 shows the diagnostic plots of drawdown and build-up data for the 70-hours pumping test at K1. Thin lines relate to the drawdown and the build-up, respectively, bold lines to the corresponding derivatives. In addition, the slope of the derivatives is given by numbers. Figure 6.15 suggests that pumping test interpretation at the site is complex. Dependent on which aquifer unit a particular well taps, different flow regimes are observed. Therefore, Table 6.2 summarizes identified flow regimes and reservoir properties by combining information form Figures 6.14 and 6.15. In doing so, early pumping time data is disregarded, as it commonly relates to well effects. From Table 6.2, it can be seen that the hydraulic response at wells K1 and K2 indicates a reservoir delimited by two parallel sealing boundaries. Note that both wells tap aquifer units B and C (Figure 6.12). On the contrary, the hydraulic response at wells K5 and K6, which solely tap aquifer unit B, indicates a closed reservoir, or a reservoir of double porosity, respectively. The pumping test interpretation model is derived and discussed in the following.

Starting with the interpretation of the hydraulic response at the pumped well K1, the

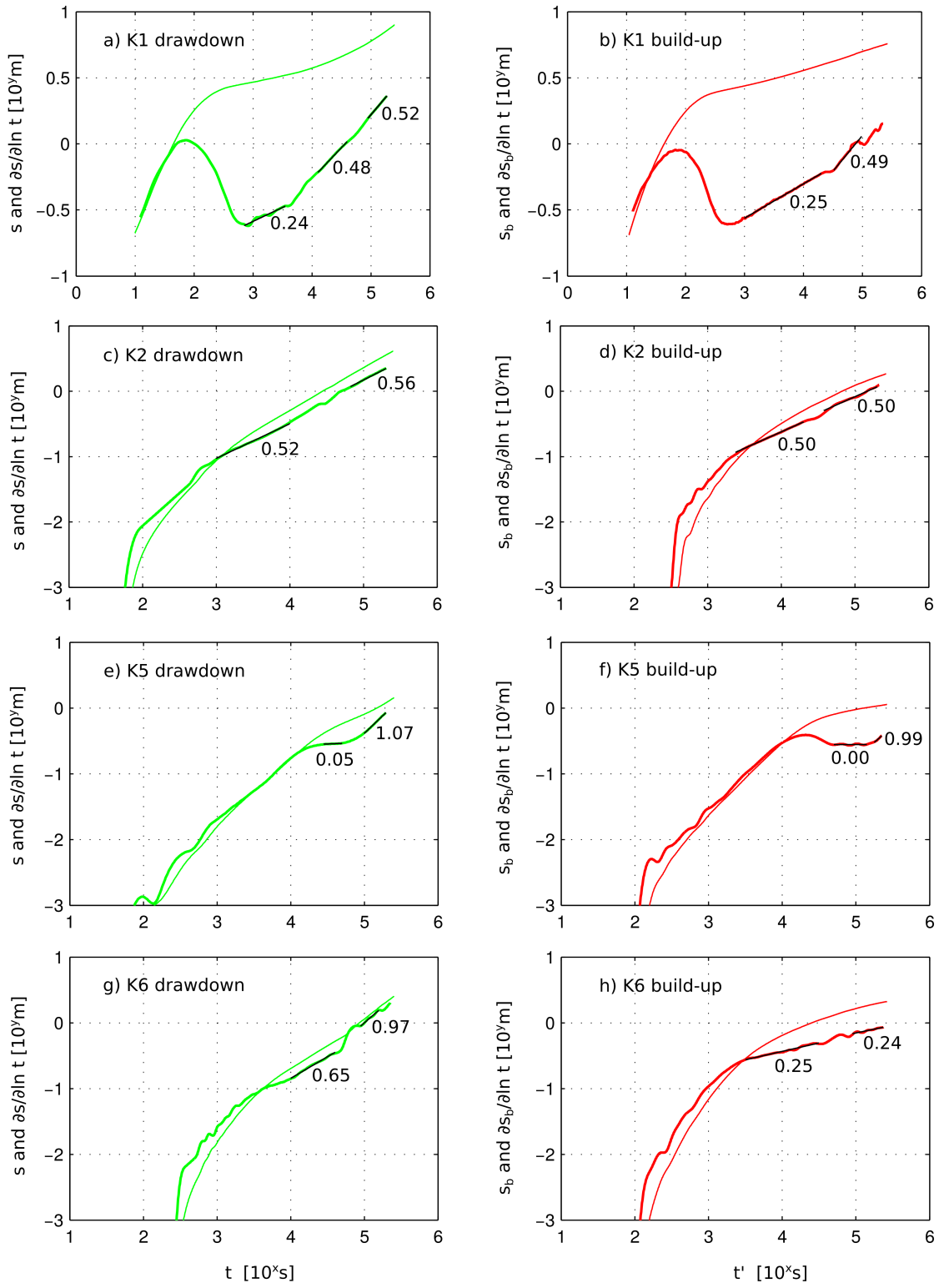

Figure 6.15: Diagnostic plots. Well K1 is active, wells K2, K5 and K6 are observation wells. Thin lines show the drawdown and build-up data, respectively; bold lines the corresponding derivatives. Black lines indicate periods over which the slope of the derivative was calculated.

Table 6.2: Reservoir properties obtained by evaluating the diagnostic plots in Figure 6.15.

Well	Slope of the derivative and associated reservoir properties for	
	Intermediate times	Late times
K1	≈ 0.25: layered/double porosity	≈ 0.5: parallel sealing boundaries
K2	≈ 0.5: parallel sealing boundaries	≈ 0.5: parallel sealing boundaries
K5	≈ 0: radial-infinite acting flow	≈ 1: closed reservoir
K6[1]	≈ 0.25: layered/double porosity	≈ 0.25: layered/double porosity

[1] drawdown response is not interpretable

drawdown and build-up derivatives show a characteristic hump during early pumping times associated to well effects, not representing reservoir properties. After the influence of well effects vanished, both derivatives show a slope of about 0.25 (bilinear flow) which changes with continuous pumping to about 0.5 (linear flow). The shapes of the drawdown and build-up derivatives at K1 agree well with a theoretical model reported by *Stewart* [1997] (as cited by *Bourdet* [2002]), which relates to a double porosity configuration within a channel reservoir. That is, the well taps a reservoir delimited by two parallel sealing boundaries, which consists of two layers with the permeability of the bottom layer being larger than in the higher part. Regarding the preliminary hydrogeological model (Figure 6.12), this implies that the permeability of the pyroclastic deposits (unit C) is considerably larger than that of the basaltic breccia (unit B). This seems reasonable, as the porosity of pyroclastic deposits is commonly larger than that of a basaltic breccia. However, drawdown and build-up data also show differences, e.g., in the time when the slopes of the derivatives change from 0.25 to 0.5. Since well K1 taps aquifer units B and C, this effect is attributed to the specific withdrawal from each aquifer unit. That is, even though the pumping rate is kept constant on the surface, the withdrawal from each aquifer unit may be fluctuating, dependent on the hydraulic properties and the available amount of groundwater. In this regard, groundwater flow within the basaltic breccia is considered to be restricted to fracture flow with the effective porosity of the matrix being almost negligible. Thus, the bilinear flow regime extends during build-up, as unit C is primarily producing.

With regard to the aquifer response at observation well K2, both, the drawdown and build-up derivatives show a slope about 0.5 indicating that two parallel sealing boundaries are recognized. Though, bilinear flow which can be attributed to a layered reservoir is not observed. In fact, the influence of the outer boundaries is recognized quite early. This fortifies the assumption of unit B being less productive, barely contributing to the drawdown at K2, and unit C providing the main share in extracted groundwater.

Well K5 is solely screened in the upper part of aquifer unit B of lower permeability (basaltic breccia). Accordingly, the drawdown and build-up derivatives at well K5 indicate

different reservoir properties than at wells K2 and K1. After the influence of well effects vanished, the slopes of the derivatives stabilize for a rather short intermediate period at about 0, indicating a radial infinite acting flow regime. During late pumping times, a slope of about 1 suggests a closed reservoir. However, the hydraulic response at the other wells contradicts the closed reservoir hypothesis. Thus, it is suggested that within aquifer unit B, the cone of depression does not reach the reservoir boundaries. The late-time slope of 1 does rather indicate that unit B is barely producing at the end of the test, thus acting like a closed reservoir.

With regard to the hydraulic response at well K6, the drawdown derivative does not allow for drawing conclusions on reservoir properties as its slope does not correlate with available flow regimes. This might be due to the fact that well K6 taps unit C for about one meter. Furthermore, when considering the clay layers as fault gouge, the deeper part of aquifer unit B might be intensively disturbed. Nevertheless, the build-up derivative shows a quite constant slope of about 0.25, suggesting that the well is screened within a double-porosity layer, or a layered reservoir, respectively. However, the hydraulic response at well K6 does not show any influence of outer boundary. This again points to a restricted groundwater flow in aquifer unit B.

Another feature which is observed at all wells is some disturbance at $t = 10^{4.5}$ to 10^5 seconds. The reason for this disturbance is not clear. It might be related to some hydraulic interaction between the aquifer units, as it temporally correlates with the infinite acting flow period at K5. Beyond that, it could also indicate a change in the allover reservoir permeability during late times, which would point to the existence of the semi-permeable fault, as suggested by the preliminary hydrogeological model.

In summary, the questions on reservoir properties raised at the beginning of this section can be answered by defining the pumping test interpretation model as follows. The investigated reservoir is considered to be delimited by two parallel sealing boundaries. The proposed division of the Cretaceous bedrock formation into two aquifer units B and C is supported. With regard to aquifer properties, the permeability of unit C is assumed to be considerably larger than that of unit B, with unit C providing the main share of extracted groundwater. Furthermore, pumping test interpretation suggest that a double-porosity model is applicable for aquifer unit B. Though, additional information on aquifer heterogeneity of aquifer unit C can not be provided as the hydraulic response is dominated by the reservoir boundaries.

Parameter Estimation

In order to verify the proposed pumping test interpretation model, further investigations would necessitate to establish a numerical model. However, the above investigations also

show that the investigated aquifer system is not bounded by the Black Sea, but by two impermeable boundaries. As the focus of this thesis is on pumping test interpretation in coastal aquifers, establishing a sophisticated numerical model of the site is beyond the scope of this work. Anyway, in order to provide preliminary estimates of hydraulic parameters, this section utilizes a simplified analytical model. In this regard, parameter estimation is restricted to solving the direct problem to reproduce the drawdown response at the pumped well K1.

The relation between hydraulic aquifer parameters and the geometry of a homogeneous channel reservoir is given by [*Bourdet*, 2002, Equation (5.6)]

$$L_1 + L_2 = 1.246 \frac{qB}{b\, m_{\mathrm{Ch}}} \sqrt{\frac{\mu}{k\phi c_{\mathrm{t}}}}, \tag{6.2}$$

with L_1 and L_2 being the perpendicular distances between the pumped well and the channel boundaries in meters, q the pumping rate in m^3/d, B the formation factor, b the aquifer thickness, μ the viscosity of water in centipoise (cp), k the permeability in millidarcy (md), the effective porosity ϕ, and the total compressibility of the formation and water c_{t} in bar^{-1}. $\mathrm{m_{Ch}}$ relates to the slope of the drawdown with respect to $\sqrt{t}$, with t in hours and s in bar.

Figure 6.16a shows the drawdown and build-up at well K1 as a function of $\sqrt{t}$. The corresponding slopes are $m_{\mathrm{Ch}} = 0.06$ for the drawdown, and, $m_{\mathrm{Ch}} = 0.02$ for the build-up. However, in order to utilize Equation (6.2), several assumptions are needed for the parameters of porosity and total compressibility. The corresponding values are given in Table 6.3. Furthermore, the thickness of the aquifer is set equal to the screen length at well K1, as no data on the true thickness is available. The formation coefficient B was set to one, i.e., the volume of one kilogram of water is considered the same under surface and subsurface conditions.

In order to get a first estimate for the permeability k or transmissivity T, respectively, it is recognized that immediately after well effects vanished at K1, the drawdown and build-up derivatives show a slope of about 0 for a rather short period between $10^{2.75}$ and $10^{2.85}$ seconds (Figure 6.15a/b). A slope of 0 indicates a period of radial infinite-acting flow (Figure 6.14). Under radial infinite-acting flow, the Cooper-Jacob method [*Cooper and Jacob*, 1946] can be applied to get a first estimate of the transmissivity. In doing so, a value of $T = 2.1 \cdot 10^{-3}$ m^2/s is obtained from this short period of the drawdown and the build-up ($m_{\mathrm{s}} = 0.09$, $u \approx 4 \cdot 10^{-5}$). This estimate of T is subsequently used within Equation (6.2), along with the presumed values for porosity and compressibility, to obtain a first estimate for the width of the channel $L_1 + L_2$. The channel width is thus estimated to 253 m from drawdown, and 784 m from build-up data, respectively.

However, the results from the diagnostic plots indicated that the medium is of double-porosity. Hence, the estimated transmissivity, which is quite large, might represent the

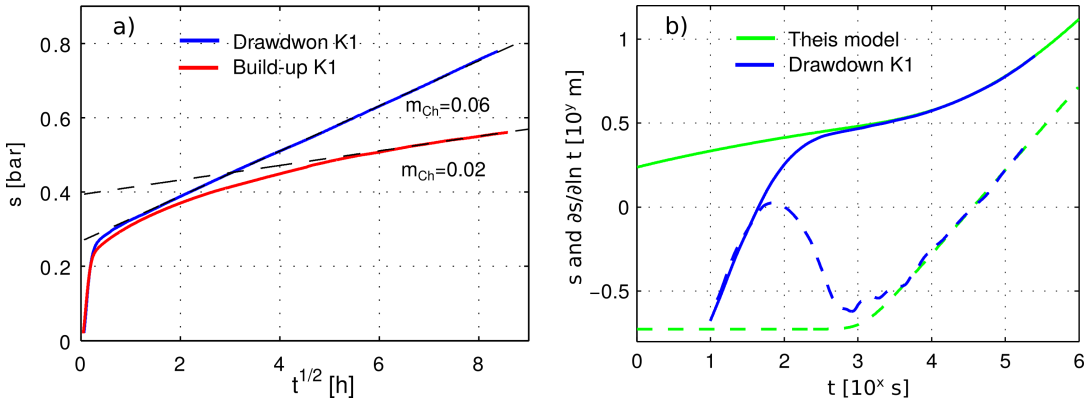

Figure 6.16: Parameter estimation from drawdown data at well K1. a) Drawdown and build-up as function of $\sqrt{t}$. b) Best fit between the real drawdown at well K1 and the calculated drawdown from the Theis-model.

"early" flow through the fractures. Furthermore, the channel width estimated from the build-up might also be too large, because the hydraulic head did not completely recover to its initial value prior to pumping (Figure 6.11). To check the obtained estimates for plausibility a simple model for a channel reservoir was established, by using Theis' equation along with the principle of superposition. Afterwards, the model was used to adjust the hydraulic parameters and channel width, to obtain the best agreement with the real drawdown at K1.

Figure 6.16b shows the best fit between the real drawdown at well K1 (blue) and the calculated drawdown from the Theis-model (green), as well as the corresponding derivatives. The aquifer parameters estimated from the best fit are summarized in Table 6.3. For early-intermediate times (about 10^3 seconds), the model overestimates the drawdown and consequently underestimates the hydraulic conductivity, as it ignores double-porosity and the presence of two aquifer units, respectively. However, for late times the model fits the real data quite well. The estimated channel width is about 420 m. The hydraulic conductivity of the entire aquifer system considered to be homogeneous is $1.08 \cdot 10^{-5}$ m/s. The early-time transmissivity estimated above is considered to approximate the transmissivity of fractures. Please note that the aquifer thickness, which was assumed to equal the screen length at well K1, has significant impact on the estimated hydraulic conductivities, since the Theis-model yields the transmissivity of the aquifer.

Furthermore, the presumed value for the porosity of the aquifer (0.12) might be regarded quite large for a basalt formation. However, presuming a lower porosity does not significantly impact the estimated hydraulic conductivity, though, estimates of storativity and the channel width. For example, assuming a porosity of $7 \cdot 10^{-3}$ yields a channel width of 1.6 m. This would basically mean that K1 is screened in a narrow fracture/fault zone of high conductivity. By considering that the outer reservoir boundaries are also recognized

Table 6.3: Estimated reservoir properties obtained by fitting a Theis-model to the drawdown at the pumped well K1.

Assumed parameters	
Porosity	0.12
Total compressibility (water + rock)	$8.6 \cdot 10^{-5}$ bar^{-1}
Aquifer thickness	44 m
Estimated parameters	
Hydraulic conductivity (fractures)	$4.66 \cdot 10^{-5}$ m/s
Hydraulic conductivity (entire formation)	$1.08 \cdot 10^{-5}$ m/s
Storativity	$4.3 \cdot 10^{-5}$
Channel width	420.5 m
Distances K1 to outer boundaries	176.6 m / 243.9 m

at well K2, such a scenario is considered unlikely to represent the hydrogeological situation at the site.

6.4 Hydrochemical Investigations

Hydrogeological investigations suggest that the investigated reservoir is not influenced by the Black Sea. To provide further data in support of this conclusion, hydrochemical investigations are evaluated in the following. Furthermore, it is examined whether the hydrochemistry at the site supports the current understanding of the aquifer system.

6.4.1 Groundwater Sampling and Analysis

Groundwater sampling was realized by different techniques, namely, by pumping and by using a vacuum sampler to obtain depth oriented groundwater samples. That is, a vacuum is created within a metal probe with a capacity of 2 liters. Afterwards, the probe is lowered into the well and a valve is opened. After the groundwater entered the sampler the valve is closed and the probe is lifted. Besides, groundwater samples at well K1 were directly taken from the extracted water when a pumping test was performed. Seawater from the Black Sea and precipitation was also sampled. Moreover, water samples from a spring were taken, which originates at an elevation of about 30 m msl on the Western flank of the Pleistocene dune between wells K1 and K2. Chemical analysis was performed in the laboratories of the Helmholtz-Centre for Environmental Research in Halle. Analysis results were checked for plausibility by means of an ion balance.

The following characterization concentrates on determining the type of groundwater by examining the bulk chemical composition. Subsequently, conservative tracers such as

chloride and the stable isotopes ^{2}H and ^{18}O are used for a more detailed interpretation. The applied methods are in general state-of-the-art techniques, e.g., *Clark and Fritz* [1997] and *Appelo and Postma* [2005]. A table which summarizes results of the chemical analysis is presented in Appendix A.

6.4.2 Hydrochemical Characterization

The electric conductivity of sampled groundwater varies between 0.54 and 6.62 mS/cm. Spring water from the Pleistocene dune shows the lowest value, whereas water from the deeper part of wells K2 and K3 is most conductive. At well K4, the electric conductivity of the pumped water is about 1 mS/cm. Groundwater from wells K1, K5 and K6 is a bit more conductive with about 1.3 mS/cm. With continuous pumping, the electric conductivity at well K1 increased to 2.4 mS/cm. Seawater samples from the Black Sea yield about 28 mS/cm.

The pH of sampled groundwater varies between 7.3 and 9.34, with spring water showing the lowest value again. Groundwater from well K5 shows the highest pH, whereas groundwater from the deeper part of the aquifer system has a pH of about 8. At K1, the pH changes with continuous pumping from 9.2 to 9.08. At K4 the pH is about 8.2, slightly less than the pH of sampled seawater, which is 8.4.

Figure 6.17 compares the electric conductivity to the pH of all taken groundwater samples. It can be seen that two groundwater volumes are present within the Cretaceous formation, an upper unit of fresh groundwater which relates to groundwater from aquifer unit B (basaltic breccia), and a deeper volume of brackish groundwater relating to aquifer unit C (pyroclastic deposits).

The temperature of sampled waters ranges from about 15.8 to 22.2°C. Disregarding the few uppermost meters of the water column affected by surface temperature, the water temperature increases with depth with about 3°C/100m. Thus, no evidence on geothermal impact is found. Despite the sampled spring water, which has an oxygen content of

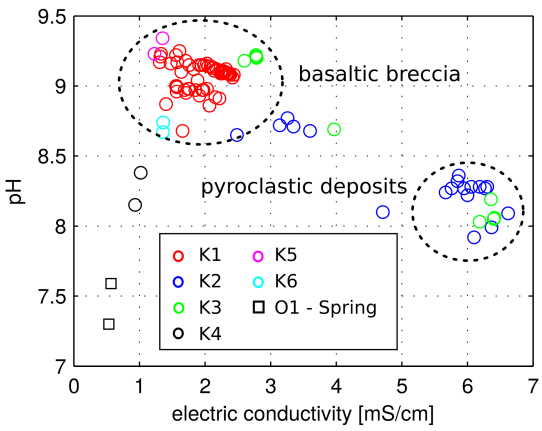

Figure 6.17: Electric conductivity and pH of sampled groundwater. Two groups can be distinguished relating to the corresponding geologic units.

5.8 mg/l, groundwater samples generally show an oxygen content <0.1 mg/l. The average redox-potential of groundwater is about -50 to -75 mV and does not vary significantly between wells and depths, respectively.

Figure 6.18 presents the relative molar composition of cations and anions of sampled waters by means of a Piper diagram. The composition of groundwater from the Cretaceous formation can be clearly distinguished from spring water and seawater. Spring water is of Ca-HCO_3-type, whereas seawater is of Na-Cl-type with a Na/Cl-ratio of about 0.88.

Closer examination of the groundwater from the Cretaceous formation reveals that groundwater from aquifer unit B, i.e., from wells K1, K5 and K6, is of Na-HCO_3-(Cl)-type. With continuous pumping, the composition of the extracted groundwater at well K1 changes to Na-Cl-(HCO_3)-(SO_4). Thus, the character of the pumped water changes towards the composition of the groundwater which prevails in the deeper part of the aquifer system tapped by wells K2 and K3. The corresponding groundwater from depths of about -125 m msl is of Na-Cl-(SO_4)-type. Consequently, two groundwater volumes are distinguished, a Na-HCO_3-type groundwater within unit B and a Na-Cl-type groundwater in unit C.

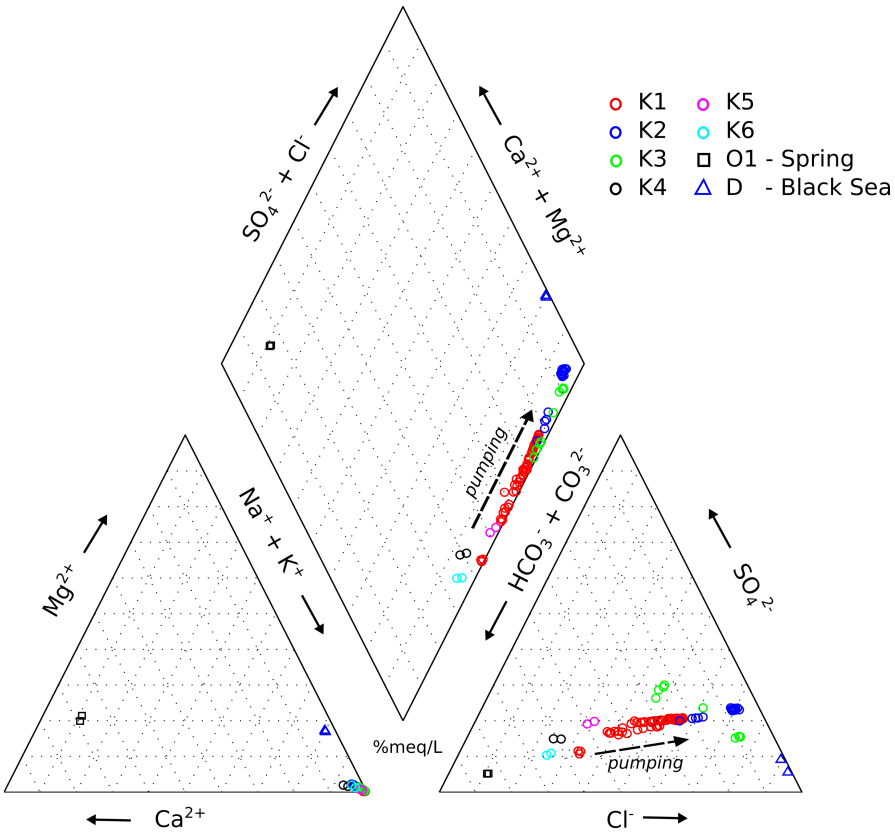

Figure 6.18: Piper diagram of sampled waters. Note that the total load of dissolved solutes or the electric conductivity at K1 increases with pumping, and with depths at wells K2 and K3, respectively.

With regard to the origin of the groundwater it is interesting to note that sodium accounts for >90% of cations, whereas the percentage of calcium and magnesium is less than 5%. An explanation for this composition might be long residence times within basaltic rock. Thus, recharging CO_2-charged meteoric water of Ca-Mg-HCO_3-type can change to a Na-HCO_3-water and eventually to a Na-Cl-type groundwater. That is, silicate/silica hydrolysis and dissolution occurs along the flow path of the water, resulting in a gradual increase in pH while chloride is leached, e.g., from glass within the partly hyaloclastic basaltic breccia. Precipitation and ion-exchange reactions further modify the water by removing calcium and magnesium in exchange for sodium [*Hearn et al.*, 1985; *Reidel et al.*, 2002]. Thus, the chemical composition of the groundwater is considered to mainly result from water-rock interaction.

However, groundwater from aquifer unit C is brackish with Na/Cl-ratios of 1.5. The increased ion content might result from either very long residence times, much longer than for the groundwater from unit B, or, from secondary solution of sodium salts. In this regard, brackish groundwater is considered to only prevail in the deeper parts of aquifer unit C, not comprising the entire formation of pyroclastic deposits. Note that the salinity of the pumped water at well K1, which is assumed to tap only the upper part of unit C, increases with continuous pumping, thus indicating up-coning within unit C. However, suggesting secondary solution of sodium salts would presume the availability of halite. Corresponding intercalated layers within the volcanic sequence might relate to sedimentation and evaporation between eruptive events. Though, evidence for such geologic conditions does not exist.

6.4.3 Conservative Tracers

Figure 6.19 shows the δ^2H-δ^{18}O diagram for groundwater and precipitation samples collected at the site. It further shows the global meteoric water line (GMWL) and the local meteoric water line of the Marmara region (MWL) [*Dirican et al.*, 2005]. From Figure 6.19 it can be seen that precipitation samples plot close to the MWL and GMWL, respectively, at which the most depleted sample relates to a sample of snow. Groundwater samples form well K4 and the spring plot almost on the MWL with $\delta^2\mathrm{H} = -52\,‰$ and $\delta^{18}\mathrm{O} = -8.2\,‰$, thus indicating an origin of groundwater from recent meteoric water. This is also supported by ^{3}H-data of 4.7 TU for groundwater from well K4, indicating that groundwater derives from meteoric water younger than 50 years.

The groundwater at the remaining wells is depleted in ^{2}H and ^{18}O isotopes. The depletion increases with increasing depth, as groundwater samples from aquifer unit C plot further away from the MWL than samples from unit B. Furthermore, ^{3}H-data indicates that groundwater from aquifer unit B is slightly affect by modern meteoric water. Based on

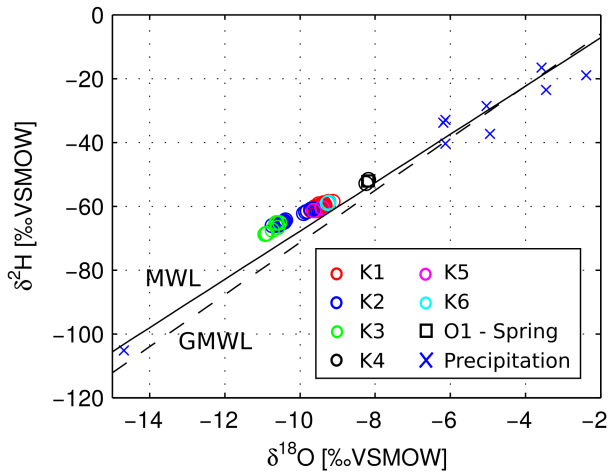

Figure 6.19: δ^2H and δ^{18}O of groundwater and precipitation samples at Saritepe Campus. GMWL is the global meteoric water line, MWL is the local meteoric water line of the Marmara region [*Dirican et al.*, 2005].

14 samples from wells K1, K5 and K6, groundwater form aquifer unit B shows in average ^{3}H=0.7 TU. On the contrary, groundwater from aquifer unit C is tritium free. Accordingly, the isotopic data supports the hypothesis of a paleo-water prevailing within the Cretaceous formation. In this regard, groundwater from aquifer unit B shows a rather weak impact of recent meteoric water, whereas groundwater from unit C might be considered as trapped groundwater not showing any interaction with modern water.

Figure 6.20 compares the concentration of Chloride to δ^{18}O-data. It can be seen that in wells K2 and K3 both groundwater volumes are encountered. Groundwater samples with about 20 meq/l Chloride relate to the interface between both groundwater volumes. Note that samples from well K2 were taken before the well was capped, thus indicating mixing of both groundwater volumes. At well K1, the presented data indicates up-coning with continuous pumping. Furthermore, groundwater from the upper part of well K3 shows a relatively low concentration of Chloride but is most depleted in δ^{18}O. This supports the hypothesis from pumping test interpretation, which suggested that well K3 is isolated from the groundwater reservoir perturbed by the pumping test. In this regard, groundwater from the upper part of the aquifer at well K3 is considered to be not influenced by mixing or dilution with recent meteoric water, nor by a possible secondary solution of sodium salts from deeper parts.

In summary, the evaluation of hydrochemical and isotopic data reveals that groundwater from the pumped reservoir relates to paleo-water. Even though the Na-Cl water in the deeper part of aquifer unit C, and Na-HCO_3 water of aquifer unit B exhibit a different chemistry, they are both assumed to originate from the same kind of paleo-water. Groundwater from aquifer unit B is considered to be slightly affected by modern recharge, whereas groundwater from the deeper part of unit C is regarded as trapped water, not showing any influence by modern water. As groundwater from the upper part of the Cretaceous formation at well K3 is isolated from recent recharge, it might represent the unaffected

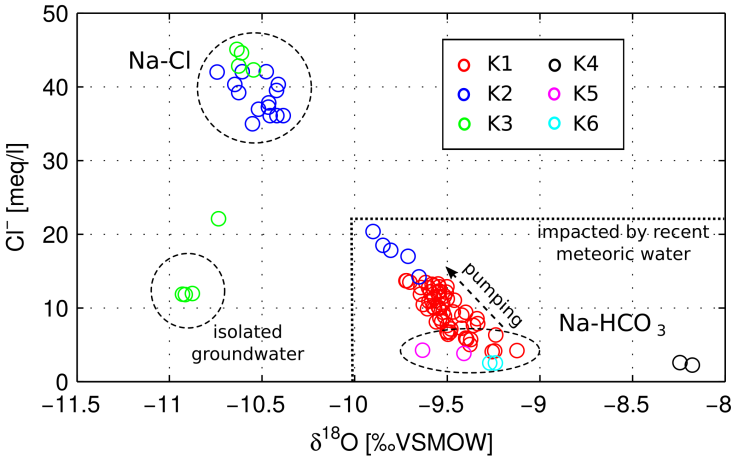

Figure 6.20: Chloride concentration versus δ^{18}O-data of groundwater samples at Saritepe Campus.

paleo-water. Whether the increased salinity of the deep groundwater from aquifer unit C results from long residence times, or is impacted by secondary solution of sodium salts could not eventually be resolved. However, an impact of seawater on the investigated reservoir can be excluded.

6.5 Conceptual Hydrogeological Model of Saritepe Campus

Within a regional tectonic environment of dextral shear Saritepe Campus is considered to be affected by block rotation, as discussed in Section 6.2.3. Within the block, the tectonic situation is complex and can not be resolved in detail. However, geologic investigations reveal that Saritepe Campus is affected by subsidence, most probably resulting from sinistral strike-slip tectonics. Furthermore, hydraulic testing yielded that the investigated groundwater reservoir is delimited by two impermeable, most probably parallel striking boundaries. Accordingly, it is considered most likely that faults constitute the boundaries of the investigated reservoir.

By recognizing that Saritepe Campus is located between two roughly NE-SW trending streams whose trend correlates well with the main strike direction of strike-slip faults observed in the surrounding of the campus, the corresponding NE-SW direction potentially represents the strike of the reservoir bounding faults. Thus, the faults might relate to R-Riedel shears with respect to sinistral strike-slip on a local scale, or, to R'-Riedel with respect to dextral shear and block-rotation on a regional scale. From pumping test interpretation, the width of the investigated channel reservoir was estimated to about 420 m. In this regard, the Western reservoir boundary is assumed to trace the stream in the West of Saritepe Campus, whereas the Eastern boundary is assumed to intersect the Pleistocene dune in NE-SW direction. The trace of the Eastern fault might thus correlate with a topographic step in the dune, and a fault documented at the cliffs of the campus, respectively.

Figure 6.21 shows a transect trough the investigated reservoir, also pointing to the hydrochemical situation at the site. The transect is in NNE-SSW direction, i.e., roughly parallel to the reservoir bounding faults. By considering the location of well K1 within the channel reservoir as given in Table 6.3, it is rather unlikely that one of the reservoir bounding faults cuts between wells K2 and K3. However, well K3 showed a delayed response on pumping at well K1. Hence, it is suggested that the channel reservoir is cut by another WNW-ESE striking semi-permeable fault. The semi-permeable character of the fault may argue for an inactive fault which has undergone weathering. However, the existence of a hydraulic barrier between wells K2 and K3 is evident, and supported by isotopic groundwater data. Note that such a reservoir-boundary configuration produces diagnostic plots comparable to that of a channel reservoir, as a semi-permeable boundary would just be recognized during late pumping times, as difference in permeability.

With regard to the hydraulic properties of the investigated channel reservoir, two aquifer units are distinguished within Cretaceous rock, basically confirming the preliminary model presented in Figure 6.12. Thus, aquifer unit B relates to a basaltic breccia, whereas the deeper aquifer unit C comprises basaltic to andesitic pyroclastic deposits. Both units are considered to dip with about 10° North, and are separated by clay layers whose genesis is unclear. In order to keep the model simple, the clay layers are treated as continuous geological units. However, geologic investigations also point to the fact that clay layers may relate to fault gouge, indicating an intensively disturbed lower part of

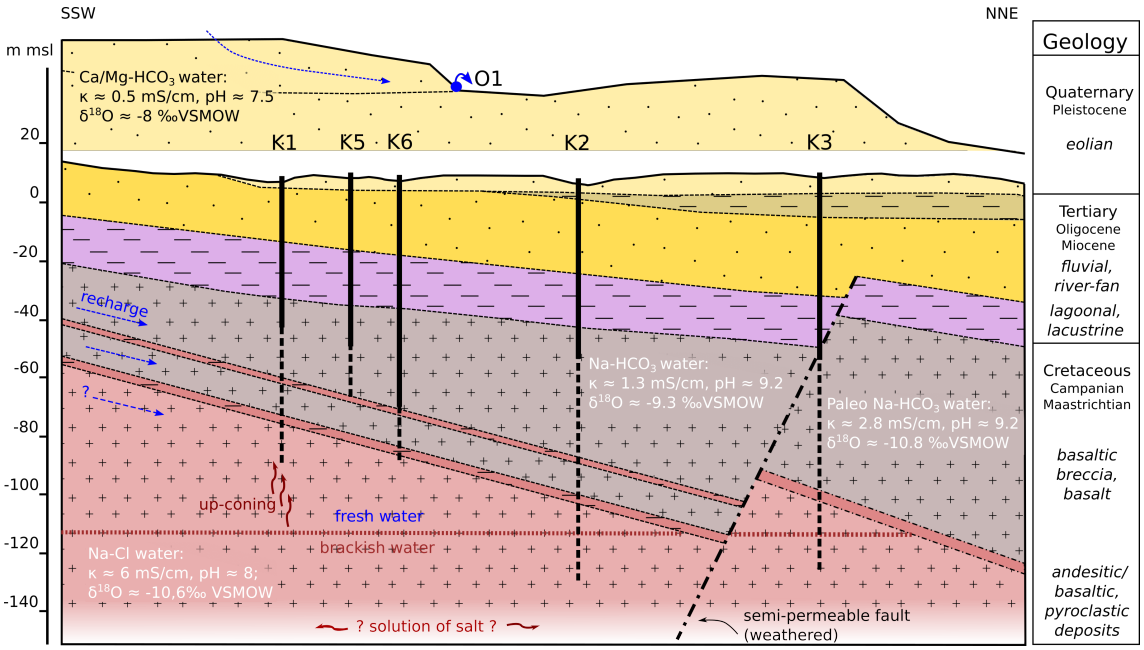

Figure 6.21: Hydrogeological transect through the pumped reservoir at Saritepe Campus. The transect is in NNE-SSW direction, approximately parallel to the impermeable reservoir bounding faults.

unit B. In this regard, aquifer unit B might be divided into two sub-aquifers.

Pumping test evaluation by means of diagnostic plots further indicates that the hydraulic conductivity of aquifer unit C is considerably larger that that of unit B. Due to the complex geology of the investigate reservoir, hydraulic aquifer parameters were approximated by means of a simplified analytical model. For that purpose, both aquifer units were treated as one homogeneous formation, an aquifer thickness was set equal to the screened section at well K1. This yielded an hydraulic conductivity of $K = 1.08 \cdot 10^{-5}$ m/s and a storativity of $S = 4.3 \cdot 10^{-5}$. The hydraulic conductivity of fractures was estimated from the early drawdown at the pumped well, which yielded $K = 4.66 \cdot 10^{-5}$. In order to get more reliable estimates a sophisticated numerical model would be needed.

The question on seawater intrusion affecting the investigated reservoir has to be answered in the negative. In fact, hydrochemical and isotopic data indicate that brackish water might be related to long residence times, or originate from the secondary solution of sodium salts, respectively. However, evidence for intercalated salt layers in the deeper part of aquifer unit C were not found. In general the groundwater of the investigated reservoir is addressed as paleo-water, with the reservoir being considered as groundwater trap. A discharge area of the reservoir could not be identified, as reservoir boundaries in the West, East and North are addressed as impermeable to semi-permeable faults. However, isotopic data suggests that at least aquifer unit B is slightly influenced of modern meteoric water. The corresponding recharge area is considered to be located to the SW of Saritepe Campus, where small outcrops of Cretaceous volcanic rock are documented in the geological map (Figure 6.3). However, the main part of modern water might discharge at higher elevations SW of the site, not reaching the Northern part of the reservoir, which is strongly confined.

With regard to the hydraulic situation at well K4, which currently provides water supply for Saritepe Campus, no detailed information on the corresponding reservoir can be derived from this study. Well K4 is obviously situated within a different reservoir than the investigated one. In general, results from the present study suggest that Saritepe Campus consists of relatively small adjoined reservoirs which are not necessarily hydraulically connected. Thus, the hydraulic situation is strongly dependent on the hydraulic properties of the tectonic inventory, with faults constituting reservoir boundaries. However, tritium data confirms that groundwater at well K4 is impacted by recharge from modern meteoric water. The corresponding reservoir is thus considered to be flushed, not being delimited by a semi-permeable fault.

Last but not least, the present study shows that an integrated evaluation of hydraulic testing and geologic site investigations, accompanied by hydrochemical data can provide fundamental information on the structural inventory of aquifers. In this regard, pumping test interpretation which utilizes the time derivative for evaluation can provide fundamental information on reservoir boundaries and their hydrogeological properties, which is not easily

accessible by conventional exploration methods.

Chapter 7

Synthesis

7.1 Summary and Conclusions

Groundwater flow and transport are strongly influenced by the heterogeneity of the subsurface, which complicates the estimation of subsurface flow parameters, such as transmissivity and storativity. The accurate definition of flow parameters is an essential step in any hydrogeological study. Accordingly, appraising the impact of aquifer heterogeneity on groundwater flow and the estimation of aquifer parameters became a key aspect of hydrogeologic research. Pumping tests are an established technique to estimate hydraulic aquifer parameters. Although aquifers are intrinsically heterogeneous, the interpretation of pumping tests is commonly performed under the assumption of aquifer homogeneity, by utilizing Theis' equation [*Theis*, 1935]. Several studies indicate that even though Theis-based techniques presume the aquifer to be homogeneous, their application to heterogeneous systems can yield information on aquifer heterogeneity, in particular when using the time derivative of the drawdown for parameter estimation. It is recognized that the time derivative of the drawdown is much more sensitive to aquifer properties than the drawdown itself. However, the relation of Theis-based interpreted hydraulic parameters to the underlying heterogeneity of the aquifer is not clear. In order to estimate the impact of aquifer heterogeneity on groundwater flow, knowledge on how a pumping test interpretation method renders the underlying heterogeneity is crucial.

In this regard, the present study provides insight on how Theis-based interpreted hydraulic parameters relate to the underlying heterogeneity of the aquifer. To investigate this relation, time-dependent spatial weighting functions are established to estimate upscaled transmissivities from a given heterogeneous distribution. The derived spatial weighting functions are verified numerically by means of Monte Carlo simulations. The spatially weighted transmissivities are then compared to the interpreted transmissivity, obtained by evaluating synthetically generated pumping tests. Therefor, various Theis-based interpre-

tation techniques are considered, namely, the Cooper-Jacob method [*Cooper and Jacob*, 1946] and the Continuous-Derivation method [*Copty et al.*, 2011] for infinite aquifers, and, the Hantush method [*Hantush*, 1959] for pumping tests in the presence of an infinite linear constant head boundary (BCH). Furthermore, a new interpretation method is derived by extending the Continuous-Derivation method for an application to BCH-domains. Whereas traditional interpretation methods like the Cooper-Jacob and the Hantush method just consider the late-time drawdown for the estimation of hydraulic parameters, the Continuous-Derivation method utilizes the entire time domain of the pumping test, by continuously evaluating the ratio of the drawdown and the drawdown derivative. Thus, the Continuous-Derivation method provides time-dependent hydraulic parameters. Since the hydraulic conductivity or transmissivity, respectively, is considered the ruling hydraulic parameter governing groundwater flow, investigated systems are heterogeneous with regard to transmissivity, which is modeled as log-normally distributed spatial random function. The storativity is considered uniform.

In a first step, investigations focused on single-well pumping tests in heterogeneous aquifers of infinite extent. The sensitivity of the drawdown to aquifer heterogeneity was investigated by utilizing Fréchet kernels [*Knight and Kluitenberg*, 2005], and two types of time-dependent spatial weighting functions were derived. One spatial weighting uses the Fréchet kernel for transmissivity as spatial weight, providing an upscaled homogeneous transmissivity which solves Theis' equation for the drawdown in the true heterogeneous domain. The other spatial weighting uses the time derivative of the Fréchet kernel for transmissivity as spatial weight, providing an upscaled heterogeneous transmissivity field. For a single-well pumping test, when the pumping well coincides with the observation well, the upscaled heterogeneous transmissivity field is radially symmetric. It starts from the local transmissivity at the pumped well and approaches the geometric mean of point transmissivities within about 15 to 20 correlation lengths. Pumping in the upscaled heterogeneous transmissivity field reproduces the drawdown in the true heterogeneous domain. By comparing the spatially weighted transmissivity to the interpreted transmissivity from pumping tests it was found that the upscaled heterogeneous transmissivity agrees well with the interpreted transmissivity from the Cooper-Jacob method and the Continuous-Derivation method, respectively.

Since the focus of this work is on pumping test interpretation in coastal aquifers, the proposed spatial weighting was adapted for an application to heterogeneous domains, in the presence of an infinite linear constant head boundary (BCH). That is, the Fréchet kernel for BCH-domains was derived, and utilized within the proposed spatial weighting to estimate the upscaled homogeneous transmissivity in BCH-domains. Subsequently, the spatially weighted transmissivity was compared to the interpreted transmissivity from the Hantush method, and the newly derived Continuous-Derivation method for BCH-domains,

respectively. This comparison revealed that at early times when the BCH does not affect the drawdown at an observation well, the meaning of the interpreted transmissivity is equivalent to that in an infinite domain. Consequently, the corresponding interpreted transmissivity relates to an upscaled heterogeneous transmissivity field. At late pumping times when the BCH affects the drawdown, quickly leading to steady-state conditions, the interpreted transmissivity approaches the upscaled homogeneous transmissivity. In this regard, the steady-state transmissivity from the Continuous-Derivation method for BCH-domains equals the Hantush transmissivity.

Accordingly, the meaning of the interpreted transmissivity, or its relation to the underlying heterogeneity, respectively, depends on the properties of the Theis' equation, used during the interpretation process. That is, if the interpreted transmissivity is inferred from the drawdown derivative, the resulting transmissivity relates to an upscaled heterogeneous transmissivity field. This relationship is valid for the interpreted transmissivity from the Cooper-Jacob method and the Continuous-Derivation method in infinite domains, as well as, for the interpreted transmissivity from the Continuous-Derivation method for BCH-domains, when the BCH does not affect the drawdown. On the contrary, at late pumping times in BCH-domains, the drawdown derivative approaches zero, and, the interpreted transmissivity is directly related to the drawdown. As a result, the interpreted steady-state transmissivity in BCH-domains does not relate to an upscaled heterogeneous transmissivity field, but substitutes the true heterogeneous transmissivity distribution by a homogeneous transmissivity value.

By considering the transmissivity in a BCH-domain as log-normally distributed spatial random function, it was found that the ratio of two distances strongly influences well flow and transmissivity estimates, namely, the ratio of the distance between the pumping well and the BCH, and the correlation length of the spatial random function. If this ratio is small, the pumping test perturbs an aquifer volume not representative for the entire system, which generally prevents the estimation of the geometric mean of the transmissivity. If the above ratio is larger than about 15 to 20, the cone of depression is considered to sample a representative aquifer volume. In that case, the interpreted transmissivity reaches the geometric mean of the transmissivity before the BCH affects the drawdown. However, under steady-state conditions the geometric mean can not generally by estimated, but may be approximated from an observation well sufficiently far from the pumping well and the BCH, respectively. In this regard, the examination of the Fréchet kernel for BCH-domains shows that a sub-domain between the observation well and the BCH has pronounced impact on the steady-state drawdown. The impact of the transmissivity in this sub-domain, again depends on the ratio of the correlation length to the size of the sub-domain. The closer an observation well to the BCH, the more narrow this sub-domain becomes.

Besides the estimation of transmissivity, Theis-based interpretation methods allow for

the estimation of the storativity. The interpreted storativity is calculated from the interpreted transmissivity, and can not directly be linked to the drawdown. The interpreted storativity has therefore been evaluated in combination with the corresponding transmissivity, providing subsequent information on the heterogeneity in the transmissivity. Thus, the true storativity of the aquifer can only be estimated when the interpreted transmissivity is not influenced by heterogeneity, i.e., from the very early drawdown at the pumping well, when the interpreted transmissivity equals the local transmissivity at the well. In practice, the very early drawdown is often influenced by well effects, which complicates the estimation of the true storativity. However, in all other cases the interpreted storativity is considered to provide information on flow connectivity. With regard to single-well pumping tests in infinite domains, numerical results indicate that the interpreted storativity allows for appraising how the local transmissivity at the well relates to some average transmissivity of the entire system. Thus, a small interpreted late-time storativity indicates a low transmissivity at the pumping well, and vice versa.

In BCH-domains, the evaluation of the interpreted storativity as an indicator for flow connectivity is more complex because the BCH represents an additional source. However, as the interpreted transmissivity becomes a homogeneous parameter under steady-state conditions, its variability decreases. Accordingly, the variability of the interpreted late-time storativity decreases as well appearing to approximate the true storativity of the aquifer. But, the interpreted steady-state storativity still includes information on flow connectivity and does not match the true storativity of the aquifer. Disregarding this fact during the interpretation process may lead to inadequate conclusions.

In general, the theoretical part of this thesis is considered to provide the framework for an improved understanding on how Theis-based interpreted hydraulic parameters relate to aquifer heterogeneity, thus enhancing pumping test interpretation. It was shown that the meaning of the interpreted transmissivity depends on the properties of the Theis equation, used during the interpretation process. Furthermore, the interpreted storativity does not generally allow to estimate the true storativity of the aquifer, but is rather understood to compensate for applying a homogeneous theory to heterogeneous systems. In this regard, the interpreted storativity has to be evaluated with the corresponding interpreted transmissivity to provide additional information on aquifer heterogeneity, which may be considered as an indicator for flow connectivity.

The theoretical/numerical investigations are followed by an applied part, which evaluates real pumping tests in an aquifer system strongly affected by tectonics, at Saritepe Campus, Boğaziçi University, Istanbul. Pumping tests were accompanied by geological and hydrochemical investigations, which included the installation of two new wells, drilled up to depths of 100 meters. The goal of investigations was to provide a conceptual hydrogeologic model of the investigated groundwater reservoir to estimate the impact of the

nearby Black Sea. By using the drawdown derivative for the identification of reservoir boundaries, pumping test interpretation revealed that the investigated groundwater reservoir is bounded by two impermeable faults, not showing a hydraulic connection to the sea. Furthermore, pumping test interpretation suggests that the reservoir consists of two aquifers. The division of aquifers is supported by geological and hydrochemical findings. Accordingly, the investigated groundwater reservoir comprises two groundwater volumes of paleo-water, with the occurrence of brackish water being restricted to the deeper aquifer. The analysis of δ^2H and δ^{18}O data confirmed that the brackish groundwater does not originate from seawater intrusion. The investigated reservoir is rather considered as a groundwater trap, which does barely experience recharge by modern meteoric water. The elevated salt content of the groundwater is thus attributed to rock-water interaction. These results basically confirm the pumping test interpretation model. In this regard, this study shows that pumping test interpretation which utilizes the time derivative for evaluation can provide fundamental information on reservoir boundaries and their hydrogeological properties, which are not easily accessible by conventional exploration methods.

7.2 Outlook

The herein presented concept of spatial weighting functions is not restricted to the presented system configurations, but may serve for investigating the impact of heterogeneity on pumping test interpretation for a variety of systems. In this regard, estimating the Fréchet kernel for heterogeneous domains in the presence of an infinite no-flow boundary, would allow to investigate the relation of Theis-based hydraulic parameters and aquifer heterogeneity in corresponding systems. Moreover, comparing spatially averaged transmissivities to Theis-based hydraulic parameters may serve for investigating other pumping test interpretation techniques, e.g., the Theis method which uses the quasi steady-state drawdown in infinite domains for parameter estimation.

With regard to the Continuous-Derivation method, further research may consider how interpreted hydraulic parameters relate to aquifer properties in media of double-porosity. By now, available pumping test interpretation methods for media of double-porosity generally rely on curve-matching procedures. It seems worthwhile to investigate whether the application of the Continuous-Derivation method can simplify and enhance the interpretation process, as it may immediately provide transient estimates of hydraulic parameters, which then relate to fracture, or matrix-flow, respectively.

Another advantage of using the Continuous-Derivation method is that it allows for inferring time-dependent estimates of the interpreted storativity. It has been shown that very early estimates of the interpreted storativity from single-well pumping tests allow for potentially assessing the true storativity of the aquifer, whereas late-time estimates include

information on flow connectivity. However, investigating the meaning of the interpreted storativity over the entire time domain of a pumping test may be subject of further research. This applies in particular for BCH-domains when multiple sources/sinks affect groundwater flow.

Moreover, the present study suggests that instead of replacing the heterogeneous domain by an equivalent homogeneous transmissivity, an upscaled heterogeneous domain may be a promising approach for a more comprehensive interpretation of pumping tests in heterogeneous media, and, for modeling purposes.

Appendix A

Hydrochemical and Isotopic Data from Saritepe Campus, Istanbul

The following tables summarize the analytical results of sampled water from Saritepe Campus, over a period of two years from October 2010 to October 2012. The following abbreviations are used: GW = groundwater, S = seawater, Sp = spring water, P = precipitation, n.a. = not analyzed. If a sampling depth is mentioned, a vacuum sampler was used for groundwater sampling. All other samples relate to pumped groundwater, with the pump installed at about 50 m below surface level. Spring and seawater was ladled. Precipitation was collected with a precipitation collector.

Table A.1: Isotopic results of sampled waters.

	Typ	Date	Time	δ^{18}O [‰VSMOW]	δ^{2}H [‰VSMOW]	D-exess [‰VSMOW]	δ^{2}H [TU]	$\pm 2\sigma$ [TU]
K1 $_{53m}$	GW	23/10/10	13:10	-9.24	-58.50	15.45	0.8	0.5
K1 $_{74m}$	GW	23/10/10	13:45	-9.12	-58.55	14.45	n.a.	n.a.
K1	GW	24/10/10	11:45	-9.26	-58.74	15.31	n.a.	n.a.
K1	GW	24/10/10	13:00	-9.40	-59.52	15.68	n.a.	n.a.
K1	GW	24/10/10	14:30	-9.37	-59.71	15.28	n.a.	n.a.
K1	GW	24/10/10	15:30	-9.39	-59.55	15.61	n.a.	n.a.
K1	GW	24/10/10	16:15	-9.50	-59.99	15.97	n.a.	n.a.
K1	GW	24/10/10	16:45	-9.48	-60.33	15.55	n.a.	n.a.
K1	GW	24/10/10	17:30	-9.50	-60.47	15.53	n.a.	n.a.
K1	GW	24/10/10	19:00	-9.50	-60.43	15.56	n.a.	n.a.
K1	GW	24/10/10	20:00	-9.53	-60.37	15.88	n.a.	n.a.
K1	GW	24/10/10	20:45	-9.54	-60.31	16.01	n.a.	n.a.
K1	GW	24/10/10	21:30	-9.52	-60.28	15.91	n.a.	n.a.
K1	GW	24/10/10	23:00	-9.57	-60.68	15.86	n.a.	n.a.
K1	GW	24/10/10	23:59	-9.63	-60.95	16.08	n.a.	n.a.
K1 $_{55m}$	GW	27/10/10	14:15	-9.24	-58.49	15.41	0.8	0.5
K1 $_{90m}$	GW	27/10/10	14:30	-9.58	-60.73	15.88	0.7	0.5
K1	GW	09/10/11	10:35	-9.38	-58.91	16.10	1.2	0.8
K1	GW	13/06/12	11:28	-9.48	-59.68	16.17	n.a.	n.a.
K1	GW	13/06/12	13:12	-9.56	-60.53	15.94	n.a.	n.a.
K1	GW	13/06/12	16:20	-9.52	-60.33	15.79	n.a.	n.a.

Table A.1: Isotopic results of sampled waters.

	Typ	Date	Time	$\delta^{18}O$ [‰VSMOW]	$\delta^{2}H$ [‰VSMOW]	D-exess [‰VSMOW]	$\delta^{2}H$ [TU]	$\pm 2\sigma$ [TU]
K1	GW	13/06/12	18:06	-9.40	-60.48	14.72	n.a.	n.a.
K1	GW	13/06/12	19:45	-9.54	-60.33	16.03	0.5	0.3
K1	GW	18/07/12	15:25	-9.50	-59.28	16.73	0.3	0.3
K1	GW	18/07/12	17:50	-9.42	-60.17	15.23	n.a.	n.a.
K1	GW	18/07/12	20:00	-9.36	-60.20	14.67	n.a.	n.a.
K1	GW	18/07/12	22:00	-9.34	-59.81	14.87	n.a.	n.a.
K1	GW	18/07/12	23:55	-9.34	-59.76	14.96	n.a.	n.a.
K1	GW	19/07/12	02:00	-9.42	-59.94	15.43	0.8	0.3
K1	GW	19/07/12	04:00	-9.47	-60.13	15.60	n.a.	n.a.
K1	GW	19/07/12	06:00	-9.61	-60.12	16.74	n.a.	n.a.
K1	GW	19/07/12	08:00	-9.55	-60.17	16.22	n.a.	n.a.
K1	GW	19/07/12	10:00	-9.53	-60.44	15.77	n.a.	n.a.
K1	GW	19/07/12	12:00	-9.60	-60.22	16.57	0.6	0.3
K1	GW	19/07/12	14:00	-9.58	-60.54	16.13	n.a.	n.a.
K1	GW	19/07/12	16:00	-9.46	-60.62	15.07	n.a.	n.a.
K1	GW	19/07/12	18:00	-9.50	-60.70	15.29	n.a.	n.a.
K1	GW	19/07/12	20:00	-9.57	-60.46	16.10	0.6	0.3
K1	GW	19/07/12	22:00	-9.54	-60.57	15.79	n.a.	n.a.
K1	GW	19/07/12	23:55	-9.51	-60.97	15.15	n.a.	n.a.
K1	GW	20/07/12	02:00	-9.54	-60.83	15.51	n.a.	n.a.
K1	GW	20/07/12	03:30	-9.54	-60.92	15.44	n.a.	n.a.
K1	GW	20/07/12	05:00	-9.51	-61.03	15.02	n.a.	n.a.
K1	GW	20/07/12	07:00	-9.64	-61.07	16.09	n.a.	n.a.
K1	GW	20/07/12	09:00	-9.55	-61.05	15.36	n.a.	n.a.
K1	GW	20/07/12	10:55	-9.59	-60.80	15.94	n.a.	n.a.
K1	GW	20/07/12	12:55	-9.50	-60.74	15.26	0.4	0.4
K1	GW	20/07/12	14:55	-9.54	-61.11	15.25	n.a.	n.a.
K1	GW	20/07/12	16:55	-9.60	-61.01	15.80	n.a.	n.a.
K1	GW	20/07/12	18:50	-9.64	-61.39	15.75	n.a.	n.a.
K1	GW	20/07/12	21:10	-9.58	-61.00	15.66	n.a.	n.a.
K1	GW	20/07/12	23:10	-9.57	-61.36	15.22	n.a.	n.a.
K1	GW	21/07/12	01:10	-9.55	-61.12	15.28	n.a.	n.a.
K1	GW	21/07/12	03:10	-9.62	-61.18	15.76	n.a.	n.a.
K1	GW	21/07/12	05:10	-9.70	-61.25	16.37	n.a.	n.a.
K1	GW	21/07/12	09:50	-9.72	-61.18	16.61	n.a.	n.a.
K1	GW	21/07/12	11:50	-9.72	-61.21	16.55	0.7	0.3
K2 70m	GW	22/10/10	16:00	-9.65	-60.80	16.42	<0.7	0.4
K2 90m	GW	22/10/10	16:50	-9.71	-60.89	16.80	n.a.	n.a.
K2 110m	GW	22/10/10	17:10	-10.61	-65.44	19.42	n.a.	n.a.
K2 134m	GW	22/10/10	17:50	-10.65	-65.98	19.19	n.a.	n.a.
K2	GW	25/10/10	11:12	-9.80	-61.53	16.91	n.a.	n.a.
K2	GW	25/10/10	11:40	-9.85	-61.84	16.94	n.a.	n.a.
K2	GW	25/10/10	12:25	-10.52	-65.17	18.98	n.a.	n.a.
K2	GW	25/10/10	13:55	-10.47	-65.10	18.63	n.a.	n.a.
K2	GW	25/10/10	15:55	-10.42	-64.93	18.45	n.a.	n.a.
K2	GW	25/10/10	16:35	-10.39	-64.31	18.77	n.a.	n.a.
K2	GW	25/10/10	16:55	-10.41	-64.78	18.52	n.a.	n.a.
K2	GW	25/10/10	17:40	-10.48	-65.24	18.58	n.a.	n.a.
K2	GW	25/10/10	19:10	-10.46	-65.01	18.71	n.a.	n.a.
K2	GW	25/10/10	20:10	-10.42	-64.76	18.60	n.a.	n.a.
K2	GW	25/10/10	21:10	-10.46	-65.00	18.65	n.a.	n.a.

Table A.1: Isotopic results of sampled waters.

	Typ	Date	Time	δ^{18}O [‰VSMOW]	δ^{2}H [‰VSMOW]	D-exess [‰VSMOW]	δ^{2}H [TU]	$\pm 2\sigma$ [TU]
K2 $_{65m}$	GW	27/10/10	11:30	-9.90	-62.26	16.94	<0.5	0.3
K2 $_{80m}$	GW	27/10/10	12:00	-10.63	-65.46	19.55	n.a.	n.a.
K2 $_{123m}$	GW	27/10/10	12:15	-10.55	-65.87	18.54	n.a.	n.a.
K2	GW	07/10/11	14:55	-10.74	-66.06	19.88	n.a.	n.a.
K3 $_{66m}$	GW	21/10/10	17:45	-10.88	-68.53	18.48	<0.5	0.3
K3 $_{77m}$	GW	21/10/10	18:40	-10.74	-67.53	18.35	n.a.	n.a.
K3 $_{100m}$	GW	21/10/10	19:00	-10.55	-65.23	19.14	n.a.	n.a.
K3	GW	26/10/10	14:45	-10.91	-68.61	18.71	n.a.	n.a.
K3	GW	26/10/10	15:30	-10.93	-68.76	18.68	n.a.	n.a.
K3 $_{85m}$	GW	08/10/11	-	-10.63	-65.22	19.80	n.a.	n.a.
K3 $_{89m}$	GW	08/10/11	-	-10.61	-65.28	19.60	n.a.	n.a.
K3 $_{100m}$	GW	08/10/11	-	-10.64	-65.20	19.89	n.a.	n.a.
K4	GW	27/10/10	17:00	-8.24	-52.79	13.16	4.7	0.5
K4	GW	06/10/12	-	-8.18	-51.69	13.73	n.a.	n.a.
K5	GW	30/08/12	15:10	-9.63	-61.38	15.68	0.6	0.3
K5	GW	30/08/12	17:43	-9.41	-60.50	14.78	1.2	0.3
K6	GW	15/04/12	15:35	-9.24	-58.76	15.17	n.a.	n.a.
K6	GW	15/04/12	18:35	-9.27	-59.10	15.07	0.4	0.4
O1	Sp	23/06/11	-	-8.20	-52.17	13.46	n.a.	n.a.
O1	Sp	08/10/11	-	-8.17	-51.93	13.43	n.a.	n.a.
D	S	22/10/10	14:00	-2.93	-23.98	-0.56	7.4	0.8
D	S	26/10/10	14:00	-2.89	-24.04	-0.93	7.7	0.9
N	P	2/17/12	-	-14.69	-105.24	12.31	n.a.	n.a.
N	P	3/30/12	-	-3.58	-16.50	12.10	n.a.	n.a.
N	P	4/19/12	-	-4.95	-37.32	2.25	n.a.	n.a.
N	P	5/5/12	-	-2.38	-19.02	0.06	n.a.	n.a.
N	P	5/22/12	-	-3.45	-23.56	4.02	n.a.	n.a.
N	P	6/8/12	-	-6.13	-40.36	8.70	n.a.	n.a.
N	P	8/14/12	-	-6.13	-32.97	16.06	n.a.	n.a.
N	P	8/29/12	-	-6.19	-33.87	15.61	n.a.	n.a.
N	P	10/6/12	-	-5.03	-28.58	11.68	n.a.	n.a.

Table A.2: Analytical results of sampled waters.

	Typ	Date	Time	Con (25°) [mS/cm]	T [°C]	O_2 [mg/l]	pH	m-V C_A 4,3	p-V C_B 8,2	Redox [mV]	Cl^- [mg/l]	SO_4^{2-} [mg/l]	Ca^{2+} [mg/l]	K^+ [mg/l]	Mg^{2+} [mg/l]	Na^+ [mg/l]
K1 53m	GW	23/10/10	13:10	1.33	16.3	n.a.	9.23	7.01	n.a.	n.a.	148	64.40	2.11	0.90	0.24	282
K1 74m	GW	23/10/10	13:45	1.321	16.6	n.a.	9.21	6.98	n.a.	n.a.	149	69	0.94	0.86	0.31	283
K1	GW	24/10/10	11:45	1.313	17.8	0.092	9.17	6.99	n.a.	n.a.	144	69.30	0.74	0.82	0.38	282
K1	GW	24/10/10	13:00	1.571	18.2	0.042	9	6.39	n.a.	-164.58	209	121	2.41	1.10	1.14	332
K1	GW	24/10/10	14:30	1.576	18.2	0.044	8.99	6.6	n.a.	-120.49	202	117	2.74	0.84	0.66	332
K1	GW	24/10/10	15:30	1.561	18.2	0.037	9	6.54	n.a.	-140.52	204	117	1.20	0.76	0.51	336
K1	GW	24/10/10	16:15	1.692	18.2	0.042	8.97	6.63	n.a.	-84.28	228	129	3.22	1.10	1.26	359
K1	GW	24/10/10	16:45	1.711	18.2	0.044	8.95	6.53	n.a.	-64.49	238	140	1.83	1.22	0.86	362
K1	GW	24/10/10	17:30	1.743	18.4	0.077	8.98	6.55	n.a.	-34.61	238	129	1.67	1.12	0.72	369
K1	GW	24/10/10	19:00	1.854	18.2	0.042	8.97	7	n.a.	-78.42	271	138	9.33	1	3.09	399
K1	GW	24/10/10	20:00	1.917	18.1	0.057	8.93	6.5	n.a.	-66.24	289	149	1.86	1.17	0.83	416
K1	GW	24/10/10	20:45	1.98	18.1	0.042	8.97	6.33	n.a.	-66	305	156	5.79	1.74	2.20	416
K1	GW	24/10/10	21:30	2.07	18.1	0.049	8.86	6.21	n.a.	-71.56	334	168	2.52	1.26	1.74	432
K1	GW	24/10/10	23:00	2.16	17.7	0.029	8.92	6.11	n.a.	-77.34	354	174	2.75	1.07	1.34	448
K1	GW	24/10/10	23:59	2.22	17.9	0.039	8.91	6.08	n.a.	-75.85	370	181	2.72	1.21	1.53	460
K1 55m	GW	27/10/10	14:15	1.64	16.5	n.a.	9.1	6.49	n.a.	n.a.	224	118	1.57	1.14	0.93	343
K1 90m	GW	27/10/10	14:30	1.57	15.8	n.a.	8.96	6.09	n.a.	n.a.	359	174	2.01	1.32	1.17	454
K1	GW	09/10/11	10:35	1.405	17.2	0.17	8.87	6.36	0.38	-87.46	178	107.9	1.48	1.07	0.60	327
K1	GW	13/06/12	11:28	1.48	18.1	0.1	9.16	6.32	0.43	-28.63	253	156.2	4.11	1.31	1.86	362
K1	GW	13/06/12	13:12	1.89	18.6	0.26	9.04	6.2	0.38	-37.73	287	164.4	3.02	1.15	1.41	374
K1	GW	13/06/12	16:20	1.76	18.5	0.03	8.98	6.16	0.44	-68.71	314	173.7	3.36	1.20	1.62	395
K1	GW	13/06/12	18:06	2.03	18.5	0.03	8.98	6.55	0.45	-83.71	332	180.8	4.56	1.27	1.84	412
K1	GW	13/06/12	19:45	1.96	18.5	0.05	8.97	6.05	0.47	-74.71	352	189.2	4.23	1.28	2.01	417
K1	GW	18/07/12	15:25	1.56	18.3	0.04	9.22	6.36	0.5	-82.67	240	144.1	2.66	1.10	1.20	332
K1	GW	18/07/12	17:50	1.58	18.5	0.06	9.17	6.33	0.58	-71.71	256	151.1	2.49	1.10	1.20	350
K1	GW	18/07/12	20:00	1.61	18.5	0.05	9.25	6.3	0.54	-60.71	270	156.8	2.55	1.12	1.24	358
K1	GW	18/07/12	22:00	1.709	18.5	0.06	9.18	6.29	0.58	-64.71	279	158.7	2.79	1.11	1.38	371
K1	GW	18/07/12	23:55	1.76	18.5	0.06	9.15	6.22	0.56	-63.71	302	168.6	3.06	1.14	1.51	378
K1	GW	19/07/12	02:00	1.83	18.5	0.01	9.12	6.18	0.54	-68.71	319	175.9	3.21	1.18	1.67	392
K1	GW	19/07/12	04:00	1.91	18.5	0.04	9.15	6.1	0.5	-66.71	335	181.2	3.34	1.15	1.77	404
K1	GW	19/07/12	06:00	1.947	18.5	0.04	9.15	6.16	0.57	-63.71	345	187.4	3.66	1.20	1.90	413
K1	GW	19/07/12	08:00	1.986	18.6	0.06	9.15	6.14	0.57	-64.73	358	189.2	3.91	1.26	2.05	424

Table A.2: Analytical results of sampled waters.

	Typ	Date	Time	Con (25°) [mS/cm]	T [°C]	O_2 [mg/l]	pH	m-V C_A 4,3	p-V C_B 8,2	Redox [mV]	Cl^- [mg/l]	SO_4^{2-} [mg/l]	Ca^{2+} [mg/l]	K^+ [mg/l]	Mg^{2+} [mg/l]	Na^+ [mg/l]
K1	GW	19/07/12	10:00	2.03	18.8	0.03	9.16	6.31	0.54	-67.77	373	195.1	4.11	1.25	2.18	427
K1	GW	19/07/12	12:00	2.05	18.9	0.06	9.14	6.13	0.52	-70.79	387	200	4.17	1.26	2.22	433
K1	GW	19/07/12	14:00	2.09	18.6	0.03	9.14	6.07	0.57	-57.73	387	204	4.32	1.25	2.32	440
K1	GW	19/07/12	16:00	2.11	18.6	0.04	9.13	6	0.49	-67.73	391	207	4.51	1.26	2.46	444
K1	GW	19/07/12	18:00	2.13	18.6	0.05	9.13	6	0.54	-66.73	398	208	4.74	1.29	2.54	452
K1	GW	19/07/12	20:00	2.14	18.6	0.05	9.11	5.95	0.52	-76.73	404	211	4.64	1.28	2.56	443
K1	GW	19/07/12	22:00	2.18	18.6	0.03	9.12	5.99	0.52	-69.73	408	209	4.94	1.31	2.68	455
K1	GW	19/07/12	23:55	2.14	18.6	0.03	9.11	5.91	0.49	-82.73	412	213	4.97	1.32	2.72	449
K1	GW	20/07/12	02:00	2.26	18.5	0.05	9.09	5.88	0.48	-87.71	432	217.9	5.12	1.30	2.80	459
K1	GW	20/07/12	03:30	2.24	18.6	0.03	9.10	5.9	0.49	-87.73	435	218.8	5.18	1.32	2.78	464
K1	GW	20/07/12	05:00	2.24	18.6	0.03	9.09	5.9	0.5	-78.73	430	219.8	5.26	1.36	2.81	469
K1	GW	20/07/12	07:00	2.27	18.5	0.06	9.11	5.89	0.5	-78.71	420	215.1	5.39	1.31	2.83	473
K1	GW	20/07/12	09:00	2.27	18.5	0.03	9.10	6.01	0.51	-79.71	427	212.5	5.34	1.30	2.83	461
K1	GW	20/07/12	10:55	2.29	18.5	0.08	9.10	5.97	0.52	-76.71	433	213.5	5.38	1.32	2.86	470
K1	GW	20/07/12	12:55	2.3	18.5	0.04	9.10	5.95	0.53	-81.71	456	224.3	5.29	1.28	2.83	472
K1	GW	20/07/12	14:55	2.31	18.5	0.04	9.10	5.95	0.53	-83.71	455	226	5.66	1.32	2.87	465
K1	GW	20/07/12	16:55	2.32	18.5	0.15	9.12	6	0.53	-49.71	451	224.6	5.51	1.37	2.93	469
K1	GW	20/07/12	18:50	2.33	18.7	0.08	9.09	5.98	0.5	-57.75	453	229.2	5.64	1.31	2.97	484
K1	GW	20/07/12	21:10	2.34	18.6	0.07	9.09	5.93	0.5	-54.73	467	229	5.67	1.30	3.03	478
K1	GW	20/07/12	23:10	2.34	18.6	0.14	9.09	5.85	0.48	-55.73	461	229.9	5.77	1.30	3.09	478
K1	GW	21/07/12	01:10	2.36	18.6	0.15	9.09	5.91	0.5	-60.73	469	229.1	5.87	1.31	3.12	481
K1	GW	21/07/12	03:10	2.38	18.6	0.13	9.09	5.87	0.49	-61.73	477	237.2	6	1.33	3.14	474
K1	GW	21/07/12	05:10	2.39	18.6	0.13	9.08	5.88	0.49	-61.73	477	233.1	6.01	1.34	3.16	478
K1	GW	21/07/12	09:50	2.42	18.7	0.16	9.06	5.87	0.48	-64.75	485	237.2	6.10	1.34	3.23	479
K1	GW	21/07/12	11:50	2.44	18.7	0.09	9.08	5.88	0.47	-65.75	484	241.2	6.12	1.32	3.24	495
K2 $_{70m}$	GW	22/10/10	16:00	2.49	15.8	n.a.	8.65	6	n.a.	n.a.	504	242	5.85	1.40	3.13	558
K2 $_{90m}$	GW	22/10/10	16:50	3.14	16.2	n.a.	8.72	5.71	n.a.	n.a.	602	283	5.82	1.57	2.81	647
K2 $_{110m}$	GW	22/10/10	17:10	6.62	16.1	n.a.	8.09	3.57	0	n.a.	1490	676	32	3.14	15.10	1340
K2 $_{134m}$	GW	22/10/10	17:50	6.37	16.2	n.a.	7.99	3.81	0	n.a.	1430	647	31.40	4.34	13.70	1290
K2	GW	25/10/10	11:12	3.26	18.1	0.09	8.77	5.58	n.a.	-74.37	631	294	8.64	2	5.03	657
K2	GW	25/10/10	11:40	3.35	18.4	0.05	8.71	5.52	n.a.	-97.45	655	302	8.15	2.18	4.90	681
K2	GW	25/10/10	12:25	6	18.9	0.07	8.22	3.87	0	-12.18	1310	592	25	3.58	11.70	1220

Table A.2: Analytical results of sampled waters.

	Typ	Date	Time	Con (25°) [mS/cm]	T [°C]	O_2 [mg/l]	pH	m-V C_A 4,3	p-V C_B 8,2	Redox [mV]	Cl^- [mg/l]	SO_4^{2-} [mg/l]	Ca^{2+} [mg/l]	K^+ [mg/l]	Mg^{2+} [mg/l]	Na^+ [mg/l]
K2	GW	25/10/10	13:55	5.95	19.2	0.04	8.27	3.5	0	-42.16	1320	601	27.20	3.46	13.40	1180
K2	GW	25/10/10	15:55	6.27	19.2	0.04	8.27	3.9	0	-57.61	1400	640	34.90	2.84	15.70	1250
K2	GW	25/10/10	16:35	5.87	18.9	0.05	8.36	4.1	n.a.	-9.37	1280	584	31	4.52	14.50	1170
K2	GW	25/10/10	16:55	6.3	19.1	0.02	8.28	3.87	n.a.	-43.36	1430	650	34.60	2.86	15.80	1270
K2	GW	25/10/10	17:40	6.19	18.8	0.10	8.28	3.98	n.a.	-41.53	1490	675	34.40	4.09	14.70	1240
K2	GW	25/10/10	19:10	6.06	18.6	0.04	8.28	4.01	n.a.	-53.64	1340	604	32.80	3.68	14.50	1210
K2	GW	25/10/10	20:10	5.85	18.3	0.05	8.32	4.03	n.a.	-54.13	1280	569	30	3.84	12.70	1160
K2	GW	25/10/10	21:10	5.76	18.4	0.07	8.27	4.06	n.a.	-42.24	1280	571	28.30	3.29	11.90	1150
K2 $_{65m}$	GW	27/10/10	11:30	3.6	16.5	n.a.	8.68	5.48	n.a.	n.a.	722	331	11	1.78	6.01	727
K2 $_{80m}$	GW	27/10/10	12:00	4.71	16.4	n.a.	8.1	3.79	0	n.a.	1390	616	31.40	3.10	13.60	1260
K2 $_{123m}$	GW	27/10/10	12:15	5.67	16.2	n.a.	8.24	3.99	0	n.a.	1240	580	26	3.95	10.90	1150
K2	GW	07/10/11	14:55	6.1	19.3	0.06	7.92	3.36	0	-49.07	1489	654	29.24	4.28	13.42	1327
K3 $_{66m}$	GW	21/10/10	17:45	2.78	17.1	n.a.	9.22	6.76	0.97	n.a.	423	365	2.58	3.65	1.52	580
K3 $_{77m}$	GW	21/10/10	18:40	3.97	17.2	n.a.	8.69	6.11	0.51	n.a.	784	412	5.68	3	4.08	826
K3 $_{100m}$	GW	21/10/10	19:00	6.36	17.1	n.a.	8.19	6.16	0	n.a.	1500	415	17.30	5.52	10.20	1310
K3	GW	26/10/10	14:30	2.6	19.3	0.07	9.18	6.61	n.a.	-72.83	402	308	1.82	2.54	1.08	546
K3	GW	26/10/10	14:45	2.79	20.2	n.a.	9.2	5.89	n.a.	n.a.	419	355	2.56	2.49	1.62	579
K3	GW	26/10/10	15:30	2.78	20.3	n.a.	9.21	6.47	n.a.	n.a.	420	353	3.24	2.31	1.70	577
K3 $_{85m}$	GW	08/10/11	-	6.19	22.2	n.a.	8.03	5.49	0	-71.55	1517	431	15.28	4.04	9.43	1396
K3 $_{89m}$	GW	08/10/11	-	6.4	19.3	n.a.	8.05	5.48	0	-30.97	1581	444	12.84	4.91	9.09	1445
K3 $_{100m}$	GW	08/10/11	-	6.41	21.5	n.a.	8.06	5.54	0	-50.71	1598	445	15.70	3.43	10.05	1465
K4	GW	27/10/10	17:00	1.02	15.9	n.a.	8.38	5.78	n.a.	n.a.	90.9	69.9	7.92	0.82	1.79	197
K4	GW	06/10/12	-	0.936	18.9	n.a.	8.15	5.65	0	n.a.	79	66.4	9.36	1.13	2.09	182
K5	GW	30/08/12	15:10	1.355	17.3	n.a.	9.34	6.86	0.72	n.a.	151	123	2.21	0.91	0.84	278
K5	GW	30/08/12	17:43	1.231	17.4	n.a.	9.23	6.69	0.62	n.a.	135	112	3.52	0.95	1.22	263
K6	GW	15/04/12	15:35	1.366	17.9	0.12	8.74	7.42	0.65	-17.09	90	51.7	8.80	2.48	3.38	305
K6	GW	15/04/12	18:35	1.361	17.6	0.62	8.67	6.95	0.65	-32.23	89	51.8	7.05	1.63	2.18	313
O1	Sp	23/06/11	-	0.567	21.3	5.84	7.59	5.38	0	423.93	24.06	15.79	76.34	0.79	14.64	14
O1	Sp	08/10/11	-	0.538	18.5	5.82	7.3	4.99	0	378.69	23.17	15.04	79.27	0.74	13.93	14
D	S	22/10/10	14:00	26.8	17.2	7.15	8.4	3.35	0.31	288	9180	746	168	196	619	5280
D	S	26/10/10	14:00	29.2	18.9	7.4	8.25	3.44	0	220.11	8930	1230	174	207	603	5300

Bibliography

Ababou, R., and E. F. Wood (1990), Comment on "Effective groundwater model parameter values: Influence of spatial variability of hydraulic conductivity, leakance, and recharge" by J. J. Gómez-Hernández and S. M. Gorelick, *Water Resources Research*, *26*(8), 1843–1846, doi:10.1029/WR026i008p01843.

Abramowitz, M., and I. A. Stegun (1964), *Handbook of Mathematical Functions: With Formulas, Graphs, and Mathematical Tables*, Courier Corporation, New York.

Agarwal, R. G. (1980), A New Method To Account For Producing Time Effects When Drawdown Type Curves Are Used To Analyze Pressure Buildup And Other Test Data, *SPE 9289*, doi:10.2118/9289-MS.

Akartuna, M. (1963), Die Fortsetzung der Überschiebung von Sile an der Nordküse des Bosporus, *Bulletin of the Mineral Research and Exploration Institute of Turkey*, *61*(Foreign Edition), 15–21.

Appelo, C. A. J., and D. Postma (2005), *Geochemistry, Groundwater and Pollution*, 2 rev ed. ed., A a Balkema Publishers, Leiden.

Attinger, S. (2003), Generalized Coarse Graining Procedures for Flow in Porous Media, *Computational Geosciences*, *7*(4), 253–273, doi:10.1023/B:COMG.0000005243.73381.e3.

Bear, J. (1972), *Dynamics of Fluids in Porous Media*, Dover Publ., New York.

Beauheim, R. L., R. M. Roberts, and J. D. Avis (2004), Well testing in fractured media: flow dimensions and diagnostic plots, *Journal of Hydraulic Research*, *42*(sup1), 69–76, doi:10.1080/00221680409500049.

Bourdet, D. (2002), *Well Test Analysis: The Use of Advanced Interpretation Models*, Elsevier, Amsterdam; Boston.

Bourdet, D., J. A. Ayoub, V. Kniazeff, Y. M. Pirard, and T. M. Whittle (1983), Interpreting Well Tests in Fractured Reservoirs, *World Oil; (United States)*, *197:5*.

Bourdet, D., J. Ayoub, and Y. Pirard (1989), Use of Pressure Derivative in Well Test Interpretation, *SPE Formation Evaluation*, *4*(2), doi:10.2118/12777-PA.

Butler, J. J. (1990), The Role of Pumping Tests in Site Characterization: Some Theoretical Considerations, *Ground Water*, *28*(3), 394–402, doi:10.1111/j.1745-6584.1990.tb02269.x.

Butler, J. J., C. D. McElwee, and G. C. Bohling (1999), Pumping tests in networks of multilevel sampling wells: Motivation and methodology, *Water Resources Research*, *35*(11), 3553–3560, doi:10.1029/1999WR900231.

Cardwell, W., Jr., and R. Parsons (1945), Average Permeabilities of Heterogeneous Oil Sands, *SPE-945034-G*, doi:10.2118/945034-G.

Chapuis, P., C. Bélanger, and D. Chenaf (2006), Pumping Test in a Confined Aquifer Under Tidal Influence, *Ground Water*, *44*(2), 300–305.

Chapuis, R. P. (1994), Assessment of Methods and Conditions to Locate Boundaries: II. One Straight Recharge Boundary, *Ground Water*, *32*(4), 583–590, doi:10.1111/j.1745-6584.1994.tb00894.x.

Clark, I. D., and P. Fritz (1997), *Environmental Isotopes in Hydrogeology*, Crc, Boca Raton, FL.

Cooper, H. H., and C. E. Jacob (1946), A generalized graphical method for evaluating formation constants and summarizing well-field history, *Transactions, American Geophysical Union*, *27*(4), 526, doi:10.1029/TR027i004p00526.

Copty, N. K., and A. N. Findikakis (2004), Stochastic analysis of pumping test drawdown data in heterogeneous geologic formations, *Journal of Hydraulic Research*, *42*(Extra Issue), 59–67, doi:10.1080/00221680409500048.

Copty, N. K., P. Trinchero, and X. Sanchez-Vila (2011), Inferring spatial distribution of the radially integrated transmissivity from pumping tests in heterogeneous confined aquifers, *Water Resources Research*, *47*(5), W05,526, doi:10.1029/2010WR009877.

Dagan, G. (1986), Statistical theory of groundwater flow and transport: Pore to laboratory, laboratory to formation, and formation to regional scale, *Water Resources Research*, *22*(9S), 120S–134S, doi:10.1029/WR022i09Sp0120S.

Dagan, G. (1989), *Flow and transport in porous formations*, Berlin; New York, Springer-Verlag.

Dagan, G., and S. C. Lessoff (2007a), Transmissivity upscaling in numerical models of steady aquifer flow: Conditional statistics, *Water Resources Reasearch*, *43*(10), doi:10.1029/2007WR006028.

Dagan, G., and S. C. Lessoff (2007b), Transmissivity upscaling in numerical aquifer models of steady well flow: Unconditional statistics, *Water Resources Reasearch*, *43*(3), 12, doi:10.1029/2006WR005235.

Dagan, G., S. C. Lessoff, and A. Fiori (2009), Is transmissivity a meaningful property of natural formations? Conceptual issues and model development, *Water Resources Research*, *45*(3), W03,425, doi:10.1029/2008WR007410.

Demirbag, E., E. Gökaşan, F. Y. Oktay, M. Simsek, and H. Yüce (1999), The last sea level changes in the Black Sea: evidence from the seismic data, *Marine Geology*, *157*(3-4), 249–265.

Demirbag, E., C. Rangin, X. Le Pichon, and A. Celal Şengör (2003), Investigation of the tectonics of the Main Marmara Fault by means of deep-towed seismic data, *Tectonophysics*, *361*(1–2), 1–19, doi:10.1016/S0040-1951(02)00535-8.

Desbarats, A. J. (1992), Spatial averaging of transmissivity in heterogeneous fields with flow toward a well, *Water Resources Research*, *28*(3), 757–767, doi:10.1029/91WR03099.

Desbarats, A. J. (1993), Geostatistical analysis of interwell transmissivity in heterogeneous aquifers, *Water Resources Research*, *29*(4), 1239–1246, doi:10.1029/92WR02418.

Dietrich, P., R. Helmig, M. Sauter, H. Hötzl, J. Köngeter, and G. Teutsch (2005), *Flow and Transport in Fractured Porous Media*, Springer, Berlin; New York.

DIN 4022, T. . (1987), DIN 4022, Teil 1, Benennen und Beschreiben von Boden und Fels, Schichtenverzeichnis für Bohrungen ohne durchgehende Gewinnung von gekernten Proben im Boden und Fels.

Dirican, A., S. Ünal, Y. Acar, and M. Demircan (2005), The temporal and seasonal variation of H-2 and O-18 in atmospheric water vapor and precipitation from Ankara, Turkey in relation to air mass trajectories at Mediterranean Basin, in *Isotopic composition of precipitation in the Mediterranean Basin in relation to air circulation patterens and climate*, IAEA-TECDOC-1453, IAEA, Vienna.

Ehlig-Economides, C. (1988), Use of the Pressure Derivative for Diagnosing Pressure-Transient Behavior, *Journal of Petroleum Technology*, *40*(10), doi:10.2118/18594-PA.

Ehlig-Economides, C., P. Hegeman, and S. Vik (1994), Guidelines simplify well test interpretation, *Oil and Gas Journal*, *92:29*.

Ercan, T., A. Türkecan, H. Guillou, M. Satir, D. Sevin, and F. Saroglu (1998), Features of the Tertiary Volcanism around Sea of Marmara, *Bulletin of the Mineral Research and Exploration Institute of Turkey*, *120*, 97–118.

Fernàndez-Garcia, D., P. Trinchero, and X. Sanchez-Vila (2010), Conditional stochastic mapping of transport connectivity, *Water Resources Research*, *46*, 14 PP., doi:201010.1029/2009WR008533.

Ferris, J. G., D. B. Knowles, R. H. Brown, and R. H. Stallman (1962), Theory of aquifer tests, *Tech. Rep. WSP - 1536-E*, United States Geological Survey.

Fetter, C. W. (2000), *Applied Hydrogeology*, 4 edition ed., Prentice Hall, Upper Saddle River, N.J.

Fiori, A., P. Indelman, and G. Dagan (1998), Correlation structure of flow variables for steady flow toward a well with application to highly anisotropic heterogeneous formations, *Water Resources Research*, *34*(4), 699–708, doi:10.1029/97WR02491.

Freeze, R. A. (1975), A stochastic-conceptual analysis of one-dimensional groundwater flow in nonuniform homogeneous media, *Water Resources Research*, *11*(5), 725–741, doi:10.1029/WR011i005p00725.

Freeze, R. A., and J. A. Cherry (1979), *Groundwater*, 1 edition ed., Prentice Hall, Englewood Cliffs, N.J.

Gelhar, L. W. (1993), *Stochastic Subsurface Hydrology*, Prentice-Hall, Englewood Cliffs, N.J.

Gringarten, A. (2008), From Straight Lines to Deconvolution: The Evolution of the State of the Art in Well Test Analysis, *SPE Reservoir Evaluation & Engineering*, *11*(1), doi:10.2118/102079-PA.

Grinsted, A. (2014), Tidal fitting toolbox - File Exchange - MATLAB Central, 2014, http://www.mathworks.com/matlabcentral/fileexchange/19099-tidal-fitting-toolbox.

Guadagnini, A., and S. P. Neuman (1999a), Nonlocal and localized analyses of conditional mean steady state flow in bounded, randomly nonuniform domains: 1. Theory and computational approach, *Water Resources Research*, *35*(10), 2999–3018, doi:10.1029/1999WR900160.

Guadagnini, A., and S. P. Neuman (1999b), Nonlocal and localized analyses of conditional mean steady state flow in bounded, randomly nonuniform domains: 2. Computational examples, *Water Resources Research*, *35*(10), 3019–3039, doi:10.1029/1999WR900159.

Guadagnini, A., and M. Riva (2003), Three-dimensional steady state flow to a well in a randomly heterogeneous bounded aquifer, *Water Resources Reasearch*, *39*(3), 1–16, doi:10.1029/2002WR001443.

Gómez-Hernández, J. J., and S. M. Gorelick (1989), Effective groundwater model parameter values: Influence of spatial variability of hydraulic conductivity, leakance, and recharge, *Water Resources Research*, *25*(3), 405–419, doi:10.1029/WR025i003p00405.

Gökaşan, E., E. Demirbag, F. Y. Oktay, B. Ecevitoglu, M. Şimşek, and H. Yüce (1997), On the origin of the Bosphorus, *Marine Geology*, *140*(1-2), 183–199, doi:10.1016/S0025-3227(97)00022-4.

Gökaşan, E., C. Gazioğlu, B. Alpar, Z. Yücel, c. Ersoy, O. g. Gündoğdu, and B. Tok (2001a), Evidence of NW-extension of the North Anatolian Fault Zone in the Marmara Sea: A new interpretation of the Marmara Sea (Izmit) earthquake on 17 August 1999, *Geo-Marine Letters*, *21*(4), 183–199, doi:10.1007/s00367-001-0088-0.

Gökaşan, E., B. Alpar, C. Gazioğlu, Z. Yaşar Yücel, B. Tok, E. Doğan, and C. Güneysu (2001b), Active tectonics of the Izmit Gulf (NE Marmara Sea): from high resolution seismic and multi-beam bathymetry data, *Marine Geology*, *175*(1–4), 273–288, doi:10.1016/S0025-3227(01)00133-5.

Gökaşan, E., T. Ustaömer, C. Gazioğlu, Z. Y. Yucel, K. Öztürk, H. Tur, B. Ecevitoğlu, and B. Tok (2003), Morpho-tectonic evolution of the Marmara Sea inferred from multi-beam bathymetric and seismic data, *Geo-Marine Letters*, *23*(1), 19–33, doi:10.1007/s00367-003-0120-7.

Görür, N. (1988), Timing of opening of the Black Sea basin, *Tectonophysics*, *147*(3–4), 247–262, doi:10.1016/0040-1951(88)90189-8.

Görür, N., O. Monod, A. I. Okay, A. M. C. Sengor, O. Tüysüz, E. Yigitbas, M. Sakinc, and R. Akkok (1997), Palaeogeographic and tectonic position of the Carboniferous rocks of the western Pontides (Turkey) in the frame of the Variscan belt, *Bulletin De La Societe Geologique De France*, *168*(2), 197–205.

Gürbüz, A. (2009), Orientations of palaeotectonic features as a key to understanding the neotectonic block rotation of the Kocaeli peninsula, NW Turkey, *International Geology Review - INT GEOL REV*, *51*(4), 329–344, doi:10.1080/00206810802655963.

Hantush, M. S. (1959), Analysis of data from pumping wells near a river, *Journal of Geophysical Research*, *64*(11), 1921–1932, doi:10.1029/JZ064i011p01921.

Harbaugh, M., E. Banta, M. Hill, and M. McDonald (2000), *Modflow-2000: The US Geological Survey modular ground-water model-user guide to modularization concepts and the ground-water flow process*, USGS Open-File Rep. 00-92.

Hearn, P. P., W. C. Steinkampf, G. C. Boptleson, and B. W. Drost (1985), Geochemical controls on dissolved sodium in basalt aquifers of the Columbina plateau, Washington, *Tech. rep.*, USGS, Tacoma.

Hoeksema, R. J., and P. K. Kitanidis (1985), Analysis of the Spatial Structure of Properties of Selected Aquifers, *Water Resources Research*, *21*(4), 563–572, doi:10.1029/WR021i004p00563.

Horne, R. N. (1996), *Modern Well Test Analysis: A Computer-Aided Approach*, pap/cdr ed., Petro Way, Palo Alto, CA.

Illman, W. A., and S. P. Neuman (2001), Type curve interpretation of a cross-hole pneumatic injection test in unsaturated fractured tuff, *Water Resources Research*, *37*(3), 583–603, doi:10.1029/2000WR900273.

Indelman, P. (2003), Transient pumping well flow in weakly heterogeneous formations, *Water Resources Reasearch*, *39*(10), 10, doi:10.1029/2003WR002036.

Indelman, P., and B. Abramovich (1994), Nonlocal properties of nonuniform averaged flows in heterogeneous media, *Water Resources Research*, *30*(12), 3385–3393, doi:10.1029/94WR01782.

Indelman, P., A. Fiori, and G. Dagan (1996), Steady flow toward wells in heterogeneous formations:

Mean head and equivalent conductivity, *Water Resources Reasearch*, *32*(7), 1975–1983, doi: 10.1029/96WR00990.

Kaymakci, N., E. Aldanmaz, C. Langereis, T. L. Spell, O. F. Gurer, and K. A. Zanetti (2007), Late Miocene transcurrent tectonics in NW Turkey: evidence from palaeomagnetism and 40ar–39ar dating of alkaline volcanic rocks, *Geological Magazine*, *144*(02), 379–392, doi: 10.1017/S0016756806003074.

Keskin, M., T. Ustaömer, and M. Yeniyol (2003), Stratigraphy, petrology and tectonic setting of Upper Cretaceous volcano-sedimentary units, North of Istanbul, Turkey, *Symposium on the Geology of Istanbul*, pp. 23–25.

Kinzelbach, W., and R. Rausch (1995), *Grundwassermodellierung: Eine Einführung mit Übungen*, Borntraeger, Berlin.

Knight, J., and G. Kluitenberg (2005), Some analytical solutions for sensitivity of well tests to variations in storativity and transmissivity, *Advances in Water Resources*, *28*(10), 1057–1075, doi:10.1016/j.advwatres.2004.08.018.

Knudby, C., and J. Carrera (2005), On the relationship between indicators of geostatistical, flow and transport connectivity, *Advances in Water Resources*, *28*(4), 405–421, doi: 10.1016/j.advwatres.2004.09.001.

Koral, H. (2007), Sea-level changes modified the Quaternary coastlines in the Marmara region, northwestern Turkey: What about tectonic movements?, in *The Black Sea Flood Question: Changes in Coastline, Climate, and Human Settlement*, edited by V. Yanko-Hombach, A. S. Gilbert, N. Panin, and P. M. Dolukhanov, pp. 571–601, Springer Netherlands.

Kruseman, G. P., N. A. d. Ridder (1990), *Analysis and evaluation of pumping test data*, International Institute for Land Reclamation and Improvement, Wageningen.

Langguth, H. R., and R. Voigt (1980), *Hydrogeologische Methoden*, Springer DE, Berlin.

Langguth, H. R., and R. Voigt (2004), *Hydrogeologische Methoden: Mit 304 Abbildungen*, Springer DE, Berlin, Heidelberg.

Leven, C., and P. Dietrich (2006), What information can we get from pumping tests?-comparing pumping test configurations using sensitivity coefficients, *Journal of Hydrology*, *319*(1–4), 199–215, doi:10.1016/j.jhydrol.2005.06.030.

Lu, Z., and V. V. Vesselinov (2015), Analytical sensitivity analysis of transient groundwater flow in a bounded model domain using the adjoint method, *Water Resources Research*, 5060–5080, doi:10.1002/2014WR016819.

Mantoglou, A., and J. L. Wilson (1982), The Turning Bands Method for simulation of random fields using line generation by a spectral method, *Water Resources Research*, *18*(5), 1379–1394, doi:10.1029/WR018i005p01379.

Matheron, G. (1967), *Elements pour une theorie des milieux poreux*, Masson et Cie, Paris.

McClusky, S., S. Balassanian, A. Barka, C. Demir, S. Ergintav, I. Georgiev, O. Gurkan, M. Hamburger, K. Hurst, H. Kahle, K. Kastens, G. Kekelidze, R. King, V. Kotzev, O. Lenk, S. Mahmoud, A. Mishin, M. Nadariya, A. Ouzounis, D. Paradissis, Y. Peter, M. Prilepin, R. Reilinger, I. Sanli, H. Seeger, A. Tealeb, M. N. Toksöz, and G. Veis (2000), Global Positioning System constraints on plate kinematics and dynamics in the eastern Mediterranean and Caucasus, *Journal of Geophysical Research: Solid Earth*, *105*(B3), 5695–5719, doi:10.1029/1999JB900351.

Meier, P. M., J. Carrera, and X. Sánchez-Vila (1998), An evaluation of Jacob's Method for the interpretation of pumping tests in heterogeneous formations, *Water Resources Research*, *34*(5), 1011–1025, doi:10.1029/98WR00008.

Moix, P., L. Beccaletto, H. W. Kozur, C. Hochard, F. Rosselet, and G. M. Stampfli (2008), A new classification of the Turkish terranes and sutures and its implication for the paleotectonic history of the region, *Tectonophysics*, *451*(1–4), 7–39, doi:10.1016/j.tecto.2007.11.044.

MTA (2005), Geological Map of Turkey F22-d (No:10), Maden Tektik ve Arama Genel Müdürlügü, Ankara.

MTA (2012a), Geological Map of Turkey, Istanbul-F21-c2, Maden Tektik ve Arama Genel Müdürlügü, Ankara.

MTA (2012b), Geological Map of Turkey, Istanbul-F22-d1, Maden Tektik ve Arama Genel Müdürlügü, Ankara.

MTA (2012c), Geological Map of Turkey, Istanbul-F21-b3, Maden Tektik ve Arama Genel Müdürlügü, Ankara.

Neuman, S. P., and S. Orr (1993), Prediction of steady state flow in nonuniform geologic media by conditional moments: Exact nonlocal formalism, effective conductivities, and weak approximation, *Water Resources Research*, *29*(2), 341–364, doi:10.1029/92WR02062.

Neuman, S. P., A. Guadagnini, and M. Riva (2004), Type-curve estimation of statistical heterogeneity, *Water Resources Reasearch*, *40*(W04201), 1–7, doi:10.1029/2003WR002405.

Nikishin, A. M., M. V. Korotaev, A. V. Ershov, and M.-F. Brunet (2003), The Black Sea basin: tectonic history and Neogene-Quaternary rapid subsidence modelling, *Sedimentary Geology*, *156*(1-4), 149–168, doi:10.1016/S0037-0738(02)00286-5.

Okay, A. (2008), Geology of Turkey: A synopsis, Anschnitt, 21, 19-42.

Okay, A. I., and O. Tüysüz (1999), Tethyan sutures of northern Turkey, *Geological Society, London, Special Publications*, *156*(1), 475–515, doi:10.1144/GSL.SP.1999.156.01.22.

Okay, A. I., A. Celal Sengor, and N. Gorur (1994), Kinematic history of the opening of the Black Sea and its effect on the surrounding regions, *Geology*, *22*(3), 267–270, doi:10.1130/0091-7613(1994)0220267:KHOTOO2.3.CO2.

Okay, A. I., I. Tansel, and O. Tüysüz (2001), Obduction, subduction and collision as reflected in the Upper Cretaceous–Lower Eocene sedimentary record of western Turkey, *Geological Magazine*, *138*(02), 117–142, doi:10.1017/S0016756801005088.

Okay, A. I., M. Satir, and W. Siebel (2006), Pre-Alpide Palaeozoic and Mesozoic orogenic events in the Eastern Mediterranean region, *Geological Society, London, Memoirs*, *32*(1), 389 –405, doi:10.1144/GSL.MEM.2006.032.01.23.

Oktay, F. Y., and R. H. Eren (1995), The geological map (1/50000) of Istanbul metropolitan area, Istanbul.

Oktay, F. Y., E. Gökasan, M. Sakınc, C. Yaltirak, C. Imren, and E. Demirbag (2002), The effects of the North Anatolian Fault Zone on the latest connection between Black Sea and Sea of Marmara, *Marine Geology*, *190*(1-2), 367–382, doi:10.1016/S0025-3227(01)00246-8.

Oliver, D. (1990), The Averaging Process in Permeability Estimation From Well-Test Data, *SPE Formation Evaluation*, *5*(3), doi:10.2118/19845-PA.

Oliver, D. S. (1993), The influence of nonuniform transmissivity and storativity on drawdown,

Water Resources Research, *29*(1), 169–178, doi:10.1029/92WR02061.

Oppenheim, A. V., and R. W. Schafer (1999), *Discrete-Time Signal Processing*, Prentice-Hall, Upper Saddle River, NJ. Limited.

Osnes, H. (1995), Stochastic analysis of head spatial variability in bounded rectangular heterogeneous aquifers, *Water Resources Research*, *31*(12), 2981–2990, doi:10.1029/95WR01956.

Osnes, H. (1998), Stochastic analysis of velocity spatial variability in bounded rectangular heterogeneous aquifers, *Advances in Water Resources*, *21*(3), 203–215, doi:10.1016/S0309-1708(96)00041-3.

Özgül, N. (2011), *Istanbul il alaninin jeolojisi - yönetici özeti*, Istanbul Municipality, Istanbul.

Özgül, N., K. Üner, I. Akmese, I. Bilgin, R. Kokuz, and I. Özcan (2005), *Istanbul il alanini genel jeologji özellikleri*, Istanbul Municipality, Istanbul.

Paleologos, E. K., S. P. Neuman, and D. Tartakovsky (1996), Effective Hydraulic Conductivity of Bounded, Strongly Heterogeneous Porous Media, *Water Resources Research*, *32*(5), 1333–1341, doi:10.1029/95WR02712.

Peaceman, D. (1983), Interpretation of Well-Block Pressures in Numerical Reservoir Simulation With Nonsquare Grid Blocks and Anisotropic Permeability, *Society of Petroleum Engineers Journal*, *23*(03), 531–543, doi:10.2118/10528-PA.

Reidel, S. P., V. G. Johnson, and F. A. Spane (2002), Natural Gas Storage in Basalt Aquifers of the Columbia Basin: A Guide to Site Characterization, *Tech. Rep. PNNL-13962*, U.S. Department of Energy, Pacific Northwest National Laboratory, Richland, Washington.

Reilinger, R. E., S. C. McClusky, M. B. Oral, R. W. King, M. N. Toksoz, A. A. Barka, I. Kinik, O. Lenk, and I. Sanli (1997), Global Positioning System measurements of present-day crustal movements in the Arabia-Africa-Eurasia plate collision zone, *Journal of Geophysical Research: Solid Earth*, *102*(B5), 9983–9999, doi:10.1029/96JB03736.

Renard, P. (2007), Stochastic Hydrogeology: What Professionals Really Need?, *Ground Water*, *45*(5), 531–541, doi:10.1111/j.1745-6584.2007.00340.x.

Renard, P., D. Glenz, and M. Mejias (2009), Understanding diagnostic plots for well-test interpretation, *Hydrogeology Journal*, *17*(3), 589–600, doi:10.1007/s10040-008-0392-0.

Riva, M., and M. Willmann (2009), Impact of log-transmissivity variogram structure on groundwater flow and transport predictions, *Advances in Water Resources*, *32*(8), 1311–1322, doi:10.1016/j.advwatres.2009.05.007.

Riva, M., A. Guadagnini, S. P. Neuman, and S. Franzetti (2001), Radial Flow in a Bounded Randomly Heterogeneous Aquifer, *Transport in Porous Media*, *45*(1), 139–193, doi:10.1023/A:1011880602668.

Rubin, Y. (2003), *Applied Stochastic Hydrogeology*, Oxford Univ Pr, Oxford ; New York.

Rubin, Y., and G. Dagan (1988), Stochastic analysis of boundaries effects on head spatial variability in heterogeneous aquifers: 1. Constant head boundary, *Water Resources Research*, *24*(10), 1689–1697, doi:10.1029/WR024i010p01689.

Sanchez-Vila, X. (1997), Radially convergent flow in heterogeneous porous media, *Water Resources Reasearch*, *33*(7), 1633–1641, doi:10.1029/97WR01001.

Sanchez-Vila, X., and D. M. Tartakovsky (2007), Ergodicity of pumping tests, *Water Resources Research*, *43*(3), W03,414, doi:10.1029/2006WR005241.

Sanchez-Vila, X., C. L. Axness, and J. Carrera (1999a), Upscaling transmissivity und radially convergent flow in heterogeneous media, *Water Resources Reasearch*, *104*(3), 613–621, doi:10.1029/1998WR900056.

Sanchez-Vila, X., P. M. Meier, and J. Carrera (1999b), Pumping tests in heterogeneous aquifers: An analytical study of what can be obtained from their interpretation using Jacob's Method, *Water Resources Research*, *35*(4), 943–952, doi:10.1029/1999WR900007.

Sanchez-Vila, X., A. Guadagnini, and J. Carrera (2006), Representative hydraulic conductivities in saturated groundwater flow, *Reviews of Geophysic*, *44*(RG3002), 46, doi:10.1029/2005RG000169.

Schad, H., and G. Teutsch (1994), Effects of the investigation scale on pumping test results in heterogeneous porous aquifers, *Journal of Hydrology*, *159*, 61–77, doi:10.1016/0022-1694(94)90249-6.

Schneider, C., and S. Attinger (2008), Beyond Thiem: A new method for interpreting large scale pumping tests in heterogeneous aquifers, *Water Resources Research*, *44*(W04427), 14, doi:10.1029/2007WR005898.

Şengör, A., and Y. Yilmaz (1981), Tethyan evolution of Turkey: A plate tectonic approach, *Tectonophysics*, *75*(3-4), 181–241, doi:10.1016/0040-1951(81)90275-4.

Şengör, A., O. Tüysüz, C. İmren, M. Sakınç, H. Eyidogan, N. Görür, X. Le Pichon, and C. Rangin (2005), The North Anatolian Fault: A New Look, *Annual Review of Earth and Planetary Sciences*, *33*(1), 37–112, doi:10.1146/annurev.earth.32.101802.120415.

Spane, F. A., and S. K. Wurstner (1993), DERIV: A Computer Program for Calculating Pressure Derivatives for Use in Hydraulic Test Analysis, *Ground Water*, *31*(5), 814–822, doi:10.1111/j.1745-6584.1993.tb00855.x.

Stampfli, G. M. (2000), Tethyan oceans, *Geological Society, London, Special Publications*, *173*(1), 1 –23, doi:10.1144/GSL.SP.2000.173.01.01.

Stewart, G. (1997), Future Developments In Well Test Analysis: Introduction of Geology, *Hart's Petroleum Engineer International*, pp. 73–76.

Sudicky, E. A. (1986), A natural gradient experiment on solute transport in a sand aquifer: Spatial variability of hydraulic conductivity and its role in the dispersion process, *Water Resources Research*, *22*(13), 2069–2082, doi:10.1029/WR022i013p02069.

Sun, N.-Z., and W. W.-G. Yeh (1985), Identification of Parameter Structure in Groundwater Inverse Problem, *Water Resources Research*, *21*(6), 869–883, doi:10.1029/WR021i006p00869.

Tartakovsky, D. M., A. Guadagnini, F. Ballio, and A. M. Tartakovsky (2002), Localization of Mean Flow and Apparent Transmissivity Tensor for Bounded Randomly Heterogeneous Aquifers, *Transport in Porous Media*, *49*(1), 41–58, doi:10.1023/A:1016092910797.

Theis, C. V. (1935), The relation between the lowering of the Piezometric surface and the rate and duration of discharge of a well using ground-water storage, *Transactions, American Geophysical Union*, *16*(2), 519, doi:10.1029/TR016i002p00519.

Thiem, G. (1906), Hydrologische Methoden, Ph.D. thesis, Gebhardt, Leipzig.

Toll, N. J., and T. C. Rasmussen (2007), Removal of Barometric Pressure Effects and Earth Tides from Observed Water Levels, *Ground Water*, *45*(1), 101–105, doi:10.1111/j.1745-6584.2006.00254.x.

Trinchero, P., X. Sánchez-Vila, and D. Fernàndez-Garcia (2008), Point-to-point connectivity, an abstract concept or a key issue for risk assessment studies?, *Advances in Water Resources*, *31*(12), 1742–1753, doi:10.1016/j.advwatres.2008.09.001.

Tüysüz, O. (1999), Geology of the Cretaceous sedimentary basins of the Western Pontides, *Geological Journal*, *34*(1-2), 75–93.

Walker, D. D., and R. M. Roberts (2003), Flow dimensions corresponding to hydrogeologic conditions, *Water Resources Research*, *39*(12), 1349, doi:10.1029/2002WR001511.

Warren, J., and H. Price (1961), Flow in Heterogeneous Porous Media, *Society of Petroleum Engineers Journal*, *1*(03), 153–169, doi:10.2118/1579-G.

Winter, C. L. (2004), Stochastic hydrology: practical alternatives exist, *Stochastic Environmental Research and Risk Assessment*, *18*(4), 271–273, doi:10.1007/s00477-004-0198-0.

Wu, C.-M., T.-C. J. Yeh, J. Zhu, T. H. Lee, N.-S. Hsu, C.-H. Chen, and A. F. Sancho (2005), Traditional analysis of aquifer tests: Comparing apples to oranges?, *Water Resources Research*, *41*(9), W09,402, doi:10.1029/2004WR003717.

Yeh, W. W.-G. (1986), Review of Parameter Identification Procedures in Groundwater Hydrology: The Inverse Problem, *Water Resources Research*, *22*(2), 95–108, doi:10.1029/WR022i002p00095.

Yilmaz, N., H. Güven, M. Senkaya, H. Safak, and M. Artut (2009), Kocaeli il cevre durum raporu 2009, Istanbul.

Yilmaz, Y. (2007), Morphotectonic development of the southern Black Sea region and the Bosphorus channel, in *The Black Sea Flood Question: Changes in Coastline, Climate, and Human Settlement*, edited by V. Yanko-Hombach, A. S. Gilbert, N. Panin, and P. M. Dolukhanov, pp. 537–569, Springer Netherlands.

Yilmaz, Y., A. M. C. Sengör, O. Tüysüz, E. Yigitbas, and S. C. Genc (1997), Chapter 11: Geology and Tectonic Evolution of the Pontides, in *AAPG Memoir 68: Regional and Petroleum Geology of the Black Sea and Surrounding Region.*, pp. 183–226, American Association of Petroleum Geologists.

Zech, A., S. Arnold, C. Schneider, and S. Attinger (2015), Estimating Parameters of Aquifer Heterogeneity Using Pumping Tests - Implications for Field Applications, *Advances in Water Resources*, doi:10.1016/j.advwatres.2015.05.021.

Selbstständigkeitserklärung

Ich erkläre, dass ich die vorliegende Arbeit selbstständig und unter Verwendung der angegebenen Hilfsmittel, persönlichen Mitteilungen und Quellen angefertigt habe.

11. Juni 2016, Leipzig

Armin Pechstein